transnationale
UNIVERSITEIT LIMBURG

School voor Levenswetenschappen

Cellular defence mechanisms in renal distal tubular A6 cells facing metabolic inhibition

A study of Na^+ handling, intracellular pH, cell volume regulation and their inter-relationships

Proefschrift voorgelegd tot het behalen van de graad van
Doctor in de Biomedische Wetenschappen,
te verdedigen door

Ilse SMETS

Promotoren : Prof. dr. P. Steels,
Prof. dr. M. Ameloot

2001

DOCTORAATSPROEFSCHRIFT

Universiteit Maastricht

LIMBURGS UNIVERSITAIR CENTRUM
PARTNER IN DE UNIVERSITEIT LIMBURG

Abbreviations and symbols

A6 : cell line derived from the kidney of *Xenopus laevis*
ADP : adenosine diphosphate
AM : acetoxymethyl ester (form of a fluorescent indicator)
AMI : amiloride
AMP : adenosine monophosphate
ap. : apical
ARF : acute renal failure
ATN : acute tubular necrosis
ATP : adenosine triphosphate
BCECF : 2', 7'-bis-(2-carboxyethyl)-5-(and6) carboxyfluorescein
bl. : basolateral
cAMP : 3'5'-cyclic adenosine monophosphate
CCD : charge coupled device
CCT : cortical collecting tubule
CDPC : 6-chloro-3,5-diamino-pyrazine-2-carboxamide
CMF(DA) : 5-chloromethyl fluorescein (diacetate)
CN : anion cyanide
C_T : transepithelial capacitance
CTR : control
cpm : counts per minute
DMSO : dimethyl sulfoxide
DOG : 2-deoxyglucose
DOG-6-P : 2-deoxyglucose-6-phosphate
$\Delta\Psi_m$: mitochondrial membrane potential
EB : ethidium bromide
EDTA : ethylenediaminetetraacetic acid
EIPA : 5-(N-ethyl-N-isopropyl)amiloride
E_M : apical membrane potential
E_{Na} : Nernst potential for Na^+
ENaC : epithelial Na^+ channel
ER : endoplasmic reticulum
ETC : electron transport chain
f : frequency
f_c : corner frequency
F : fluorescence intensity
FCCP : carbonyl cyanide p-trifluoromethoxy-phenylhydrazone
FCS : fetal calf serum
γ : single channel conductance
G_{Cl} : chloride conductance
GSH : reduced glutathione
GSSH : oxidised glutathione
G_T : transepithelial conductance
HEPES : 4-(2-hydroxyethyl)-1-piperazine sulphonic acid
Hz : Hertz
i : single channel current
IF_1 : inhibitory protein of the mitochondrial F_1F_0-ATPase
i_{max} : maximal value of single channel current

I_{max}	: maximal value of transepithelial current
IMP	: inosine monophosphate
I_{Na}	: transepithelial Na^+ current
I_{sc}	: short-circuit current
I.U.	: international units
JC-1	: 5,5',6,6'-tetrachloro-1,1',3,3'-tetra-ethylbenzimidazolylcarbocyanine iodide
K_B	: microscopic equilibrium constant for the channel fluctuation reaction
Kir	: inward rectifier K^+ channels
K_m	: Michaelis-Menten constant
k_{on}	: rate constant for blockage of the ion channel
k_{off}	: rate constant for unblockage of the ion channel
λ	: wavelength
MDCK	: Madin-Darbey Canine Kidney cells
MI	: metabolic inhibition
N	: number of tissues
$[Na^+]_{ap}$	: apical sodium concentration
NAD(P)H	: nicotinamide adenine dinucleotide (phosphate)
N_B	: number of beads (cells) used to calculate the mean of T_c
Nedd4	: neuronal precursor cell-expressed developmentally downregulated
NHE	: Na^+/H^+ exchanger
NMDG	: N-Methyl-D-Glucamine
NPPB	: 5-nitro-2-[(3-phenylpropyl)amino]-benzoic acid
N_o	: number of open channels per unit area of the membrane
N_T	: total (open + closed) channel number per unit area of the membrane
OUAB	: ouabain
π	: extracellular osmolality
π_{bl}	: osmolality of the basolateral solution
PDS	: power density spectrum
P_K	: basolateral membrane K^+ permeability
P_{Na}	: apical membrane Na^+ permeability
P_o	: open probability of an ion channel
pH_c	: intracellular pH
pH_{sol}	: external solution pH
R	: ratio of fluorescence intensities
ROS	: reactive oxygen species
R_T	: transepithelial resistance
RVD	: regulatory volume decrease
RVI	: regulatory volume increase
SEM	: standard error of the mean
S(f)	: spectral density or power density
S_o	: Lorentzian plateau value
S_1	: amplitude of the low frequency component at f = 1 Hz
T_c	: cell thickness
TEA	: tetraethylammonium
TCA	: tricarboxylic acid
Tricine	: N-Tris-(hydroxymethyl)-methylglycine
TRIS	: Tris-(hydroxymethyl)-aminomethane
V_{sc}	: intracellular potential in short-circuit conditions
V_T	: transepithelial voltage

U

transnationale
UNIVERSITEIT LIMBURG

L

School voor Levenswetenschappen

Cellular defence mechanisms in renal distal tubular A6 cells facing metabolic inhibition

A study of Na^+ handling, intracellular pH, cell volume regulation and their inter-relationships

Proefschrift voorgelegd tot het behalen van de graad van
Doctor in de Biomedische Wetenschappen,
te verdedigen door

Ilse SMETS

Promotoren : Prof. dr. P. Steels,
Prof. dr. M. Ameloot

2001

According to the guidelines of the Limburgs Universitair Centrum,
a copy of this publication
has been filed in the Royal Library Albert I, Brussels,as publication
D/2001/2451/35

Table of Contents

Abbreviations and symbols

A6	: cell line derived from the kidney of *Xenopus laevis*
ADP	: adenosine diphosphate
AM	: acetoxymethyl ester (form of a fluorescent indicator)
AMI	: amiloride
AMP	: adenosine monophosphate
ap.	: apical
ARF	: acute renal failure
ATN	: acute tubular necrosis
ATP	: adenosine triphosphate
BCECF	: 2', 7'-bis-(2-carboxyethyl)-5-(and6) carboxyfluorescein
bl.	: basolateral
cAMP	: 3'5'-cyclic adenosine monophosphate
CCD	: charge coupled device
CCT	: cortical collecting tubule
CDPC	: 6-chloro-3,5-diamino-pyrazine-2-carboxamide
CMF(DA)	: 5-chloromethyl fluorescein (diacetate)
CN	: anion cyanide
C_T	: transepithelial capacitance
CTR	: control
cpm	: counts per minute
DMSO	: dimethyl sulfoxide
DOG	: 2-deoxyglucose
DOG-6-P	: 2-deoxyglucose-6-phosphate
$\Delta\Psi_m$	: mitochondrial membrane potential
EB	: ethidium bromide
EDTA	: ethylenediaminetetraacetic acid
EIPA	: 5-(N-ethyl-N-isopropyl)amiloride
E_M	: apical membrane potential
E_{Na}	: Nernst potential for Na^+
ENaC	: epithelial Na^+ channel
ER	: endoplasmic reticulum
ETC	: electron transport chain
f	: frequency
f_c	: corner frequency
F	: fluorescence intensity
FCCP	: carbonyl cyanide p-trifluoromethoxy-phenylhydrazone
FCS	: fetal calf serum
γ	: single channel conductance
G_{Cl}	: chloride conductance
GSH	: reduced glutathione
GSSH	: oxidised glutathione

G_T	: transepithelial conductance
HEPES	: 4-(2-hydroxyethyl)-1-piperazine sulphonic acid
Hz	: Hertz
i	: single channel current
IF_1	: inhibitory protein of the mitochondrial F_1F_0-ATPase
i_{max}	: maximal value of single channel current
I_{max}	: maximal value of transepithelial current
IMP	: inosine monophosphate
I_{Na}	: transepithelial Na^+ current
I_{sc}	: short-circuit current
I.U.	: international units
JC-1	: 5,5',6,6'-tetrachloro-1,1',3,3'-tetra-ethylbenzimidazolylcarbocyanine iodide
K_B	: microscopic equilibrium constant for the channel fluctuation reaction
Kir	: inward rectifier K^+ channels
K_m	: Michaelis-Menten constant
k_{on}	: rate constant for blockage of the ion channel
k_{off}	: rate constant for unblockage of the ion channel
λ	: wavelength
MDCK	: Madin-Darbey Canine Kidney cells
MI	: metabolic inhibition
N	: number of tissues
$[Na^+]_{ap}$	: apical sodium concentration
NAD(P)H	: nicotinamide adenine dinucleotide (phosphate)
N_B	: number of beads (cells) used to calculate the mean of T_c
Nedd4	: neuronal precursor cell-expressed developmentally downregulated
NHE	: Na^+/H^+ exchanger
NMDG	: N-Methyl-D-Glucamine
NPPB	: 5-nitro-2-[(3-phenylpropyl)amino]-benzoic acid
N_o	: number of open channels per unit area of the membrane
N_T	: total (open + closed) channel number per unit area of the membrane
OUAB	: ouabain
π	: extracellular osmolality
π_{bl}	: osmolality of the basolateral solution
PDS	: power density spectrum
P_K	: basolateral membrane K^+ permeability
P_{Na}	: apical membrane Na^+ permeability
P_o	: open probability of an ion channel
pH_c	: intracellular pH
pH_{sol}	: external solution pH
R	: ratio of fluorescence intensities
ROS	: reactive oxygen species
R_T	: transepithelial resistance
RVD	: regulatory volume decrease
RVI	: regulatory volume increase

SEM	: standard error of the mean
S(f)	: spectral density or power density
S_o	: Lorentzian plateau value
S_1	: amplitude of the low frequency component at f = 1 Hz
T_c	: cell thickness
TEA	: tetraethylammonium
TCA	: tricarboxylic acid
Tricine	: N-Tris-(hydroxymethyl)-methylglycine
TRIS	: Tris-(hydroxymethyl)-aminomethane
V_{sc}	: intracellular potential in short-circuit conditions
V_T	: transepithelial voltage

Chapter 1

General Introduction

1.1 INTRODUCTION

Ischemia *in vivo* is characterised by a decrease of blood flow with subsequent limitation of substrate, particularly glucose, and oxygen supply. The typical consequences of ischemic acute renal failure will be described in section 1.5. In this thesis, renal ischemia was mimicked via an experimental *in vitro* model: renal distal tubular A6 cells were exposed to metabolic inhibitors for both cellular metabolic pathways. The use of metabolic inhibition (MI) as an *in vitro* model of ischemic acute renal failure, as well as the use of the A6 cell culture model, are described in detail in sections 1.6 and 1.7 respectively.

The objective of this study was to investigate cellular events occurring in renal epithelial cells facing metabolic inhibition and to examine the relationships between them. In particular, we focussed on Na^+ handling, cell volume regulation and intracellular pH regulation. To better understand their modifications and correlations during MI, these three topics are first described for normal physiological conditions in sections 1.2, 1.3 and 1.4 respectively.

At the end of this chapter the different aims of this thesis are summarised.

1.2 TRANSEPITHELIAL SODIUM TRANSPORT IN TIGHT EPITHELIA

Epithelia are structurally well-organised cell layers that are specialised in the net unidirectional movement of ions or other substances from one side of the epithelium to the other side. Therefore, epithelia serve to maintain the fluid and electrolyte balance of the surrounding compartments. Tight epithelia are epithelia with a transepithelial resistance in the range of $k\Omega.cm^2$. High concentration differences can be created since passive backflow through the paracellular pathway is largely prevented. Moreover, marked transepithelial potential differences can exist because active electrogenic transepithelial transport of ions is not followed immediately by the paracellular flux of the counter ions.

Vectorial sodium ion transport in high-resistance epithelia (Fig. 1.1) is mediated by apical Na^+ influx through highly selective low-conductance amiloride sensitive epithelial Na^+ channels (ENaC). Subsequent cellular Na^+ efflux occurs through Na^+K^+-ATPases at the basolateral cell surface. Under most physiological circumstances, the Na^+K^+-ATPase is not the rate limiting step in electrogenic sodium reabsorption, but rather the ENaC (Biber and Curran, 1970). The number of pumps is high (up to 10^6 per cell). In most cases, the Na^+K^+-ATPase operates at only one fifth or one third of its maximal capacity (Rossier, 1997). This series arrangement of apical (ap.) and

basolateral (bl.) membranes, which contain distinct proteins (Na^+ channel versus Na^+K^+-ATPase), allows vectorial transport of Na^+ across the epithelium.

The rate-limiting Na^+ entry through ENaCs is the site of regulation of net transepithelial transport (Garty and Benos, 1988; Garty and Palmer, 1997; Rossier, 1997). The ENaC is a channel consisting of at least three subunits, sharing limited (~30-40%) sequence similarity and called α-, β-, and γ-ENaC (Canessa et al., 1994; Alvarez de la Rosa et al., 2000). Although the α-subunit alone can form functional amiloride-sensitive Na^+ channels, the combination of the three subunits is required for maximal conductance and for obtaining the typical properties of the native ENaC (McNicholas and Canessa, 1997). ENaC is a 'low copy number' protein: only a few hundred molecules are expressed per cell and its tissue distribution is highly restricted to a few organs (Rossier, 1997). ENaC is expressed at the ap. surface of: the distal part of the nephron in the kidney (from distal convoluted tubule to inner medullary collecting duct), the distal colon, the ducts of secretory glands (salivary and sweat glands), the respiratory airways and in amphibian skin.

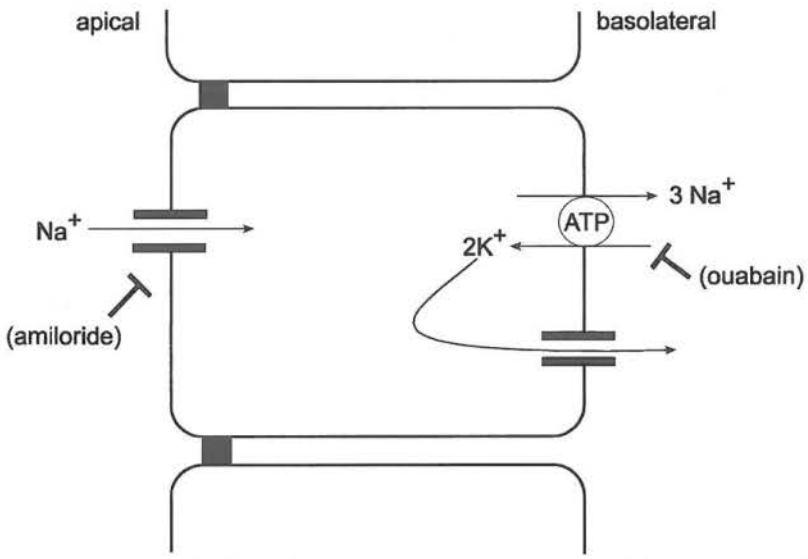

Fig. 1.1 Transepithelial Na^+ reabsorption in tight epithelia. *Na^+ is reabsorbed from the luminal space into the cell down its electrochemical gradient via the amiloride-sensitive ENaC. In the basolateral membrane, the Na^+K^+-ATPase extrudes Na^+ in exchange for K^+ to maintain a low intracellular Na^+ concentration, and basolateral K^+ channels recycle K^+.*

Several hormones, including aldosterone, arginine vasopressin, atrial natriuretic peptide, and insulin, as well as cellular kinases, regulate the ap. membrane ENaC (Garty and Benos, 1988; Duchatelle et al., 1992; Eaton et al., 1995; Garty and Palmer, 1997;

Stockand et al., 2000). General mechanisms of ENaC regulation are likely to involve at least one of three processes, i.e., 1) changes in the number of ENaCs that are expressed at the plasma membrane, 2) changes in the open probability of the channels, P_o, or 3) changes in the current through individual Na^+ channels, i. Concerning the regulation of cell surface expression of ENaCs, the rapid internalisation of ENaCs can serve as a control mechanism of channel density. The turnover of ENaCs at the ap. plasma membrane is known to be very fast (less than one hour) (Rossier, 1997). Rapid channel retrieval of ENaCs from the plasma membrane can occur via clathrin-mediated endocytosis (Shimkets et al., 1997) or via ubiquitination (Staub et al., 1996; Malik et al., 2001). The relevance of ENaC regulation via ubiquitination became clear when specific mutations at the β-, and γ-ENaC induced the 'Liddle syndrome' (Snyder et al., 1995). Although not yet formally demonstrated in the human kidney, an excessive number of functional channels is probably expressed in the cortical collecting duct, causing an increased sodium reabsorption, increased blood volume, and hence hypertension. The described mutations (Snyder et al., 1995) were different alterations in one specific conserved sequence found in the three ENaC subunits, which normally allows binding to the ubiquitin protein ligase Nedd4 (Staub et al., 1996). Normally this interaction with Nedd4 would promote a rapid internalisation and degradation of ENaC molecules. In the Liddle syndrome or in the Liddle mutations, Nedd4 cannot bind with high affinity to ENaC, thus, the turnover of ENaCs is slowed down and the number of channels at the cell surface increases (Rossier, 1997).

Besides ENaC regulation to control the overall homeostasis of the organism, e.g. by hormones or regulatory proteins as described above, regulation of ENaCs by factors intrinsic to the Na^+ transporting cells themselves is essential to control their own Na^+ content and cellular volume (Garty and Palmer, 1997). 'Na^+ self-inhibition' and 'feedback inhibition' are terms used in the literature to describe these processes. The concept of 'self-inhibition' is that extracellular Na^+ itself can modify the activity of the channels via an allosteric receptor for Na^+ on the outside of the cell, and thus, independent of changes in intracellular ion composition (Lindemann, 1984). The clearest evidence for such an effect came from experiments in which the Na^+ concentration at the outer surface of the frog skin was abruptly increased. The current through the channels rose to a peak and relaxed subsequently to a significantly lower steady-state level over a period of a few seconds, a time period in which intracellular Na^+ did not increase (Fuchs et al., 1977).

The term 'feedback-inhibition' refers to the modulation of ENaC activity by intracellular Na^+. Early experiments provided little evidence for this inhibitory mechanism since acute elevation of intracellular Na^+ did not decrease the ap. membrane Na^+ permeability (P_{Na}) in rabbit and toad urinary bladder (Eaton, 1981; Palmer, 1985), neither decreased the ENaC activity in excised patches of rat cortical collecting tubules during complete replacement of intracellular K^+ with Na^+ (Palmer et al., 1989). On the other hand,

current fluctuation measurements on frog skin demonstrated that adding ouabain, to block the Na^+K^+-ATPase, resulted in a decrease of the ap. ENaC density (Erlij and Van Driessche, 1983). This decrease could result from feedback inhibition due to increased levels of intracellular Na^+ after the addition of ouabain. Recently, Nedd4 was proposed as the mediator for Na^+ feedback inhibition of ENaCs in salivary glands, since blocking of the Nedd4 activity abolished the inhibitory effect of increased internal Na^+ on ENaC (Dinudom et al., 1998; Alvarez de la Rosa et al., 2000). Increased levels of intracellular Na^+ mostly result in parallel changes of cytosolic Ca^{2+} concentrations, presumably via the Na^+/Ca^{2+} exchanger (Yang et al., 1988) or via mitochondrial Ca^{2+} release (Hayworth et al., 1980). Furthermore, an inverse relationship between cytosolic Ca^{2+} and P_{Na} was observed (Taylor and Windhager, 1979), possibly involving activation of protein kinase C, which has been shown to inhibit apical Na^+ flux at both a macroscopic and single-channel level in A6 epithelia (Yanase and Handler, 1986; Ling and Eaton, 1989; Stockand et al., 2000) and mammalian cortical collecting tubules (Snyder et al., 1995).

1.3 CELL VOLUME HOMEOSTASIS

The volume regulatory system in animal cells is extremely sensitive. Changes as small as 2-5% of the original volume may result in the activation of specific transport pathways. Most cells of higher animals are not subjected to osmotic stress since the tonicity of extracellular fluid is nearly constant. However, epithelia in the kidney, red blood cells or intestinal epithelial cells can face significant changes in extracellular osmolality. Especially for these cells it is crucial to possess adequate volume regulatory mechanisms: a regulatory volume decrease (RVD) as a response to sudden osmotic swelling and a regulatory volume increase (RVI) to counteract shrinkage. During both phases, volume activated intracellular phenomena result in the activation of transport pathways to restore resting conditions. This introduction will only deal with the RVD mechanism, since, within the framework of this thesis, only the RVD phenomenon is investigated (Chapter 7).

In hypotonic media, cells initially swell by osmotic water uptake and subsequently regulate their volume by a net loss of solutes and water. In most cell types, this swelling results in a loss of K^+, Cl^- and organic molecules. The loss of K^+ and Cl^- via activation of ion channels -which are not necessarily identical to the native K^+ and Cl^- channels- was described for most cell types investigated including Ehrlich ascites cells (Hoffmann, 1992), lymphocytes (Grinstein and Foskett, 1990), hepatocytes (Haussinger and Lang, 1991), frog skin (Ussing, 1985) and many other epithelia (Banderali and Roy, 1992) including A6 cells (De Smet et al., 1995b). The nature of the swelling-induced K^+ pathway is unknown. In some cell types, cell swelling induces an increase in intracellular free $[Ca^{2+}]$, which in turn activates high-conductance Ca^{2+}-

activated K^+ channels. This has been shown in e.g. principal cells of rat and rabbit cortical collecting tubule (Ling et al., 1992; Stoner and Morley, 1995) and rabbit proximal tubule cells (Dube et al., 1990). In addition to the swelling-induced opening of K^+ channels, a Cl^- conductance is activated allowing a rapid loss of KCl and water. The volume-activated Cl^--channels can transport other small, monovalent anions (NO_3^-), but no large organic anions such as gluconate. Volume-activated Cl^- channels differ from both the adenosine 3'5'-cyclic monophosphate (cAMP) activated and the Ca^{2+} and calmodulin activated Cl^- channels.

KCl loss during RVD can also occur via KCl cotransport, e.g. in red blood cells of many species (Hall et al., 1989) or via K^+/H^+ exchange coupled to Cl^-/HCO_3^- exchange in *Amphiuma* red blood cells (Cala, 1985).

1.4 INTRACELLULAR pH HOMEOSTASIS AND THE REGULATORY FUNCTION OF INTRACELLULAR pH

Epithelial cells maintain their intracellular pH (pH_c) within a narrow range (6.9-7.5) (Ives and Rector, 1984). This is well above the electrochemical equilibrium value of ~ 6.0 - 6.5 that is predicted by the Nernst equation from the interior negative potential difference of 60-90 mV and an extracellular pH of ~ 7.4. Intracellular buffers and acid-base transport systems regulate pH_c. The role of intracellular buffering in pH_c regulation is to attenuate large variations in pH_c: they cannot prevent a change in pH_c but they can merely reduce its magnitude. Furthermore, buffering mechanisms cannot return pH_c towards its initial value following an acid or alkali load. This recovery is brought about by transport of acid and/or base across the cell membrane. There are several mechanisms of acid extrusion or loading in epithelial cells (reviewed by Boron, 1992). Probably the most widespread is the Na^+/H^+ exchanger (NHE). The antiporter exchanges intracellular H^+ for extracellular Na^+ in a 1:1 stoichiometry and is driven by the large inward chemical gradient of Na^+ and the outward H^+ gradient. Intracellular acidification activates the exchanger whereas a decrease in the extracellular pH inhibits its activity. Amiloride and its derivatives inhibit the NHE activity by competing with Na^+ for binding to the same external site (Moolenaar, 1986).

Another transport system involved in pH_c regulation is the Na^+-dependent Cl^-/HCO_3^- exchanger (Boyarsky et al., 1988). This antiporter has an absolute requirement for external Na^+, external HCO_3^- and internal Cl^-. Removing any one of these three ions from the appropriate side of the membrane completely blocks acid extrusion. A Na^+-independent Cl^-/HCO_3^- exchanger that mediates the exchange of external Cl^- for internal HCO_3^- in a 1:1 ratio has also been observed (Boyarsky et al., 1988). In the basolateral membrane of several epithelia, including the renal proximal tubule, an electrogenic Na^+/HCO_3^- cotransporter is present (Boron and Boulpaep, 1983). In epithelia, the

cotransporter normally mediates a net efflux of Na^+ and HCO_3^-. An electrogenic H^+ pump is present in the distal nephron of the kidney as well as in the urinary bladder of the reptile (Al-Awqati et al., 1983) and in frog skin (Klein et al., 1997). It has been shown (Selvaggio et al., 1988) that the H^+ pump contributes to the recovery of pH_c after an acid load in collecting duct cells. In the parietal cells of the stomach (Sachs et al., 1989) and in renal cells (Lang et al., 1990) an ATP-driven pump is present that extrudes H^+ in exchange for K^+ (H^+/K^+ pump).

There is an absolute need for the maintenance of pH_c within a narrow range, since many cellular processes are sensitive to pH_c. The most obvious way pH_c affects the cell metabolism is via regulation of enzyme activity. This results in the regulation of protein synthesis as well as in the control of energy production and utilization. Other cellular processes which are regulated by pH_c include the cell cycle and proliferation, fertilisation and signal transduction (Epel, 1990; Ganapathy and Leibach, 1991; LaPointe and Battle, 1994). The efficiency of contractile elements and the conductivity of some ion channels -including these involved in transepithelial Na^+ reabsorption in tight epithelia- also depend upon cytosolic pH (Ganapathy and Leibach, 1991). Early findings demonstrated that increased CO_2 pressures of the bathing medium -a procedure that may be expected to acidify the cytoplasm- reduced Na^+ reabsorption in frog skin (Ussing and Zerahn, 1951) and in toad urinary bladder (Palmer, 1985). Acidification of the solution on the cytosolic side of excised patches of rat cortical collecting tubule ap. membranes markedly decreased the P_o of the ENaCs (Palmer and Frindt, 1987). More recent experiments on ap. membrane patches of A6 cells demonstrated that acidosis of the cytosolic bath decreased the ENaC open probability and the number of active channels in the membrane patch without altering the single channel conductance (Harvey, 1995). Internal hydrogen ions affected channel closure by interacting with high cooperativity at a titration site with an apparent pK of ~ 7.2 (Harvey, 1995). pH_c directly regulates the α-subunit of the ENaC, presumably via titration of one or more amino acids (e.g. His-94) in the cytoplasmic amino and carboxy termini (Chalfant et al., 1999). Furthermore, pH_c is an important determinant of the bl. K^+ conductance (Fig. 1.1) in Na^+ absorbing tight epithelia. Intracellular acidification closes inward rectifier K^+ (Kir) channels rapidly and with a steep pH dependence (Ruppersberg, 2000). Kir1.1 (expressed in the nephron) is half-maximally active around pH 7.0 and fully blocked at pH 6.7 (Ruppersberg, 2000). Recent studies have contributed to the understanding of the molecular mechanism of gating of Kir channels (including the ATP sensitive and kidney-specific Kir, ROMK) by pH_c which involves protonation of lysine 80 and subsequent conformational changes (Fakler et al., 1996; Choe et al., 1997; Giebisch and Wang, 2000; Ruppersberg, 2000). Furthermore, it was demonstrated that some of the membrane transport mechanisms involved in cell volume regulation are also affected by changes in pH_c. For example, mechanisms implicated in volume regulation in various tissues include Na^+-H^+ and Cl^--HCO_3^- antiporters (Hoffmann, 1987). The activity of

swelling activated K^+ channels decreases with intracellular acidification in some cells, e.g. in primary cultures of seawater fish gill cells (Duranton et al., 2000). Recently, a role for pH_c in the activation of Ca^{2+}-activated K^+ channels upon cell swelling of villus epithelial cells has been proposed (MacLeod and Hamilton, 1999a; MacLeod and Hamilton, 1999b). Moreover, volume-regulated anion channels (VRAC) in endothelial cells display pH_c-dependent activation characteristics (Sabirov et al., 2000).

1.5 ISCHEMIC ACUTE RENAL FAILURE

1.5.1 General aspects

Approximately 5% percent of all patients in clinic, and up to 30 % of all patients in intensive care units develop acute renal failure or ARF (Brady et al., 2000). ARF is a syndrome characterised by a rapid decline in renal function resulting in retention of waste products such as urea nitrogen and serum creatinine (Brady et al., 2000). Another term conventionally used in clinical practice is acute tubular necrosis (ATN), referring to ARF that results from toxic or ischemic insults to the renal tubular cells.

Since structural differences within the kidney are of high importance in the pathophysiology of ARF, a brief anatomical description of the major anatomical regions in the kidney and in the nephron –the functional unit of the kidney- is given below (Fig 1.2). If a kidney is sectioned, two regions are seen: an outer part, called the cortex, and an inner part, called the medulla. Within the medulla an inner and outer zone are distinguished. The outer zone can be subdivided into an inner and an outer stripe. The nephron is made up of different nephron segments (Fig 1.2), which consist of highly specialised cells with typical structural and functional characteristics.

The combination of individual cell function and tissue organisation makes the mammalian kidney an efficient osmoregulatory and excretory organ. It regulates body salt and water balance (homeostasis of volume and osmolarity), acid-base balance, it eliminates the end-products of metabolism, while conserving valuable blood plasma constituents (e.g. sugars). The importance of the kidney for maintaining whole body homeostasis is illustrated by the high amount of blood granted to this organ. Although the kidneys constitute only 0.5 % of total body weight, they receive 20 to 25 % of the cardiac output. Most of this flow is directed towards the cortical region (Fig. 1.2) to optimise filtration in the glomeruli and hence to maximise flow-dependent clearance of wastes. In contrast, the blood flow to the renal medulla, and consequently the oxygen delivery to the renal medulla, is kept to a minimum which is the price to pay to maintain osmotic gradients, in order to permit concentration of urine, the inherent

function of the renal medulla (Brezis and Rosen, 1995). Moreover, oxygen tensions are low in the outer medulla of normally perfused kidneys due to countercurrent exchange of oxygen in the vasa recta: oxygen diffuses directly from the descending (arterial) to the ascending (venous) branches of the vasa recta (Brady et al., 2000).

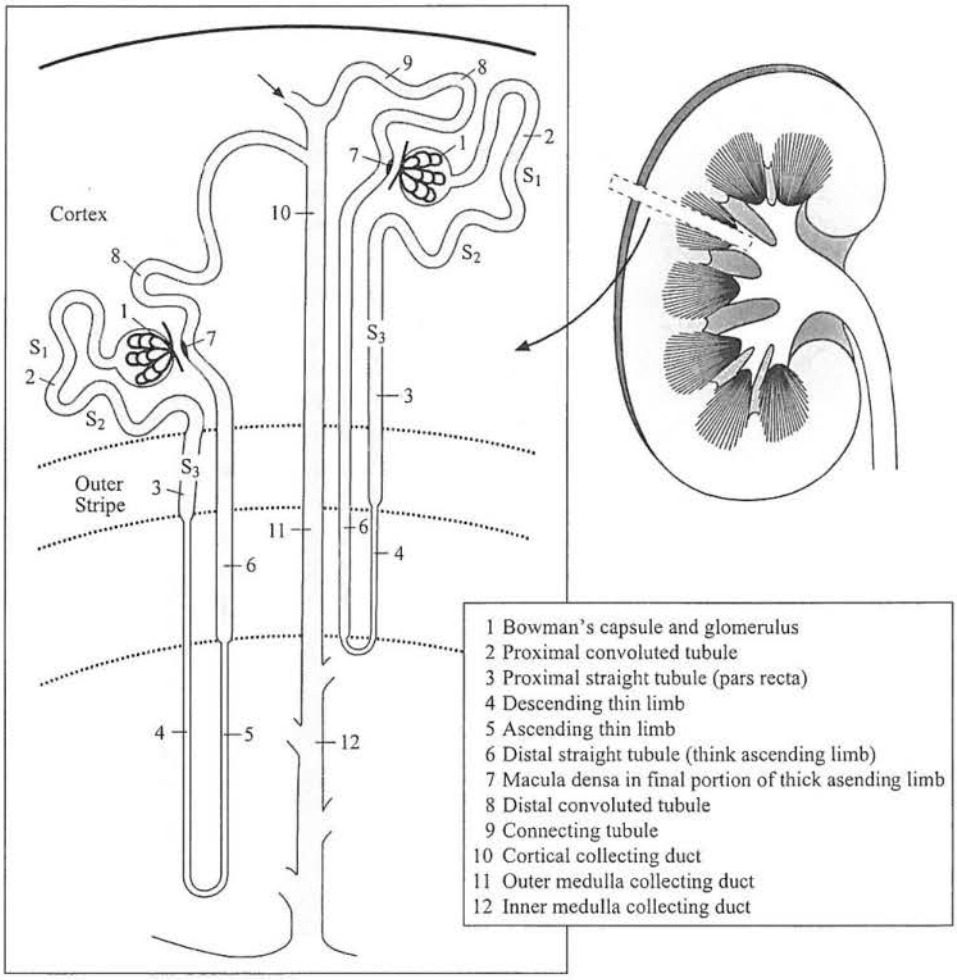

Fig. 1.2 Scheme of the nephron structure of the rat. *Modified from (Kriz and Bankir, 1988).*

Morphologically, ATN is characterised by the loss of microvilli in the proximal tubular brush border membrane. Lethally injured cells are shed, leaving denuded areas in the tubules. Cellular debris gives rise to the formation of casts, which

accumulate within the lumen of the distal segments of the nephron. Functionally, ATN leads to renal impairment by the combined action of tubular cell dysfunction, tubular obstruction, and enhanced backleak of the primary urine (Brady et al., 2000).

For decades, studies have been performed to understand the physiological and cellular basis of renal ischemic injury, using different model systems. The *in vivo* models of clamping or hypoperfusion that best mimic the clinical situation (Glaumann et al., 1975; Venkatachalam et al., 1978) and the isolated perfused kidney (Brezis et al., 1984; Shapiro J.I. et al., 1985) have been replaced more and more by *in vitro* models. These include freshly isolated renal tubules, primary renal cell cultures and renal cell lines. *In vitro* studies on cell lines enable the study of specific cell types under controlled and standardised conditions, and may help to elucidate the cellular basis of ischemic renal injury. Since *in vivo* studies (Venkatachalam et al., 1978) and biopsy data in kidneys with ATN demonstrated the very high vulnerability of the pars recta of the proximal tubule and the medullary thick ascending limb (mTAL), these segments were frequently used to investigate the effects of renal ischemia. These two nephron segments, both situated in the outer medulla, are probably most susceptible to ischemic injury because of the combination of their high ATP requirements for active solute transport and the regional differences in renal blood flow as discussed above, which render the outer medulla more hypoxic than other regions of the kidney (Bonventre et al., 1998; Brady et al., 2000). On the other hand, some cells, predominantly cortical ascending limb cells, collecting duct cells and cells of the tubules within the inner medulla, appear to escape injury or are only sublethally injured and are capable of complete functional and structural recovery if the insult is removed in time (Brady et al., 2000).

1.5.2 Cellular alterations during ischemia

When blood supply to the kidney is inadequate to sustain metabolic demands, a number of pathological changes in renal tubular cells occur, resulting in cell dysfunction or in cell death.

1.5.2.1 ATP depletion

A fall in cellular ATP levels is an early event following oxygen deprivation due to ischemia, hypoperfusion, or hypoxia and is believed to be the key-event responsible for cell dysfunction and death (Brady et al., 2000). The major consequences of cellular ATP depletion include inhibition of ATP-dependent transport pumps with loss of the ion gradients that are normally maintained across cell membranes and polarised epithelia (as discussed below), uncontrolled activation of harmful enzyme systems such as

phospholipases and proteases, and alterations in the cell cytoskeleton. Furthermore, recovery processes after the ischemic insult are hampered by the lack of ATP precursors after prolonged ischemic periods: due to the decrease in ATP synthesis, ADP and AMP accumulate, and adenosine and/or inosine will be formed by conversion of AMP. The passive efflux of adenosine and inosine out of the cell will further impair regeneration of ATP after the insult (Warnick and Lazarus, 1981).

1.5.2.2 Ion homeostasis

SODIUM, POTASSIUM AND CHLORIDE

Intracellular Na^+ and Cl^- are normally kept low, whereas intracellular K^+ is kept at a high level compared to the extracellular compartment. This ion balance is maintained by the basolateral Na^+K^+-ATPases, that function in conjunction with ATP-sensitive K^+ channels (Fig. 1.1). One immediate effect of cellular ATP depletion is a reduction of the activity of the Na^+K^+-ATPases, loss of the normal Na^+, Cl^- and K^+ concentration gradients and cell swelling (Weinberg, 1991). Cell swelling contributes to renal dysfunction by contributing to obstruction of the tubular lumen and to the vascular congestion in the outer medulla (Mason et al., 1989; Lang et al., 1995).

CALCIUM

ATP depletion inhibits the Ca^{2+}-ATPases and impairs the active calcium extrusion from the cell and sequestration of calcium in the endoplasmic reticulum. Additionally, the rise in intracellular sodium associated with inhibition of the Na^+K^+-ATPase activity potentiates calcium entry into the cell via the sodium-calcium exchanger (Gabellini et al., 2000). The early increase in calcium may activate phospholipases and calcium dependent proteases and induce cytoskeletal changes (Edelstein and Schrier, 1995). Although the increase of calcium is a general and early event in the cascade of reactions occurring in ARF, controversy remains about the extent to which this intracellular calcium is a critical mediator for lethal cellular injury (Weinberg et al., 1991; Peters et al., 1995).

ACIDOSIS

In normal aerobic metabolism, cells turn over impressive quantities of hydrogen. The main sink for this vast amount of protons is oxidative phosphorylation (Hochachka and Mommsen, 1983). The closely balanced system between the rate of H^+ production and the rate of H^+ removal in the oxidative phosphorylation dissipates in cells exposed to oxygen deprivation. In glycolytic cells the fall in pH_c is partly due to increased lactate production. However, intracellular acidosis occurs even in cells with relatively low glycolytic capacity such as proximal tubule cells (Weinberg, 1991). Hydrolysis of ATP to its breakdown products results in the release of protons, and ATP depletion

impedes the transport processes that normally maintain intracellular acid-base balance (Hochachka and Mommsen, 1983; Demaurex and Grinstein, 1994). Although severe intracellular acidosis can clearly contribute to ischemic cell injury (see section 1.4), there is convincing evidence that a decrease in pH_c might be cytoprotective in cells facing ischemic conditions (Bonventre and Cheung, 1985; Shanley et al., 1988; Weinberg, 1991). The mechanisms responsible for the protective effect of acidosis are not known, but are likely multifactorial. For instance, the activity of some isoforms of phospholipase A_2 is decreased at acidic pH (Weinberg, 1991). Moreover, the affinity of calcium for calmodulin is also reduced by a decrease in pH_c so that intracellular acidosis may also impair multiple calcium-calmodulin regulated events that are potential contributors to ischemic injury, including the conversion of xanthine dehydrogenase to xanthine oxidase (Weinberg, 1991).

1.5.2.3 Reactive oxygen species (ROS)

ROS have been implicated as important effectors of cell injury in ATN. ROS are produced by numerous sources, including mitochondrial electron transport, cyclooxygenases, lipoxygenases and oxidases e.g. the xanthine oxidase system (Sheridan and Bonventre, 2001). ROS have numerous deleterious effects on cells including lipid peroxidation, oxidation of cell proteins and damage to DNA (Greene and Paller, 1991; Nath and Norby, 2000). These effects can result in loss of plasma membrane and mitochondrial membrane integrity, impaired protein function, and inhibition of cell repair and proliferation (Greene and Paller, 1991). The ROS are inactivated by several cellular mechanisms, including oxidation of glutathione (Meister and Anderson, 1983; Weinberg, 1991). However, this antioxidant is rapidly dissipated during ATP depletion since the synthesis of glutathione requires ATP (Meister and Anderson, 1983).

1.5.2.4 Cell death and regeneration

ARF can induce either sublethal or lethal cell injury. Lethal cell injury reflects irreversible processes that culminate in either necrosis or apoptosis depending on the severity of the insult (Bonfoco et al., 1995; Formigli et al., 2000). Less severe injury often results in apoptosis rather than necrosis (Bonfoco et al., 1995; Formigli et al., 2000). Since kidney cells are exposed to varied degrees of oxygen deprivation and show different metabolic responses, it is not surprising that there is a heterogeneous response in injury. Some studies indicate that apoptosis is more important in distal tubular cells (Beeri et al., 1995; Oberbauer et al., 1999). Mitochondria seem to play a

major role in the regulation of both apoptosis and necrosis (Kroemer et al., 1998). The mitochondrial permeability transition is hypothesised to be a central coordinating event in each cell death pathway. The permeability transition has at least two major consequences: 1) disruption of cellular metabolism and 2) liberation of protease and endonuclease activators from mitochondria. Depending on which of these processes predominate, either necrosis (lysis before activation of catabolic enzymes) or apoptosis (activation of proteases and endonucleases before lysis) ensues (Kroemer et al., 1998).

Sublethal injury principally is reflected by perturbations in cytoskeletal function and structure that largely stem from reductions in ATP levels (see 1.5.2.1). These sublethal changes can be repaired if the offending ischemic insult is removed and adequate ATP synthetic capability allows restoration of cellular stores of ATP. A striking characteristic of renal ischemia is that patients usually regain sufficient renal function for normal life. This phenomenon can be ascribed to the recovery of sublethally injured cells, removal of necrotic cells and intratubular casts, and regeneration of renal cells to restore the normal continuity and function of the tubular epithelium. It is remarkable that most, if not all, surviving epithelial cells in the damaged tubules have the capacity to dedifferentiate and undergo accelerated mitosis (Bonventre, 1998; Lameire and Vanholder, 2001). An important component of the repair process in the kidney may involve the local induction of genes encoding growth factors as well as genes encoding proteins including members of the mitogen-activated protein kinases (MAPKs) such as extracellular regulated kinases (ERKs) and stress-activated protein kinases (SAPKs). Safirstein and co-workers established that the activation of ERK kinases might be essential for cell survival in renal epithelial cells (Di Mari et al., 1999). Moreover, it has been suggested (though not yet proven) that gene expression and production of growth factors, which predominantly occur in the TAL, might influence recovery and enhance epithelial cell regeneration in the proximal tubule since both segments lie adjacent to one another within the outer medulla (Bonventre et al., 1998; Bonventre, 1998). To date, the role of the induction of gene expression following ARF remains incompletely understood.

1.6 METABOLIC INHIBITION AS AN IN VITRO MODEL OF ISCHEMIC ACUTE RENAL FAILURE

In normal aerobic metabolism, cells are able to produce ATP via two distinct pathways: 1) the cytosolic glycolysis and 2) the mitochondrial oxidative phosphorylation (Fig. 1.3).

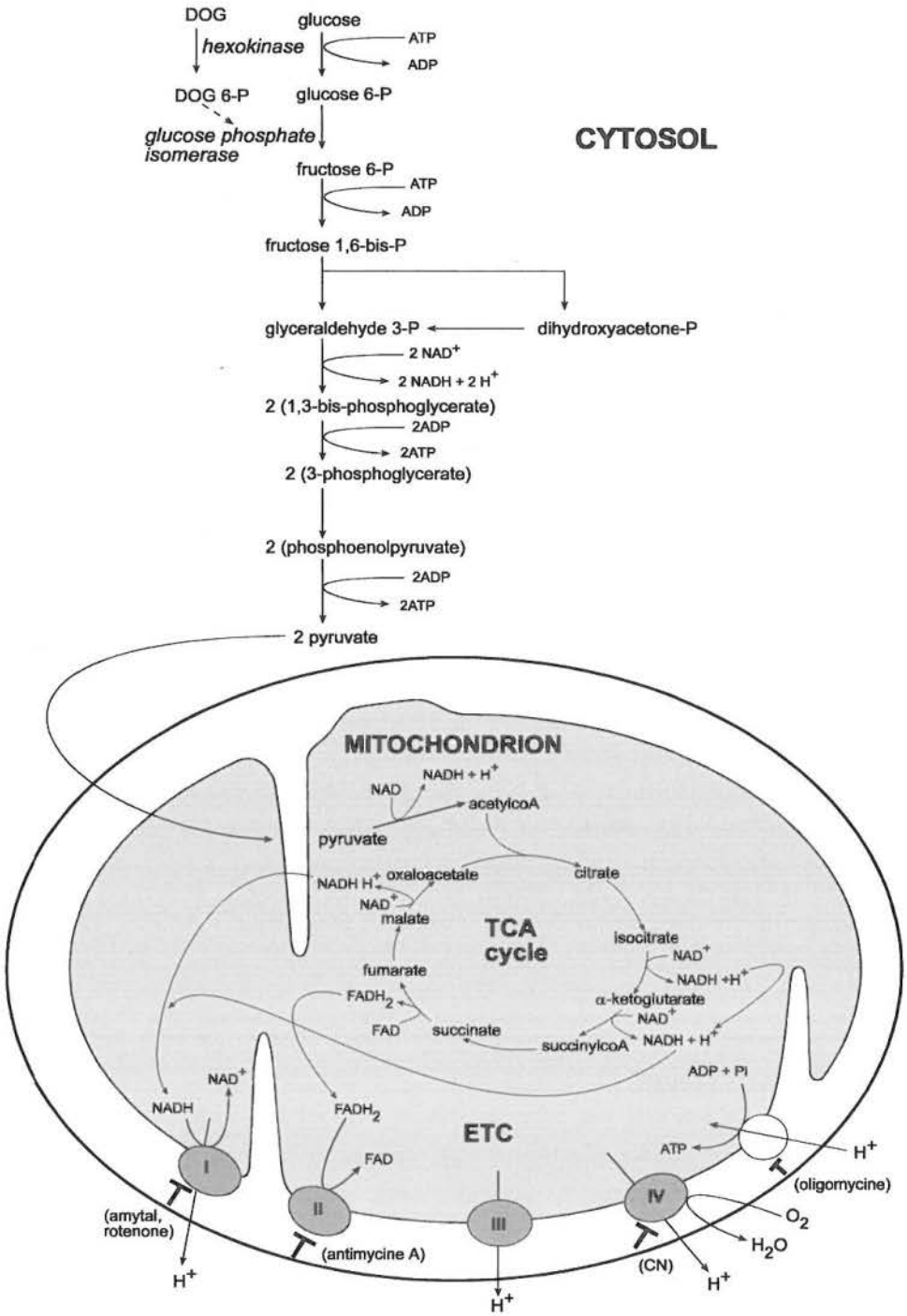
DOG
glucose
hexokinase
ATP
ADP
DOG 6-P
glucose 6-P
glucose phosphate isomerase
CYTOSOL
fructose 6-P
ATP
ADP
fructose 1,6-bis-P
glyceraldehyde 3-P
dihydroxyacetone-P
2 NAD+
2 NADH + 2 H+
2 (1,3-bis-phosphoglycerate)
2ADP
2ATP
2 (3-phosphoglycerate)
2 (phosphoenolpyruvate)
2ADP
2ATP
2 pyruvate
MITOCHONDRION
NAD
NADH + H+
acetylcoA
pyruvate
NADH H+
oxaloacetate
citrate
NAD+
malate
TCA cycle
isocitrate
NAD+
NADH +H+
fumarate
FADH2
α-ketoglutarate
NAD+
FAD
succinate
succinylcoA
NADH + H+
ADP + Pi
NAD+
NADH
FADH2
ETC
ATP
H+
FAD
(oligomycine)
I
II
III
IV
O2
H2O
(amytal, rotenone)
(antimycine A)
(CN)
H+
H+
H+

Fig. 1.3 Schematic presentation of cellular metabolic pathways. *The upper part of the figure illustrates the cytosolic glycolysis. The interference of 2-deoxyglucose (DOG) with the glycolytic enzyme glucose phosphate isomerase is indicated. The end-product of aerobic glycolysis, pyruvate, enters mitochondria and –after conversion to ac-coA- serves as a substrate for the tricarboxylic acid cycle (TCA cycle). The supply of substrate to the tricarboxylic acid cycle (TCA cycle) promotes the reduction of NAD^+ to NADH and of FAD to $FADH_2$. As these are re-oxidized, they supply electrons to the electron transport chain (ETC). In the process of electron transfer to O_2, protons are translocated across the inner mitochondrial membrane, generating a potential gradient of –150 to –180 mV. ATP synthesis takes place at a separate site, the ATP synthase (F_1F_0-ATP synthase). The enzyme is driven by the downhill movement of H^+ and phosphorylates ADP, producing ATP, which is transported out of the matrix by the adenine nucleotide translocase in exchange for ADP. The blockers for the different sites of the ETC are indicated between brackets.*

In *in vitro* cell line models, ischemia can be simulated by inhibition of both metabolic pathways (Canfield et al., 1991; Sheridan et al., 1993; Doctor et al., 1994). Respiration can be blocked either by removal of oxygen (real anoxia) or by the addition of mitochondrial inhibitors (chemical anoxia). Glycolysis is generally inhibited through the removal of glucose and/or addition of 2-deoxyglucose or iodoacetic acid. In this study, metabolic inhibition (MI) with cyanide and 2-deoxyglucose is used as an experimental model to induce cellular ATP depletion, which is known to be an early and prominent feature of ischemic cell injury (see section 1.5.2.1). The glucose-derivative, 2-deoxy-glucose (DOG), is phosphorylated to DOG-6-phosphate (DOG-6-P) by the intracellular glycolytic hexokinase (Wick et al., 1957). By undergoing extensive phosphorylation DOG depletes existing ATP stores (Lieberthal et al., 1998). DOG-6-P is not further metabolised by the glucose-6-phosphate isomerase (Newsholme and Leech, 1983). Since DOG-6-P cannot leave the cell (Chen and Gueron, 1992), it accumulates in the cytosol where it might inhibit the hexokinase, as was described for the inhibition of a mammalian hexokinase by DOG-6-P (Chen and Gueron, 1992). The mitochondrial oxydative phosphorylation was blocked by cyanide (CN). CN binds the 'metal centre' of cytochrome c oxydase, which is the enzyme of the mitochondrial respiratory chain that transfers electrons from cytochrome c to O_2 (Panda and Robinson, 1995). Although many text books refer to the CN binding as an irreversible interaction with the cytochrome c oxydase, several studies in the literature show reversible CN effects in different cell types (Weinberg et al., 1990; Donoso et al., 1992; Leyssens et al., 1996). To ameliorate cellular recovery after MI, washout of the metabolic inhibitors during the recovery phase can be done in the presence of pyruvate (Leyssens et al., 1996). Pyruvate is known to be protective against CN-toxicity since it reacts with CN to form the non-toxic cyanohydrin (Delhumeau et al., 1994). Furthermore, it has been shown that high oxygen concentrations, realised via high aeration above the sample mounted in a chamber with high surface area, may loosen CN from the metal centre and allow

pyruvate to 'catch' cyanide (Delhumeau et al., 1994). Hence, the presence of pyruvate in the recovery solution and oxygen in the air may explain the reversibility of CN effects seen in above-mentioned studies. Moreover, pyruvate, the end-product of glycolysis, served also as a mitochondrial substrate after MI because it has been reported that DOG might have an irreversible action on cellular glycolysis (Wick et al., 1957; Leyssens et al., 1996)

1.7 THE A6 CELL CULTURE MODEL

The A6 cell line is a cell line derived from distal tubules of the kidney of *Xenopus laevis* (Handler et al., 1980; Perkins and Handler, 1981). When grown on a permeable support, A6 cells orient their basolateral side to the supporting substrate, while the apical surface faces the bathing medium. A6 cells form a monolayer epithelium of high electrical resistance in the range of 2-10 $k\Omega.cm^2$. The cells, cultured on a porous substrate, generate a transepithelial potential difference (apical side negative) by active transcellular Na^+ reabsorption from the apical to the basolateral side of the epithelium. When mounted in an Ussing chamber, the short-circuit current reflects the transepithelial transport of Na^+. When grown on impermeable substrates, confluent monolayers also transport solutes and water, as indicated by dome formation.

Several considerations underlie the use of the A6 cell culture model as an in vitro model in this study of metabolic inhibition. In view of their amphibian origin and, hence, their slower metabolism, A6 cells were expected to exhibit a higher resistance to metabolic inhibition as compared to other cell lines from mammalian origin. The longer survival period allows a detailed study of some cellular processes that occur in surviving or sublethally injured cells during metabolic inhibition. Furthermore, A6 cells were chosen since they are derived from the distal part of renal tubules, which is –as outlined in section 1.5.1- more resistant to ischemic injury as compared to proximal tubular cells. Moreover, the A6 cell culture is a well-characterised and established model in epithelial transport research (Duchatelle et al., 1992; Rehn et al., 1995). Specifically, thanks to its electrophysiological accessibility, it is generally used for the study of electrogenic Na^+ transport and its regulation. The cells express many similarities with the principal cells of mammalian cortical collecting tubules (CCT) (Perkins and Handler, 1981; Duchatelle et al., 1992), but lack some typical features e.g. the vasopressin-dependent insertion of aquaporins in the ap. membrane. Na^+ reabsorption occurs –as in the principal cells of the CCT- via the typical Na^+ transport pathways in tight epithelia (Fig. 1.1): ap. Na^+ influx occurs through amiloride-sensitive ENaCs (Puoti et al., 1995) and basolateral Na^+ extrusion is mediated via the Na^+K^+-ATPase in combination with K^+ channels for K^+ recycling to the bl. side. The transepithelial Na^+ transport in A6 cells is under hormonal control (Handler et al.,

1981). Stimulation of Na^+ transport is achieved by aldosterone (Perkins and Handler, 1981; Duchatelle et al., 1992; Helman et al., 1998), vasopressin (Duchatelle et al., 1992; Chalfant et al., 1993), insulin (Erlij et al., 1994), cAMP-increasing agents such as forskolin and theophylline (Perkins and Handler, 1981; Erlij et al., 1999), and also by hyposmotic conditions (Wills et al., 1991; Niisato et al., 2000).

Fig. 1.4 schematically represents the current knowledge on ap. and bl. transport systems present in A6 cells. Besides the transport systems for transepithelial Na^+ reabsorption mentioned above, A6 epithelia possess also Cl^- conductances in the ap. and bl. membrane (Marunaka and Eaton, 1990; Brochiero et al., 1995; Zeiske et al., 1998), a bl. $Na^+/K^+/2Cl^-$ cotransporter (Brochiero et al., 1995), a bl. $Ca^{2+}/3Na^+$ exchanger (Brochiero et al., 1995), a Ca^{2+} ATPase (Brochiero et al., 1995), bl. Ca^{2+} channels (Brochiero and Ehrenfeld, 1997) and a bl. Na^+/H^+ exchanger (Casavola et al., 1992).

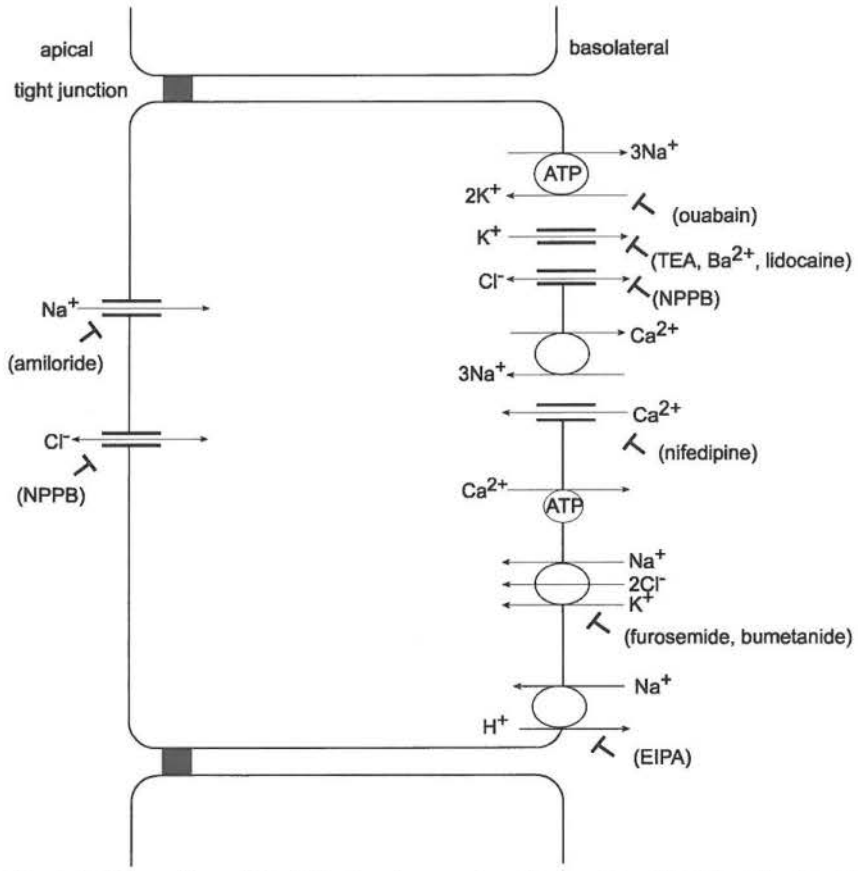

Fig. 1.4 Schematic model of the ion transport pathways identified in A6 cells. *The inhibitors of these transport systems are indicated between brackets.*

1.8 AIMS OF THIS STUDY

In view of the high resistance to ischemic injury of distal tubular cells (see section 1.5.1), a distal tubular cell line is used in this study as an *in vitro* model to examine some of the cellular defence processes occurring in surviving renal cells during energy depletion. To allow a detailed study of some cellular events and to investigate the relationships between them, a cell line with a low rate metabolism was chosen: the A6 cell line. Moreover, this cell line is a well-characterised model tight epithelium, which resembles the principal cells in mammalian collecting tubules, and that allows electrophysiological measurements to follow transepithelial transport characteristics.

To enable us to understand the survival of distal tubular cells in ischemic conditions with threatening high apical sodium levels in the distal tubular lumen, we first characterised the dependency of Na^+ transport characteristics on the apical Na^+ concentration (Chapter 3) in normal conditions. Moreover, since there is convincing evidence in literature that intracellular acidification in ischemic conditions might be cytoprotective (see section 1.5.2.2), we determined first the effects of intracellular pH-shifts on Na^+ transport in control conditions (Chapter 4).

A second objective was to investigate the time course of changes in morphology and to determine when irreversible cell death features, such as plasma membrane damage occur in A6 cells facing metabolic inhibition (MI) (Chapter 5). This allowed us to establish a 45 min protocol of MI, since in this time period no detectable cell death occurred and hence the epithelial cells were expected to be sublethally injured at most.

Since A6 cells, like mammalian distal tubular epithelia, are active Na^+ transporting epithelia, we then focussed on the suppression of Na^+ transport in energy-depleted conditions. The third aim of this study was to look for possible cellular defence strategies related with mechanisms underlying Na^+ transport suppression during MI. Moreover, it was examined whether transcellular Na^+ transport and cellular energy levels recovered after MI (Chapter 6).

One of the nefast consequences of renal ischemia is excessive tubular epithelial cell swelling, which contributes to renal dysfunction by inducing obstruction of the tubular lumen and vascular congestion in the outer medulla (Mason et al., 1989; Lang et al., 1995). Therefore, the last aim of this thesis was to examine in our experimental model the extent of cell swelling during MI, and to investigate whether metabolically challenged cells still possess the capacity to regulate their cell volume in iso- as well as in anisotonic conditions (Chapter 7).

Chapter 2

Materials and methods

2.1 CELL CULTURE

A6 cells obtained from Dr. J.P. Johnson (University of Pittsburgh, Pittsburgh, PA., USA) were used at passages 108-118 for the experiments. The cells were cultured in plastic tissue culture flasks in a humidified incubator at 28 °C in the presence of 1 % CO_2 in the air. The growth medium consisted in equal parts of Leibovitz's L-15 and HAM's F-12. This mixture was supplemented with 10 % fetal calf serum, 20 % water, 3.8 mM L-glutamine, 8 mM $NaHCO_3$, 87 I.U. penicillin, 87 µg/ml streptomycin. The osmolality of the growth medium was 260 mOsm/kgH_2O. Growth medium was replaced 2 times a week. The cells were subcultured weekly. Cell detachment was realised by incubating the cells with ethylenediaminetetraacetic acid (EDTA, Versene, Gibco) for 8-10 min at room temperature. If cells still adhered to the culture flask, a subsequent treatment with a 0.05% trypsin solution (Gibco) for 20 min at 28 °C was applied. The cells were seeded on two 75 cm^2 culture flasks and on Anopore tissue culture inserts (Nunc Intermed, Roskilde, Denmark). The Anopore inorganic membrane had a pore size of 0.2 µm and a growth area of 4.15 cm^2. Seeding density on the filter supports determined with a Fuchs-Rosenthal counting chamber was ~ 3.5 x 10^5 cells/cm^2. Cells were provided with 3 ml culture medium at the apical side (in the insert) and 2 ml at the basolateral side (in the well of the six well plate). When cultured on permeable supports A6 cells form confluent monolayers. After 4 to 21 days of culture (depending on the type of the experiment to perform) the permeable support was removed from its holder using a special cutting tool. The rigid membrane was mounted in the experimental chamber and continuously perfused at both sides during the experiment.

2.2 ELECTROPHYSIOLOGICAL METHODS

2.2.1 Transepithelial DC measurements: short circuit current (I_{sc}) and transepithelial conductance (G_T)

Polarised A6 epithelia, that actively transport Na^+ from the apical to the basolateral side, were transferred to an Ussing-type chamber (insert Fig. 2.3). The transepithelial Na^+ transport gives rise to a transepithelial potential. This transepithelial voltage was continuously clamped to zero with an automatic voltage-clamp apparatus (designed by Dr. W Van Driessche, KULeuven, Belgium) connected with Ag/AgCl voltage and current electrodes. Agar bridges containing 3% agar in 1 M KCl medium connected the electrodes with the bath solutions. The short circuit current (I_{sc}) was the current

through the external electrical circuit that was necessary to clamp the transepithelial potential to zero. Except for some active chloride secretion in A6 epithelia with elevated cAMP and/or Ca^{2+} levels (Zeiske et al., 1998; Atia et al., 1999), Na^+ is the only ion that is actively transported across the A6 epithelium. Therefore, I_{sc} reflects the active transepithelial Na^+ current (I_{Na}) in A6 cells. I_{Na} is defined as the amiloride-sensitive current i.e. I_{sc} minus the short circuit current in the presence of 0.1 mM apical amiloride. I_{sc} was recorded as well as G_T, which can be calculated from the I_{sc}-deflection induced by a brief voltage-deplacement according to Ohm's law.

2.2.2 Current fluctuation analysis

Polarised high resistance monolayers of A6 cells ($G_T \leq 0.5$ mS/cm^2) were used in blocker-induced conductance/current-fluctuation measurements. The tissues were transferred to Ussing chambers (De Wolf and Van Driessche, 1986) with 0.5 cm^2 accessible epithelial area (Fig. 2.1), and were continuously short-circuited except for brief voltage pulses (4 mV during 0.5 s duration) for determination of G_T. A low-noise voltage clamp (Van Driessche and Lindemann, 1978; De Wolf and Van Driessche, 1986) was used. After tissue mounting and perfusion with NaCl Ringer the macroscopic current I_{sc} stabilised within 45 min in most of the cases. Although the "macroscopic" current seems to attain a stable value, it nevertheless shows "microscopic" (nA) fluctuations around the mean value I_{sc}. The switching between the open and closed state of ion channels may cause fluctuations in current ("noise"). Opening and closing of ion channels can be spontaneous and/or can be induced by various agents. For instance, a reversible channel blocker (B) will randomly interrupt the current through an open channel. Blocker-induced noise can be analysed to give microscopic information about blocker rates, gating behaviour, single channel currents and channel density (Van Driessche and Lindemann, 1978). Fourier analysis of the I_{sc} noise results in power density spectra (PDS), where the variance of the current fluctuations (S(f)), normalised to the membrane area, is displayed as a function of the frequencies (f) that are contained in the current noise (Fig. 2.2). Data for PDS were calculated from an average of 60 sweeps of data with a fundamental frequency of 1 Hz. The spectra are represented in a double logarithmic plot of the variance of the current fluctuations as a function of frequency.

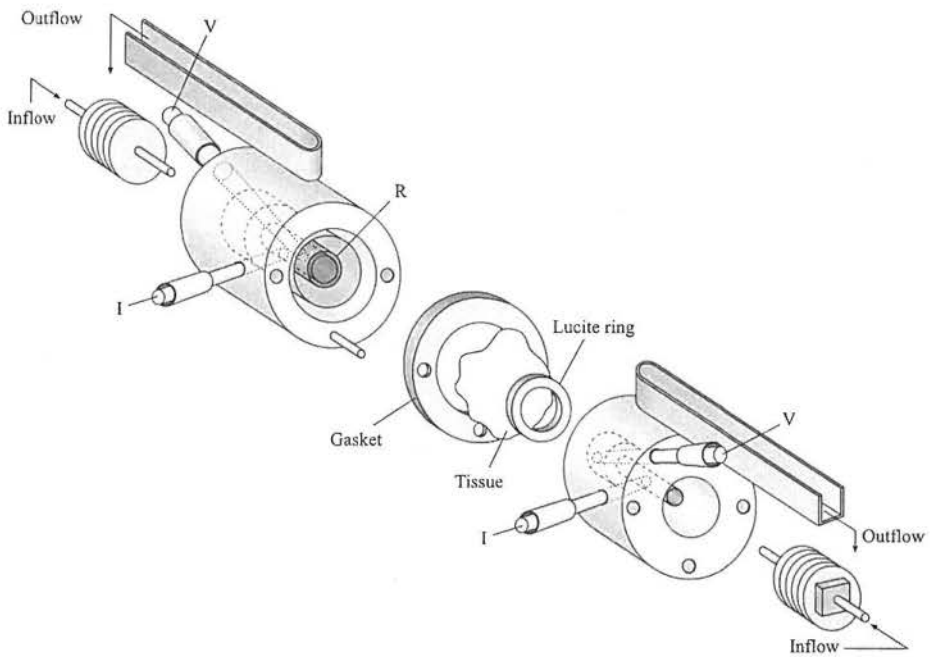

Figure 2.1 Experimental chamber for noise analysis experiments. *The tissue was mounted between the two chamber halves. The pressure exerted on the tissue, which depended on the thickness of the gasket, was adjusted to minimise edge damage. Furthermore, edge damage was reduced by a thin film of silicon vacuum grease on the rim (R) of each chamber half. Continuous flow of the solutions was maintained by gravity. The solutions left the chamber through spillways containing paper strips. V: voltage electrodes, I: current electrodes. Figure adapted from (De Wolf and Van Driessche, 1986)*

In general, simple diffusion of ions generates currents characterised by low frequency noise or 1/f noise in the PDS (Fig. 2.2), i.e. fluctuations of which the magnitude in the PDS decreases when the frequency increases. The current passing through ion channels that open and close randomly induces a Lorentzian component in the PDS in addition to the 1/f noise. Curve fitting enabled the determination of the following parameters: 1) S_o, the Lorentzian plateau value that reflects the amplitude of the current through the channels, 2) f_c, the corner frequency, which is the frequency where S(f) drops to $S_o/2$, 3) S_1, the amplitude of the low frequency component at f = 1 Hz and 4) α the slope of the 1/f line in the double-logarithmic presentation. Calculations were based on the following equations according to Van Driessche (Van Driessche and Lindemann, 1978; Van Driessche, 1994):

$$S(f) = \frac{S_o}{1+(f/f_c)^2} + \frac{S_1}{f^\alpha} \qquad (2.1)$$

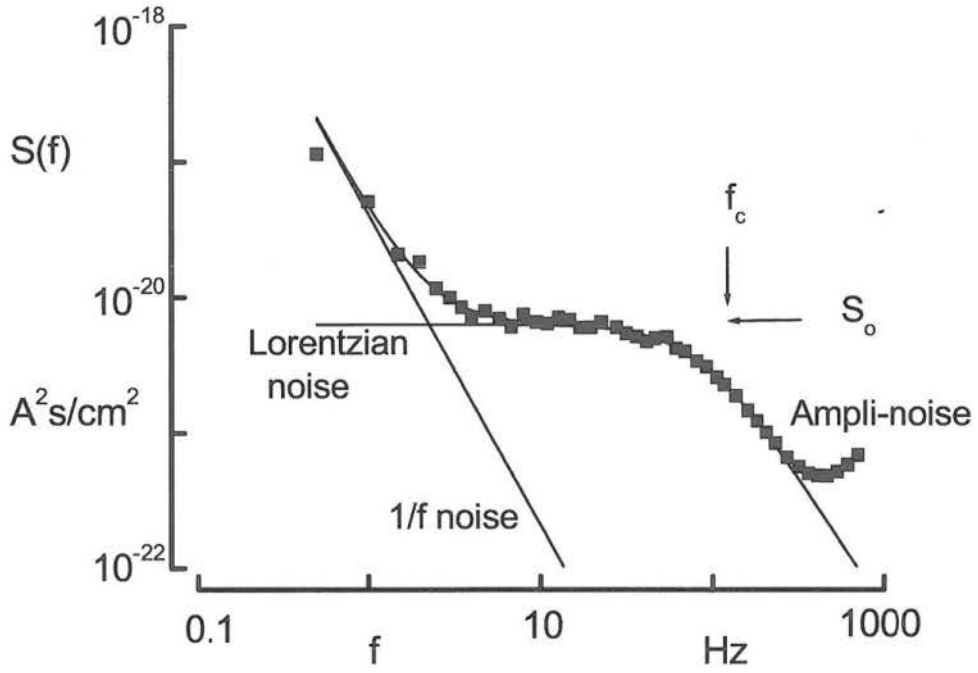

Figure 2.2 Typical power density spectrum recorded with low noise voltage clamp. *The spectrum contains a Lorentzian component which dominates in the middle frequency range. At the lower frequency end the 1/f noise overcomes the Lorentzian noise. At higher frequencies the amplifier noise surpasses the Lorentzian component. The squares represent data points of a typical experimental spectrum for which the position of the Lorentzian plateau (S_o) and corner frequency (f_c) are indicated. Adapted from (Van Driessche, 1994)*

The following two-state model was considered:

channel in open state + blocker $\rightleftharpoons$ channel in blocked state (2.2)

$2\pi f_c$ reflects the rate of the 'open-blocked' reaction (Van Driessche and Lindemann, 1978; Van Driessche, 1994). The ratio of the rate constants for unblockage (k_{off}) and blockage (k_{on}) of the channel is equal to the microscopic equilibrium constant K_B for the channel fluctuation reaction:

$$K_B = k_{off}/k_{on} \quad (2.3)$$

Assuming that Na^+ channels blockage obeys pseudo-first-order kinetics (Lindemann and Van Driessche, 1977); see also fig. 3.2 in chapter 3), Eq. 2.4 is valid at the blocker concentration [B]:

$$2\pi f_c = k_{on} [B] + k_{off} \quad (2.4)$$

The rate constants k_{on} and k_{off} can be determined by linear regression analysis of the $2\pi f_c$-data as a function of [B].
The two-state model for the blocker-channel interaction predicts that:

$$S_o = 2 N_T i^2 P_o (1 - P_o) / \pi f_c \quad (2.5)$$

with N_T the total (open + closed) channel density, i the Na^+ current carried by a single channel and P_o the open probability. P_o can be written as follows:

$$P_o = k_{off} / 2\pi f_c \quad (2.6)$$

Using the expression for the macroscopic current I_{Na}

$$I_{Na} = N_T i P_o \quad (2.7)$$

and (2.6), equation 2.5 can be rewritten as:

$$S_o = I_{Na} [B] i k_{on} / \pi^2 f_c^2 \quad (2.8)$$

With the values for k_{on}, k_{off}, I_{Na}, f_c and S_o, equation 2.8 allows to calculate the single channel current i. Then, the open channel density (N_o) can be calculated from:

$$N_o = I_{Na} / i \quad (2.9)$$

Details of the experimental procedures of noise analysis experiments are given in the corresponding chapters (chapter 3 and 4).

2.3 FLUORESCENCE MICROSCOPY

A6 monolayers grown to confluency on a porous filter were mounted in a chamber (insert Fig. 2.3) that allowed superfusion at both sides of the epithelium and were placed on the stage of an inverted epifluorescence microscope. After measuring

the background signal, the cells were loaded (for details see below) with an appropriate fluorescent indicator.

2.3.1 Fluorescence set-ups

Two different microfluorimetric set-ups were used. The first set-up used a Nikon TMD35 inverted epifluorescence microscope (Tokyo, Japan) and photomultiplier tube detection (Fig. 2.3). Fluorescence was elicited by illumination with a 100 W Xe lamp (Osram, Berlin-München, Germany). The excitation filters were inserted into a computer controlled filter wheel (Lambda 10; Sutter Instrument Company, Novato, USA), which allowed fast alternation between different excitation filters. Neutral density filters were inserted between the microscope and the filter wheel to reduce the intensity of the source. All optical filters and dichroic mirrors were obtained from Omega Optical (Brattleboro, Vermont, USA).

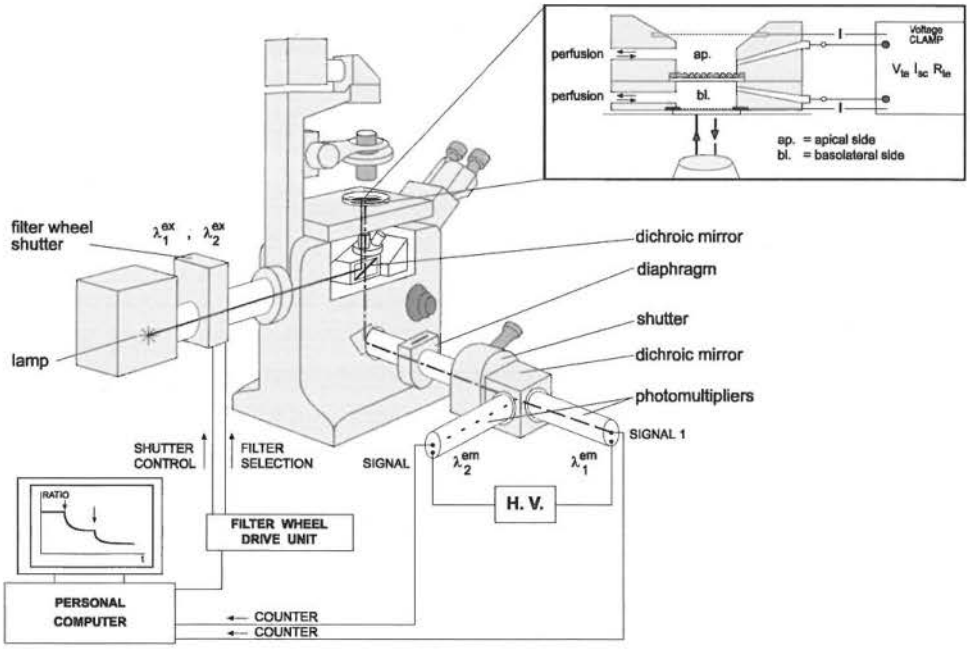

Figure 2.3 Schematic representation of the experimental microfluorescence set-up with photomultiplier detection. *Simultaneous measurements of intracellular pH and electrophysiological parameters I_{sc} and G_t were performed on this set-up. The experimental chamber was connected with a voltage clamp apparatus via voltage and current electrodes (insert).*

The excitation light was directed to the sample by a dichroic mirror and a Leitz objective (32x/0.40 corr., Leitz, Wetzlar, Germany). Although not ideal for fluorescence measurements, this objective had the appropriate working distance. The fluorescence collected by the objective was transmitted through the dichroic mirror and a bandpass emission filter to a photomultiplier tube (9124A; Thorn-EMI, Middlesex, England) which was operating in photon counting mode. The pulses were transferred to the computer through a counter/timer board C660 (Thorn-EMI, Middlesex, England). The data were corrected for the dead time of the counting system and for the background signal. The measurements were done under computer control, based on a home-written program.

Fluorescence imaging was performed on a second set-up where the fluorescence was measured with an inverted epifluorescence microscope Zeiss Axiovert 100 (Jena, Germany). Excitation light of a 75 W xenon lamp (Osram, Berlin-München, Germany) was filtered with excitation filters (Chroma Technology Corp, Brattleboro, VT), which were inserted in a computer controlled filter wheel (Lambda 10-2, Sutter Instrument Company, Novato, CA). The fluorescence collected by the objective (Zeiss LD Achroplan 20x/0.4 corr.) was transmitted through a dichroic mirror and an emission filter (Chroma Technology Corp, Brattleboro, VT, USA) to a Quantix CCD camera (Photometrix, Tucson, Arizona, USA).

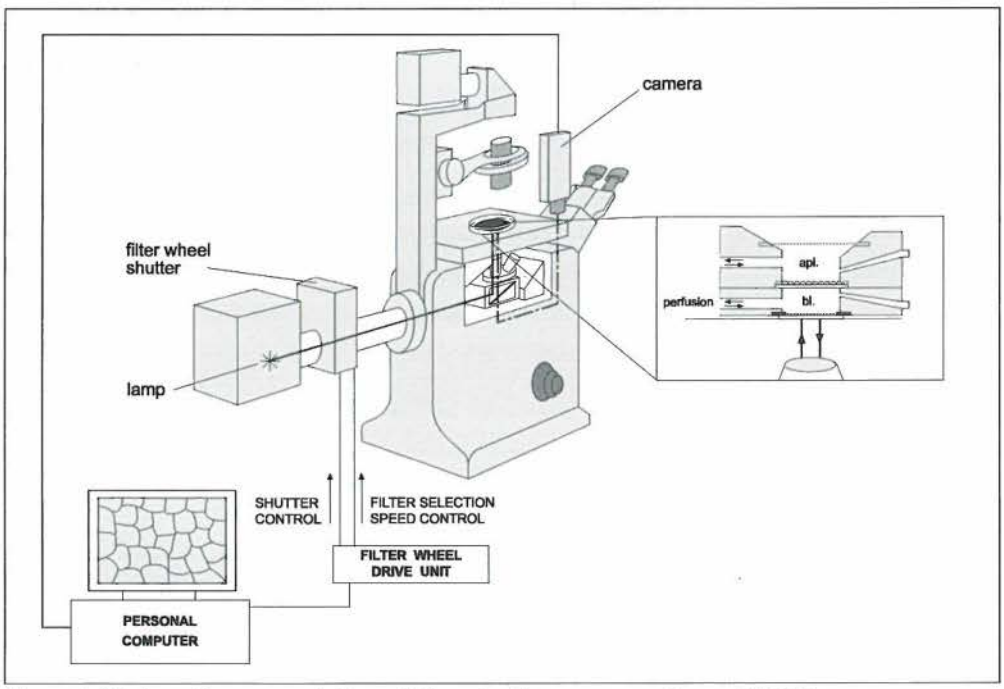

Figure 2.4 Schematic representation of the microfluorescence set-up with CCD camera.

The camera was equipped with a Kodak KAF 1400 CCD (grade 2, MPP) with 1317x1035 pixels and cooled to -25 °C by a thermoelectric cooler. The value of the detected fluorescence was increased by applying 3x3 binning and gain 3. The acquisition of pairs of images for ratiometric dyes was controlled by a home-made program which uses the V for Windows software (Digital optics, Auckland, New Zeeland). The signals were obtained by integrating spatially pixels over the field of view. The background image, due to reading noise, the dark current of the CCD camera and the autofluorescence of tissue and tissue support, was subtracted, pixel by pixel, from the fluorescence image. At the end of each experiment, the images were analysed with a home-made program, that uses the V for Windows software, to examine the heterogeneity in the response of the cells in different regions of the monolayer.

2.3.2 Intracellular pH (pH_c) measurements

2.3.2.1 Fluorescence microscopy to monitor pH_c

Intracellular pH was monitored in A6 cells using fluorescent probes. A study on leech giant glial cells showed that intracellular pH changes detected by fluorescent indicators and micro-electrodes in side-by-side measurements have been found to be very similar, although absolute values may differ by about 0.1 pH units (Nett and Deitmer, 1996). However, fluorescence measurements are less invasive and have a very high sensitivity (small signals are detected against zero background). The lower sensitivity of absorption techniques, e.g. on cell suspensions, results from the fact that the absorption signal is related to the 100% incident light intensity (Slavik, 1992). Furthermore, the greatest advantage of using the micro-fluorescence technique for the measurement of intracellular ion concentrations is the possibility to perform 'fluorescence imaging', i.e. to view the object e.g. the A6 monolayer, during measurement by detecting the fluorescence emission with a camera. This offers space-resolved information of a specific area of the monolayer and subsequent computer processing of the images is possible.

2.3.2.2 Fluorescent pH_c probes BCECF and CMFDA: spectral properties and calibration

Fluorescein is a well-known, pH_c dependent fluorescent probe. Its absorption and fluorescence properties have been thoroughly tested and are unambiguously pH dependent. Derivatives of fluorescein ($pK_a \sim 6.4$) were designed to adjust the pK_a to a

value more convenient for pH measurements near physiological pH. The most popular fluorescein derivative is 2', 7'-bis-(2-carboxyethyl)-5-(and6) carboxyfluorescein (BCECF, Fig. 2.5A), which has a pK_a value of ~7. BCECF (Molecular Probes, Eugene, OR, USA) was used in this study (chapter 4) in dual excitation mode to measure pH_c in A6 cells. Intracellular pH measurements with BCECF were made in this study by determining the pH-dependent ratio of emission intensity (detected at 535 nm) when the dye is excited at ~495 nm versus the emission intensity when excited at its isosbestic point of ~440 nm (Fig. 2.5B and 2.5C for spectral properties). At the end of each experiment, calibration of the BCECF fluorescence (F) ratio $R = F_{495\ nm}/F_{440\ nm}$ versus a given pH_c was performed using the nigericin-high K^+ technique where intracellular pH was forced to equilibrate with the external pH according to the method of Thomas et al. (Thomas et al., 1979). The calibration solutions had different pH values and contained a high $[K^+]$, ideally identical to the intracellular $[K^+]$, and the ionophore nigericin, which acts as a K^+/H^+ exchanger. At equilibrium, if the incorporation of nigericin in the membranes is sufficient, the transmembrane K^+ and H^+ gradients will be the same; $[K^+]_c/[K^+]_o = [H^+]_o/[H^+]_c$, and hence if $[K^+]_o = [K^+]_c$, then $pH_o = pH_c$ (subscripts o and c denote extracellular and intracellular compartments respectively). A6 cells were exposed to solutions containing 137 mM KCl, 1 mM $CaCl_2$, 10 mM HEPES and 13 μM nigericin. The K^+ concentration used approximated closely the reported cytosolic K^+ concentration in A6 cells (Nakanishi et al., 1988). Different pH values of the calibration solutions were obtained with TRIS. Figure 2.5D shows the resulting linear fit through data of 16 in vivo calibrations on different A6 monolayers. When individual tissue calibration at the end of the experiment failed, we used the pooled calibration curve {pH = [R + 19.0 (±0.6)]/3.45 (±0.08)} to evaluate the experimental data. Fig 2.5D illustrates that in A6 cells the calibration procedure was quite reproducible.

Figure 2.5. The classical pH-probe BCECF. (A) *The chemical structure of the tri-acetoxymethyl ester form of BCECF-AM which is one of the three different molecular species of BCECF-AM in synthetic preparations. The two other species contain only 1 or 2 acetoxymethyl esters. The pH-dependent emission spectra and excitation spectra of BCECF are shown in panel* ***(B)*** *and* ***(C)*** *respectively. When excitation occurs at 505 nm, the intensity of the fluorescence signal is maximal at 535 nm (panel B). The excitation spectra in panel C reveal that the fluorescence intensity at 535 nm strongly depends on the excitation wavelength. When excited at 439 nm, the fluorescence emission is pH-independent (see enlargement on the left side of the panel), whereas excitation at 495 nm is highly pH-dependent. (copied from Haugland; the Molecular Probes Catalogue 2001)* ***(D)*** *Calibration curve for cellular pH (pH_c) in A6 cells using BCECF. The ratio, R, of the emitted fluorescence light intensities (F) at 495 and 440 nm ($R = F_{495}/F_{440}$) can be approximated by a linear function of pH_c (N=16). This can be seen for the 2 arbitrary selected individual tissues (squares and triangles respectively) as well as for the averaged data, with pH = [R+19(±0.6)]/3.45(±0.08). The other 14 tissues are, for clarity, represented only as dots. The fitted linear relationship for all pooled data is shown as a bold line.*

A

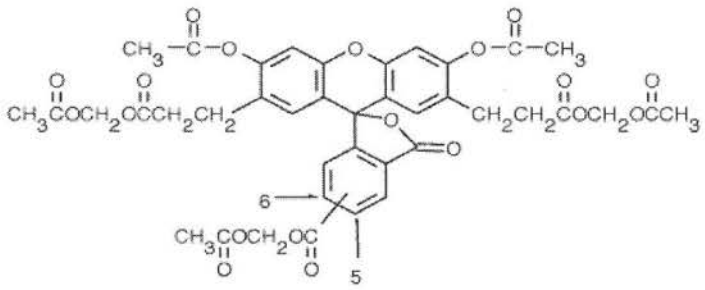

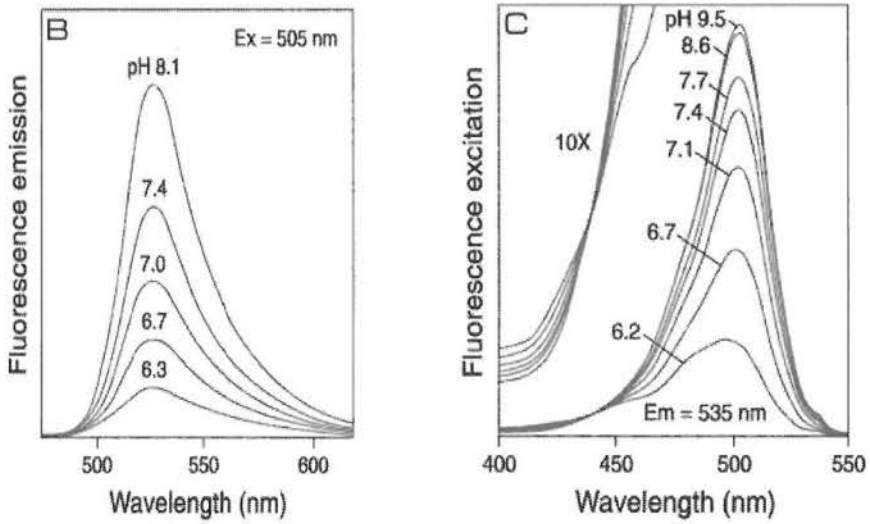
B
Ex = 505 nm
pH 8.1
7.4
7.0
6.7
6.3
Fluorescence emission
500
550
600
Wavelength (nm)
C
pH 9.5
8.6
7.7
7.4
7.1
6.7
6.2
10X
Em = 535 nm
Fluorescence excitation
400
450
500
550
Wavelength (nm)

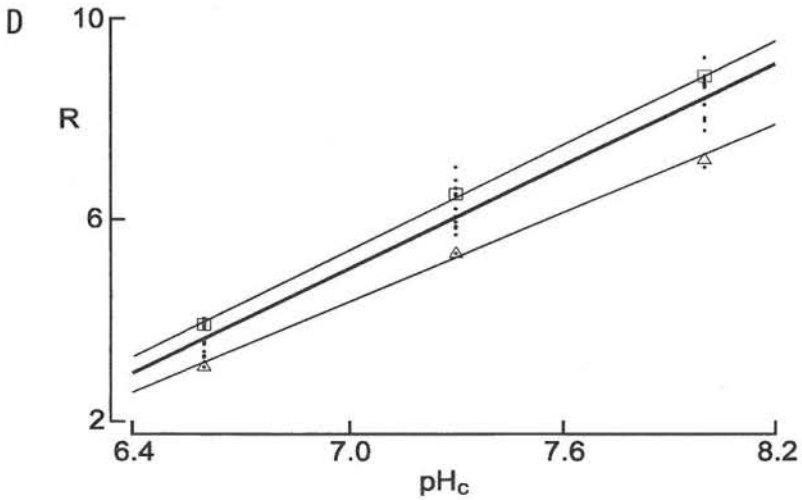
D
10
R
6
2
6.4
7.0
7.6
8.2
pHc

The BCECF acid is formed by esterase-mediated hydrolysis of its acetoxymethyl ester form (BCECF-AM) inside the cell. The leakage of the dye was thought to be slow because of the high electric charge (-4) of the cleaved probe inside the cell. However, in some cell types, including A6 cells, BCECF shows a high leakage rate out from the cells, probably mediated via yet unidentified anion transport pathways. Therefore, another fluorescein derivative, 5-chloromethyl fluorescein diacetate (CMFDA), was tested on its suitability for pH_c measurements in A6 cells. CMFDA retains far better into A6 cells than BCECF. The fluorescence to background ratio for the F440 signal in BCECF loaded A6 monolayers was only one third of that in CMFDA loaded cells at the end of an identical protocol of 2 hours. Moreover, the F495 fluorescence to background ratio in CMFDA loaded tissues was twice that of BCECF loaded cells at the end of an identical protocol. The better retention of the dye in CMFDA loaded cells is probably due to a reaction of the fluorescent 5-chloromethylfluoresceine, the intracellular hydrolysis product of the membrane-permeant non-fluorescent CMFDA, with intracellular thiols to yield well-retained products (Johnson, 1998). Cytotoxic effects caused by this intracellular reaction are unlikely since many cell types loaded with CMFDA remained viable for at least 24 hours after loading and often through several cell divisions (Boleti et al., 2000). Because of these long-term cell-labelling properties, CMFDA was already used in a variety of studies including studies of cell migration and cell tracing in mixed cultures (Johnson, 1998). Since fluorescein is a part of the structure of CMFDA (Fig. 2.6A), the dye exhibits the pH-dependent spectral properties of fluorescein. CMFDA shows pH dependent spectral shifts in a somewhat more acidic cytosolic pH range than BCECF since the pK_a is ~6.4 (determined for the unconjugated hydrolysed product in buffer). Note that after conjugation to an intracellular thiol or amine the pK_a value may be different.

At first, we checked whether CMFDA was a suitable pH-probe for A6 cells, since in the literature, there was only one abstract where the use of CMFDA as a pH probe in MDCK cells was mentioned (Parkinson and Hendry, 1995). Therefore, CMFDA calibrations were performed as shown for one typical experiment in Figure 2.6B. CMFDA - like BCECF - was used in the dual excitation (495 nm and 440 nm) mode (for details see below).

Figure 2.6 The pH-sensitivity of CMFDA. ***(A)*** *The chemical structure of the fluorescein derivative CMFDA. (copied from Haugland; the Molecular Probes Catalogue 2001)* ***(B)*** *The ratio R of the CMFDA fluorescence intensities (F) in A6 cells measured at 535 nm due to excitation at 495 nm and 440 nm, R = F(495)/F(440), is shown at various pH values for one representative example of a CMFDA calibration. The different symbols indicate the cellular response in six different regions of a single monolayer.* ***(C)*** *The six imposed pH values of panel B and their corresponding CMFDA ratios for one representative region are plotted in panel C. The fit (solid line) through the data indicates that CMFDA displays the highest pH-sensitivity (linear range of this fit) from pH ~6 to ~7.*

A

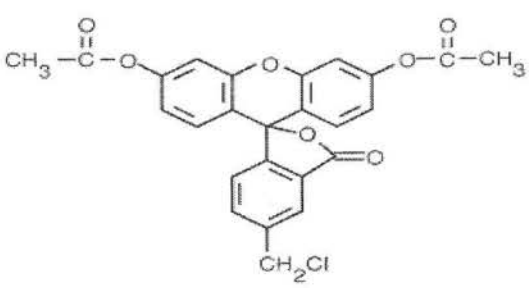
CH3
O
O
O
O
O
CH3
O
CH2Cl

B

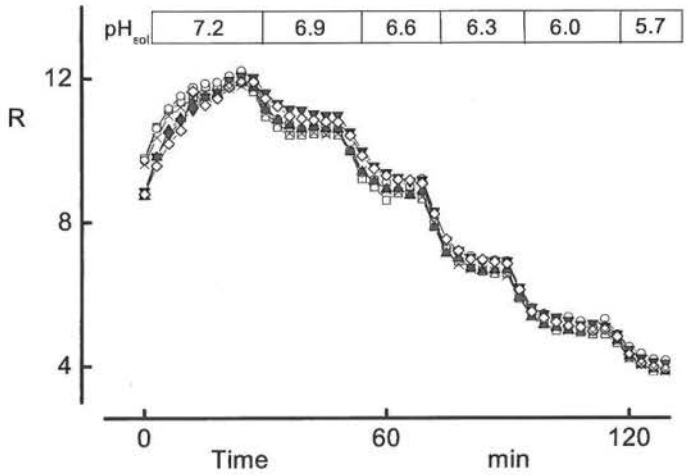
pHsol
7.2
6.9
6.6
6.3
6.0
5.7
R
12
8
4
0
Time
60
min
120

C

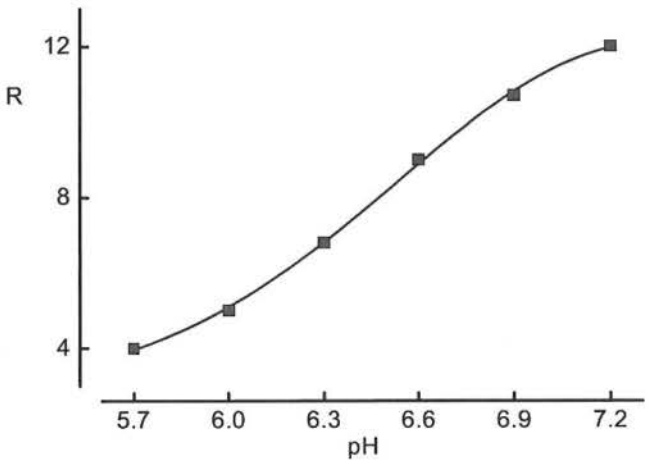
R
12
8
4
5.7
6.0
6.3
6.6
6.9
7.2
pH

The CMFDA fluorescence ratio R = F495 / F440 *versus* the different imposed pH_c values are depicted in panel C of Figure 2.6. The linear part of the curve (from pH ~6 to ~7) indicates the range where the CMFDA ratio is most sensitive to pH_c changes. The control pH of A6 cells measured with CMFDA is 7.00 ± 0.03 (N=14, Table 2.1). Hence, CMFDA was a very useful pH-probe for monitoring pH_c changes during the acidifying manipulations applied in the experimental protocols of this study.

Secondly, pH_c values of A6 cells measured with the commonly used pH dye BCECF were compared with those measured with CMFDA. Table 2.1 reveals that both dyes indicate similar absolute pH values in control conditions as well as after an acidifying treatment.

Table 2.1 Comparison of pH_c values obtained with CMFDA and BCECF

	CMFDA	N	BCECF	N
Control	7.00 ± 0.03	14	7.07 ± 0.09	5
After 45 min CN+DOG	6.44 ± 0.04	6	6.54 ± 0.07	5

pH_c values indicated are mean values ± standard errors for N different monolayers. The compositions of the control Ringer and the Ringer with 2.5 mM NaCN (CN) in combination with 20 mM 2-deoxyglucose (DOG) are given below. The pH of both solutions was 7.4 and osmolalities were 200 mOsm/kgH_2O.

Therefore, it can be concluded that CMFDA is a reliable pH_c indicator. Moreover, the improved cellular retention of the fluorescent probe allows to perform long-lasting experiments (5-6 hours) and overcomes the cell leakage problem encountered when using BCECF.

2.3.2.3 Experimental procedure

For fluorimetric pH_c measurements polarised A6 monolayers of only 4 to 6 days old were used to obtain higher fluorescence to background ratios. The monolayers were mounted in an Ussing-type chamber (chamber opening 0.7 cm^2). After measurement of the background signal, cells were loaded from the apical side with the (ratiometric) pH probe (BCECF or CMFDA). Cells were exposed to a final concentration of 10 µM of the acetoxymethyl ester form of BCECF or the diacetate form of CMF (stock solution in DMSO). Loading was performed for 45-60 min, at room temperature, in apical control Ringer solution (see *Solutions*). After loading, excessive dye was removed by replacing the apical bath solution several times and subsequent bilateral perfusion for 30-45 min

before the start of the experiment. During the experiment, monolayers were continuously superfused (0.75 ml/min) on both sides.

Excitation light was filtered at 440 and 495 nm with excitation filters. A neutral density filter of 1.0 was inserted in the excitation pathway. The fluorescence collected by the objective was transmitted through a >500 nm long-pass dichroic mirror and a 535/50nm bandpass emission filter (Chroma Technology Corp, Brattleboro, VT). On the photomultiplier set-up, the data were collected with a dwell time of 1 s at each wavelength. The camera exposure time for each image was 1 s.

At the end of each experiment, a calibration was performed using the nigericin-high K^+ technique (Thomas et al., 1979) as described earlier. Heterogeneity in the cellular response of different regions in the monolayer was checked after each experiment on the set-up equipped with the CCD camera. Analysis with a home-made program, that uses the V for Windows software, revealed that no significant differences existed in the cellular responses of different regions in one monolayer to pH_c changing manipulations.

2.3.3 Mitochondrial potential ($\Delta\Psi_m$) measurements

2.3.3.1 The fluorescent probe JC-1

$\Delta\Psi_m$ was evaluated using the potentiometric indicator JC-1 (5,5',6,6' - tetrachloro - 1,1',3,3' - tetra - ethylbenzimidazolylcarbocyanine iodide)(Molecular Probes, Inc. Eugene, OR, USA). JC-1 is a lipophilic cation that partitions into mitochondria according to the Nernst potential. JC-1 exists as a monomer at low concentrations and as aggregates, called J-aggregates, at high concentrations. JC-1 aggregates are formed in mitochondria with a high membrane potential (Reers et al., 1991). The monomeric form emits fluorescence with a maximum intensity at 530 nm when excited at 490 nm, while the maximum intensity of the fluorescence emitted by J-aggregates occurs at 590 nm. Depolarisation of the mitochondrial inner membrane leads to a redistribution of the dye with dissociation of J-aggregates (Reers et al., 1995; Reers et al., 1991; Cossarizza et al., 1993; Di Lisa et al., 1995). Consequently, the ratio of the fluorescence emission at 590 nm over that at 530 nm decreases upon depolarisation of the mitochondrial membrane. It has been shown that the membrane potential reported by JC-1 is not significantly affected by changes in pH above ~6.5 (Reers et al., 1991).

2.3.3.2 Experimental Procedure

A6 cells were loaded with 10 μM JC-1 (from a 10 mM stock solution in DMSO) for at least 30 minutes at 28° C in the CO_2 incubator. Dual-emission ratiometric imaging was performed by manually changing the emission cube. The excitation was done through a 10 nm bandpass filter centred at 495 nm. A neutral density filter of 0.3 was inserted in the excitation pathway. The fluorescence emitted by the JC-1 monomers was collected through a >500 nm long-pass dichroic mirror and a 535/50 nm bandpass emission filter. The emission cube used to detect the J-aggregates consisted of a >560 nm long-pass dichroic mirror and a 590/55 nm emission filter. Data collection time for each image was 2 seconds. The mitochondrial uncoupler carbonyl cyanide p-trifluoromethoxy-phenylhydrazone (FCCP, 10 μM) was added at the end of each experiment (from a 10 mM stock solution in ethanol) to determine the JC-1 emission ratio associated with a collapsed $\Delta\Psi_m$. DOG (20 mM) was administered simultaneously with FCCP to rule out glycolytic ATP provision for the reverse action of the mitochondrial F_1F_0-ATPase.

2.3.4 NAD(P)H autofluorescence measurements

For autofluorescence measurements, A6 cells were cultured on polytetrafluoroethylene (PTFE) permeable supports (pore size 0.4 μm) especially selected for their low autofluorescence at the excitation wavelength used (Biocoat Fibrillar collagen/Fibronectin Inserts, Becton Dickinson, Bedford, MA, USA). Confluent monolayers were used after 8 to 15 days of growth in the culture medium.

NAD(P)H was excited via a 360/40 nm excitation filter. The fluorescence collected by a Zeiss objective LD Achroplan (40x/0.6 corr.) was transmitted to the camera through a >380 nm long-pass dichroic mirror and a 450/50 nm emission filter. Data collection time for each image was 2.5 seconds. At the end of each experiment, the cells were lysed with 0.1 % Triton X-100 to evaluate the background signal due to the support. The results are expressed as a percentage change compared to control. The signal to background ratio in these experiments was 2 to 3.

2.4 MEASUREMENT OF THE CELLULAR ATP CONTENT

Confluent monolayers of A6 cells (6 to 10 days old) on Nunc Anopore Membranes were washed and equilibrated in control Ringer solution for at least 1.5 hours. Subsequent incubation with metabolic inhibitors (combined with inhibitors of

other cellular transport pathways in some experiments) was performed in non-perfusion conditions. At the start of the recovery phase cell layers were washed three times with recovery Ringer (for composition: see below) and each subsequent 15 min the recovery solution was renewed. Control cells were incubated in normal saline solution. ATP measurements were performed with a luciferin-luciferase based assay kit (Molecular Probes, Eugene, OR). The assay is based on luciferase's requirement for ATP in producing light (emission maximum ~560 nm at pH 7.8) according to the reaction:

$$\text{luciferin} + \text{ATP} + O_2 \xrightarrow{Mg^{2+},\ \text{luciferase}} \text{oxyluciferin} + \text{AMP} + \text{pyrophosphate} + CO_2 + \text{light}$$

The reaction buffer contained 150 µg ml^{-1} luciferin, 1.25 µg ml^{-1} luciferase, 5 mM $MgSO_4$, 1 mM dithiothreitol (DTT), 25 mM Tricine buffer, 0.1 mM EDTA and 0.1 mM azide, pH=7.8. The cells were solubilised in 650 µl of somatic cell ATP-releasing agent (Sigma, St Louis, MO) for 30 seconds. 50 µl of cell extract was added to 450 µl reaction buffer. ATP levels were measured with a luminometer type 1250 from Wallac (Turku, Finland). Calibration was performed with several standard ATP solutions (Molecular Probes, Eugene, OR) in the concentration range 10^{-5}-10^{-4} M. The results are expressed as a percentage change compared to control.

2.5 TECHNIQUES TO EXAMINE PROLIFERATION CAPACITY AND CELL VIABILITY

2.5.1 ^{3}H-Thymidine uptake proliferation experiments

A6 cells were seeded on flat bottom 96 well plates (10,000 cells/well). Measuring proliferation by detection of newly synthesised DNA via incorporation of ^{3}H-thymidine is dependent on the number of cells used. To avoid differences in seeding density for different wells, the cell suspension was carefully mixed during the seeding procedure in order to avoid inhomogeneity of the cell suspension due to sedimentation of the cells. After 3 days of growth (80 % confluency), the cells were first equilibrated in control Ringer solution and subsequently incubated during 0 (control) to 6 hours in a Ringer solution with metabolic inhibitors (see section 2.8). To ensure complete removal of metabolic inhibitors afterwards, the cell layers were carefully rinsed 3 times with culture medium before subsequent overnight incubation in pyruvate (2.1 mM) containing culture medium. To rule out waste of eventually detached cells during the washing procedure, all removed solutions were collected in a separate 96 well plate. Subsequently, that plate was centrifuged, supernatants were discarded, wells were re-filled with culture medium and resuspended cells were added to the original flat bottom

plate. The proliferation capacity after MI was measured using the ^{3}H-thymidine incorporation assay. The cells were incubated overnight with 1 µCi ^{3}H-thymidine (Amersham, Buckinghamshire, U.K.) per well in the culture medium and afterwards harvested by an automated cell harvester (Betaplate 1295-004, Pharmacia, Uppsala, Sweden). Incorporated radioactivity was measured using a Beta-plate liquid scintillation counter (Wallac, Turku, Finland). The counts per minute (cpm) for each well with A6 cells were corrected for the 'background' cpm of empty wells (no cells, only culture medium). Data were expressed as percentages of 'maximal' ^{3}H-Thymidine incorporation as determined for the untreated controls.

2.5.2 DNA gel electrophoresis to detect DNA fragmentation

Polarised epithelial cells were detached from the permeable support (EDTA and trypsine, see section *cell culture*) after incubation with metabolic inhibitors (for the composition of the Ringer solution: see section 2.8) during a period ranging from 0 to 24 hours. Subsequently, cells were subjected to lysis buffer (in mM: 100 NaCl, 10 TRIS, 25 EDTA and 0.5 % Triton-X-100, pH=8) during 1 hour at 4 °C. To remove cellular proteins, lysates were incubated overnight at 50 °C with 200 µg/ml Proteinase K. To remove RNA, lysates were incubated during 4 hours at 37 °C with 20 µg/ml RNASE A. DNA was extracted from the cells with an ammoniumacetate (7.5 M)-ethanol mixture (20:80). DNA in the aqueous phase was precipitated with 70% ice-cold ethanol. The concentration of DNA in each sample was determined by UV absorbance at 260 nm. The same amount of nucleic acid from each sample was subjected to electrophoresis on 2% agarose gel. A 100 base pair DNA ladder (Gibco) was used as reference. After electrophoresis, DNA was visualised by UV fluorescence after staining with ethidium bromide (0.5 µg/ml).

2.5.3 Ethidium bromide exclusion experiments

A6 cells were seeded on glass cover slips (seeding density = 50,000 cells/cover slip) and were grown to confluency during 9 to 10 days before they were used in the fluorescence microscopy experiment. The monolayers displayed 'domes' due to transepithelial transport of salt and water, which indicates the polarised character of the cells. Cell layers were incubated during 1 hour in normal Ringer solution containing 10 µg/ml ethidium bromide (EB). The cell layers were incubated during 20 hours with metabolic inhibitors in the presence of 10 µg/ml EB. EB is a red, cationic dye that cannot enter living cells. Only when cellular plasma membrane integrity is lost (necrotic cells), EB can enter and intercalate double-stranded DNA. The probe was excited at 540

nm (25 nm bandwidth) and fluorescence was collected using a dichroic mirror at 565 nm and an emission filter of 590 nm (55 nm bandwidth). Data collection time for an image was 1 s and a neutral density filter of 1.0 was inserted in the excitation pathway.

2.5.4 Trypan blue exclusion experiments

Polarised A6 cell layers grown on glass cover slips were incubated in a Ringer solution with metabolic inhibitors (see section 2.8) during a period ranging from 0 (control) to 24 hours. A short incubation period of 2 min in trypan blue containing Ringer (12 vol %) allowed trypan blue to enter necrotic cells via holes in the plasma membrane. Trypan blue binds to intracellular proteins and hence, necrotic cells appear as obvious blue-stained cells in light microscopic pictures, whereas living cells, which exclude the dye, remain unstained.

2.5.5 Transmission electron microscopy

Confluent monolayers on Nunc permeable supports were cut from the plastic insert and fixed in a solution of 2 % glutaraldehyde in 0.05 M cacodylate buffer (pH 7.3) during 18 hours at 4 °C. After fixation, the tissue was cut into approximately 1 mm square blocks. The small pieces were washed in 0.05 M cacodylate buffer for 10 min, postfixed with 2% osmiumtetroxide for 1 hour, stained with 2% uranylacetate in 10% acetone for 20 min, dehydrated through graded concentrations of acetone and embedded in Araldite. Ultrathin sections (0.06 mm) from the tissue blocks were mounted on 0.7% formvar-coated grids, stained with uranyl acetate and lead citrate and examined with a Philips EM 208 electron microscope (Eindhoven, The Netherlands).

2.6 CELL THICKNESS MEASUREMENTS

For the volume measurements the Anopore membranes were coated with fluorescent microspheres of 1 µm diameter (L5081, Molecular Probes, Eugene, OR) embedded in a thin gelatine layer before seeding the cells (Fig 2.7). Confluent and polarised A6 tissues were mounted in an Ussing-type chamber enabling solution exchange on both sides. Cell thickness (T_c) was used as an index for cell volume of confluent monolayers. The apical (upper) side of the monolayer was labelled with fluorescent biotin-coated microbeads. Focussing of the microbeads was automatically performed with a piezoelectric focussing device (PIFOC, Physik Instrumente, Waldbronn,

Germany). The image of the fluospheres is captured by a videocamera and processed with a computer-based video-imaging system (designed by W. Van Driessche, KULeuven, Belgium: for details see (Van Driessche et al., 1993)). Cell thickness is defined as the vertical distance between the basolateral and apical beads. Measured T_c values were corrected for the diameter of the fluorescent microbeads by subtracting 1 µm. The method has an accuracy better than 0.1 µm in the vertical direction. Changes in cell height are expressed as percentage of the value recorded just before the hyposmotic challenge or metabolic inhibition is imposed. Averaged values of T_c were calculated using the recordings from a number of beads (n_B) that remained attached to the monolayer during the entire experiment. The tissues were short-circuited during the entire course of the experiment and G_T and I_{sc} were recorded simultaneously with T_c.

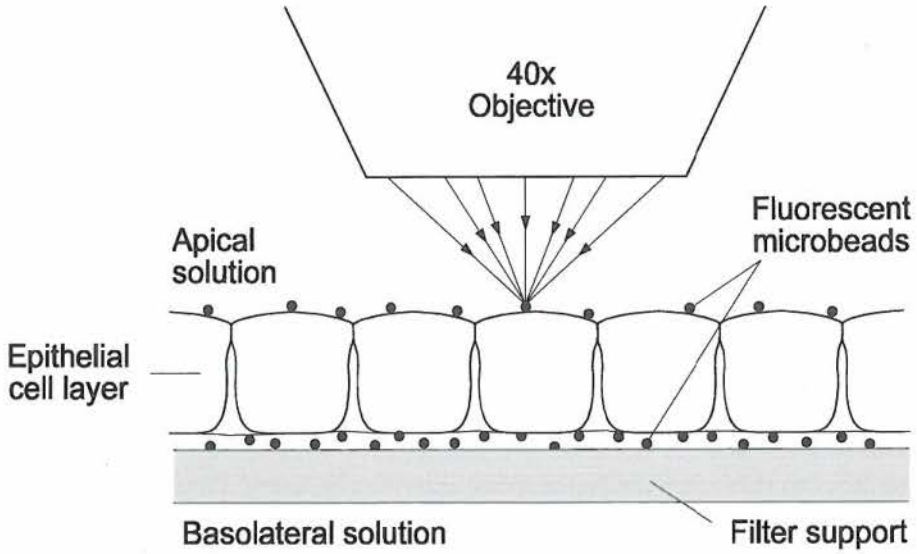

Figure 2.7 Schematic presentation of the cross section of the preparation used for epithelial cell thickness measurements. *Dimensions: filter support for epithelial cells: 40-45 µm; gelatine layer with 1 µm bead: less than 1.5 µm; epithelial cells: ~8 µm. (Adapted from Van Driessche et al., 1993)*

2.7 STATISTICAL ANALYSIS

All reported data are given as mean values from N experiments (different monolayers) ± standard errors (SEM). The Student's unpaired two-tailed t-test was used to evaluate differences between means. $P < 0.05$ was considered statistically significant.

2.8 SOLUTIONS AND CHEMICALS

The **normal control Ringer solution** used for A6 cells had the following composition (in mM): 70 NaCl, 3 KCl, 1 $CaCl_2$, 10 glucose, 35 sucrose and 10 HEPES buffered with TRIS to a final pH of 7.4. (osmolality ~200 mOsm/kgH_2O). In some tissues with a low basal transport rate 10 mM theophylline was added to the saline. In noise analysis experiments, theophylline was omitted from the solution because it induces additional Cl^--dependent Lorentzian noise (De Smet and Van Driessche, 1992) that interferes with the 6-chloro-3,5-diamino-pyrazine-2-carboxamide (CDPC)-induced Na^+-current noise. In case of variations on this Ringer composition for specific experimental protocols, the changes are indicated in the Materials and Methods section of that particular chapter, e.g. the composition of the solutions used in cell volume experiments are indicated in Table 7.1.

Metabolic inhibition was realised by bilateral perfusion with a solution containing (in mM): 70 NaCl, 3 KCl, 1 $CaCl_2$, 20 2-deoxyglucose (DOG), 2.5 NaCN (CN), 20 sucrose and 10 HEPES buffered with TRIS to a final pH of 7.4 (osmolality ~200 mOsm/kgH_2O).

Washout of the metabolic inhibitors during the **recovery phase** was done in the presence of 10 mM Na^+ pyruvate that substituted for glucose in the Ringer solution (with a reduction in sucrose concentration to maintain constant osmolality).

All fluorescent indicators used in this work were from Molecular Probes, Inc. (Eugene, OR). Amiloride, dexamethasone, gramicidin D, nigericin, carbonyl cyanide p-trifluoromethoxy-phenylhydrazone (FCCP), 5-nitro-2-[(3-phenylpropyl)amino]-benzoic acid (NPPB), Triton-X-100, ethylisopropylamiloride (EIPA), DOG, the sodium salt of pyruvic acid and thapsigargin were obtained from Sigma (St. Louis, MO). CDPC was obtained from Aldrich (Milwaukee, Wis., USA), ethylisopropylamiloride from Research Biochemicals Inc. (Natick, MA), NaCN from UCB (Brussels, Belgium). Oligomycin (mixture of types A, B and C) was purchased from Acros Organics (Geel, Belgium). Final concentrations in the Ringer solutions were obtained by adding these substances from a stock solution in H_2O (amiloride, NaCN), or in ethanol (dexamethasone, FCCP, gramicidin D, nigericin, oligomycin), or in DMSO (CDPC, EIPA, fluorescent indicators, NPPB, thapsigargin).

All experiments were carried out at room temperature and under normal atmospheric oxygen pressure.

Chapter 3

Na^+-dependence of single channel current and channel density generate saturation of Na^+-uptake in A6 cells

3.1 INTRODUCTION

In high-resistance epithelia such as A6 cells, transcellular sodium reabsorption occurs as a two-step process: 1) the rate limiting Na^+ entry through apical ENaCs, which is the principal site of regulation of Na^+ transport, and 2) the ATP-dependent extrusion via the basolateral Na^+/K^+-ATPase.

Different hormones control the activity of the apical ENaC: in kidney epithelia, for instance, aldosterone and vasopressin stimulate Na^+ reabsorption by increasing channel open probability and channel number, respectively (Duchatelle et al., 1992). Other factors such as intracellular Na^+, Ca^{2+} and pH levels or the activity of guanine nucleotide regulated (G) proteins, tyrosine and serine/threonine kinases and membrane lipid metabolites also participate in the regulation of apical Na^+ uptake (Eaton et al., 1995).

An interesting kinetic property of apical Na^+ uptake is that it differs from simple passive diffusion because it saturates at high apical Na^+. This was also observed in the cultured epithelial cell line A6 (Sariban-Sohrabi et al., 1983; Wills and Millinoff, 1990; Chuard and Durand, 1992). Saturation is also seen in *Xenopus oocytes* with functional expressed Na^+ channels after injection of mRNA from A6 cells (Palmer et al., 1990; Puoti et al., 1995).

To further elucidate this saturating behaviour of Na^+ uptake through the apical membrane in A6 cells, it is necessary to examine the Na^+-dependence of all parameters underlying the Na^+ current (I_{Na}) which are given by:

$$I_{Na} = \gamma \ (E_M - E_{Na}) \ N_T \ P_o = i \ N_o \qquad (3.1)$$

where γ is the single channel conductance, E_M is the apical membrane potential and E_{Na} is the Nernst potential for Na^+. The product γ (E_M - E_{Na}) is the single channel current (i). N_T is the total number of channels present per unit area of the membrane and P_o is the open probability of a single channel (either the spontaneous and/or blocker-induced gating). Therefore, N_T P_o is the number of open channels present per unit area of the membrane, or the open channel density (N_o).

Any of these factors can be responsible for alterations in and -especially- saturation of apical Na^+ uptake with increasing apical Na^+ concentrations. Since the Na^+ concentration in the lumen of distal tubules significantly increases in ischemic conditions (Schnermann et al., 1966; Braam et al., 1993), distal tubular epithelial cells are threatened with Na^+ overloading and loss of the intracellular ion homeostasis in these conditions. The aim of this chapter is to determine how distal tubular A6 cells handle increasing apical Na^+ concentrations and whether i or/and N_o are responsible for the saturating dependence of I_{Na} on the apical Na^+ concentration.

3.2 MATERIALS AND METHODS

3.2.1 Solutions and chemicals

Experiments were performed with A6 cells which had been incubated for 24 hours with $5 \cdot 10^{-7}$ mol/l dexamethasone in the basolateral culture medium. The basolateral solution had the following composition (mM): 70 NaCl, 3 KCl, 1 $CaCl_2$, 10 theophylline, 40 sucrose, 5 glucose and 10 HEPES buffered with TRIS to a final pH of 7.4. The Lorentzian noise was induced with the uncharged amiloride analogue 6-chloro-3,5-diaminopyrazine-2-carboxamide (CDPC).

In the initial phase of the experiment the apical side was perfused with control Ringer solution containing (in mmol/l): 110 NaCl, 1$CaCl_2$ and 10 HEPES buffered with TRIS to a final pH of 7.4. After an equilibration period we gradually reduced the apical Na^+ concentration ($[Na^+]_{ap}$) by replacing Na^+ by $Tris^+$ or by simply removing NaCl. The latter method gives rise to a reduction of the osmolality of the apical solution. Osmotic changes of the cellular compartment are negligible because the apical membrane is virtually impermeable for water, even after manipulations that are known to increase cellular cAMP (De Smet et al., 1995c). No differences were obtained in the results for both $[Na^+]_{ap}$-reducing methods.

3.3 RESULTS

3.3.1 Dependence of macroscopic current on apical Na^+ concentration

The relation between I_{Na} and $[Na^+]_{ap}$ was studied in Na^+ dose-response experiments. At the end of the 30-45 min equilibration period in control NaCl Ringer mean I_{Na} was 8 ± 1 $\mu A/cm^2$ (N=8) . Subsequently, $[Na^+]_{ap}$ was decreased by substituting $Tris^+$ for Na^+. The time course of I_{sc} recorded while stepwise decreasing $[Na^+]_{ap}$ is illustrated in Fig. 3.1A. At $[Na^+]_{ap}$ lower than 55 mmol/l I_{sc} was clearly reduced. In Na^+-free conditions we recorded in 4 out of 8 experiments a positive I_{sc} (I_{sc}°) which averaged 0.9 ± 0.3 $\mu A/cm^2$. This remaining current is most likely caused by cAMP-stimulated Cl^- outward movements after treatment with theophylline (Marunaka and Eaton, 1990; Zeiske et al., 1998). Therefore, at $[Na^+]_{ap} > 0$, I_{Na} was calculated as:

$$I_{Na} = I_{sc} - I_{sc}^{\circ} \qquad (3.2)$$

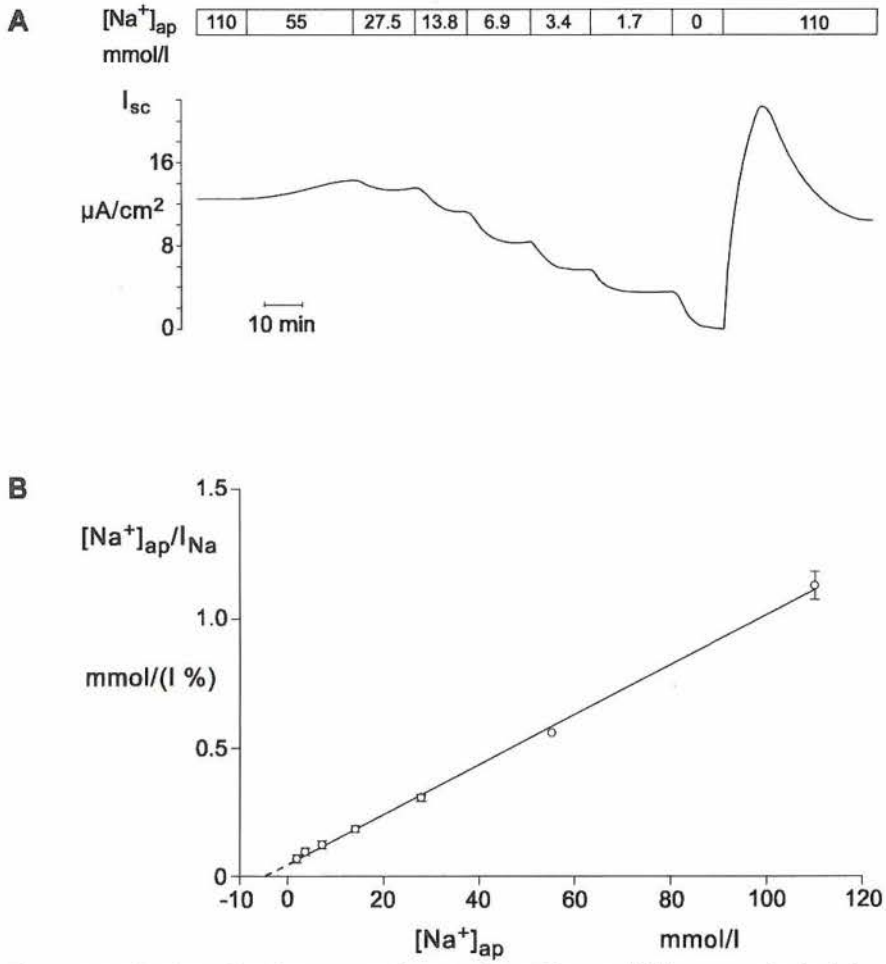

Figure 3.1 Kinetics of Na^+ transport in A6 cells. *Different $[Na^+]_{ap}$ were obtained by replacing Na^+ isosmotically with $Tris^+$.* ***(A)*** *Short-circuit current (I_{sc}) in response to stepwise decreased apical Na^+ concentrations (110, 55, 27.5, 13.8, 6.9, 3.4, 1.7 and 0 mmol/l) in a representative experiment.* ***(B)*** *Hanes-plot of the Na^+-current (I_{Na}) as a function of $[Na^+]_{ap}$. I_{Na} values of 8 distinct monolayers were normalised and defined as 100% at $[Na^+]_{ap}$ = 55 mmol/l. The averaged absolute value of I_{Na} at 55 mmol/l is 8 ± 1µA/cm². Mean values were fitted (solid line) to a linearised Michaelis-Menten equation and extrapolated (dashed line) to the abscissa where the negative intercept reveals a K_m^1 of ~ 5 mmol/l.*

After restoring $[Na^+]_{ap}$ to 110 mmol/l, I_{sc} increased rapidly. The observed overshoot in I_{sc} might be related to autoregulation of the apical Na^+ permeability after Na^+-deprivation (Abramcheck et al., 1985) or to changes in cellular composition (Turnheim, 1991). This may also explain why in this experiment (although not in others) I_{Na} at $[Na^+]_{ap}$ of 110

mmol/l at the start of the experiment was slightly smaller than at 55 mmol/l (Fig. 3.1A).

The relation between I_{Na} and $[Na^+]_{ap}$ was analysed in terms of the Hanes plot (Fig. 3.1B). The relation between $[Na^+]_{ap}/I_{Na}$ and $[Na^+]_{ap}$ is clearly linear which indicates that Na^+ reabsorption can be described by Michaelis-Menten kinetics. The apparent Michaelis-Menten constant (K_m^I) determined from the negative abscissa intercept of the linear fit extrapolation (dotted line), is equal to ~ 5 mmol/l. The maximal transport rate (inverse slope: I_{max}) was ~ 8 $\mu A/cm^2$. I_{max} was reached at a sodium concentration of 55 mmol/l (Fig. 3.1A). Thus, I_{Na} was normalised and defined as 100% at 55 mmol/l.

3.3.2 Noise analysis of I_{sc}

CDPC, a low affinity amiloride analogue, produces fluctuations in current which give rise to a Lorentzian noise component in the PDS (Helman and Baxendale, 1990). I_{Na} is only moderately reduced which enables accurate determination of I_{Na} in the presence of blocker. Noise analysis was performed with 5 apical CDPC concentrations ([CDPC]) ranging from 10 to 80 µmol/l. Figure 3.2 shows that $2\pi f_c$ increases linearly with [CDPC], which enabled us to calculate k_{on} = 6.5 ± 0.4 $(\mu mol/l)^{-1}s^{-1}$ and k_{off} = 291 ± 16 s^{-1} (N = 25). The corresponding blocker dissociation constant K_B (= k_{off}/k_{on}) was 50 ± 4 µmol/l (N = 25).

A possible effect of $[Na^+]_{ap}$ on $2\pi f_c$ was verified by recording current noise induced with a single CDPC concentration of 50 µmol/l at various $[Na^+]_{ap}$. In those experiments $[Na^+]_{ap}$ was reduced by removing NaCl. The mean values (N = 7) of $2\pi f_c$ thus recorded are depicted in Fig. 3.3A which shows that $2\pi f_c$ does not change with $[Na^+]_{ap}$. Power density spectra associated with the 5 different apical sodium concentrations recorded in a representative experiment are shown in Fig. 3.3B. In each PDS the 1/f background noise component at the lower frequency end superimposes the Lorentzian noise while at frequencies > 500 Hz the amplifier noise is dominating (Van Driessche, 1994). Lowering the apical sodium content showed a clear decrease in S_o values of the Lorentzian noise, whereas f_c values remained almost constant.

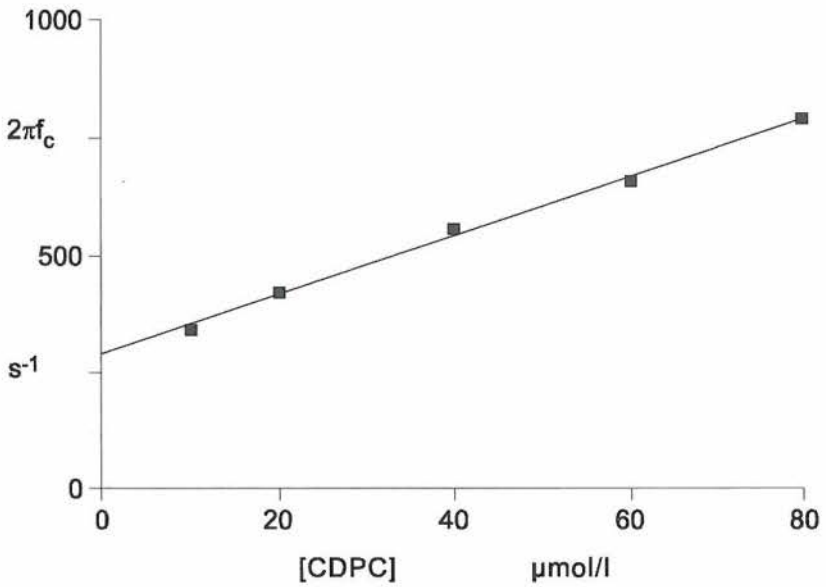

Figure 3.2 ***CDPC block of Na^+ channels in A6 cells.*** *The linear dependence of $2\pi f_c$ on increasing CDPC concentrations (10, 20, 40, 60 and 80 µmol/l) is shown for a typical experiment. The slope and intercept of the linear regression ($2\pi f_c$ = 290 + 6.2 [CDPC]) equal the "on" and "off" rates, respectively, of the interaction between CDPC and the Na^+ channel.*

We used the two-state model (Chapter 2) for CDPC blockage of the Na^+ channel to calculate the single channel currents (i) and open channel densities (N_o). Absolute values of single channel currents and open channel densities in control Ringer with 50 µmol/l CDPC were 0.18 ± 0.01 pA and 65 ± 9 million channels/cm^2 of epithelium (n=7), respectively. Data of i and N_o were normalised to their values at 55 mmol/l and the mean values of these normalised data are shown in Fig. 3.3C as a function of apical sodium concentrations. The number of open Na^+ channels shows a sharp rise by about 100 % when the apical sodium concentration is decreased below ~ 20 mmol/l. On the other hand, the current through single conducting pores displays a saturating concentration dependence. In the light of these results, the saturation of macroscopic I_{Na} must be caused by the concerted $[Na^+]_{ap}$-dependent behaviour of N_o and i. The negative abscissa intercepts (= K_m) determined by extrapolation of the regression lines (dotted lines) of the linear Hanes fits through the data (solid lines) are clearly different for i and I_{Na} as shown in the Hanes diagram (Fig. 3.3D) of normalised and averaged i and I_{Na} data. K_m^i is ~17 mmol/l and thus twice as high as K_m^I (~8 mmol/l).

Since the I_{Na} saturation must reflect the mode of both, i-saturation as well as N_o decrease in function of increasing $[Na^+]_{ap}$, the extrapolated parameter K_m^I cannot have a physical reality. Indeed, any linearisation procedure of a saturable function as I_{Na} to a

line with one slope and one intercept with the x-axis is only allowed if both the K_m and the I_{max} of the Michaelis-Menten equation are valid in the entire investigated range of substrate concentration. Since I_{Na} depends on both i and N_o, also the maximal rate of Na^+ transport (I_{max}) is determined by i_{max} as well as by a given N_o value. N_o can apparently attain different values dependent on the range of apical Na^+ concentration (Fig. 3.3C). For $[Na^+]_{ap}$ above ~ 20 mmol/l, the saturation of I_{Na} is completely described by the saturation of i. For lower $[Na^+]_{ap}$, I_{Na} will not simply reflect the behaviour of i but also that of N_o. Thus, the interpretation of a linear I_{Na} Hanes relation as fingerprint of 'saturation' is limited to the $[Na^+]_{ap}$-range above ~ 20 mmol/l.

3.4 DISCUSSION

3.4.1 Methodological aspects

In order to avoid changes of the intracellular potential governed by apical Na^+ and basolateral K^+ channels (Granitzer et al., 1991), depolarisation of the basolateral membrane with high K^+ solutions has been used to "selectively" clamp the apical membrane (Van Driessche and Lindemann, 1979). However, since it has been noted that high bl. K^+ may have severe adverse effects, such as a 7-10 fold increase in intracellular levels of cyclic AMP in frog skin (Cuthbert and Wilson, 1981), current-fluctuation experiments in this report were done in non-depolarised conditions.

Current-fluctuation measurements using CDPC as Na^+ channel blocker have been done previously (Helman and Baxendale, 1990). The relationship between $2\pi f_c$ and [CDPC] is linear (Fig. 3.2), a prerequisite for the application of the two-state model that was used for the calculation of i and N_o in this report. The high off-rate is advantageous for the accurate determination of K_B.

Since CDPC is uncharged, blocker kinetics should not be affected by competition with Na^+ (Fig. 3.3A) (Els and Helman, 1991) and should also be independent of membrane voltage.

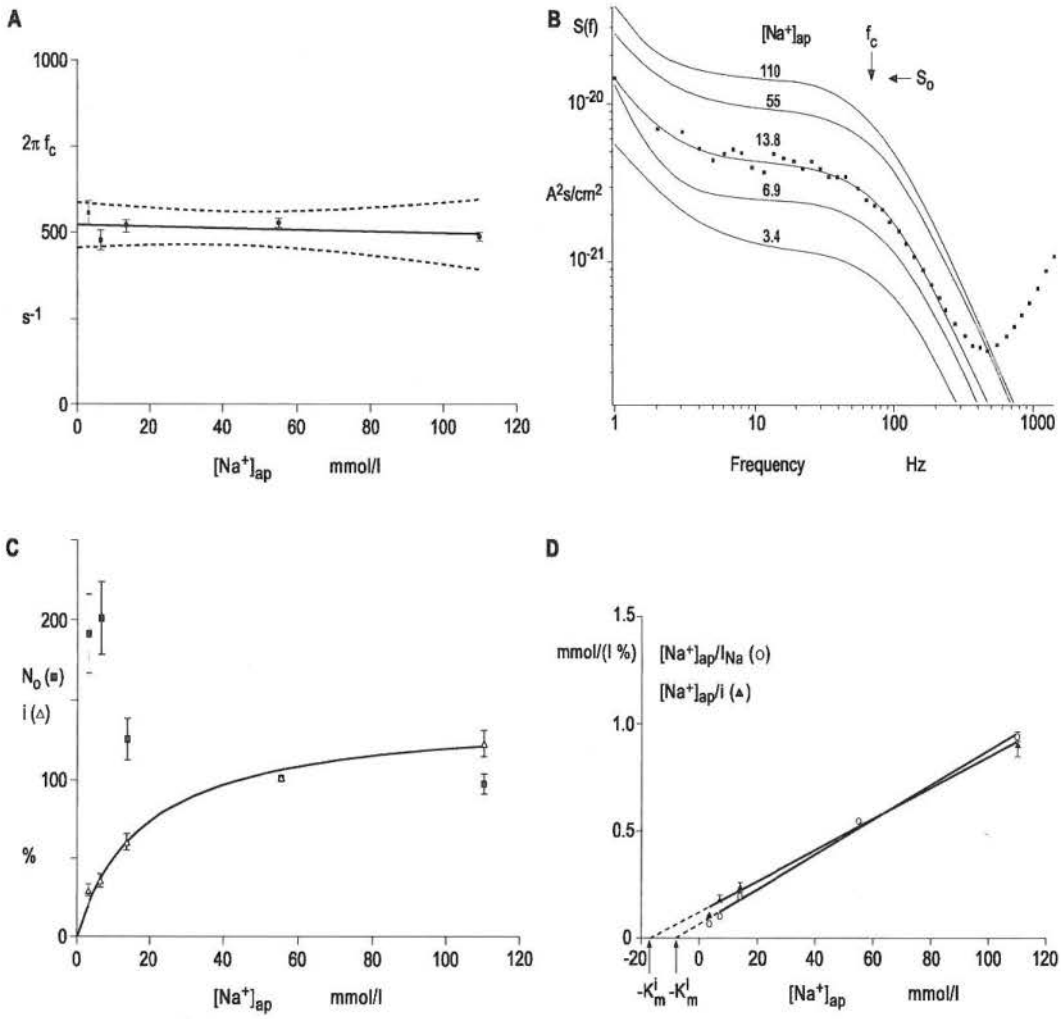

Figure 3.3 (A) *Effect of apical sodium concentrations on blocker kinetics. $[Na^+]_{ap}$ (110, 55, 13.8, 6.9 and 3.4 mmol/l) was lowered by dilution with a Tris/Hepes buffer solution. 50 µmol/l CDPC was continuously present in the apical Ringer solution. Dashed lines indicate the 95% confidence interval of the linear regression. The near horizontal character of the linear fit illustrates the Na^+-independence of [CDPC] interaction with Na^+ channels.* ***(B)*** *Power density spectra of I_{Na} fluctuations in conditions with different $[Na^+]_{ap}$ are shown for one representative experiment. The spectral data are fitted (smooth lines) by the sum S(f) of a Lorentzian component and a linear background component (Van Driessche, 1994). Data points are only shown for $[Na^+]_{ap}$ = 13.8 mmol/l. For $[Na^+]_{ap}$ = 110 mmol/l, the position of the Lorentzian plateau (S_o) and corner frequency (f_c) are indicated.* ***(C)*** *Dependence of i (Δ) and N_o (■) on $[Na^+]_{ap}$. Data were calculated according to the two-state model and were normalised to 100% at $[Na^+]_{ap}$ = 55 mmol/l. Averaged*

absolute values of i and N_o at $[Na^+]_{ap}$ = 55 mmol/l are 0.17 ± 0.01 pA and 64 ± 10 million channels/cm² epithelium respectively. ***(D)*** *Comparison of Hanes fits for the kinetics of i (triangles) and I_{Na} (circles). Solid lines represent a traditional linearised Michaelis-Menten fit of the data plotted according to Hanes. Dashed lines indicate the extrapolation of the fit for $[Na^+]_{ap}/I_{Na}$ data and $[Na^+]_{ap}$ /i data towards the abscissa where the intercept with the abscissa reveals $-K_m^I$ and $-K_m^i$, respectively.*

In current-fluctuation measurements, the calculation of single channel currents and channel densities is based upon chemical reaction schemes. For CDPC-induced current fluctuations, a kinetic scheme that proposes four different states of the ion channel (open blocked, open, closed and closed blocked) seems inappropriate since it was shown that CDPC interacts principally -if not solely- with open channels (Helman and Baxendale, 1990). Moreover, because of the very rapid off-rate of CDPC, a CDPC-blocked channel rarely closes in presence of the blocking molecule (Eaton and Marunaka, 1990). For A6 Na^+ channels which fluctuate spontaneously between the open and closed state (Hamilton and Eaton, 1985) the three-state model (open blocked, open and closed) seems to be the proper model but, a two-state model (open blocked and open) can still be considered if the interferences between the binding of the blocker and the spontaneous transitions are negligible (Van Driessche, 1994). This seems indeed to be the case for CDPC-induced Na^+ noise in A6 cells since the rate of spontaneous open-close transitions of Na^+ channels in A6 cells is much smaller (0.4 - 0.7 s^{-1}) (Hamilton and Eaton, 1985) than the CDPC reaction rate (~ 616 s^{-1} at a [CDPC] of 50 µmol/l, Fig. 3.2).

Helman and Baxendale (Helman and Baxendale, 1990) still suggest the use of the three-state model to determine channel densities, because it allows to correct for the [CDPC]-dependent changes of N_o (the open channel density) and N_{ob} (the sum of open and blocked channel densities) they measured in frog skin Na^+ current noise experiments. However such blocker-dependent changes of channel densities were not observed in CDPC noise measurements on A6 cells (Wills et al., 1991). Furthermore, a blocker-dependent change in i or N_o cannot play a role in those experiments where we determined the Na^+-dependence of these parameters since we used a constant [CDPC].

3.4.2 Factors that may generate Na^+ current saturation

According to Eq. 3.1, candidates for inducing saturation of I_{Na} include γ (Olans et al., 1984), E_M (Granitzer et al., 1991) and P_o (Ling and Eaton, 1989). These parameters will be reflected by i and N_o (Eq. 3.1), the data obtained from blocker-induced noise analysis. In order to estimate the values in the absence of blocker, we

will need to extrapolate the findings from fluctuation analysis for the case when no blocker is present.

In A6 cells Hanes analysis of the I_{Na} kinetics yielded a K_m^I value of ~5 mmol/l which is lower than reported before in A6 epithelia (18 mmol/l, (Sariban-Sohrabi et al., 1983)) but comparable with other reports of A6 Na^+ channels (9.5 mmol/l, (Wills and Millinoff, 1990); 10 mmol/l, (Palmer et al., 1990) and 5 mmol/l, (Puoti et al., 1995)). Despite this considerable accumulation of data, there is no report to date that elucidates the mechanism(s) underlying this Na^+ current saturation behaviour of I_{Na} for A6 cells. In other tight epithelia it has been observed that I_{sc} increased but then declined within seconds to a steady state level following a rapid step increase in apical Na^+ concentrations ("Na^+ self-inhibition") (Fuchs et al., 1977; Lindemann, 1984). Using the noise-analysis technique for amiloride-induced current fluctuations in frog skin, Van Driessche and Lindemann (Van Driessche and Lindemann, 1979) found that the open channel number steeply decreased, whereas single channel current linearly increased when $[Na^+]_{ap}$ was raised. This observation could indeed explain the saturating behaviour of I_{Na} in apical solutions with high Na^+ content.

Besides external Na^+ that may influence the number of open channels in a direct way, the observed non-linear behaviour of I_{Na} in high sodium solutions might also be caused by indirect modulation of transport properties e.g. via intracellular Na^+, a phenomenon called Na^+ 'feedback inhibition' (see section 1.2). Moreover, increased levels of intracellular Na^+ mostly result in parallel changes of cytosolic Ca^{2+} concentrations (Yang et al., 1988; Hayworth et al., 1980) and an inverse relationship between cytosolic Ca^{2+} and P_{Na} was observed (Taylor and Windhager, 1979), possibly involving activation of protein kinase C, which has been shown to inhibit apical Na^+ flux at both a macroscopic and single-channel level in A6 epithelia (Yanase and Handler, 1986; Ling and Eaton, 1989; Stockand et al., 2000) and mammalian cortical collecting tubules (Palmer and Frindt, 1987). On the other hand, I_{Na} reduction can be ascribed to a Na^+-induced decrease in cell negativity (Granitzer et al., 1991) that outweighs the Na^+-dependent increase in chemical driving force.

Any combination of the above mentioned processes could also underlie the I_{Na} overshoot seen after zero-$[Na^+]_{ap}$ treatment (Fig. 3.1A).

3.4.3 Contribution of Na^+-dependent single channel currents and open channel densities to the saturating behaviour of I_{Na}

For $[Na^+]_{ap}$ —> 0 mmol/l the density N_o of conducting pores is at least twice as high as for $[Na^+]_{ap}$ > ~ 20 mmol/l. In frog skin, Van Driessche and Lindemann (Van Driessche and Lindemann, 1979) found that N_o steadily increases with decreasing $[Na^+]_{ap}$ and the lowest tested apical Na^+ concentration in amiloride-induced Na^+-noise measurements was 11 mmol/l. This monotonous increase of N_o, when lowering apical

Na^+ concentrations down to 11 mmol/l, was thought to continue for lower $[Na^+]_{ap}$. Within our statistical limits, our finding for A6 cells may confirm their results.

The mean single channel current was, in our experiments for $[Na^+]_{ap}$ = 110 mmol/l, 0.18 pA. Wills and Millinoff (Wills and Millinoff, 1990) reported about the same i, whereas that reported by Helman et al. (Helman et al., 1986) was twice as large. At present, the reason for these discrepancies is unknown.

Contrary to the observations in frog skin (Van Driessche and Lindemann, 1979), hen cloaca (Christensen and Bindslev, 1982) and rabbit urinary bladder (Lewis et al., 1984), the single channel current i does saturate with $[Na^+]_{ap}$ in A6 cells (Fig. 3.3C). The Hanes plot of this process (Fig. 3.3D) yields a Michaelis-Menten constant K_m^i of ~17 mmol/l. With respect to the behaviour of the single channel current, our observation is consistent with the non-linear dependence of i on $[Na^+]_{ap}$ in A6 cells which was reported by Helman and co-workers (Helman et al., 1986). There, no K_m^i was given. The expected effects of increasing $[Na^+]_{ap}$, i.e. depolarisation of E_M (Granitzer et al., 1991) in parallel with an increase in E_{Na} (cf. Eq. 3.1), will tend to cancel each other and so are not likely to contribute to the saturation of i. We cannot strictly exclude that Na^+-dependent cell depolarisation contributes to the saturation of i. However, the A6 Na^+ channel reconstituted in lipid bilayers, when held at constant voltage, also showed a saturation of i due to saturation of γ (Olans et al., 1984). A saturation of γ with increasing Na^+ concentrations was also observed for cloned rat epithelial ENaCs in planar lipid bilayers (Ismailov et al., 1997). Thus, a saturating γ may account for the saturating $[Na^+]_{ap}$-dependence of i.

3.4.4 Summary

In this chapter, we evaluated how A6 cells handle increasing apical Na^+ concentrations. Our results are consistent with the literature in that the Na^+ uptake through the apical ENaCs saturates with increasing apical Na^+ concentrations. The single channel current clearly saturates with an apparent Michaelis-Menten constant (K_m) of ~ 17 mmol/l. Physiologically, the limited transport capacity of the amiloride-sensitive ENaC may be an important property to protect the cells from Na^+ overloading and subsequent changes in intracellular electrolyte composition in situations with increased outer Na^+ concentrations, e.g. during ischemia (Schnermann et al., 1966; Braam et al., 1993).

At a given CDPC concentration (tacitly extending our results to the situation of absence of the blocker), I_{Na} is equal to the product i N_o. The single channel current saturates according to

$$i = i_{max} \{[Na^+]_{ap} / ([Na^+]_{ap} + K_m^i)\} \qquad (3.3)$$

Since the change in N_o below ~ 20 mmol/l occurs with an unknown steep function of $[Na^+]_{ap}$, we must refrain from representing I_{Na} as an explicit function of $[Na^+]_{ap}$, i_{max}, K_m^i and the parameters that govern the relationship between $[Na^+]_{ap}$ and N_o.

Chapter 4

Intracellular pH-shifts in cultured kidney (A6) cells: effects on apical Na^+ transport

4.1 INTRODUCTION

Cell pH (pH_c) is under strict control (Chen and Boron, 1991; Ganapathy and Leibach, 1991). Unexpectedly, cytosolic acidification, resulting from a lack of oxygen, appeared to be, at least at short term, beneficial against major cell damage from ischemia (Weinberg et al., 1991). Prior treatment of several cell types including kidney cells with salines of pH<7 reduced or prevented cell damage like leak of enzymes or complete lysis during anoxia. Interestingly, analogous cytoprotective effects were obtained by treatment with glycine and alanine during ischemia. So far, the mechanism underlying either type of cytoprotection could not be settled (Rose et al., 1995; Weinberg et al., 1991). In the context of using A6 cells as model epithelium for the study of the cellular consequences of metabolic inhibition and the possible protective effects of protons, this chapter focusses first on the effects of intracellular acidification on transepithelial Na^+ transport in normal functioning A6 cells.

Recently, it has been argued that pH_c is also a cytosolic second messenger, like Ca^{2+}, cAMP and ATP (Harvey, 1994; Harvey, 1995). For instance, in tight epithelia like frog skin or the cultured distal kidney cell line A6 from the clawed toad, *Xenopus laevis*, pH_c was found to influence apical and basolateral cation permeabilities resulting in a concerted up- and downregulation occurred of apical Na^+ (P_{Na}) and basolateral K^+ (P_K)-permeabilities (so-called "cross-talk"). Upon gradual acidification from pH 8.0 to 6.5, P_{Na} as well as P_K became negligible (Harvey, 1994; Harvey, 1995). This might shed some light on the mechanism of the protective effect of protons. A closure of epithelial cation channels by cellular acidification could prevent the accumulation of intracellular Na^+ in ATP-depleted cells facing ischemic conditions. Hence, the gain in cellular NaCl and the resulting cell swelling might be avoided or, at least, reduced.

To study the dependence of plasma membrane ion permeability on pH_c, the so-called 'NH_4^+-pulse' method (De Weer, 1978) has become a popular way to alter pH_c. Usually, when more than millimolar concentrations of ammonium salts are added to the extracellular saline, an alkalinisation of the cytosol due to hydrolysis of the easily permeant NH_3 has been observed (Chuard and Durand, 1992; Cougnon et al., 1996; Harvey et al., 1988). NH_3 enters through the lipid or via a possible aquaporin permeation route (Scholz et al., 1993). Extracellular ammonium removal would in turn acidify the cell ('NH_4^+-prepulse' method (Casavola et al., 1992)). The rate of the subsequent re-alkalinisation will reflect the activities of pH_c-regulating transporters, such as the Na^+/H^+ exchanger or primary active H^+ pumps. If -otherwise K^+-permeable-entrance pathways for NH_4^+ (Cougnon et al., 1996; Knepper, 1991) are present, a cytosolic pH_c drop may occur as a consequence of the intracellular release of protons by entered NH_4^+ ions. When tissue pH changes are evoked by simple addition (Casavola et

al., 1992; Cougnon et al., 1996; Harvey et al., 1988; Reuss, 1998) of 10 to 30 mM ammonium salts to a saline, without being balanced osmotically, cell volume changes may influence ion channel permeabilities as well (De Smet et al., 1995c).

In this chapter, the NH_4^+-pulse was performed without or with osmotic control. For each method, alterations in cell volume were recorded. pH_c was monitored using a membrane-permeant derivative of the pH-sensitive fluorescent dye, BCECF (Casavola et al., 1992; Chuard and Durand, 1992). To inspect transepithelial Na^+ uptake, we monitored transepithelial conductance and the short-circuit current carried by Na^+. In order to establish whether pH_c-dependent changes in apical Na^+ permeability are related to changes in single-channel current or channel density we conducted fluctuation analysis with the Na^+ channel blocker CDPC (see Chapter 3). Finally, the influence of pH_c changes on Na^+ current (I_{Na})-kinetics were evaluated and compared with the results obtained from noise analysis.

Depending on the side of application, and the tonicity of the NH_4Cl-containing saline, pH_c and I_{Na} changed in a complex manner. Under strict conditions, however, changes in pH_c affected only N_o, the number of open apical Na^+ channels, whereas the single-channel current (i), and also the blocker kinetics appeared invariant.

4.2 METHODS AND MATERIALS

4.2.1 Cell culture

In this study A6 cells obtained from Dr. S. Helman were used at passages 71-75 for pH_c measurements. The cells were cultured in the same way as the A6 cells obtained from Dr. J.P. Johnson (see Chapter 2 for details).

4.2.2 Solutions and chemicals

The control NaCl Ringer solution had the following composition (in mM): 70 NaCl, 3 KCl, 1 $CaCl_2$, 40 sucrose, 5 glucose and 10 HEPES (N-[2-Hydroxyethyl] piperazine-N'-[2-ethanesulfonic acid]) and was buffered with TRIS (Tris[hydroxymethyl]aminomethane) to a final pH of 7.4 (osmolality ~200 mosm/kgH_2O). Under these conditions the average pH_c was 7.34 ± 0.06 (N=11) which is comparable with the pH_c of 7.30 ± 0.02 as earlier reported for A6 cells (Casavola et al., 1992). Lorentzian noise was induced with the uncharged amiloride analogue 6-chloro-3,5-diaminopyrazine-2-carboxamide (CDPC; 50 μM). In order to investigate pH_c-effects

on I_{Na}-kinetics from dose-response experiments, the apical Na^+ concentration ($[Na^+]_{ap}$) was gradually reduced by substituting $Tris^+$ for Na^+.

4.3 RESULTS

4.3.1 Influence of hyper- and iso-osmotic NH_4^+-containing salines on cell volume

In many reports where the influence of NH_4^+ ions on cytosolic pH was investigated, high concentrations of the NH_4^+ salt were added to the bath, giving rise to a noticeable increase in osmolality. In a number of tight epithelia, hyperosmotic cell shrinking strikingly reduces transepithelial Na^+ transport as for instance in A6 cells (Wills et al., 1991). On the other hand, due to the permeability of the cell membrane for NH_3, or NH_4^+ with Cl^-, cell shrinkage will be counteracted by solute influx followed by an obligatory water flow. Even when NaCl or sucrose in the saline is isosmotically replaced with ammonium chloride, so-called "isosmotic swelling" due to net NH_4Cl entrance into the cells could occur. Such a phenomenon has already been described for A6 cells when basolateral NaCl was replaced by KCl or glycerol (Van Driessche et al., 1997). Finally, the side of application of the pH_c-shifting agent may be of prime importance. Indeed, as NH_4^+ can enter cells via K^+ selective pathways and thus give rise to cell acidification, its basolateral (bl.) application will have a more distinct effect on pH_c decrease than a treatment of the apical (ap.) barrier that has a negligible K^+ permeability.

Fig. 4.1 demonstrates experiments where 20 mM NH_4Cl were isosmotically applied by replacing 40 mM sucrose with 20 mM NH_4Cl (top trace), or hyperosmotically, by simply adding NH_4Cl to the NaCl Ringer's solution (bottom trace). Disturbance of the cytosolic osmotic condition was assessed by recording the cell height T_c that reflects cell volume changes as described in section 2.6. Apical application of ammonium chloride, independent of the solution osmolality, did not influence T_c. When NH_4Cl was applied basolaterally, T_c remained unchanged after isosmotical sucrose replacement by NH_4Cl whereas a remarkable but reversible decrease in T_c was observed upon simple hyperosmotic NH_4Cl addition. This result confirms previous observations (De Smet et al., 1995c) that cell volume does not respond to ap. anisotonicity as the ap. membrane of A6 cells is known to be quite impermeable to water. We also see that the expected isosmotic volume increase does not occur. This may indicate that there is no massive influx of solute/water or that the volume regulation occurs as fast as the isosmotic cell swelling (De Smet et al., 1995c). Regarding the high osmotic sensitivity of the bl. side, putatively pH_c-related transport changes that result from NH_4^+ exposure must therefore be studied in the absence of any osmotic imbalance. Moreover, the side of the

application of a pH_c-shifting agent must be under strict control. Only isosmotic experiments are reported below. Also, a strictly unilateral treatment with pH_c-influencing substances was employed.

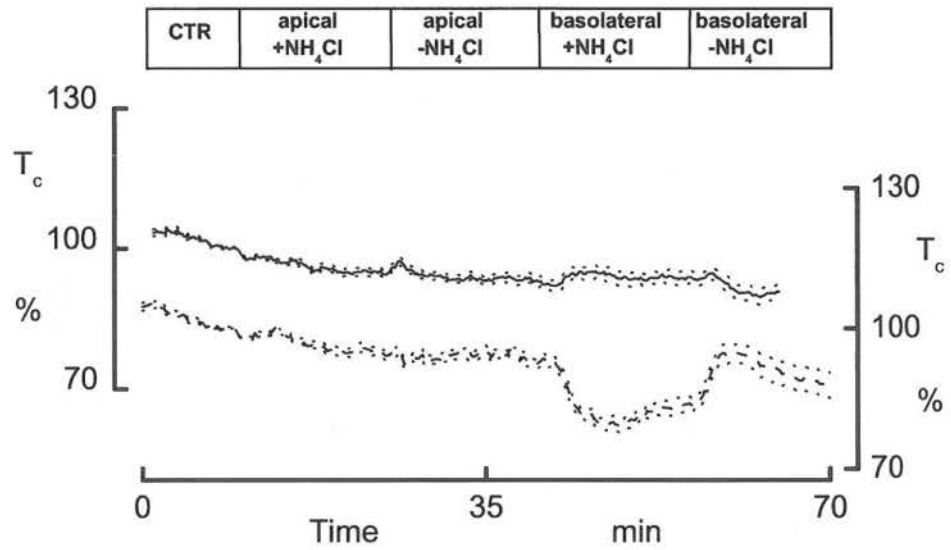

Figure 4.1 Measurements of cell thickness (T_c) during exposure to NH_4^+-containing NaCl saline. *The top trace represents the averaged time course of T_c when 20 mM NH_4Cl is replacing 40 mM sucrose at constant osmolality (N = 5 tissues; total number of beads: 34, ± SEM indicated by dots). T_c (scale on left) has been normalised to the value recorded just before ap. NH_4^+ addition. Average control T_c was 7.7 ± 0.3 µm for all beads. The bottom trace shows the average percentage change in T_c (scale on right) when NH_4Cl did not replace sucrose but was added to yield hyperosmotic solutions (N = 2, N_B = 24). We used 2 tissues with 24 beads. NH_4Cl was first introduced apically and, after removal, subsequently in the basolateral Ringer solution. CTR, control.*

4.3.2 pH_c and I_{Na} changes during apical or basolateral isovolumetric NH_4Cl exposure

Fig. 4.2, A and B, depicts recordings (from two different epithelia) of pH_c and I_{sc}, respectively, when tissues were isosmotically exposed to ap. NH_4Cl-containing NaCl saline. Typically, a very similar time course in the change of both parameters is observed: ap. NH_4^+ alkalinises the cells which raises I_{Na}. In the presence of ap. amiloride, I_{sc} remains close to zero despite the change in pH_c (not shown). Fig. 4.2D shows the rise in I_{Na} induced by ap. NH_4^+ (N = 8), whereas Fig. 4.2C illustrates (N = 5)

the underlying shifts in pH_c demonstrating that an increase in pH_c correlates with an increase in I_{Na}.

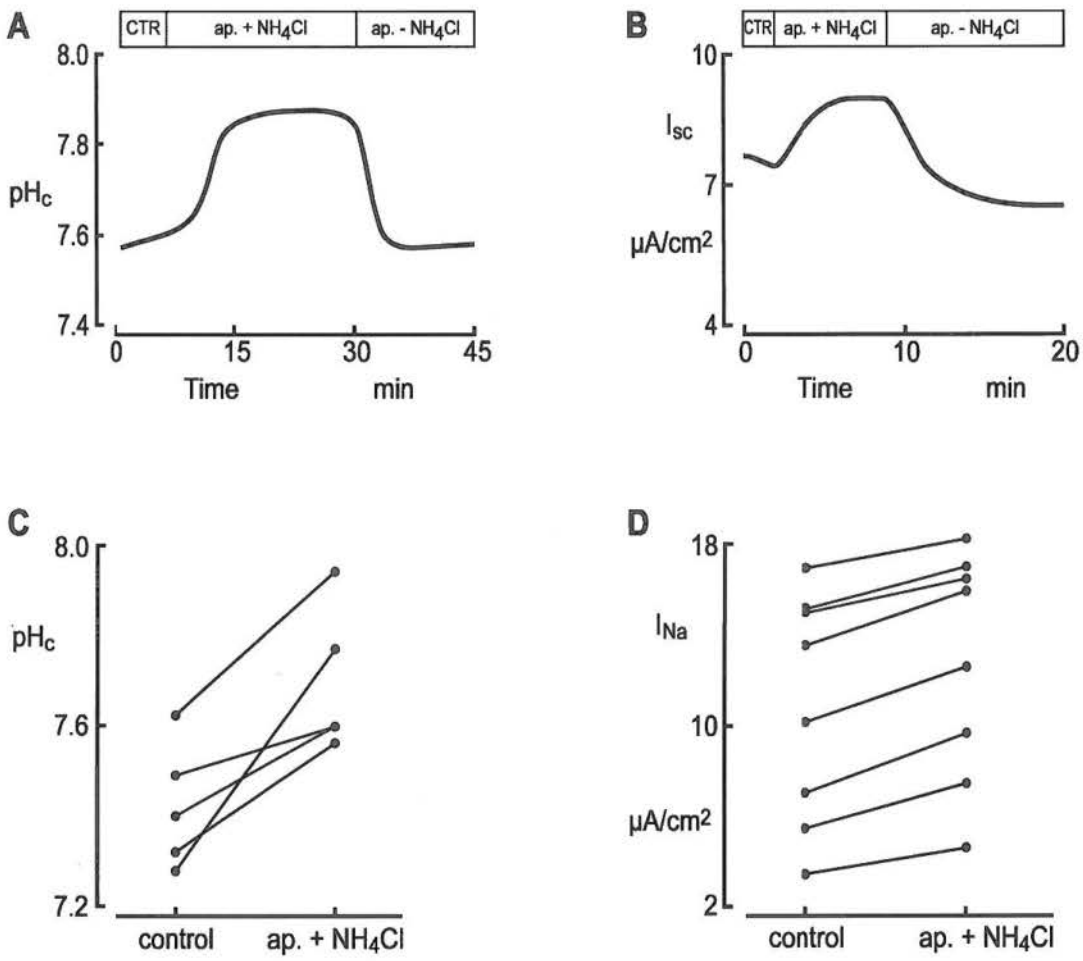

Figure 4.2 Effect of NH_4^+ on pH_c and I_{sc}. ***(A)*** *Typical time course of changes in pH_c when 20 mM NH_4Cl is added isosmotically (replacement of 40 mM sucrose) to the apical (ap.) NaCl saline, and after subsequent withdrawal.* ***(B)*** *Typical time course of changes in (mainly Na^+-carried) I_{sc} for another tissue treated as in panel A.* ***(C)*** *Comparison (5 tissues) of steady-state pH_c before (control) and after isosmotic ap. NH_4Cl addition with pH_c at maximal point of cell alkalinisation.* ***(D)*** *Comparison of I_{Na} before and at maximal response to ap. isotonic treatment with NH_4Cl. Shown are the data for 8 tissues.*

With bl. isosmotic NH_4Cl treatment (Fig. 4.3, A-D) the situation is considerably more complex. Panels A and B show simultaneously recorded traces of pH_c and I_{sc} from the same tissue. In Fig. 4.3A, during the first phase after NH_4^+ addition, pH_c rises similarly as with ap. NH_4^+. However, this pH_c rise is quickly reversed into a marked drop.

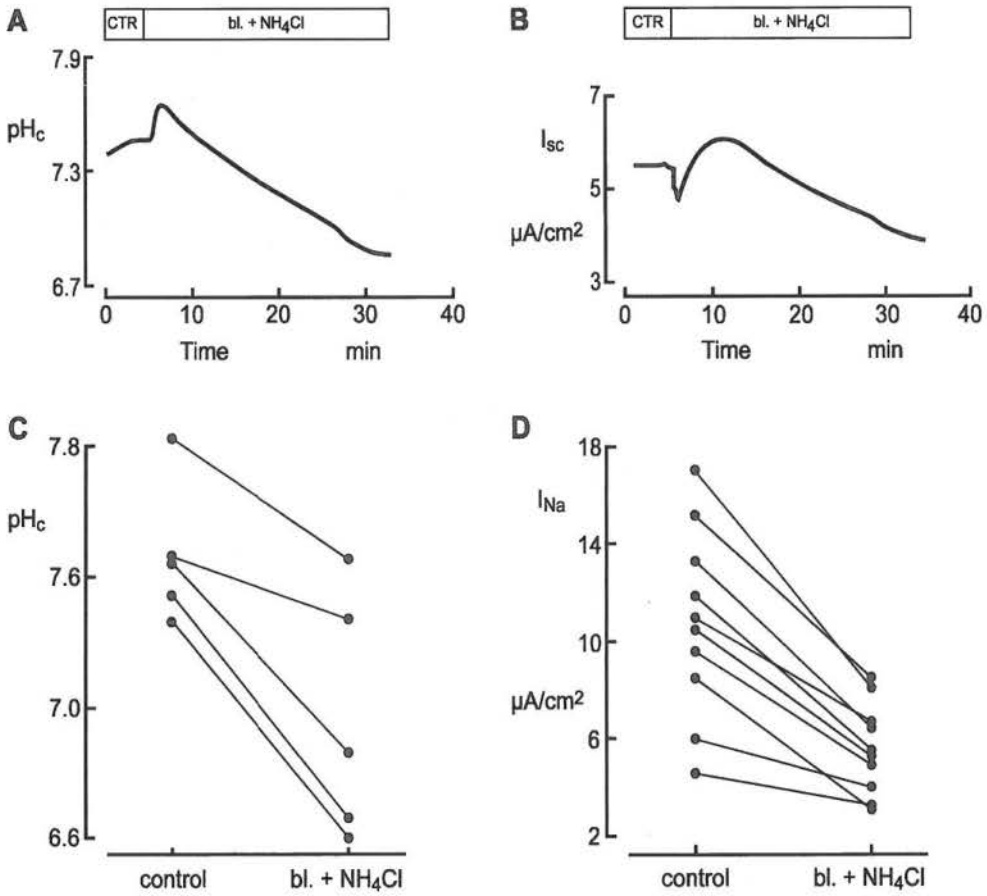

Figure 4.3 (A) *Typical time course of changes in pH_c when 40 mM basolateral (bl.) sucrose is replaced by 20 mM NH_4Cl.* ***(B)*** *Changes in Na^+-carried I_{sc} for the same tissue as shown in Fig. 4.3A.* ***(C)*** *Comparison (5 tissues) of steady-state pH_c before (control) and after isosmotic bl. NH_4Cl addition with pH_c at its minimum.* ***(D)*** *Comparison of Na^+ current (I_{Na}) before and at maximal response to bl. isotonic treatment with NH_4Cl. Shown are the data for 10 tissues*

In addition, another typical feature is observed only in the time course of I_{sc}. Right after the introduction of bl. NH_4^+ and before any change of pH_c, a sharp and immediate current drop occurs, followed by a gradual increase synchronously with pH_c, first increasing and then dropping below the control value. So, the initial fall in I_{sc} cannot be related to pH_c changes whereas the subsequent changes in I_{Na} and pH_c are quite similar. Fig. 4.3, C and D, summarises the late phase drop in pH_c (N = 5) and I_{Na} (N =10). At this point we may state that a probably causal relationship exists between pH_c and the magnitude of I_{Na}, disregarding for a moment the initial "blip" event in I_{sc} obtained with bl. NH_4^+. Cell alkalinisation and current rise occur simultaneously with NH_4^+ on either side (basolaterally only in the beginning). Cell acidification takes place in the late phase with bl. NH_4^+. Below we investigate, by means of noise analysis, which ap. parameters of Na^+ transport are influenced by pH_c.

4.3.3 Evaluation of Na^+ channel blocker noise: influence of pH_c on I_{Na} and N_o

4.3.3.1 NH_4^+ pulses

To generate a Na^+ channel blocker noise in I_{sc}, we employed CDPC, a non-charged amiloride analogue rather than amiloride itself. Since simultaneous measurements of pH_c and noise analysis could not be done we assume, for the experiment depicted in Fig. 4.4 and the following ones, that the respective alterations of pH_c due to isosmotic NH_4Cl exposure are analogous to those reported in the absence of an inhibitor. A typical protocol for noise analysis is shown in Fig. 4.4A. In the presence of 50 µM CDPC, ap. sucrose replacement by NH_4Cl led to the already known rise in I_{Na}. A similar behaviour of the transepithelial conductance (G_T), mainly determined by the ap. membrane resistance, was seen. When the agent was applied basolaterally (Fig. 4.4A), again the same features for I_{Na} as shown for I_{sc} in Fig. 4.3B were seen. The I_{Na} changes during the bl. NH_4^+ exposure (Fig. 4.4A) were accompanied by an almost completely proportional behaviour of G_T, with the notable exception of the negative initial blip characteristic for I_{sc}. After removal of bl. NH_4Cl, both G_T and I_{Na} show a marked negative overshoot. The protocol (Fig. 4.4A) ends with exposure to ap. amiloride in order to determine the Na^+-specific part in I_{sc}. The reason for the current undershoot after bl. NH_4^+ removal becomes clear from pH_c measurements: ammonium removal leads to a considerable further pH_c-drop (Fig. 4.4B) and I_{Na} decrease (Fig. 4.4C), which are followed by a slow recovery (Fig. 4.4, B and C). When this protocol is repeated, however, in the absence of bl. Na^+ as in the end of the experiment in Fig. 4.4C, I_{sc} recovery does not occur which strongly suggests the involvement of a bl. Na^+/H^+ antiporter (Casavola et al., 1992) in the backregulation of pH_c and, consequently, of I_{Na} and G_T.

We used noise analysis of the CDPC-induced fluctuation in I_{sc} at various points in time where stable current values had been attained (at the positions indicated by numbers in Fig. 4.4A). The period of the initial putative pH_c rise after bl. NH_4^+ was too short to perform data recording for noise analysis. The results from this experiment are given in Table 4.1. pH_c had no influence on the f_c of the CDPC-induced Lorentzian noise (Fig. 4.5A). However, the Lorentzian plateau magnitude was altered dramatically and reflected the direction of changes in G_T and I_{Na} (Fig. 4.4).

Analysis on the basis of the two-state channel model for interaction with the blocker clearly revealed (Table 4.1) that i remained unaffected by changes in pH_c. Therefore, pH_c exerts a direct control upon Na^+ channel activity as expressed by N_o. A rise in pH_c augments G_T by means of Na^+ channel opening, and vice versa (internal channel pH_c-'titration'). Fig. 4.5, B and C, summarise such results for 8 tissues.

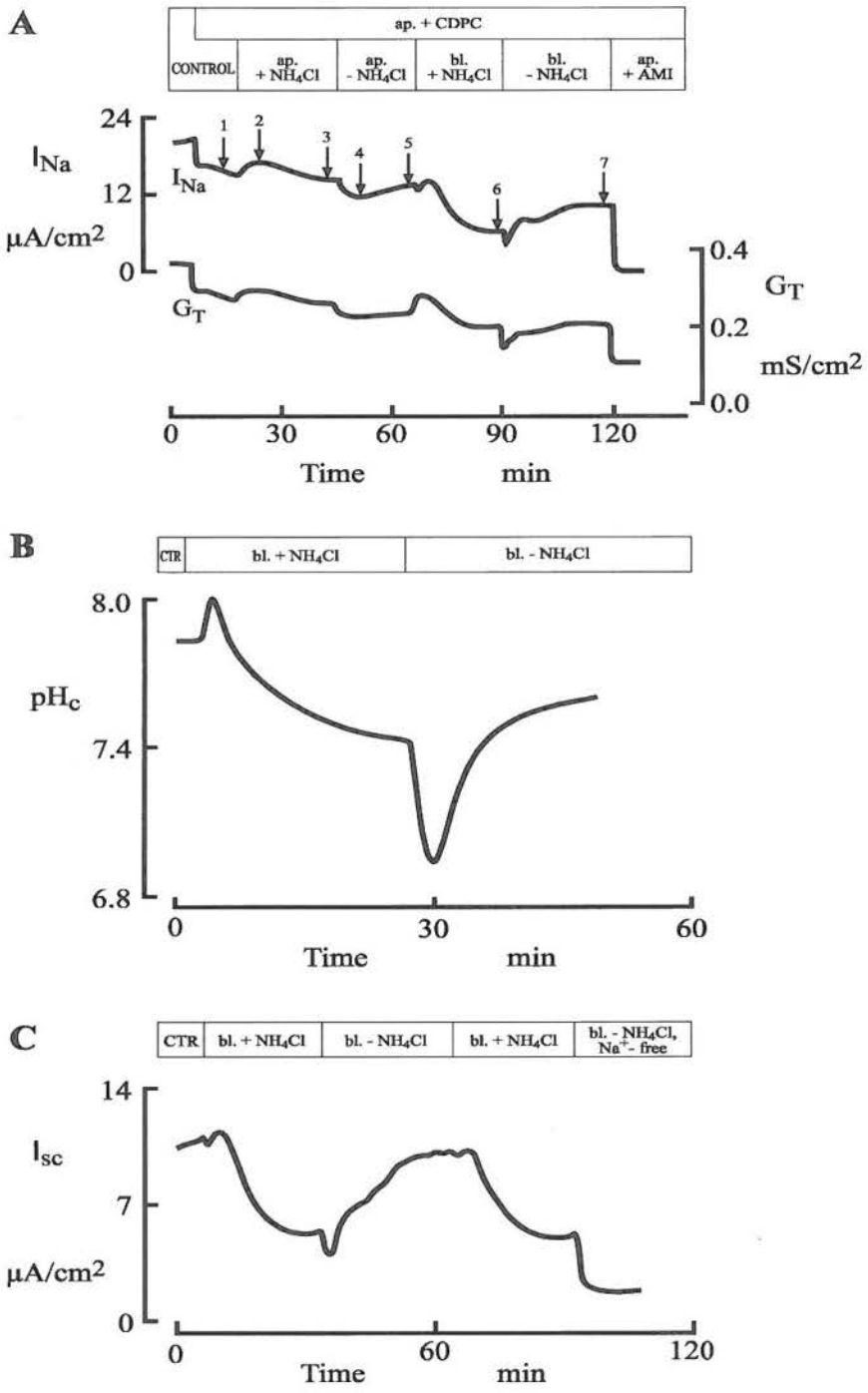
A
ap. + CDPC
CONTROL
ap. + NH4Cl
ap. - NH4Cl
bl. + NH4Cl
bl. - NH4Cl
ap. + AMI
24
12
0
INa
μA/cm2
1
2
3
4
5
6
7
INa
GT
0.4
0.2
0.0
GT
mS/cm2
0
30
60
90
120
Time
min
B
CTR
bl. + NH4Cl
bl. - NH4Cl
8.0
7.4
6.8
pHc
0
30
60
Time
min
C
CTR
bl. + NH4Cl
bl. - NH4Cl
bl. + NH4Cl
bl. - NH4Cl, Na+- free
14
7
0
Isc
μA/cm2
0
60
120
Time
min

Figure 4.4 (A) *Time courses of I_{Na} and G_T during ap. or bl. isotonic treatment (for order of application, see horizontal bar) with 20 mM NH_4Cl for a selected tissue. Before NH_4^+, 50 µM CDPC was added to the ap. NaCl saline. At the positions indicated by numbers, CDPC-induced I_{Na} noise was recorded. The respective values of the Lorentzian plateau (S_o), the corner frequency (f_c) and - after further evaluation - i and N_o are listed in Table 4.1. Amiloride (0.1 mM, AMI) was added apically for the determination of zero I_{Na}.* ***(B)*** *Time course of pH_c during isotonic basolateral (bl.) NH_4Cl addition and subsequent removal in the presence of bl. NaCl.* ***(C)*** *I_{sc} time-course during isosmotic bl. NH_4Cl addition and removal, in the presence (left) and in the absence of bl. NaCl (Tris replacement simultaneously with NH_4Cl withdrawal; right). CTR: control*

Table 4.1 Lorentzian parameters, i and N_o from the CDPC I_{sc} noise at the time periods indicated by numbers for the experiment shown in Fig. 4.4A.

	F_c (Hz)	S_o ($10^{-20}A^2s/cm^2$)	i (pA)	N_o (10^4channels/cm^2)
1	101.9	9.50	0.20	77
2	99.9	10.3	0.18	93
3	101.3	8.45	0.18	77
4	109.2	7.26	0.22	52
5	110.2	8.66	0.24	56
6	109.5	3.13	0.18	36
7	108.2	6.30	0.22	48

The current i was calculated according to Eq. 2.8. Since f_c was independent of pH_c, we chose the parameter value k_{on} = 6.48 $\mu M^{-1} s^{-1}$ from Chapter 3.

In order to compare different epithelia with sometimes very different transport capacities we plotted, in Fig. 4.5B, the relative magnitude of the Lorentzian plateaus (ratio of S_o in the presence of NH_4^+) as a function of the respective relative currents. These parameters turned out to be strictly proportional for a number of different conditions (see legend for Fig. 4.5). In the framework of the equations used for noise analysis (see Chapter 2), we thus conclude that only N_o is responsible for the observed pH_c-dependent alterations in I_{Na}, as already suggested by the typical experiment depicted in Table 4.1 and Fig. 4.4A.

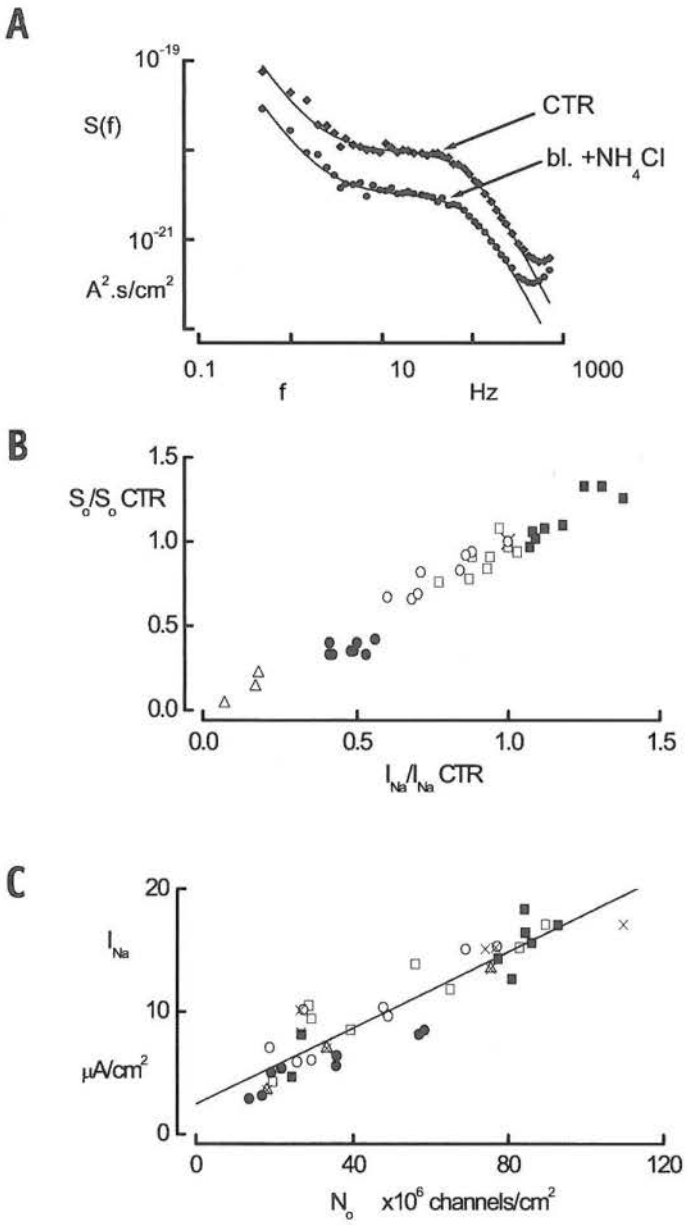

Figure 4.5 (A) *Power density spectrum of the I_{sc} noise in the presence of 50 µM ap. CDPC. The control (CTR, ◆) spectrum is calculated for position 1, the lower spectrum (labelled '+NH_4Cl', ●) for position 6 as indicated in Fig. 4.4A. Fitted and calculated parameters are listed in Table 4.1.* ***(B)*** *Ratio (normalised to control, CTR) of S_o at 50 µM CDPC plotted versus the analogous relative I_{Na} for different tissues and various treatments. According to theoretical considerations, this*

*function must intercept both abscissa and ordinate at zero. The finding of a linear relationship S_o/S_o CTR = (i/i CTR).(I_{Na}/I_{Na} CTR) suggests, that the i (i/i CTR) remains fairly constant over all tissues and pH_c conditions. ✕, control; ■, NaCl in the presence of ap. NH_4^+ (cell alkaline); □, after removal of ap. NH_4^+; ●, in the presence of bl. NH_4^+ (cell acidic); ○, after removal of bl. NH_4^+; △, removal of bl. NH_4^+ combined with bl. Na^+ replacement by $Tris^+$. **(C)** I_{Na} plotted as a function of N_o for the same tissues and for the same conditions (cf. symbols) depicted in B. According to theory (cf. Chapter 2, Eq. 2.9), the slope of the resulting linear relationship for the pooled data (solid line) equals the average single-channel current, i (mean i = 0.196 ± 0.005 pA).*

Consistently, the corresponding relationship between I_{Na} and N_o is roughly linear (Fig. 4.5C) for the cumulated data, which strongly suggest that the individual i values (the slope of the solid line in Fig. 4.5C equals averaged i values; Eq. 2.9) for all the investigated tissues are of comparable magnitude and remain unchanged during shifts of pH_c. Thus, the ap. P_{Na} reflects the N_o, and no attention must be given to i or blocker kinetics as revealed in f_c.

4.3.3.2 Arrest of the basolateral Na^+/H^+ exchanger

4.3.3.2.A BASOLATERAL Na^+ OMISSION

Casavola et al. (Casavola et al., 1992) previously reported for A6 cells the existence of a Na^+/H^+ antiporter exclusively in the bl. membrane. Presumably, removal of Na^+ from the bl. saline could acidify the cytosol. We tested this by measuring pH_c when bl. Na^+ was replaced by Tris or choline. In Fig. 4.6 we show an experiment with Tris (also representative for choline).

It can be seen (Fig. 4.6A) that pH_c drops after Na^+ removal. At the same time, and tested here (Fig. 4.6B) with another epithelium, the Na^+ current drops eventually, thus a picture similar to that seen with bl. NH_4^+-induced acidification of the cytosol. One more salient and for this sort of manipulation typical feature can be discovered in Fig. 4.6B: Na^+ removal causes a remarkable initial current overshoot. This might reflect the P_{Na} of the tight junctions and a paracellular Na^+ flux along the ap. to bl. concentration gradient, since in experiments where the Na^+/H^+ exchanger was arrested with EIPA in the presence of bl. Na^+ (see below), this phenomenon was not seen. However, control experiments (not shown) where bl. Na^+ was omitted in the absence of ap. Na^+ still exhibited such an overshoot which seems to rule out a Na^+ flux.

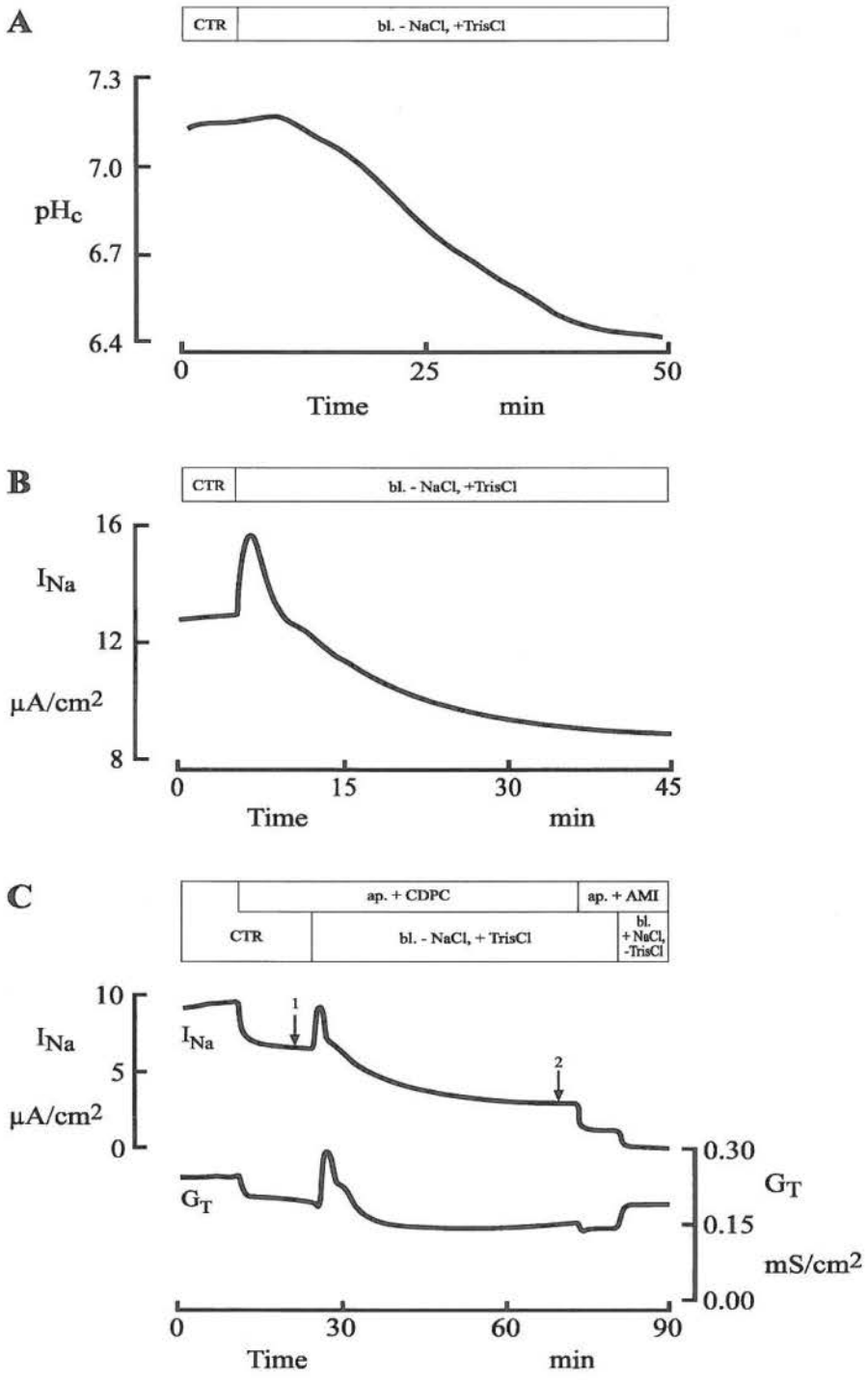
A
CTR
bl. - NaCl, +TrisCl
7.3
7.0
6.7
6.4
pHc
0
25
50
Time
min
B
CTR
bl. - NaCl, +TrisCl
16
12
8
INa
μA/cm2
0
15
30
45
Time
min
C
ap. + CDPC
ap. + AMI
CTR
bl. - NaCl, + TrisCl
bl. + NaCl, -TrisCl
10
5
0
INa
μA/cm2
1
2
GT
0.30
0.15
0.00
mS/cm2
0
30
60
90
Time
min

Figure 4.6 (A) *Effect of bl. replacement of Na^+ by $Tris^+$ on pH_c.* ***(B)*** *Same experiment as in A for another tissue; shown, however, is the time course of I_{Na}.* ***(C)*** *Time course of I_{Na} and G_T when 50 µM CDPC was first added ap. followed by bl. Na^+ replacement by $Tris^+$ (CDPC present), plus 0.1 mM ap. amiloride (AMI), and bl. cation reversal (presence of amiloride). Parameters from CDPC noise at times indicated in the figure: arrow 1: f_c = 93.4 Hz, S_o = 4.23 .10^{-20} A^2s/cm^2, i = 0.17 pA, N_o = 38.17 x 10^6 channels/cm^2; arrow 2: f_c = 97.9 Hz, S_o = 0.91 . 10^{-20} A^2s/cm^2, i = 0.16 pA, N_o = 10.42 x 10^6 channels/cm^2.*

Furthermore, since the ap. Cl^- channel blocker (Niisato and Marunaka, 1997b) NPPB had no influence on this (not shown), a contribution from Cl^- secretion (De Smet and Van Driessche, 1992; Niisato and Marunaka, 1997b) is unlikely, and the origin of this phenomenon remains obscure.

Noise analysis (a typical experiment is shown in Fig. 4.6C) led for the case of bl. Na^+ substitution by $Tris^+$ to exactly the same finding as for the cell acidification during the late phase of bl. NH_4^+ treatment (Fig. 4.4A): only N_o was reduced by Na^+ removal while i and CDPC kinetics remained unaffected. Figure 4.7 summarises the results for 8 tissues. Again, as outlined in Fig. 4.5 for the effects of ap. or bl. NH_4^+, a linear relationship was found not only between the relative Lorentzian plateaus and the relative I_{Na} (Fig. 4.7A) but also for the dependence of I_{Na} on N_o (Fig. 4.7B).

4.3.3.2.B Na^+/H^+ EXCHANGE BLOCKING BY EIPA

To check our above hypothesis that omission of bl. Na^+ brings the bl. Na^+/H^+ exchanger to a halt, we tried to inhibit it directly (Casavola et al., 1992), in the presence of Na^+, with 50 µM EIPA in the bl. bath. In Table 4.2, we show results from noise analysis of three tissues that were studied under these conditions, before and after a treatment with bl. EIPA of at least 15 min. Again, the results fully mirror those obtained above with Na^+ removal in that N_o was the sole parameter affected by the EIPA-dependent arrest of the exchanger; these results point to an EIPA-induced drop in pH_c.

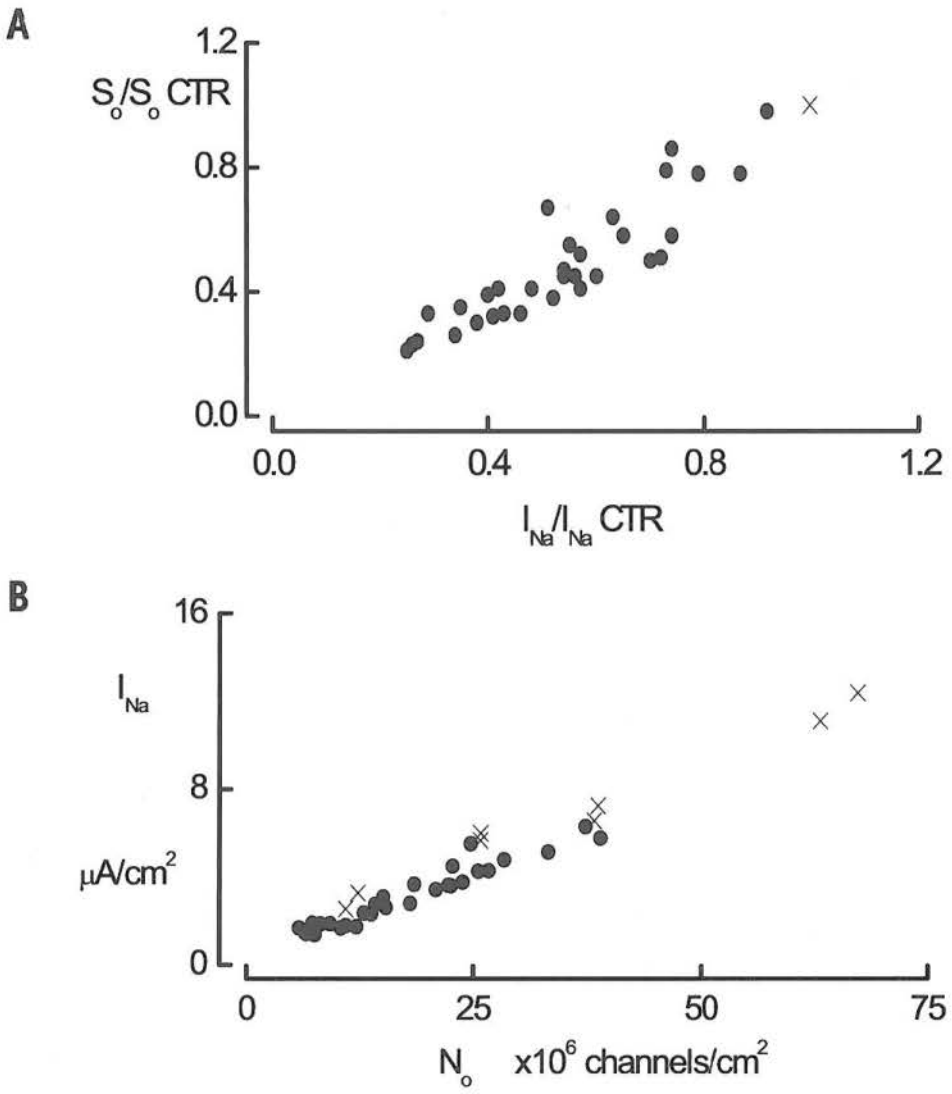

Figure 4.7 *Relationship between the relative S_o magnitudes vs. the relative Na^+ currents* ***(A)****, and linear function I_{Na} vs. N_o* ***(B)*** *from experiments where bl. Na^+ (CTR, ×) was replaced by $Tris^+$ (●). For further details, Fig. 4.5, B and C. From the slope in Fig. 4.7B we obtain a mean, pH_c-independent i = 0.178 ± 0.003 pA.*

Table 4.2 Effect of 50 μM EIPA in the bl. NaCl saline on I_{Na}, i and N_o for 3 tissues

Tissue		I_{Na} μA/cm²	i pA	N_o 10^6channels/ cm²
1	control	18.2	0.17	104
	bl. + EIPA	8.5	0.15	58
2	control	7.9	0.11	74
	bl. + EIPA	3.0	0.11	28
3	control	3.5	0.20	17
	bl. + EIPA	2.7	0.18	15

4.3.4 Cytosolic pH and macroscopic I_{Na} kinetics

Most tight epithelia display a saturating dependence of Na^+ uptake on $[Na^+]_{ap}$. This is also the case with A6 cells, and we could elucidate (Chapter 3) that two phenomena are responsible for the saturation of the macroscopic I_{Na}. With rising $[Na^+]_{ap}$, i increases and saturates with an apparent Michaelis-Menten constant K_m of 17 mM. In addition, a saturation-like decrease in N_o with even faster kinetics was found when raising $[Na^+]_{ap}$. The combined result is the fairly Michaelis-Menten-like saturation of I_{Na} with, however, an apparent 'macroscopic' K_m of ~ 5 mM (Chapter 3). These results, obtained from noise analysis, suggest that N_o plays the decisive role in determining pH_c-regulated I_{Na}.

Since both, the pH_c-independent i and the pH_c-dependent N_o are a function (both in hyperbolical but opposite ways) of $[Na^+]_{ap}$, the question arises in which manner pH_c influences N_o, i.e. by changing the channel density, or rather the K_m of its $[Na^+]_{ap}$-dependence (or both). For instance, for a rise in pH_c, an increase of N_o should become visible as an increase in maximal I_{Na} when plotting current-saturation kinetics (Fig. 4.8). An alternative would be a shift of the K_m, the half-maximal $[Na^+]_{ap}$. For many experiments, where pH_c was increased by ap. NH_4^+, or decreased by bl. NH_4^+ or Na^+ withdrawal, we obtained exactly the same result which is exemplified for the case of 20 mM bl. NH_4^+ in Fig. 4.8 in which the I_{Na} saturation function, obtained with ap. Na^+/$Tris^+$ mixtures is displayed. As shown in Fig. 4.8, we could fit a hyperbola (solid lines) to the data using a Hill-coefficient of 1, without observing any change of the apparent

macroscopic K_m. The cell acidification after bl. NH_4 had only one effect, namely, shifting the maximal current level downwards. Therefore, we do not deal with a Na^+-competitive but rather with an allosteric block of I_{Na} by cytosolic H^+.

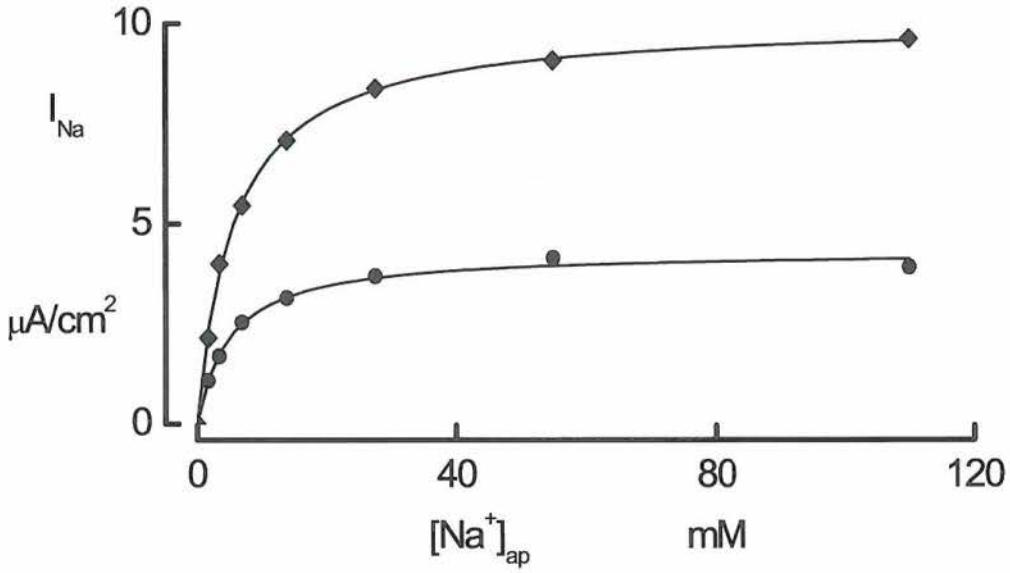

Figure 4.8 Typical example of ap. I_{Na} kinetics *(I_{Na} vs. $[Na^+]_{ap}$) in control conditions (◆), or when bl. NH_4Cl (20 mM) was introduced isosmotically (●). $[Na^+]_{ap}$ was varied by substitution for $Tris^+$. Solid lines represent hyperbolic fits to the data. The so-obtained maximal I_{Na} is 10.1 μA/cm² for control (◆) and 4.3 μA/cm² after the pH_c drop induced by bl. NH_4^+ (●). The corresponding apparent K_m values for Na^+ are 5.7 (◆) and 5.0 (●) mM, respectively.*

4.4 DISCUSSION

A6 cells possess the mechanisms for active, cAMP- and Ca^{2+}-controlled Na^+ reabsorption (Hayslett et al., 1995), and also Cl^- secretion (De Smet and Van Driessche, 1992; Niisato and Marunaka, 1997b; Zeiske et al., 1998). The virtual absence of ap. water channels (De Smet et al., 1995c) renders the cells sensitive to bl. osmotic disturbances only. There is much evidence (Harvey, 1994) that second messengers not only operate on the ap. rate-limiting barrier for ion transport processes, but also that they are able to couple properties of ap. and bl. membranes in concert for optimal transcellular ion movements. A novel coupling agent may be pH_c: in A6 and other tight epithelia (Harvey, 1994; Harvey, 1995; Harvey et al., 1988), pH_c regulates ap. P_{Na} and bl. P_K in much the same manner and within a narrow pH_c range, with maximal permeabilities at pH > 7.6 but vanishing permeabilities at pH < 6.6. In the present

chapter, we explored which ap. parameters are responsible for the pH_c-dependent modulation of ap. Na^+ channels.

So far, we may conclude that, whatever means is used to modify pH_c: (1) kinetics of blocker-induced channel fluctuations appear unaffected by pH_c; (2) with an invariant i, pH_c-invariant single-channel conductance and electrochemical ap. driving force seem reasonable assumptions; and (3) N_o available for interaction with ap. CDPC is the only parameter which plays a role in the pH_c-regulated Na^+ transport in the A6 cell line.

4.4.1 Methodological aspects

In order to evaluate pH_c-dependent parameter shifts when using either hyper- or isosmotic, NH_4Cl-containing solutions, we used a Ringer solution where NH_4Cl had been added (hyperosmotic), or replaced isosmotically 40 mM sucrose. Anisotonic addition of NH_4Cl is commonly used (Casavola et al., 1992; Cougnon et al., 1996; Harvey et al., 1988) to evoke pH_c changes. The inherent dangers are clear, and earlier data show that hypertonic salines as such decrease cell volume and N_o (Wills et al., 1991). We therefore established conditions of zero volume changes when using NH_4Cl (Fig. 4.1).

4.4.2 Complexities arising from attempts to shift pH_c with NH_4^+ pulses

With extracellular media containing NH_4^+, cell alkalinisation is a direct consequence of ammonia entry. Afterwards, acidification of the cytosol follows withdrawal of external NH_4^+ as a consequence of NH_3 efflux. (Harvey et al., 1988) Furthermore, entering of NH_4^+ through normally K^+-permeable pathways (Lyall et al., 1993), may lead to direct intracellular acidification as a result of intracellular H^+ release by NH_4^+ (De Weer, 1978; Cougnon et al., 1996). Moreover, as NH_4^+ will then compete with K^+, it may contribute to otherwise typically K^+-dependent phenomena (cation transporter fluxes, membrane polarisation or channel currents) or else, impede K^+-transporters (Zeiske and Van Driessche, 1983). Therefore, effects additional to the ones from pH_c shifts may be expected, for instance, changes in bl. membrane K^+-channel resistance and ensuing hyper- or depolarisation of a normally K^+-dependent membrane potential difference. In A6 cells at short-circuit, such a change in the negative intracellular electrical potential V_{sc} (Eq. 3.1) would immediately affect the net ap. driving force for Na^+ entry. If, as in other tissues, the bl. permeability of K^+ channels for NH_4^+ is finite (Harvey et al., 1988; Cougnon et al., 1996), the addition of K^+-mimicking ammonium to the bl. side could cause a V_{sc}-depolarisation that would impede Na^+ influx (Eq. 3.1). Such a mechanism could explain the transient initial blip-like current reduction as seen in Fig. 4.3B or Fig. 4.4A, although i, and thus V_{sc} as part of the driving force, seems unchanged at steady-state conditions (Table 4.1).

There are also hints for cellular pH-back-regulation after an externally provoked pH_c shift. The ubiquitous Na^+/H^+ antiporter which exists basolaterally in A6 cells mediates re-alkalinisation (Figs. 4.4, B and C) after NH_4^+ removal-induced acidification, an effect only observed in the presence of bl. Na^+ and in the absence of EIPA. A block of the Na^+/H^+ antiporter with EIPA excludes that a putative stop of the bl. Na^+/Ca^{2+} antiporter (Brochiero et al., 1995) with subsequent rise in cell Ca^{2+}, which has been discussed to inhibit P_{Na} (Blokkebak-Poulsen et al., 1991; Garty and Palmer, 1997; Palmer and Frindt, 1987), is responsible for the I_{Na} drop after Na^+ omission. In contrast, augmented cell calcium, e.g. after hormones that enhance I_{Na} like vasopressin, has recently been shown to have the dominant function in the stimulatory hormone action on I_{Na} in A6 cells (Hayslett et al., 1995). In fact, Lyall and co-workers (Lyall et al., 1995) suspected that a number of Na^+ uptake-activating hormones exert their effects via cell alkalinisation.

As it is generally assumed (Casavola et al., 1992) that the Na^+/H^+ exchanger (NHE) is activated only if after a certain degree of cell acidification is present, it was surprising that our manipulations that putatively stopped the exchanger caused an immediate fall in pH_c and I_{Na}. One reason could be that metabolism produces enough protons, another, that ion channels allow a constant 'leak' of protons into the cells (Lyall et al., 1993), so that the exchanger is permanently active. This was indeed the case for A6 cells, since addition of the specific NHE inhibitor HOE-694 induced an intracellular acidification of ~0.23 pH units (Casavola et al., 1997) and for frog skin (Harvey and Ehrenfeld, 1988).

In some reports on A6 cells, the points discussed above and problems arising from the choice of ill-defined experimental conditions (e.g., simple bilateral NH_4Cl exposure, including bilateral isosmotic NaCl replacement by NH_4Cl to study the Na^+/H^+ exchanger (Casavola et al., 1992) or I_{Na} kinetics (Chuard and Durand, 1992)) have been ignored. Such studies of pH_c-related transport activities are bound for erroneous interpretations, such as claiming a 'mixed competition' (Chuard and Durand, 1992) of intracellular protons with extracellular sodium ions.

4.4.3 Parameters of apical Na^+ transfer

Our data provide strong evidence that the kinetic parameters, i.e. K_m with respect to ap. Na^+ (Fig. 4.8) and f_c with respect to CDPC block (Figs. 4.4 and 4.6) are unaffected by manoeuvres that change pH_c. If i does not change with pH_c, this may infer that both γ and the net ap. driving force (Eq. 3.1) are virtually pH_c-independent: 1) at Ringer-$[Na^+]_{ap}$, the ap. Nernst potential for Na^+ is stable as the rate of the bl. Na^+/K^+-ATPase was found to be relatively insensitive to acid loading (Ehrenfeld et al., 1992; Homareda and Matsui, 1985); and 2) the practically indistinguishable pH_c-titration curves of ap. P_{Na} and bl. P_K (Harvey, 1994; Harvey, 1995) ensure that pH_c

changes both permeabilities always by the same factor, therefore yielding constant fractional membrane resistances and constant V_{sc}.

With respect to 'spontaneous' open-closed conformational changes and our inference, that N_o is pH_c-dependent whether CDPC is present or not, the 'inherent' (when blocker is absent) ENaC open probability (P_o) could be subject to pH_c which would result in a change in N_o, being the product of P_o and the total number N_T of Na^+ channels (open plus closed). Indeed, a recent report (Chalfant et al., 1999) demonstrated for the α-subunit of ENaC, expressed in *Xenopus* oocytes or reconstituted in planar lipid bilayers, that cytosolic-side acidification from pH 8 to 6.9 reduced P_o by a factor of almost 4 and reduced mean open time while increasing the mean closed time, with unaffected single channel conductance. In addition, N_T could vary if a fraction of channels, as a consequence of acidification, disappeared, either by becoming permanently closed or by endocytotic removal. With respect to the findings on the pH_c-sensitivity of patch-clamped ENaC-type epithelial Na^+ channels (Harvey, 1994; Harvey, 1995), reversible vesicle fusion may seem less likely than reversible allosteric opening-closing (by de-/protonation) of permanently resident ap. Na^+ channels, e.g. by affecting P_o. On the other hand, a drop in cell pH is known to result in ap. exocytosis of H^+ pumps in some tight epithelia (Cannon et al., 1985; Harvey, 1992). Moreover, a low intracellular pH is known to alter the cytoskeletal structure (Eskelinen et al., 1992) and the role of exocytotic events underlying the stimulatory action of several hormones on Na^+ transport in tight epithelia is heavily discussed (Garty and Palmer, 1997). For instance in A6 cells, the increase of ap. P_{Na} in the presence of either forskolin or insulin is due to the insertion of channels residing in intracellular pools (Erlij et al., 1999). Furthermore, it was shown in A6 cells that the I_{Na} stimulation by cell volume increase could be prevented by interaction with cytoskeleton-directed drugs (Niisato and Marunaka, 1997a). It was also reported that cytoskeletal elements, such as small actin filaments, induce Na^+ channel activity in A6 cells (Cantiello et al., 1991). Although some preliminary transepithelial capacitance (C_T) measurements showed no C_T decrease in acidified A6 cells, suggesting no decrease in membrane area, we are presently unable to rule out endocytosis of Na^+ channel containing vesicles. Thus, we cannot decide whether pH_c affects only P_o or also N_T.

4.4.4 Modelling of the pH_c-dependence of P_{Na}

The mechanism by which lowering the pH modulates ENaCs may involve direct interaction of protons with the channel pore or may be mediated by proton-induced conformational changes of the pore-forming membrane proteins. Fig. 4.8 suggests that we deal with an allosteric site where the interaction of internal protons should be non-competitive with external Na^+. This may also explain the pH_c-independency of i (and,

thus single channel conductance; Eq. 3.1) which is under dominant influence of external Na^+. At present, most recent publications about the presumable structure of the epithelial Na^+ channel (McNicholas and Canessa, 1997; Schild et al., 1997) do not yet provide conclusive hints for a tentative identification of the titrated allosteric intracellular site(s). However, according to the published pH_c-titration curve of the A6 Na^+ channel with $pK_a \sim 7.2$ (Harvey, 1994; Harvey, 1995) as well as for the cloned rat α-ENaC with $pK_a \sim 7.4$ (Chalfant et al., 1999) and for the wild-type rat $\alpha\beta\gamma$-ENaC expressed in Xenopus laevis oocytes with $pK_a \sim 6.6$ (Konstas et al., 2000), the pK_a-range may point to a histidine as titrated group. For instance, His-94 in the α-ENaC has been discussed by Chalfant et al. (Chalfant et al., 1999) to be a proton target during intracellular titration. Alternatively, we cannot rule out that pH-sensitive regulatory proteins of the ENaC mediate its' pH_c-dependence.

4.4.5 Summary

With respect to our data, we arrive at the following conclusions: (1) The ap. A6 cell membrane is only permeant for NH_3, and not for NH_4^+. Entry of NH_3 causes a cytosolic alkalinisation. The concomitant rise in G_T and I_{Na} is exclusively due to a rise of N_o, probably caused by allosteric opening of ap. Na^+ channels. All other parameters of ap. Na^+ transfer remain unaffected. (2) Basolateral NH_4^+ first increases pH_c (and therefore G_T and I_{Na}) due to effects identical to those discussed for ap. NH_4^+ exposure. Secondly, as pointed out also by other groups for other tissues (Cougnon et al., 1996; Harvey et al., 1988), NH_4^+ ions enter the cells. This occurs probably (Harvey et al., 1988; Knepper, 1991; Zeiske, 1990) via otherwise K^+ permeable conductive pathways, since we see an immediate rise in G_T in parallel to a drop in I_{Na}. This can easily be understood if -initially- NH_4^+, as imitator of K^+, depolarises the cell-negative short-circuit potential which reduces the net driving force for ap. Na^+ entry. Subsequent H^+ release from entered NH_4^+ ions would decrease pH_c and the ap. P_{Na} which is possibly due to a shortened open time as well as a prolonged closure (Chalfant et al., 1999), thus leading to a decrease in time-averaged open-channel density, N_o. Subsequent NH_4^+ withdrawal will tend to further acidify the cell and, depending on the activity of bl. Na^+/H^+ exchange, pH_c will recover.

Alkali ion channels deliver protons to the cytosol (Lyall et al., 1995) that will pile up in the cell when cellular metabolism is impeded (Demaurex and Grinstein, 1994) as in condition of ischemia or anoxia. This would tend to deregulate cell life. If the alkali ion channels are closed down in a negative feedback loop by cytosolic protons, the threatening acidification process might be brought to a halt. In addition, the cells would no more lose K^+ basolaterally or gain Na^+ apically and, consequently, Cl^- and water. This may prevent further cell swelling and rupture. Such mechanisms might, at least in part, account for the observed protective effects of internal H^+ when they are

derived from the 'therapeutical' acidification of the extracellular bath. Furthermore, it is most interesting that EIPA and similar drugs that stop the Na^+/H^+ exchanger –and thus lead to intracellular acidosis- have been shown to be protective in conditions of cardiac ischemia (Bugge and Ytrehus, 1995; Scholz et al., 1993).

Chapter 5

Effects of metabolic inhibition on proliferation capacity and cell viability in A6 cells

5.1 INTRODUCTION

Renal epithelial cells are morphologically and functionally specialised cells for vectorial transport of ions, water and macromolecules across the cell layers. Mostly, these transport processes are energy-dependent and, consequently, perturbed by ischemic injury. It has been shown in renal cells that ATP depletion, resulting from ischemia or from chemically induced metabolic inhibition not only affects transport processes and intracellular ion homeostasis (Brady et al., 2000) but also affects the cytoskeleton (Sutton and Molitoris, 1998; Ashworth et al., 2001), intracellular organelles such as the mitochondria (Kroemer et al., 1998), tight junctions (Canfield et al., 1991; Sutton and Molitoris, 1998), the plasma membrane (Brady et al., 2000), enzymes (Kobryn and Mandel, 1994), and the transcription of genes (Price et al., 1995). Cell death, either via necrosis or via apoptosis, is the eventual end-point of this injury.

Apoptosis and necrosis have long been considered as two distinct mechanisms of cell death, each with different biochemical, morphological and functional characteristics (Majno and Joris, 1995). Indeed, necrosis is a passive process beginning with the loss of homeostatic processes, cell swelling, major changes to the organelles such as mitochondria, nuclear swelling with flocculation of the chromatin and loss of plasma membrane integrity. The DNA is preserved initially and is non-specifically disintegrated later. Necrosis occurs in the course of acute accidental nonphysiological injuries, whereas apoptosis represents a silent form of cell death that plays distinctive roles in tissue development and homeostasis (Thompson, 1995). Apoptosis is an active energy-requiring process often characterised by the cleavage of DNA into distinct mono- (~ 180 base pairs) and oligosome fragments by endonuclease activity. Cells undergoing apoptosis also show characteristic morphological features including chromatin aggregation, nuclear and cytoplasmic condensation and partition of cytoplasm and nucleus into membrane-bound vesicles (apoptotic bodies) which contain ribosomes, morphologically intact mitochondria and nuclear material. *In vivo*, these apoptotic bodies are rapidly recognised and phagocytised by either macrophages or adjacent epithelial cells (Savill, 1994; Lieberthal et al., 1998). Due to this efficient mechanism that removes apoptotic cells *in vivo* without plasma membrane damage, no inflammatory response is elicited. *In vitro*, if apoptotic bodies are not taken up by adjacent cells, the remaining cell fragments ultimately swell and finally lyse. This terminal phase of in vitro cell death has been termed 'secondary necrosis'.

In the literature, there is now growing evidence to the idea that apoptosis and necrosis may share common events in the death process (Lemasters, 1999) and represent only the extremes of a continuum of intermediate biochemical and morphological forms of cell death (Raffray and Cohen, 1997; Kroemer et al., 1998; Formigli et al., 2000). In particular, it has been shown that it is the magnitude of the initial insult, rather than the

type of the stimulus, that plays a critical role in the decision of the cell to undergo either apoptosis or necrosis (Bonfoco et al., 1995; Formigli et al., 2000) and that common activators and inhibitors characterise the two forms of cell death. In fact, anti-apoptotic genes, such as *bcl-2* have been shown to inhibit both apoptotic and necrotic cell death induced by oxygen depletion (Shimizu et al., 1996). The downstream controller capable of directing the cells toward either type of cell death seems to be the intracellular ATP content (Eguchi et al., 1997) according to the well-accepted idea that high-energy levels are required for the execution of the apoptotic program, whereas they are dissipated during necrosis (Leist et al., 1997; Lieberthal et al., 1998; Formigli et al., 2000).

In this chapter, the time courses of inhibition of A6 cell proliferation and cell viability during metabolic inhibition were investigated. Moreover, we examined whether MI provokes apoptosis, necrosis or intermediate forms of cell death in A6 cells.

5.2 RESULTS

5.2.1 Proliferation capacity of A6 cells after metabolic inhibition

The DNA synthesis in A6 cells was monitored via ^{3}H-thymidine incorporation. DNA synthesis significantly ($P \leq 0.05$) decreased after exposure to metabolic inhibitors during 1 hour (Fig. 5.1). The proliferation was reduced to 61 ± 6 % (N = 19) compared to controls. After 6 hours of MI, DNA synthesis further decreased to only 3 ± 1 % (N = 23) of controls. The fact that still 61 % of the initial cell proliferation capacity is reached after 1 hour of MI suggests that the majority of cells are still alive.

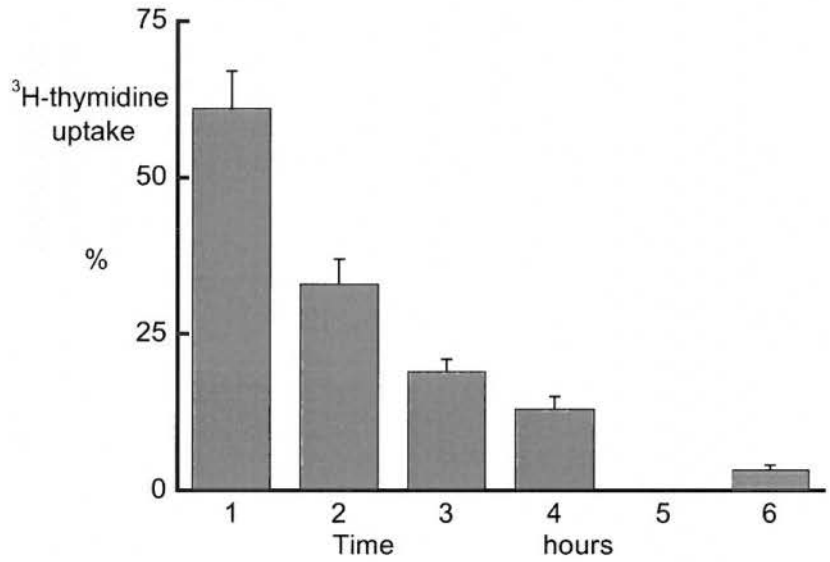

Figure 5.1 Effect of MI on DNA synthesis in A6 cells using ^{3}H-thymidine as a marker. *Data are shown as percentages (mean ± SEM) of control cells (without MI), which were set as reference (100 %).*

5.2.2 Detection of DNA fragmentation by agarose gel electrophoresis

DNA fragmentation was used as a marker for apoptosis, since laddering is found almost universally in apoptotic cells. The DNA of untreated control cells (Fig. 5.2, lane 1) or DNA of cells treated during 30 min with metabolic inhibitors (Fig. 5.2, lane 3) did not produce any DNA laddering after electrophoresis on an agarose gel. In contrast, the appearance of DNA fragments of ~180 base pairs (mononucleosomes) after 1 to 2 hours of MI (lane 4 and 5 in Fig. 5.2) might indicate apoptotic DNA disintegration. Only after at least 7 hours of exposure to metabolic inhibitors a slight DNA laddering appeared.

DNA laddering was accompanied with a smear pattern on the agarose gel, a typical feature of necrotic cell death.

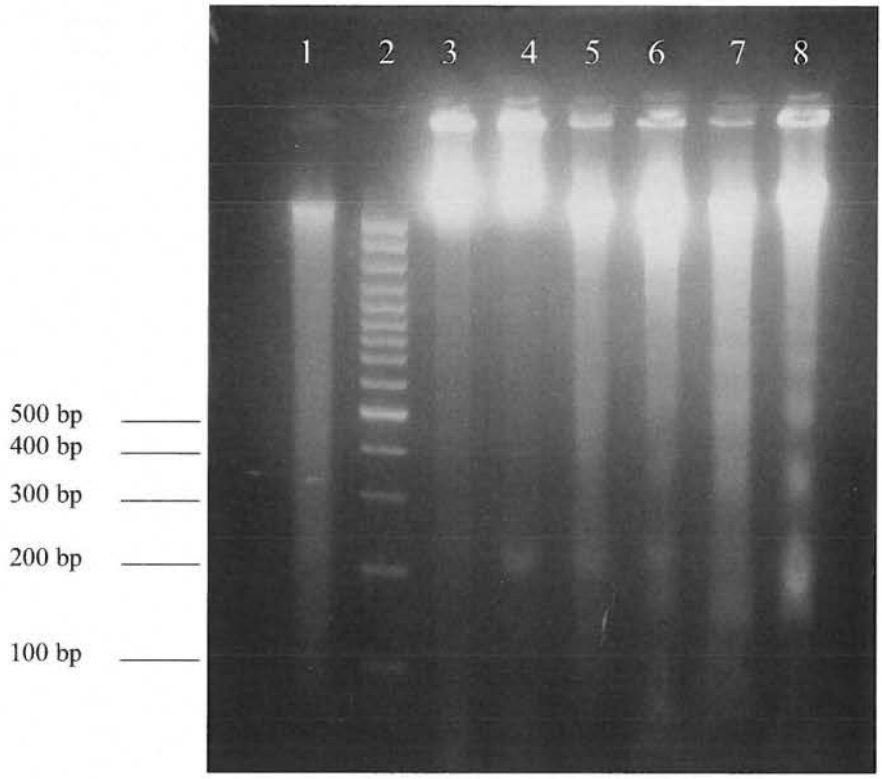

Figure 5.2 Detection of DNA fragmentation by agarose gel electrophoresis. *Lane 2 shows the 100 base pairs (bp) ladder used as standard (smallest DNA fragments of 100 bp appear at the bottom of the gel). Lane 1 shows the DNA of untreated control cells. Lanes 3 – 8 indicate DNA of A6 cells after, respectively, 0.5, 1, 2, 7, 16 and 20 hours of MI.*

5.2.3 Ethidium bromide staining of necrotic cells

Ethidium bromide (EB) was used to detect necrotic cells. Since EB can only enter cells when cellular plasma membrane integrity is lost, increased EB fluorescence intensity points to an increased number of necrotic cells in the investigated monolayers. After one hour of ATP depletion, only a very small increase was observed in the number of EB positive cells (Fig. 5.3). This observation held true during the first hours of MI. After ~ 8 hours of MI, a pronounced increase in the number of necrotic cells was seen, whereas untreated A6 monolayers did not display increased EB fluorescence on that time scale. A

prolongation of the exposure to metabolic inhibitors up to 16 hours or more, induced necrotic cell death in practically all A6 cells.

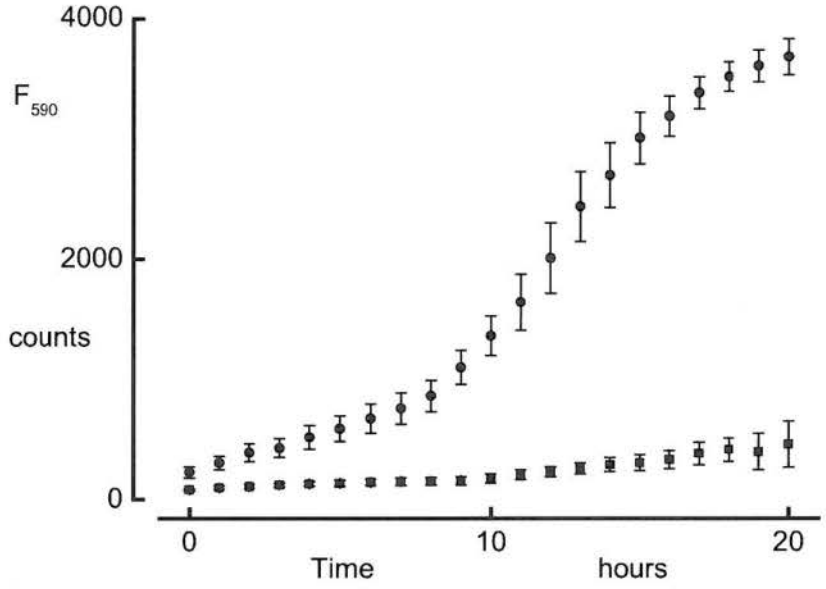

Figure 5.3 Evaluation of ethidium bromide fluorescence during 20 hours of MI in A6 cells. *The EB fluorescence (F) emission at 590 nm is plotted as a function of time for A6 monolayers exposed to Ringer without (squares, N = 3) or with metabolic inhibitors (circles, N = 5). The error bars indicate the SEM.*

5.2.4 Trypan blue exclusion

To distinguish between viable and irreversibly damaged cells, the ability of cells to exclude trypan blue was assessed in A6 monolayers exposed to CN and DOG for a period ranging from 0 (control) to 24 hours (Fig. 5.4). A qualitative light microscopic analysis confirmed the EB fluorescence measurements described in the previous paragraph. Only incubation with CN and DOG for at least 8 hours (Fig. 5.4C) resulted in a significant number of blue-stained, i.e. necrotic, cells. After 16 hours of MI, all cells were necrotic and a minority of cells detached from the support. Longer incubation periods induced a more pronounced cell detachment. Finally, complete cell lysis resulted in the cellular debris seen in Fig. 5.4F.

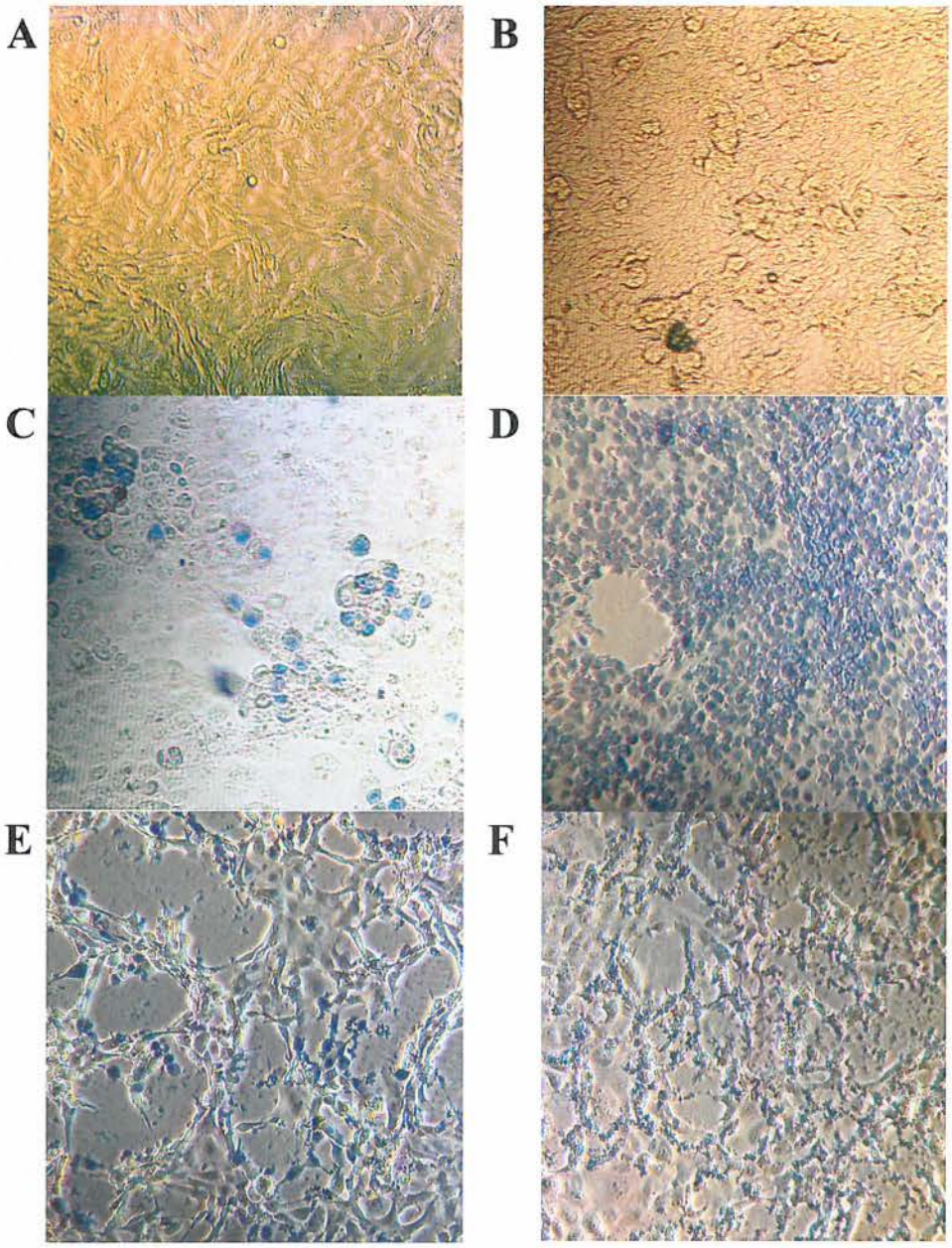

Figure 5.4 Trypan blue exclusion test of metabolically inhibited A6 cells. *Light microscopic pictures of A6 cells in control conditions (A) or after 4 (B), 8 (C), 16 (D), 20 (E) or 24 hours (F) of MI. Necrotic cells appear as blue-stained cells, whereas living cells remain unstained.*

5.2.5 Ultrastructural analysis

Ultrastructural changes during metabolic inhibition of A6 cells were evaluated by transmission electron microscopy (TEM). Control A6 cells exhibited quite normal ultrastructural features (Fig. 5.5A). They formed a homogeneous flattened monolayer well adherent to the underlying permeable support. Cells were small and oriented with their basolateral surface to the supporting substrate. The cytoplasm was well organised, containing numerous apical mitochondria (Fig. 5.5B). The control cells displayed a round-shaped euchromatin-rich nucleus. Apical microvilli, tight junctions and desmosomes were present (Fig. 5.5, C and D).

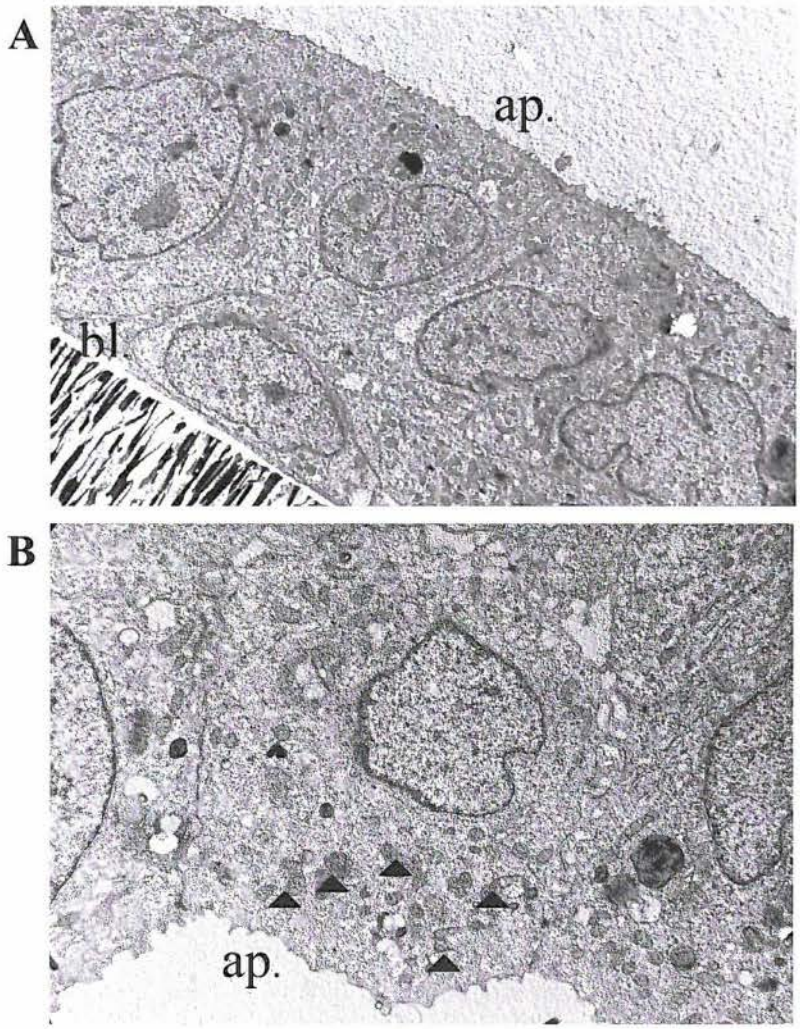

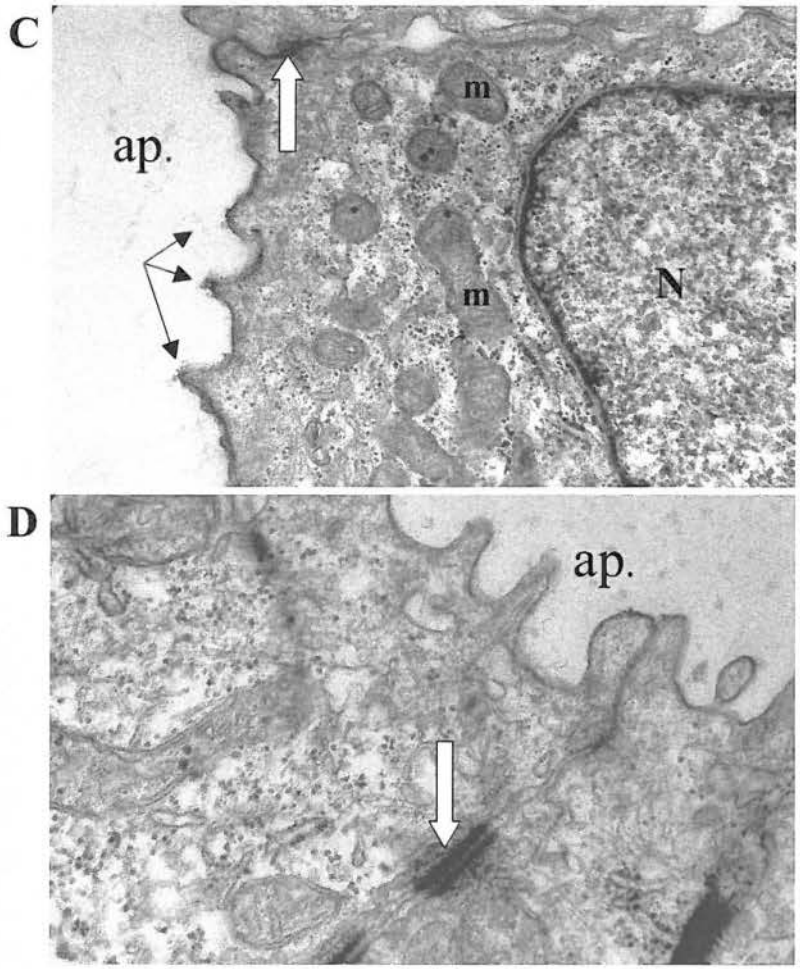

Figure 5.5 TEM analysis of A6 cells in control conditions. ***(A)*** *A6 monolayer oriented with the bl. surface to the permeable support (x2,800).* ***(B)*** *Detail of an A6 cell. Mitochondria (black arrowheads) were predominantly located at the apical (ap.) side of the epithelium (x7,100)* ***(C)*** *High power electron micrograph showing apical microvilli (black arrows), a tight junction (white arrow), mitochondria (m) and a part of the euchromatin-rich nucleus (N) (x20,000).* ***(D)*** *High power electron micrograph of a desmosome (white arrow) and a tight junction (x44,000).*

When A6 cells were subjected to 1 or 2 hours of MI, cellular morphology did not noticeably change, except for a pronounced cell swelling. Occasionally, an apoptotic cell, characterised by typical margination of the condensed chromatin in a crescent-shaped mass on the inner surface of the nuclear membrane, was detected (Fig. 5.6A). In epithelial cell cultures, apoptotic bodies are often phagocytised by neighbouring cells (Majno and Joris, 1995; Lieberthal, 1997).

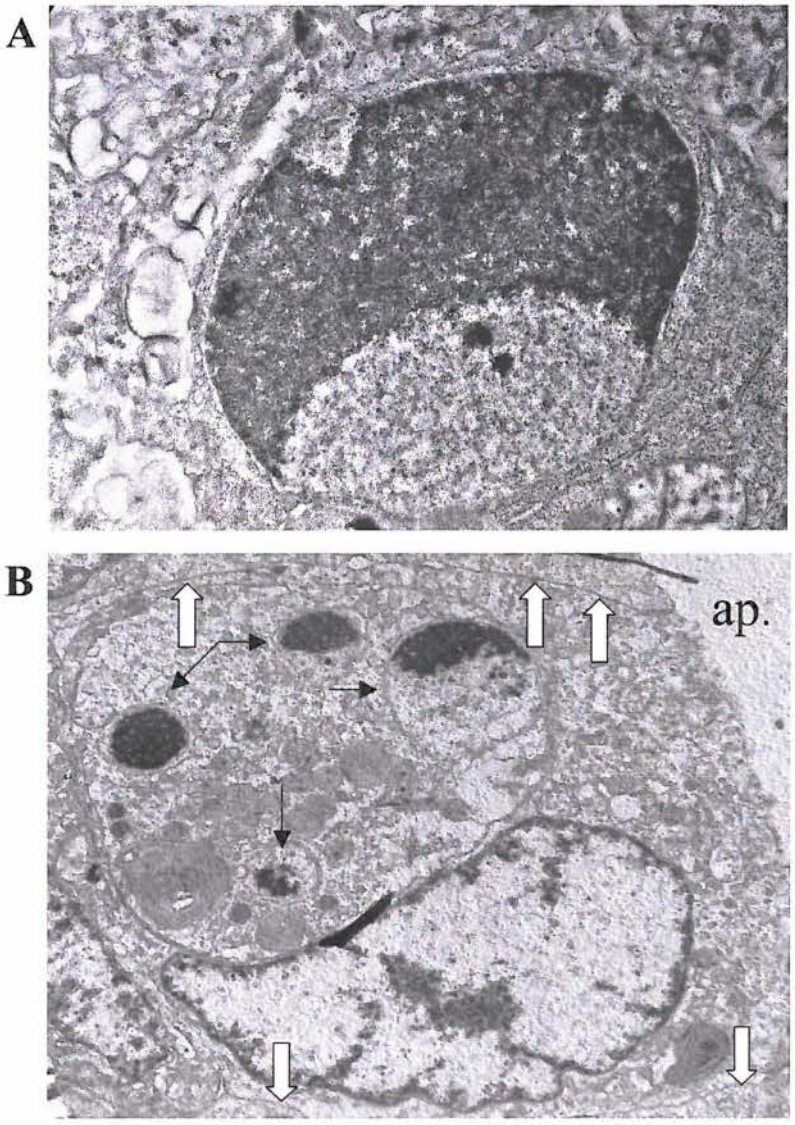

Figure 5.6 Ultrastructure of apoptotic cell remnants after short-term metabolic inhibition. ***(A)*** *The cell, detected after 1 hour of MI, displayed typical nuclear modifications namely formation of a crescent-like mass of highly condensed chromatin against the nuclear envelope. (x18,000) (B) Detail of apoptotic bodies(black arrows) incorporated in a neighbouring epithelial cell, detected after 2 hours of MI. Note the closure of the lateral intercellular spaces (white arrows) and the disappearance of apical microvilli due to epithelial cell swelling. (x7,100)*

Fig. 5.6B illustrates the phagocytosis of apoptotic bodies by neighbouring cells. The surrounding epithelial cell is clearly swollen, accompanied by the disappearance of apical microvilli and the closure of the lateral intercellular spaces.

After treatment with metabolic inhibitors, the cells displayed progressive phases of necrosis. Rupture of the plasma membrane was preceded by the appearance of morphological abnormalities that were indicative of grossly disturbed cellular homeostasis, including cell swelling, clumping of nuclear chromatin along the nuclear envelope, mitochondrial swelling and disturbance of the mitochondrial architecture, surface blebbing and nuclear degeneration (Fig. 5.7).

In contrast with the condensation of chromatin seen in apoptotic cells, the clumped chromatin is not significantly redistributed in necrotic cells. Moreover, the aggregates are less uniform in texture, have less sharply defined edges and are irregularly scattered through the nucleus (Fig. 5.7 B) rather than being sharply segregated at its periphery (Kerr et al., 1995). At a late stage of necrosis, the chromatin degenerates and disappears completely. After 8 hours of MI, plasma membrane rupture was detected in some cells.

Surface blebs are typical of ischemic cell death (Majno and Joris, 1995). They are blister-like, fluid-filled structures, typically devoid of organelles, that arise from the cell membrane. Usually they gradually swell and burst. Some blebs are reversible. Blebs differ from the budding phenomenon seen in apoptotic cells. Contrary to blebs, buds do not swell and buds may contain cell organelles, including nuclear fragments (Majno and Joris, 1995).

The ultrastructural changes in the late phase of necrosis are illustrated in Fig. 5.8.

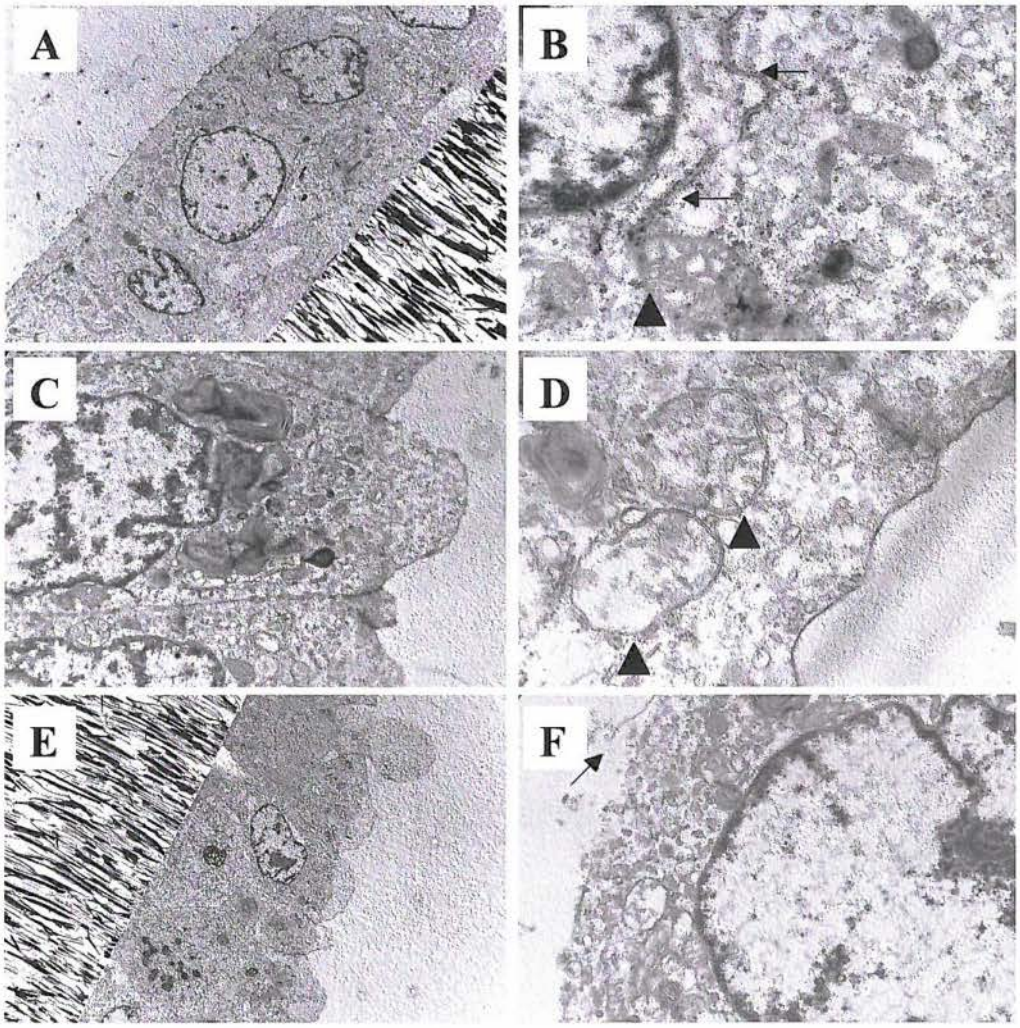

Fig. 5.7 Overview of the ultrastructural changes preceding necrotic plasma membrane rupture in metabolically inhibited A6 cells. ***(A)*** *After 4 hours of MI, nuclear chromatin was clumped. (x3,500)* ***(B)*** *Detail of clumped chromatin in the nucleus. The cytoplasm contained intact RER with adhered ribosomes (black arrows). Some mitochondria (arrowhead) were clearly swollen. (x28,000)* ***(C)*** *Surface blebbing appeared after 6 hours of MI. (x8,900)* ***(D)*** *Mitochondria (arrowheads) were swollen and their typical structure was degenerated. (x28,000)* ***(E)*** *After 8 hours of MI, the nucleus of some epithelial cells disappeared. (x2,200)* ***(F)*** *Rupture of the plasma membrane (arrow) occurred in a minority of cells after 8 hours of MI. (x18,000)*

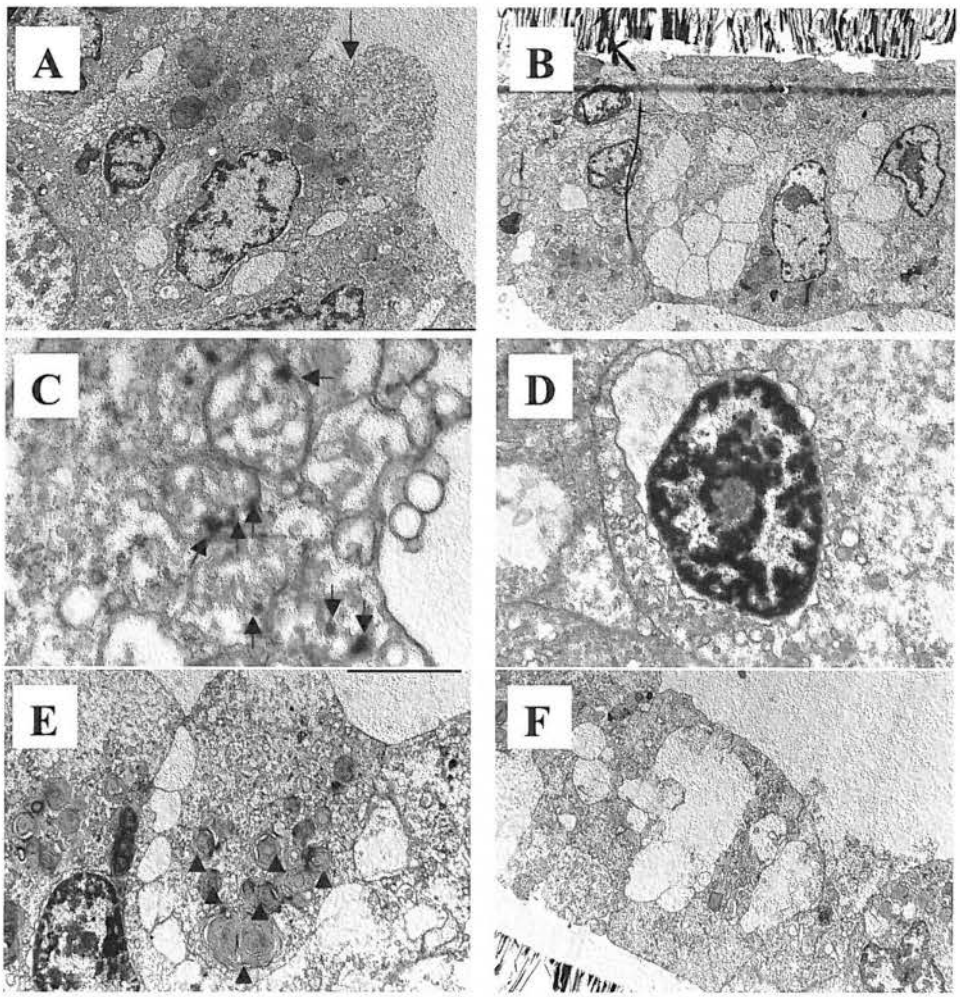

Figure 5.8 Ultrastructural changes in the late phase of necrotic cell death of A6 cells facing MI. ***(A)*** *After 12 hours of MI, ~ 50 % of the cells displayed a ruptured plasma membrane (arrow). Cells started to detach from their neighbouring cells as indicated by the appearance of vacuoles in between cells inside the monolayer. (x5,600)* ***(B)*** *Degeneration of cells within the cell layer is more pronounced after 16 hours of MI. (x2,800)* ***(C)*** *Mitochondria displayed floccular densities (arrows), a typical feature of necrotic cell death (Kerr et al., 1995). (x36,000)* ***(D)*** *Detail of chromatin clumping in the nucleus and 'blebbing' of the outer nuclear envelope. (x14,000)* ***(E)*** *Most nuclei were degenerated and the cytoplasm totally lost its architecture after 24 hours of MI. The intracellular membrane systems (Rough Endoplasmic Reticulum and Golgi apparatus) vacuolated completely. Ribosomes were dispersed as individual ribosomes and polyribosomes. Large dense bodies (arrowheads) appeared in the cytoplasm. (x7,100)* ***(F)*** *Debris of the cell layer after 24 hours of MI. (x3,500)*

5.3 DISCUSSION

5.3.1 Determination of the cell death pathway in metabolically inhibited A6 cells: apoptosis and/or necrosis ?

In the past few decades different methods were developed to recognise the different features of cell death. Unfortunately, the results of these methods are not always unequivocal. Therefore, it was recommended that independent methods were used to distinguish between apoptotic and necrotic cell death.

Many studies have focussed on the specific patterns of endonucleolytic DNA fragmentation that are a signature of apoptosis, partially because this was one of the first biochemical hallmarks identified (Wyllie, 1980), but also because of its ease of detection. The presence of oligonucleosome-sized fragments of DNA, which, when run on agarose gels, produce 'ladders', demonstrates apoptosis. However, nucleosomal ladders are not essential for demonstration of apoptosis, since the apoptotic process can occur without this type of DNA fragmentation (Ramachandra and Studzinski, 1995; Kerr et al., 1995; Raffray and Cohen, 1997). Moreover, several descriptions now exist in isolated cell systems of necrotic cell morphologies accompanied by 'apoptotic' internucleosomal DNA cleavage (Collins et al., 1992; Ojcius et al., 1991), and conversely of morphological apoptosis accompanied by 'necrotic' smearing of DNA fragments (Yoshida et al., 1996). Recently, Venkatachalam and co-workers (Dong et al., 1997) described 'necrotic DNA ladders' in ATP depleted Madin-Darby Canine Kidney (MDCK) cells, a model cell line for mammalian distal tubules. The internucleosomal DNA cleavage occurred soon after the loss of plasma membrane integrity. Moreover, provision of glycine along with the metabolic inhibitors did not modify the extent of ATP depletion, but prevented plasma membrane damage. This was accompanied by complete inhibition of DNA fragmentation. The latter illustrates that not the ATP depletion –as such- caused necrotic DNA laddering, but rather the necrotic plasma membrane rupture resulting from prolonged MI. This might explain the detection of DNA laddering along with a 'smear' pattern after at least 7 hours of MI in A6 cells. As illustrated in EB fluorescence experiments and trypan blue exclusion light microscopic pictures, necrotic plasma membrane rupture occurred only after at least ~7 hours of MI in A6 cells. This phenomenon might subsequently trigger internucleosomal DNA cleavage as described for MDCK cells (Dong et al., 1997) and result in DNA laddering superimposed on the smear DNA pattern typical for necrotic cells.

Ultrastructural analysis clearly demonstrated the occurrence of the necrotic cell death pathway of A6 cells during MI. Although almost all cells displayed necrotic cell death features, some occasional apoptotic cells or apoptotic remnants in neighbouring epithelial cells were detected after 1 hour of MI. It is known that apoptosis typically involves scattered individual cells in a tissue (Kerr et al., 1995). Apoptotic bodies formed in cell cultures frequently escape phagocytosis and spontaneously degenerate within a few

hours (Kerr et al., 1995). In epithelial cell cultures, apoptotic bodies are often phagocytised by neighbouring cells (Majno and Joris, 1995; Lieberthal, 1997). This clearance mechanism is extremely efficient, and apoptotic cells and apoptotic bodies disappear rapidly from the tissue without any trace. For this reason, apoptosis is usually difficult to detect in tissue sections, even when responsible for extensive cell loss (Lieberthal, 1997). Therefore, we cannot exclude apoptosis as an important cell death pathway in the early phase of MI when intracellular ATP levels (see section 6.3.2 in Chapter 6) are still sufficient to supply for the active cell death program. However, it is unrealistic to suppose substantial apoptotic cell death in the first phase of MI, since A6 monolayers are able to restore their transepithelial transport function completely in 2 hours time after total loss of function during 45 min of MI (see section 6.3.1 in Chapter 6). Recently, several studies have shown apoptosis in renal tubule cells including LLC-PK1 cells (Wiegele et al., 1998), MDCK cells (Wiegele et al., 1998; Allen et al., 1992), and mouse proximal tubule cells (Lieberthal et al., 1998) subjected to metabolic inhibition as well as rat kidney proximal tubules (Saikumar et al., 1998) subjected to ATP depletion. In general, the *in vitro* studies have shown apoptosis and DNA fragmentation in renal tubular cells during hypoxia as well as reoxygenation (Ueda and Shah, 2000). Based on the information in the literature, the *in vivo* studies of ischemia/reperfusion so far demonstrate apoptosis only during the reperfusion period. However, much of the evidence for the role of apoptotic mechanisms in renal tubular cell injury comes from the questionable oligonucleosome-length DNA fragmentation.

In this study almost all A6 cells died via the necrotic cell death pathway after prolonged MI. Similarly, prolonged ATP depletion induced necrotic cell death in proximal LLC-PK1 and distal MDCK epithelial cell cultures (Wiegele et al., 1998). This study and previous reports (Wiegele et al., 1998; Lieberthal et al., 1998) confirm the concept that necrosis and apoptosis are modulated by the ATP availability (Eguchi et al., 1997; Leist et al., 1997; Lieberthal et al., 1998; Formigli et al., 2000). As will be described in Chapter 6 for A6 cells, intracellular ATP levels drop to less than 20 % of the untreated cells during 45 min of incubation with metabolic inhibitors. This level of ~ 20 % in the initial phase of the insult has been reported to represent a threshold that determines whether cells die by necrosis (< 20 %) or apoptosis (> 20 %) in the later phases of the insult (Lieberthal et al., 1998; Formigli et al., 2000). Lieberthal and co-workers (Lieberthal et al., 1998) showed that cultured mouse proximal tubular cells subjected to severe ATP depletion died by necrosis, whereas moderate ATP depletion resulted in apoptosis. Thus, as in A6 cells, necrosis developed in the case of severe depletion of the energetic stores, which excluded the active apoptotic cell death pathway.

In this chapter, cell death was associated with necrotic plasma membrane rupture as demonstrated by trypan blue colouring of cytoplasmic proteins, EB intercalation in cellular DNA or morphologically via TEM. However, cell death and necrosis are two different manifestations. Cell death refers to the 'point of no return' or the point where

the cell is unable to maintain homeostasis. Cells might functionally die long before any necrotic changes can be seen by light, fluorescence or electron microscopy (Majno and Joris, 1995; Trump and Berezesky, 1998). Therefore, detection of cell death in this study probably refers to detection of late phase structural changes of dying cells.

5.3.2 Summary

The results of this chapter indicate that distal tubular A6 cells are quite resistant to MI. Plasma membrane rupture was only detected after a prolonged (> ~ 8 hours) exposure to metabolic inhibitors, which is quite a long time as compared to the substantial lactate dehydrogenase release from MDCK cells after only ~2 hours of ATP depletion (Dong et al., 1997). This characteristic makes the A6 cell culture an appropriate *in vitro* model for studying the cellular processes that occur in the surviving distal tubular cells during ischemia. We should however mention that, although the study of renal cell cultures provides valuable insights into the mechanisms determining the cellular behaviour in stress conditions, a direct extrapolation of the results from a cultured cell line to the *in vivo* situation should be done with caution. For instance, tubular cells *in vivo* can interact with other tubular and vascular segments and other extracellular factors e.g. in the blood, which is of course impossible in our A6 cell culture model.

Chapter 6

The role of intracellular ATP and pH in the reversible suppression of Na^+ transport in metabolically inhibited A6 cells

6.1 INTRODUCTION

In general, a prolonged period of renal ischemia leads to irreversible changes in structure and function of renal cells, which finally results in cell death. As a consequence, the damaged kidney fails to maintain fluid and salt homeostasis of the body. In contrast, the changes in renal cell function induced by a short exposure to ischemic conditions may be fully reversible (Brady et al., 2000). Since the regeneration of the kidney after an ischemic insult is based on the capacity of surviving cells to recover and proliferate, it is important to examine the cellular events that occur in sublethally injured epithelial cells. The results in chapter 5 demonstrate that necrotic plasma membrane rupture only occurs after at least ~ 8 hours of exposure to metabolic inhibitors in A6 cells. Therefore, the 45 min exposure time to metabolic inhibitors that is applied in this chapter and chapter 7, is expected to induce no lethal structural changes to A6 cells but rather sublethal injury at most. In this chapter, the effects of MI were investigated at the level of salt reabsorption in distal tubular A6 cells.

ATP depletion is considered to be the central mediator of ischemic cellular injury. Since the transepithelial Na^+ transport in A6 cells is ATP-dependent, the time course of the cellular ATP content was examined during MI. ATP depletion is generally followed by impairment of ion homeostasis, cell depolarisation and cellular acidification (Brady et al., 2000). Acidification in ischemic, ATP depleted cells can result from glycolytic lactate production, CO_2 accumulation, ATP hydrolysis and the failure of H^+-extrusion mechanisms to counterbalance the constant passive proton influx. It was shown in early studies on heart muscle (Bing et al., 1973), Ehrlich ascites tumor cells (Penttila and Trump, 1974) and rat hepatocytes (Bonventre and Cheung, 1985) that cytosolic acidification can be cytoprotective under hypoxic or anoxic conditions. More recently, this effect was also reported for isolated renal proximal tubules (Weinberg et al., 1991; Zager et al., 1993; Edelstein et al., 1996) and for the isolated perfused kidney (Shanley et al., 1988). Therefore, intracellular pH was measured in metabolically challenged A6 cells and pH_c effects on the evolution of I_{Na} during MI were examined.

Mitochondria are increasingly recognised as an important target of toxicity in ischemic conditions. The consequences of mitochondrial dysfunction are even thought to determine whether a cell will undergo either primary necrosis or apoptosis in conditions of prolonged ischemia (Kroemer et al., 1998). However, the role of mitochondrial dysfunction in cell injury is not yet completely understood. Recently, it has been suggested that during ischemia the mitochondrial ATP synthase could reverse and consume ATP while serving to maintain the mitochondrial membrane potential ($\Delta\Psi_m$) (Duchen and Biscoe, 1992; Leyssens et al., 1996; Di Lisa et al., 1995; Duchen, 1999; St-Pierre et al., 2000). A high $\Delta\Psi_m$ allows Ca^{2+} accumulation into mitochondria, thereby avoiding a Ca^{2+} overload of the cytoplasm (Silverman, 1993). Considering the

importance of mitochondria in the energy metabolism of cells, measurements of the mitochondrial redox state, reflected by changes in NAD(P)H autofluorescence, and of the mitochondrial membrane potential, will give valuable information about mitochondrial function in conditions of metabolic inhibition.

6.2 MATERIALS AND METHODS

6.2.1 I_{sc} and G_T measurements for comparison of ouabain (OUAB) treated and metabolically inhibited A6 cells (MI): solutions and protocol

The tissues were initially incubated in Ringer solutions (composition in mM for OUAB experiments: 102 NaCl, 2.5 $KHCO_3$, 1 $CaCl_2$; for MI experiments: normal control Ringer, see Chapter 2) with an osmolality of ~ 200 mOsm/kgH_2O. When I_{sc} attained a constant value, in both protocols Na^+ was replaced by $NMDG^+$ in the bl. solution so that only 10 mM Na^+ was left. Thirty minutes later, all ap. Na^+ was replaced with $NMDG^+$. In that way, conditions with minimised Na^+ influx were realised without disturbing the bl. Na^+/H^+ exchangers and Na^+/Ca^{2+} exchangers to the same extent as with bl. Na^+-free solutions. Subsequently, the tissues were treated with ouabain or metabolic inhibitors and ap. Na^+-free solutions were changed to the original Na^+ containing solutions after 60 or 45 min respectively. Finally, the sodium current was blocked by 100 µM ap. amiloride (AMI).

6.3 RESULTS

6.3.1 The metabolic inhibition of transepithelial Na^+ transport is fully reversible

The effect of MI on the major physiological function of distal kidney epithelial A6 cells, transepithelial salt reabsorption, was investigated. Therefore, the transepithelial transport, which mainly reflects active Na^+ reabsorption in A6 cells, was monitored as the short-circuit current (I_{sc}) in an Ussing-type set-up (see chapter 2 for details). As depicted in Fig. 6.1, I_{sc} dropped steadily during MI and disappeared completely after a 45 min incubation period with CN and DOG. Nevertheless, this loss of physiological function was not associated with irreversible cell damage, since the A6 tissues were able to repair their active salt transport completely during the subsequent recovery phase. Initial transepithelial transport levels were reached after ~ 90 minutes of superfusion with recovery Ringer. To elucidate the underlying mechanisms of I_{sc} suppression during MI, we focussed first on the energy supply for the Na^+/K^+-ATPase in the bl. membrane.

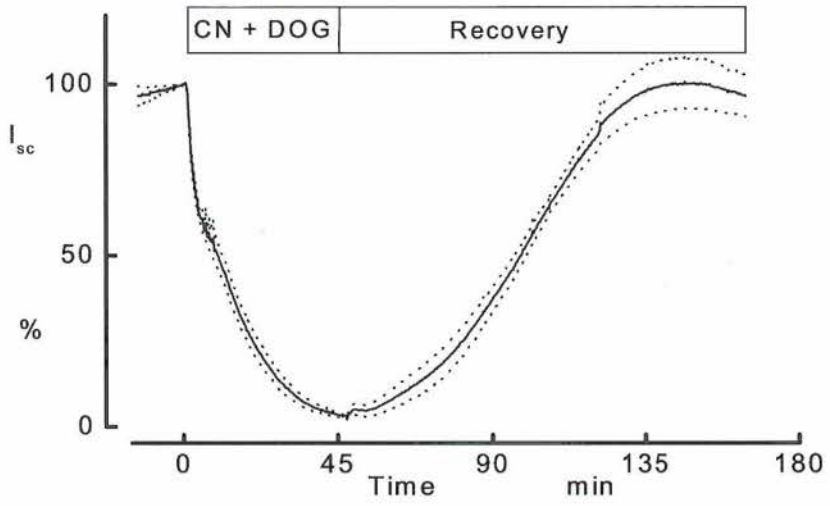

Figure 6.1 Time course of I_{sc} during MI and subsequent recovery. *The short-circuit current is expressed as percentage of the value recorded just before the tissues were exposed to CN and DOG containing solutions. The initial absolute value of I_{sc} was 22.3 ± 0.8 μA/cm², which is a high transport rate (see Chapter 7). Mean I_{sc} values (solid line) are given with SEM (dotted lines) for four different tissues during 45 min of metabolic inhibition and 2 hours of recovery.*

6.3.2 Time course of intracellular ATP content during MI and subsequent recovery

Measurements of intracellular ATP content (Fig. 6.2) revealed that ATP dropped gradually during MI. A 45 min incubation period with metabolic inhibitors reduced intracellular ATP content to 18 ± 3 % (N=7). This level of ~ 20 % of the control level in the initial phase of the insult has been reported to represent a threshold that determines whether cells die by necrosis (< 20 %) or apoptosis (> 20 %) in the later phases of the insult (Lieberthal et al., 1998). A prolongation of exposure to CN and DOG (up to 2 hours) resulted in a further drop to only 3 ± 0 % (N=6) of the initial ATP level, indicating that the rather high level of ATP after 45 min of MI was not resulting from methodological errors. After 45 min of MI, bathing of the cells in recovery Ringer allowed A6 cells to restore their ATP content to 50 % of the control level in maximally 10 min without significant changes during the remaining of the recovery phase (41 ± 6 % after 2 hours).

The mean intracellular ATP concentration, calculated from the absolute amount of ATP in the cell extracts and the estimated volume of a monolayer of A6 cells (height ~ 8 μm) on the Nunc Anopore Membrane, was 8.6 ± 0.6 mM (N=19). This estimated ATP

concentration is high as compared to the 'normal' ATP concentrations which are in the order of ~5 mM depending on the cell type (Li et al., 1993).

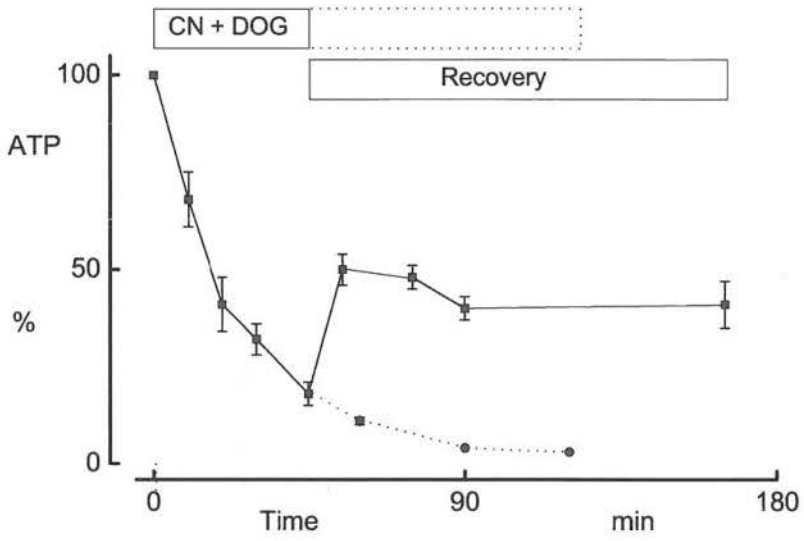

Figure 6.2 Effect of MI and recovery on the intracellular ATP content of A6 cells. *ATP levels are indicated as % of the level in control tissues. The solid line shows the evolution of the intracellular ATP content during 45 min of MI and a subsequent recovery of 2 hours. The dotted line indicates the further drop of ATP during a prolonged MI up to 2 hours. Shown are the mean ± SEM values from different monolayers with N varying between 5 and 9.*

6.3.3 Time course of intracellular ATP content during separate blockage of glycolysis and mitochondrial respiration and during a subsequent recovery period

The cytoplasmic glycolysis contributes to a similar extent to the total cellular ATP production in A6 cells as the mitochondrial oxidative respiration (Fig. 6.3). Moreover, when both metabolic inhibitors are combined, their effects tend to be additive. Incubation of the cells with CN alone was performed in the presence of glucose in the Ringer solution. In these conditions glucose, derived from the external solution or from endogenous glycogen, which is present in A6 cells (Fidelman et al., 1982), is the only source for intracellular ATP production via the glycolytic pathway. Upon recovery, mitochondria participate again in the cellular ATP production provided that the action of CN is reversible and that no mitochondrial damage occurred in the preceding period. Conversely, DOG seems to block cellular glycolysis irreversibly in A6 cells, since no significant increase in ATP production was seen upon recovery. If pyruvate, the end-product of glycolysis, was the only substrate for the mitochondrial Krebs cycle, incubation with DOG would also inhibit mitochondrial ATP production. Therefore, a

similar behaviour of cellular ATP levels would be expected as in the condition of CN and DOG incubation. In A6 cells, the cellular ATP content during DOG incubation is less reduced as compared to incubation with both metabolic inhibitors. This indicates the utilisation of endogenous substrates for mitochondrial respiration in A6 cells.

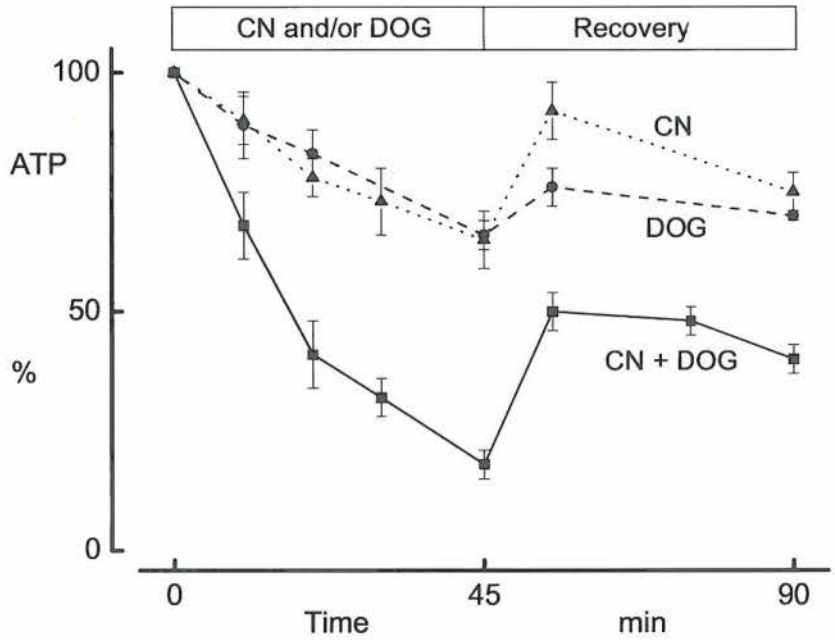

Figure 6.3 Effect of CN and/or DOG incubation and subsequent recovery on the intracellular ATP levels of A6 cells. *ATP levels are indicated as % of the level in control tissues. The solid line (copied from Fig. 6.2) shows the evolution of the intracellular ATP content during incubation with both metabolic inhibitors and a subsequent recovery. The dashed line shows the time course of intracellular ATP levels during 45 min incubation with DOG (in the absence of CN) and during a 45 min recovery period. The dotted line indicates the behaviour of A6 cells incubated with CN in the presence of glucose during 45 min and during a subsequent recovery phase providing glucose (10 mM) instead of pyruvate as substrate. Shown are the mean ± SEM values from different monolayers with N varying between 4 and 8. Solution osmolalities were kept constant (~200 mOsm/kgH_2O) by adjusting the sucrose content of the solution.*

6.3.4 NAD(P)H autofluorescence during MI and recovery

Since DOG irreversibly inhibits glycolysis (Wick et al., 1957; Leyssens et al., 1996) (Fig. 6.3), the fast recovery of intracellular ATP content seen in Fig. 6.2 implies a fast washout of CN and rapid re-activation of mitochondrial oxidative metabolism starting from either endogenous substrates (e.g. fatty acids) or pyruvate that was

provided in the recovery solution. NAD(P)H autofluorescence measurements were performed to check whether mitochondrial electron transport could indeed restart quickly on CN washout. Since mitochondrial NADH, the primary source of electrons for the electron transport chain, is only fluorescent in its reduced form, an increase in NAD(P)H autofluorescence indicates a shift of the mitochondrial NADH/NAD^+ redox state towards the reduced form. As expected, NAD^+ reduction occurred immediately following cyanide-induced inhibition of mitochondrial electron transport (Fig. 6.4). NAD(P)H autofluorescence rose to 117 ± 1 % from control level (N=6). During MI (15 min) the signal decreased gradually to 104 ± 2 % and the subsequent removal of metabolic inhibitors resulted in a fast decrease of NAD(P)H autofluorescence to values well below those observed under control conditions (81 ± 2 %). The sharp decrease in the amount of reduced NADH, during the first minutes of recovery, clearly indicates the fast reversibility of the action of CN on the cytochrome c oxidase complex.

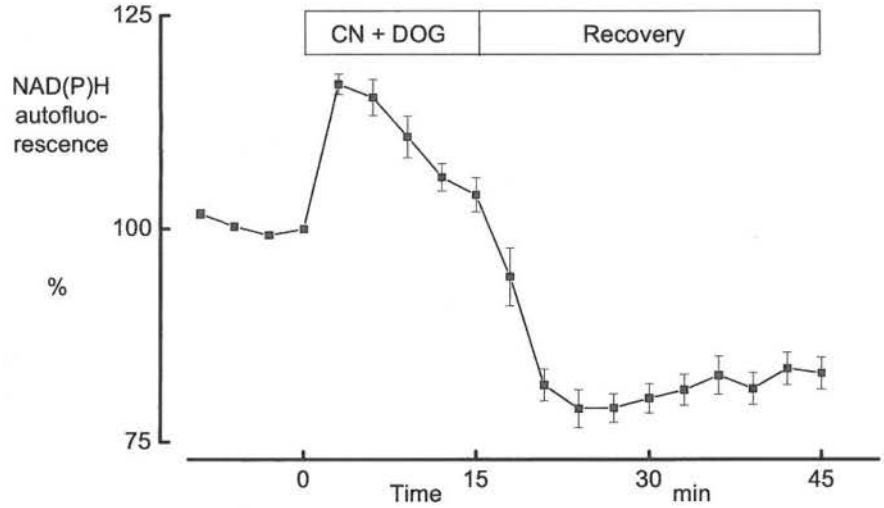

Figure 6.4 Effect of MI and recovery on NAD(P)H autofluorescence. *NAD(P)H autofluorescence is expressed as percentage of the value recorded just before the tissues were exposed to CN and DOG containing solutions. Mean values are given with standard errors for 6 different tissues during 15 min of MI and 30 min of recovery.*

6.3.5 ATP consumption during MI: contribution of I_{Na} and other ATP consumers

To determine the contribution of the active transepithelial Na^+ transport in the consumption of cellular ATP during MI, the ATP consumption was measured without and with inhibition of particular ATP consuming processes. First, the transepithelial Na^+ transport was inhibited either via blockage of Na^+ entry through ap. ENaCs with

amiloride (100 µM) or by way of arresting the bl. Na^+ pump with ouabain (100 µM)(Fig. 6.5A). The ATP consumption during MI was only slightly diminished in the presence of the transport inhibitors. Hence, the transepithelial Na^+ transport was only a minor ATP consuming activity during MI.

Secondly, other active processes that might account for major ATP consumption during MI were investigated. Recently, it was proposed that MI might reverse the mode of action of the mitochondrial ATP synthase (Duchen and Biscoe, 1992; Di Lisa et al., 1995; Leyssens et al., 1996; Duchen, 1999). This implies that the F_1F_0-ATPase consumes ATP (instead of producing it) to pump protons out from the matrix. In that way, the pump might try to avoid the collapse of the proton motive force in conditions where the electron transport chain is inhibited (St-Pierre et al., 2000). To check whether this reversal of the mitochondrial pump takes place in metabolically inhibited A6 cells, ATP measurements were performed in the absence and presence of oligomycin, a specific blocker of the mitochondrial ATP synthase. When the metabolic inhibitors were administered in combination with oligomycin, the rate of ATP depletion was markedly reduced during the first 10 min of MI (Fig. 6.5B). Afterwards, the rate of ATP consumption was similar to the condition without blockage of the mitochondrial ATP synthase. This suggests that, at least during the first 10 min of MI, the F_1F_0-ATPase might consume a major amount of intracellular ATP in an attempt to preserve mitochondrial potential. The oligomycin action on the F_1F_0-ATPase was irreversible, as illustrated by the absence of recovery of the intracellular ATP content in the subsequent recovery phase.

Figure 6.5 ATP consumption by the Na^+/K^+-ATPase and the mitochondrial F_1F_0-ATPase during MI. A, B. *The cellular ATP content, expressed as percentages from control, is indicated during MI and recovery for monolayers without (solid line) and with inhibition of active Na^+ transport (panel A) or of mitochondrial F_1F_0-ATPase (panel B). Transepithelial transport was inhibited either via blockage of Na^+ entry through ap. ENaCs with ap. amiloride (AMI, 100 µM, dashed line in panel A) or via arresting the bl. Na^+ pump with bl. ouabain (OUAB, 100 µM, dotted line in panel A). Blockage of the mitochondrial F_1F_0-ATPase was realised by adding the irreversible blocker of the ATP synthase, oligomycin (OLIG, 20 µg/ml, dashed line in panel B) to the ap. and bl. bath. The solid line in both panels was copied from Fig. 6.2. Shown are the mean ± SEM values from different monolayers with N = 5 or 6.* **C.** *Changes in the mitochondrial potential, as assessed by the ratio R_{norm} (see results for details), are shown for MI and recovery in the absence (solid line, N=6) or presence (dashed line, N=7) of oligomycin (on both sides, 20 µg/ml). Mean values are given ± SEM The symbol * indicates a statistical significant difference between both curves with $P<0.05$. The symbol (*) indicates a difference between both curves with $P<0.1$.*

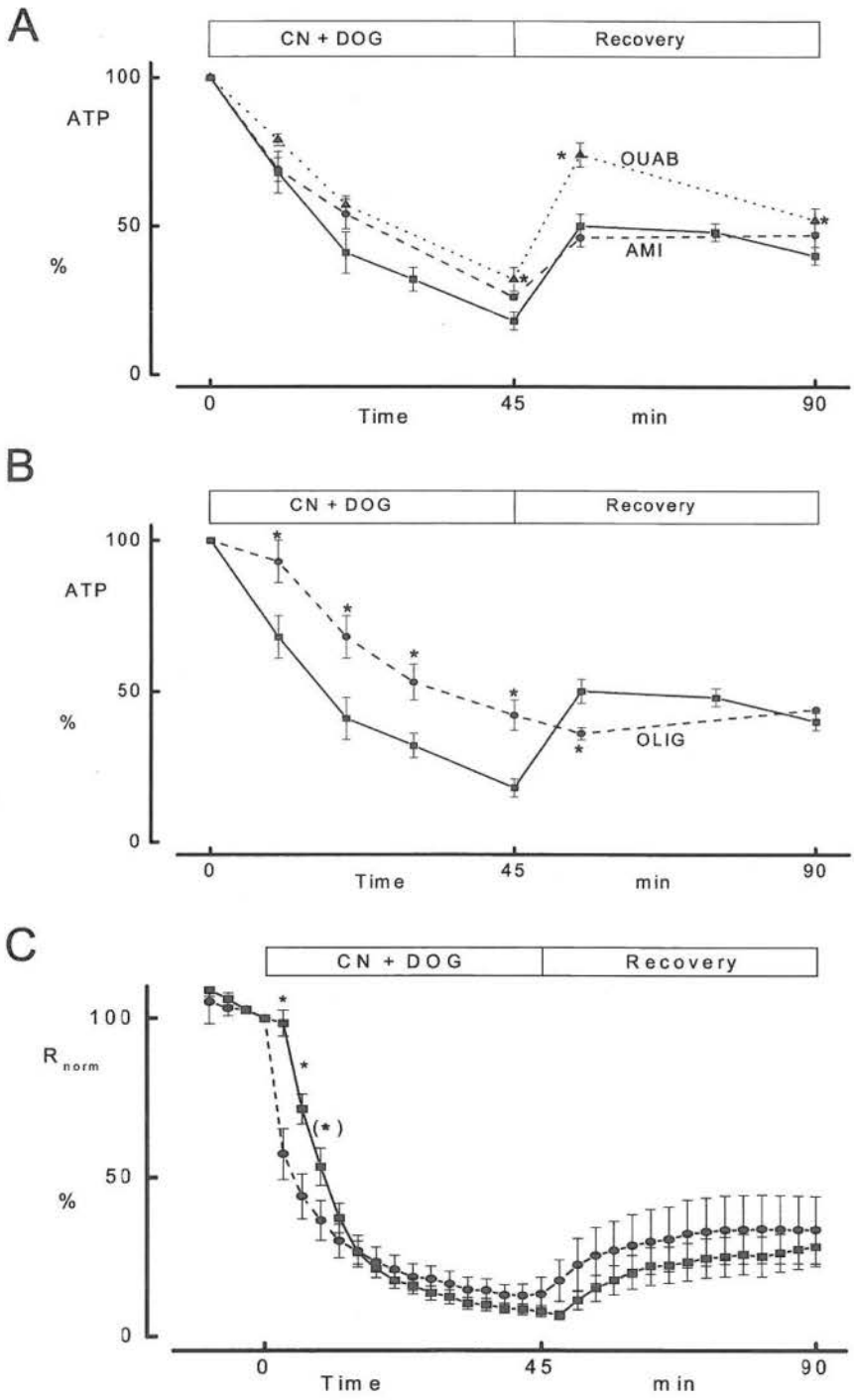
A
CN + DOG
Recovery
100
ATP
50
%
0
OUAB
AMI
0
Time
45
min
90
B
CN + DOG
Recovery
100
ATP
50
%
0
OLIG
0
Time
45
min
90
C
CN + DOG
Recovery
100
R norm
50
%
0
(*)
0
Time
45
min
90

To further test the hypothesis of mitochondrial ATP synthase reversal, the mitochondrial potential ($\Delta\Psi_m$) was evaluated with the fluorescent indicator JC-1. The emission ratio F_{590}/F_{535} was used as a parameter for $\Delta\Psi_m$ (see Methods). To allow comparison of experiments with different control ratios, the JC-1 ratios were normalised. The following expression was used to calculate the percentage of the emission ratio F_{590}/F_{535} (R_{norm}) compared to the ratio in control conditions:

$$R_{norm} = \frac{R - R_{FCCP}}{R_{control} - R_{FCCP}} \times 100 \qquad (6.1)$$

where $R_{control}$ is the ratio in control conditions and R_{FCCP} is the JC-1 ratio after adding the protonophore FCCP (10 µM) at the end of each experiment. FCCP, in the presence of DOG (20 mM), was added to determine the JC-1 emission ratio associated with a fully collapsed mitochondrial membrane potential. Mostly, large variations in dye loading efficiency were recorded among cells in one A6 monolayer. Moreover, various intensities of JC-1 fluorescence were found in mitochondria from the same cell, suggesting that the mitochondria within the same cell do not have an identical membrane potential. Similar heterogeneities have been reported for a number of cell cultures including MDCK cells, a renal distal tubular cell line (Smiley et al., 1991; Diaz et al., 1999). Despite these variations in F590, F535 and $R_{control}$ among different cells in one monolayer, the behaviour of R_{norm} during the experimental protocol was very similar for these cells.

Fig. 6.5C illustrates the time course of the drop of $\Delta\Psi_m$ in response to CN and DOG incubation and a subsequent recovery period. Although, the mitochondrial potential was maintained during the first minutes of MI, $\Delta\Psi_m$ depolarised steadily to 26 ± 4 % of control in 15 minutes. Hereafter, $\Delta\Psi_m$ declined further - but slower - to 8 ± 2 % of control after 45 min of MI. In the first 25 min of the subsequent recovery phase the mitochondrial potential partially recovered and reached a plateau value of 25 ± 6 % from the control value. The same protocol was repeated (on different monolayers) in the presence of oligomycin (20 µg/ml). Oligomycin was added to the Ringer solutions 10 min before the start of MI and did not induce a change in $\Delta\Psi_m$. In the presence of oligomycin $\Delta\Psi_m$ dropped significantly faster in the first 10 min of MI, but no differences in behaviour were seen afterwards. As in the absence of oligomycin, the mitochondrial membrane potential partially recovered upon removal of the metabolic inhibitors, suggesting that the electron transport chain restarts the pumping of protons out of the mitochondrial matrix. The acceleration of mitochondrial depolarisation in the presence of oligomycin is consistent with the putative reversal action of the F_1F_0-ATPase in the first phase of MI.

The accumulation of the cation JC-1 in cells depends on the plasma membrane potential. Subsequently, it partitions into mitochondria, which have a highly negative membrane potential. Since MI might result in cellular depolarisation, it was necessary

to check whether changes of the plasma membrane potential influenced the fluorescence of JC-1. Exposure of the cells to gramicidin D (10 μM), to depolarise the plasma membrane, induced no changes in the JC-1 ratio in A6 cells (results not shown). Hence, an interference of the plasma membrane potential with the $\Delta\Psi_m$ measurements was ruled out.

In an attempt to identify the other ATP consumers during MI, cells were exposed to metabolic inhibitors in combination with 1 μM thapsigargin, a specific inhibitor of the sarco/endoplasmic Ca^{2+}-ATPase (SERCA). To avoid the harmful effects of a cellular Ca^{2+} overload, SERCA pumps serve to accumulate cytoplasmic Ca^{2+} into the endoplasmic reticulum. In general, a rise of intracellular Ca^{2+} can be expected in ATP depleted cells (Brady et al., 2000). A study on Madin-Darby canine kidney cells, a mammalian distal tubular cell line, reported that application of 5 mM CN and 5 mM DOG resulted in a 6 fold increase in intracellular Ca^{2+} (McCoy et al., 1988). Moreover, preliminary experiments on A6 cells demonstrated a rise of intracellular Ca^{2+} to 169 ± 5 % (N=6) as compared to control during 45 min of MI with CN and DOG (Stobiecka et al., 2001). Therefore, the SERCA pumps were thought to contribute to ATP consumption during MI. However, exposure to thapsigargin simultaneous with metabolic inhibitors did not reduce ATP consumption during MI (results not shown). The plasma membrane Ca^{2+} ATPases are additional candidates to pump out the excess of intracellular Ca^{2+} ions. Their contribution to cellular ATP consumption was not tested.

6.3.6 Reduction of the apical Na^+ permeability during MI

Since transepithelial Na^+ transport recovered completely in 2 hours (Fig. 6.1), with less than 50 % of the initial cellular ATP content (Fig. 6.2), one can suppose that at least in the first 20 min of MI (ATP level > 40 % of control) pumps were fuelled with sufficient ATP to drive active Na^+ reabsorption at a normal rate. However, a pronounced drop of I_{sc} was seen in this early phase of MI (Fig. 6.1). Therefore, we investigated whether I_{sc} suppression could also result from modulation of apical Na^+ influx. Apical entry of Na^+ through ENaCs is the rate-limiting step of the transepithelial Na^+ transport in normal conditions (Biber and Curran, 1970) and therefore, up- or downregulation of transepithelial transport usually is mediated via changes in the number of open ENaCs and/or via modulation of the single channel current through the channels (e.g. Chapters 3 and 4). To examine whether apical Na^+ influx is hindered under conditions where cell metabolism is compromised, we monitored transepithelial conductance G_T and the short-circuit current I_{sc} carried by Na^+. An experimental protocol was designed that allowed comparison of I_{sc} changes monitored for epithelia treated with the Na^+ pump inhibitor ouabain (Fig. 6.6A) or exposed to CN and DOG (Fig. 6.6B).

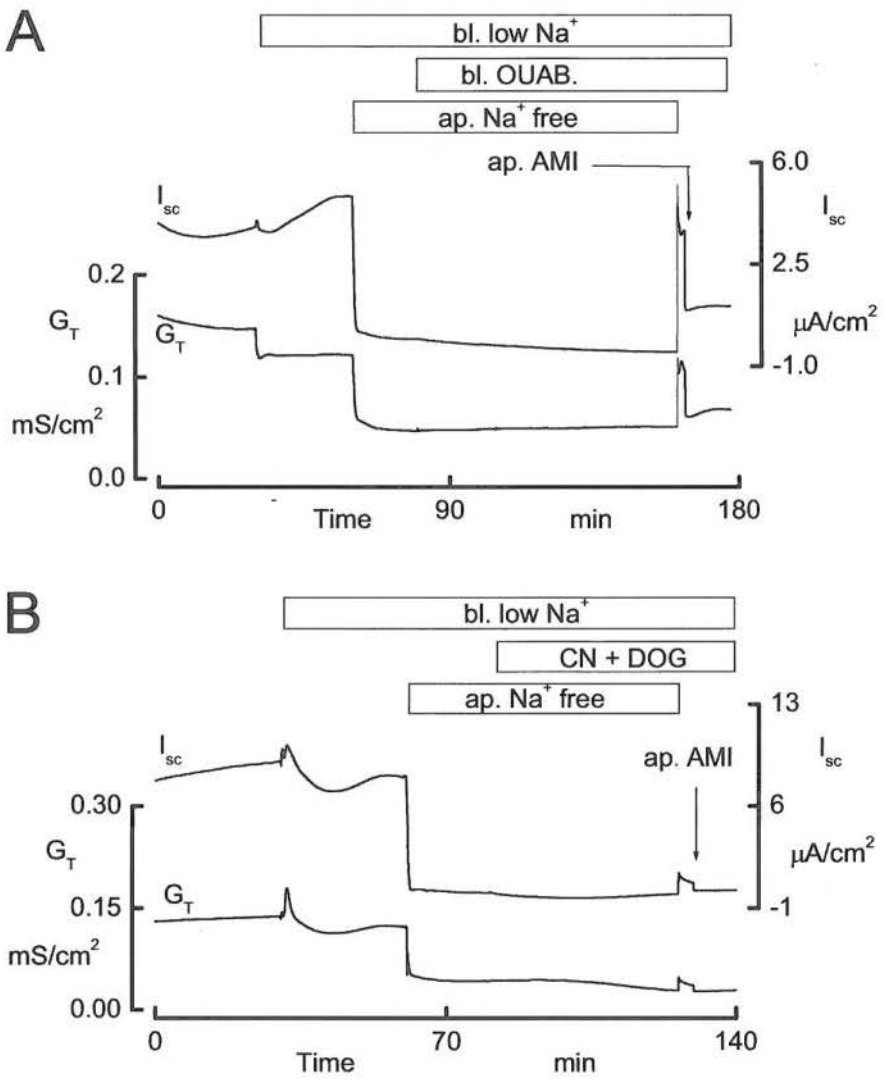

Figure 6.6 Comparison of I_{sc} and G_T changes in ouabain treated and metabolically inhibited cells in conditions with minimised Na^+ influx. *Na^+ influx was minimised by replacing apical Na^+ with $NMDG^+$ and by lowering the bl. Na^+ concentration to 10 mM NaCl.* ***A.*** *After 60 min incubation with bl. ouabain (OUAB, 100 µM) ap. $NMDG^+$ was again replaced with NaCl. Amiloride (AMI, 100 µM) was added to the apical solution to verify whether I_{sc} reflects a transepithelial Na^+ current. A representative example is shown from 4 similar experiments.* ***B.*** *MI was realised with DOG (20 mM) at both sides of the monolayer and NaCN (2.5 mM) exclusively at the bl. side to maintain Na^+ free conditions at the apical side. A typical example is shown from a series of 7 experiments.*

Since electron microprobe analysis showed that ouabain treatment of A6 cells leads to an accumulation of Na^+ in exchange for K^+ (Borgmann et al., 1994), our experiments were designed to minimise Na^+ influx into the cells. First, the bl. Na^+ concentration was lowered to 10 mmol/l in order to reduce the bl. chemical driving force for Na^+ influx. Secondly, apical Na^+ was replaced with $NMDG^+$. In that way, a 60 min incubation period with ouabain did not result in intracellular Na^+ accumulation, as confirmed by the remarkable I_{sc} peak seen when apical Na^+ was reapplied (Fig. 6.6A). Since ouabain was still present in the bl. solution at the moment of ap. Na^+ provision, the transepithelial I_{sc} current results from passive Na^+ entry through open ENaCs in the apical membrane and subsequent passive K^+ efflux via bl. K^+ channels. In contrast, cells treated with metabolic inhibitors during 45 min displayed only a very small I_{sc} increase upon apical Na^+ administration (Fig. 6.6B). Since this protocol was designed to prevent intracellular Na^+ accumulation and cellular K^+ efflux, an unfavourable electrochemical driving force for Na^+ entry was unlikely to account for the absence of the I_{sc} peak. However, G_T – that is dominated by the apical membrane Na^+ permeability (P_{Na})– clearly indicates a marked drop in P_{Na} in metabolically inhibited cells as compared with ouabain treated tissues. Therefore, these results suggest that the absence of the expected I_{sc} peak upon ap. Na^+ administration might be due to the closure of the majority of ap. ENaCs in 45 min of MI.

6.3.7 The reversible intracellular acidification of metabolically inhibited A6 cells

In Chapter 4 we showed that changes in I_{Na} and G_T, which is mainly determined by the ap. membrane conductance, are positively correlated to changes in the intracellular pH. Hence, internal protons are possible candidates to mediate the reduction of apical Na^+ entry in cells exposed to metabolic inhibitors. Therefore, pH_c measurements were performed to verify whether cells indeed acidify during MI (Fig. 6.7). Intracellular pH was assessed using the fluorescent probe CMFDA. The administration of metabolic inhibitors induced a steady intracellular acidification from $pH_c = 7.02 \pm 0.03$ to 6.46 ± 0.03 (N=6). The small drop of pH_c seen at the start of the recovery period can be ascribed to pyruvic acid, provided as substrate in the recovery solution, that enters the cell and releases its proton. This was verified in separate experiments were the replacement of glucose in the Ringer solution with pyruvate induced a slight intracellular acidification (results not shown). During the remaining of the recovery phase, cells were able to recover partially their intracellular pH ($pH_c = 6.72 \pm 0.07$, N=6) in 45 min. Probably, the pH_c recovery was not yet completed in these 45 min. These results indicate that internal protons might indeed play a role in the suppression of I_{sc} during MI since their concentration increased dramatically upon addition of metabolic inhibitors. Since cells re-alkalinise during recovery, the apical Na^+ permeability might increase again and hence, I_{sc} is allowed to recover gradually.

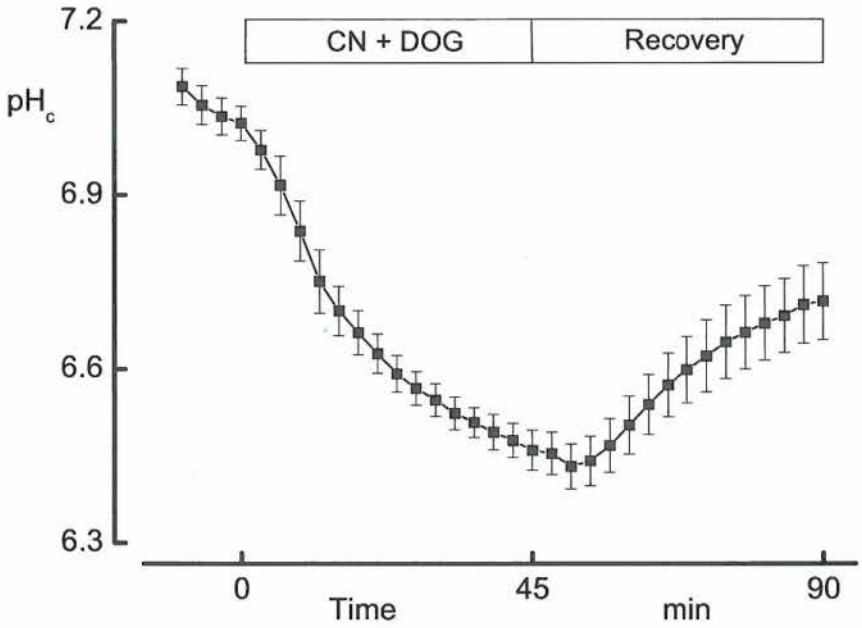

Figure 6.7 pH_c during MI and a subsequent recovery period in A6 cells. *MI was realised by superfusing the tissues at both sides during 45 min with 2.5 mM CN and 20 mM DOG. In the recovery phase metabolic inhibitors were removed from the solutions and pyruvate was added as substrate. The osmolality of the solutions was 200 mOsm/kgH_2O. Mean pH_c values are given ± SEM (N = 6).*

6.4 DISCUSSION

In this chapter, the effects of metabolic inhibition, a model that mimics the ATP depletion and associated stress of ischemia, were investigated on the active transepithelial Na^+ transport of distal tubular epithelial A6 cells.

6.4.1 The metabolic arrest of transepithelial Na^+ transport is fully reversible

The full recovery of transepithelial Na^+ transport in A6 cells proves that the cells are not lethally injured during 45 min of MI. The partial recovery of the cellular ATP

content and the cell viability experiments combined with morphological analysis in the previous chapter point toward the same conclusion.

6.4.2 The coupling of ATP depletion and intracellular acidification during MI

Measurements of the intracellular ATP content revealed that ATP dropped gradually to 18 % of the control level in 45 min of MI. A complete ATP depletion (< 3 % of control) required exposure to metabolic inhibitors for at least 2 hours. In contrast, inhibition of both glycolysis and oxidative metabolism in LLC-PK_1 cells, a model cell line for mammalian (37 °C) proximal tubular cells derived from pig kidney, resulted in a profound depletion of ATP levels to < 4% of the control level within 30 min (Doctor et al., 1994) or even within 5 min as reported for mouse proximal tubular cells and MDCK cells (Sheridan et al., 1993). The slower depletion of the cellular ATP content in A6 cells is probably due to the low metabolism of these cells cultured at 28 °C. Similarly, the rate of oxygen consumption in A6 cells is significantly lower than that for MDCK cells (Lynch and Balaban, 1987). The major role of the incubation temperature was demonstrated by the similar oxygen consumption rates of A6 cells at 37 °C as compared to MDCK cells and other cultured mammalian cells at 37 °C (Lynch and Balaban, 1987).

After 45 min of MI, bathing of the cells in recovery Ringer allowed A6 cells to restore their ATP content to 50 % of the control level in 10 min without significant changes during the remaining of the recovery phase. DOG is an irreversible blocker of cellular glycolysis in A6 cells (Fig. 6.3). Consequently, the fast recovery of the intracellular ATP content is attributed to a fast washout of CN and a rapid re-activation of mitochondrial oxidative metabolism as confirmed by NAD(P)H autofluorescence measurements. The absence of glycolytic metabolism in the recovery phase might explain that the cells only partially (~50 %) restored their cellular energy content, since the cytoplasmic glycolysis and mitochondrial oxidative respiration display an equal contribution in the total cellular ATP production in A6 cells (Fig. 6.3). These results are consistent with a recent report that showed that the ATP used by Na^+ pumps of apically digitonin-permeabilised A6 epithelia is generated to the same extent by glycolysis and oxidative phosphorylation (Guerrero et al., 1997). The difference in intracellular ATP level at the end of the recovery period after 45 min of incubation with DOG alone or incubation with both metabolic inhibitors (CN+DOG) suggests an incomplete recovery of mitochondrial ATP production in the latter case (Fig. 6.3). This might result from an incomplete washout of cyanide from the cytochrome c oxidase complex. However, this difference might also be attributed to mitochondrial dysfunction after a condition of severe ATP depletion. During limited periods of ischemia, mitochondria undergo reversible morphologic and biochemical alterations that may limit their ability to produce ATP (Bonventre et al., 1988). It has been shown for isolated mitochondria of brain neurons that respiration is severely depressed (by 50 % or more) for at least one hour after the ischemic period (Hillered et al., 1984; Sun and Gilboe, 1994). Moreover,

prolonged ischemia results in the formation of elevated concentrations of adenosine, inosine and hypoxanthine, which readily diffuse across plasma membranes, thereby reducing the pool of cellular adenine-containing compounds that serve as a reservoir for the resynthesis of purine nucleotides during recovery (Warnick and Lazarus, 1981). Recently, the release of ATP -as such- was demonstrated during cell swelling in response to a hyposmotic shock in a number of cell types, including human airway epithelial cells (Musante et al., 1999) and human intestinal epithelial cells (Dezaki et al., 2000). Since MI induces a profound cell swelling in A6 cells (see Chapter 7), swelling-induced ATP release might contribute to the incomplete recovery of the cellular ATP level in the recovery phase.

The substrates for mitochondrial respiration in A6 cells consist for the greater part of endogenous substrates. This is evidenced by the difference in the drop of intracellular ATP levels during incubation of A6 cells with DOG alone and with DOG in combination with CN (Fig. 6.3). If pyruvate, the end-product of glycolysis, was the major substrate for the mitochondrial Krebs cycle, blockage of glycolysis with DOG would inhibit mitochondrial ATP production too. Hence, a similar reduction of intracellular ATP levels as with CN and DOG incubation would be expected. Free fatty acids, if catabolised to acetyl coenzyme A, might be one source of endogenous mitochondrial substrates. Furthermore, it has been shown that A6 cells possess the creatine kinase – phosphocreatine system, a high-energy phosphate buffer, to generate cellular ATP (Guerrero et al., 1997). This system is predominantly found in distal tubules compared to the proximal segments of the nephron. Furthermore, the phosphocreatine level was acutely decreased in distal tubules when the kidney was submitted to brief ischemia (Bastin et al., 1987).

A profound intracellular acidification (from pH_c = 7.02 to 6.46) developed in parallel with the drop in cellular ATP content during MI. The similarity of both time-courses suggests that ATP hydrolysis is the main source of intracellular protons. These protons accumulate since they can not be converted to water by normal oxidative metabolism (Hochachka and Mommsen, 1983). Moreover, ATP depletion might impede the transport processes that normally maintain intracellular acid-base balance and counteract the constant passive influx of protons (Hochachka and Mommsen, 1983; Demaurex and Grinstein, 1994). Since 2-deoxyglucose was used to block cellular glycolysis, the fall in pH_c was not due to increased lactate production. A fall in intracellular pH occurs in most cells exposed to ischemic conditions (for review see (Brady et al., 2000)). As compared to A6 cells, acidification develops faster in most cell types e.g. the application of CN in combination with the glycolytic inhibitor iodoacetate induced a pH_c drop from 7.36 to 6.33 within 10 min in cultured rat hepatocytes (Gores et al., 1989). As indicated above, this difference in time course of acidification might be ascribed to the lower rate of ATP hydrolysis and metabolism in A6 cells.

6.4.3 Intracellular acidification and apical P_{Na} reduction during MI

Since changes in I_{Na} and the G_T are positively correlated to changes in pH_c (Chapter 4) in A6 cells, the intracellular acidification seen during MI might induce the decrease in ap. P_{Na} seen at the end of 45 min of MI (Fig. 6.6B). Fig. 6.6B gives no information about the moment on which the ap. ENaCs closed during MI. However, studies on excised patches from intact polarised A6 monolayers indicated that the probability of the ENaC being in the open state is greatly reduced when the bath pH (cytosolic side) was gradually reduced from 8 to 6.5 (Harvey, 1995). Harvey showed that protons affect ENaC closure by interacting with high cooperativity at a titration site with an apparent pK of ~7.2. Furthermore, a decrease of pH_c reduced the number of simultaneously active channels in the patch, whereas the single channel Na^+ conductance (5 pS) was not affected by pH_c. The gradual pH_c drop from ~7 to ~6.6 in the first 25 min of MI is - according to Harvey's titration curve - sufficient to maximally reduce the open probability P_o and thus, to inactivate a major amount of ENaCs. This inhibition of ap. Na^+ entry after 25 min of MI is consistent with the cell swelling of metabolically inhibited A6 cells only in the first ~25 min of MI. Afterwards, reduction of apical Na^+ influx is probably sufficient to allow the hindered bl. Na^+ pump to preserve cellular volume (see Chapter 7). The parallel course of both recovery of I_{sc} (Fig. 6.1) and re-alkalinisation of pH_c (Fig. 6.7) after MI, further support the possibility of ENaC inhibition by intracellular acidification during MI.

The I_{sc} suppression during MI could also be a consequence of the pH_c sensitivity of the bl. Na^+ pump as demonstrated for rabbit urinary bladder (Eaton et al., 1984). However, the ouabain-sensitive Na^+ fluxes were found to be relatively insensitive to acid loading in nystatin-treated frog skin (Ehrenfeld et al., 1992). These findings are comparable to the pH_c-insensitivity of isolated Na^+/K^+-ATPase enzymatic activity (Homareda and Matsui, 1985). Furthermore, G_T, which is predominantly determined by the apical membrane conductance, was reduced after MI in A6 cells (Fig. 6.6B). Therefore, the effects of pH_c on I_{sc} were probably due to a reduction of the apical Na^+ uptake. However, it can not be excluded that other ENaC regulatory mechanisms are activated during MI e.g. 'feedback inhibition' of ap. ENaCs when the intracellular Na^+ content is augmented or inhibitory effects on ENaC due to the cellular ATP depletion. However, the latter explanation is less likely since lowering of the intracellular ATP concentration from 5 mM to nominally free did not influence the activity of rat ENaCs expressed in *Xenopus laevis* oocytes (Abriel and Horisberger, 1999).

6.4.4 Mitochondrial function during MI

With inhibition of both electron transport chain and glycolysis, the NAD(P)H autofluorescence rises rapidly and $\Delta\Psi_m$ can not be retained. The inhibition of the mitochondrial ATP synthase with oligomycin markedly retarded the ATP depletion seen during MI, and accelerated the mitochondrial depolarisation in the first 10 min of MI. These results suggest that the mitochondrial F_1F_0-ATPase might operate in the reverse mode during the first phase of MI in A6 cells: it hydrolyses ATP to pump protons out from the mitochondrial matrix in an attempt to preserve the mitochondrial potential in the absence of electron transport. The reversal of the mitochondrial ATP synthase in conditions of MI was observed in several types of cells (Rouslin, 1991; Duchen and Biscoe, 1992; Leyssens et al., 1996; Di Lisa et al., 1995). The conservation of $\Delta\Psi_m$ might be advantageous since it prevents mitochondrial swelling (Duchen, 1999) and allows mitochondria to accumulate Ca^{2+} via the Ca^{2+} uniporter (Gunter et al., 1994).

The initial increase in NAD(P)H autofluorescence induced by the application of metabolic inhibitors was followed by a decline of the signal to 104 % during 15 min of MI (Fig. 6.4). This decrease of the autofluorescence signal during metabolic inhibition suggests that the inhibitory action of CN on the electron transport chain is faster compared to the action of DOG on cellular glycolysis. However, to determine the underlying mechanism(s) for this decrease of the autofluorescence signal during metabolic inhibition, further experiments are needed. It was beyond the scope of this thesis to unravel the possible metabolic pathways involving NAD(P)H production or consumption and their modification during metabolic inhibition, to explain the drop in autofluorescence during MI. Nevertheless, these autofluorescence measurements clearly demonstrate the inhibitory action of CN on the mitochondrial electron transport chain and, even more important, the reversibility of this inhibition. The onset of the recovery phase after MI resulted in a rapid decrease of the NAD(P)H autofluorescence to a level below that observed under control conditions (Fig. 6.4). This undershoot in NAD(P)H autofluorescence on restoration of the oxidative metabolism after MI was also reported for isolated rat myocytes (Esumi et al., 1991). The undershoot can be attributed to the accumulation of ADP - a compound known to stimulate oxidative phosphorylation - during the preceding period. Moreover, the presence of pyruvate in the recovery solution might also contribute to the observed undershoot, since it might decrease the amount of cytosolic NADH through the lactate dehydrogenase reaction.

6.4.5 Summary

The results described in this chapter are consistent with the conclusion of previous chapter that A6 cells show no loss of cell viability after 1 hour of MI. Moreover, this study indicates that A6 cells can restore their abolished physiological function (transepithelial Na^+ transport) completely in a subsequent recovery period. On the one hand, the I_{sc} suppression during MI is probably due to the reduction of apical

Na^+ entry associated with intracellular acidification. The closure of ap. ENaCs – if occurring in time - can prevent a cellular overload with external Na^+. On the other hand, the limited amount of ATP available for the Na^+ pump might contribute to the suppression of I_{sc} during MI. The re-alkalinisation of the cells during recovery and the availability of ~ 45 % of the initial ATP level allows the epithelial cells to gradually restore their transepithelial transport up to the initial transport levels.

The closure of ion channels in metabolically inhibited A6 cells might play a role in their high resistance to MI. Furthermore, the putative cytoprotective effect of intracellular acidosis is in accordance with the observed protective effects of mild acidosis in several organ systems, including the kidney (Weinberg, 1991; Weinberg et al., 1991; Edelstein et al., 1996) and with the cytoprotective action of EIPA and similar drugs that stop the Na^+/H^+ exchanger in conditions of cardiac ischemia (Bugge and Ytrehus, 1995).

Chapter 7

Loss of cell volume regulation during metabolic inhibition in A6 cells: role of intracellular pH

7.1 INTRODUCTION

A fundamental property of animal cells is the ability to maintain cell volume constant. Cellular volume is determined ultimately by two factors: the total cell content of osmotically active particles and the osmolality of the bathing medium. The principal threat to cell volume *in vivo* is a change in the amount of osmotically active molecules in cells bathing in isosmotic solutions. A change in total solute content of cells can occur if the balance is altered between solute entry and extrusion from the cells. A dramatic example of such isosmotic swelling *in vivo* occurs during ischemia. In ischemic renal injury, cellular ATP depletion inhibits the basolateral Na^+ pump that normally maintains constant cell volume by offsetting the tendency of cells to swell because of impermeant cellular solutes. The resulting swelling of tubular cells is an early, important step in the development of tubular necrosis. Furthermore, cell swelling has been proposed to contribute to renal dysfunction by leading to obstruction of the tubular lumen and thus to a decrease of glomerular filtration rate (GFR) (Brady et al., 2000). Mason and co-workers (Mason et al., 1989) described that the inwardly directed swelling of the thick ascending limb cells predominantly contributed to the occlusion of the tubular lumen, whereas the outwardly directed swelling of the proximal tubule cells depleted the interstitial and vascular space of the cortex and outer medullary outer stripe. Since the outwardly directed cell swelling occurs at the expense of vascular space, blood vessels are compressed and therefore tubular cell swelling may impede the reflow through the injured tissue (Lang et al., 1995). On the other hand, vascular congestion as a consequence of leukocyte-endothelial interactions and red blood cell accumulation in the vasa recta also contributes to the poor reperfusion after ischemia (De Greef et al., 2001). Nevertheless, the understanding of epithelial cell regulatory volume mechanisms and their modulation by ischemia could be extremely valuable for designing novel therapeutic strategies to improve organ function e.g. in transplantations.

The aim of this part of the study was to examine whether metabolic inhibition (MI) causes swelling of distal epithelial A6 cells and - if so - whether the cells can re-adjust their volume by a mechanism known as regulatory volume decrease (RVD). Furthermore, we investigated whether and how MI interferes with cell volume control mechanisms in anisotonic solutions. In most cell types, including A6 cells, exposure to a hypotonic solution elicits an RVD that is accomplished mainly by KCl efflux induced by parallel activation of K^+ and Cl^- channels (De Smet et al., 1995b; Grosse et al., 2001). Although RVD activation and regulation has been studied in detail, data on proton modulation are rather scarce. Recently, it was reported that internal protons are able to inactivate apical ENaCs (Zeiske et al., 1999) and basolateral K^+ channels (Harvey, 1995)

in A6 cells. Therefore, the hypothesis was verified whether intracellular protons might also inhibit RVD, possibly via inhibition of volume-activated K^+ and/or Cl^- channels.

We observed that cell swelling during MI depends on the salt transport rate of the epithelial cell. We demonstrate that MI inhibits the RVD in response to isosmotic cell swelling (due to the MI itself) as well as to anisosmotic cell swelling (elicited via a reduction of the extracellular tonicity). Furthermore, our findings suggest that the intracellular acidification that accompanies MI might play a role in RVD inhibition.

7.2 MATERIALS AND METHODS

7.2.1 Solutions

The compositions of the solutions used in this study are given in Table 7.1. Isosmotic solutions had an osmolality of 260 ± 4 mOsm/kgH_2O, which is the osmolality of the growth medium for the cells. Hyposmotic solutions had an osmolality of 140 ± 4 mOsm/kgH_2O. All apical (ap.) solutions in Fig. 7.2 to 7.7 were hyposmotic to avoid an osmotic gradient from ap. to basolateral (bl.) side during the reduction of bl. osmolality (π_{bl}). Reduction of ap. osmolality does not alter the volume of A6 cells (De Smet et al., 1995c). The osmolality of the solutions was verified with a cryoscopic osmometer (Osmomat 030, Gonotec, Berlin, Germany).

7.3 RESULTS

7.3.1 Influence of metabolic inhibition on cell volume in high and low rate salt transporting epithelia

To investigate whether metabolic inhibition had an influence on cell volume, we monitored epithelial cell height, T_c, during a 45 min incubation period with CN and DOG and during a subsequent 45 min recovery period. We found a striking difference between high and low rate Na^+ transporting A6 cells. As reported earlier (Wills et al., 1991; Niisato et al., 2000), high rates of Na^+ transport (I_{sc} = 22.3 ± 0.8 μA/cm^2, N=6) in A6 cells are obtained by perfusion of the monolayers with a hypotonic (200 mOsm/kgH_2O) Ringer solution. Metabolic inhibition in these epithelia resulted in a progressive increase of cell volume reaching a plateau-value of 120 % within 25 min (Fig 7.1A). Perfusion with recovery Ringer during 30 min allowed the cells to partially recover to 107 %. Fig. 7.1B illustrates the behaviour of low rate Na^+ transporting epithelia (I_{sc} = 2.9 ± 0.3 μA/cm^2, N=4) that were perfused with isotonic Ringer solution (260 mOsm/kgH_2O). Interestingly, in these conditions, cells were able to maintain cell volume constant during metabolic inhibition and the recovery phase.

Table 7.1 Composition of solutions

	NaCl	NMDGCl	KCl	sucrose	glucose	Napyr	NH_4Cl	HEPES	MES
Fig. 7.1									
Control Ringer 200	70		3	35	10			10	
CN+DOG Ringer 200	70		3	20				10	
Recovery Ringer 200	70		3	30		10		10	
Control Ringer 260	70		3	80	10			10	
CN+DOG Ringer 260	70		3	70				10	
Recovery Ringer 260	70		3	75		10		10	
Fig. 7.2 - 7.5									
Control Ringer ap. (Fig. 7.3, 7.4 & 7.5) and Hypo ringer bl.	55		3		10			10	
Iso Ringer bl.	55		3	109	10			10	
CN+DOG Ringer ap.	55		3					10	
CN+DOG Iso Ringer bl.	55		3	107				10	
CN+DOG Hypo Ringer bl.	55		3					10	
Control Ringer ap. Fig. 6		55	3		10			10	
NH_4Cl Iso Ringer bl.	55		3	77	10		20	10	
Fig. 7.6 & 7.7									
Control Ringer ap.		65	2.5					5	
Iso Ringer bl.	65		2.5	112				5	
Hypo Ringer bl.	65		2.5					5	
pH_{sol}=6 Ringer ap.		65	2.5						5 (K)
pH_{sol}=6 Iso Ringer bl.	65		2.5	112					5 (Na)
pH_{sol}=6 Hypo Ringer bl.	65		2.5						5 (Na)
pH_{sol}=5 Ringer ap.		65	2.5						5 (K)
pH_{sol}=5 Iso Ringer bl.	65		2.5	112					5 (Na)
pH_{sol}=5 Hypo Ringer bl.	65		2.5						5 (Na)

Concentrations are indicated in mM. All solutions also contained 1 mM $CaCl_2$. Numbers in solution names for Fig. 7.1 indicate solution osmolalities in mOsm/kgH_2O. For Fig. 7.2 to 7.7: 'Hypo' refers to 140 mOsm/kgH_2O, 'Iso' to 260 mOsm/kgH_2O and all ap. solutions were hyposmotic. Solutions to inhibit cellular metabolism contained 2.5 mM NaCN and 20 mM DOG. 'Low Na^+' solutions (Fig. 7.3) contained 10 mM NaCl and 45 mM NMDGCl instead of 55 mM NaCl. Solutions were HEPES/TRIS-buffered to pH 7.4 except for low pH_{sol} Ringers where MES/KOH- or MES/NaOH-buffering was applied.

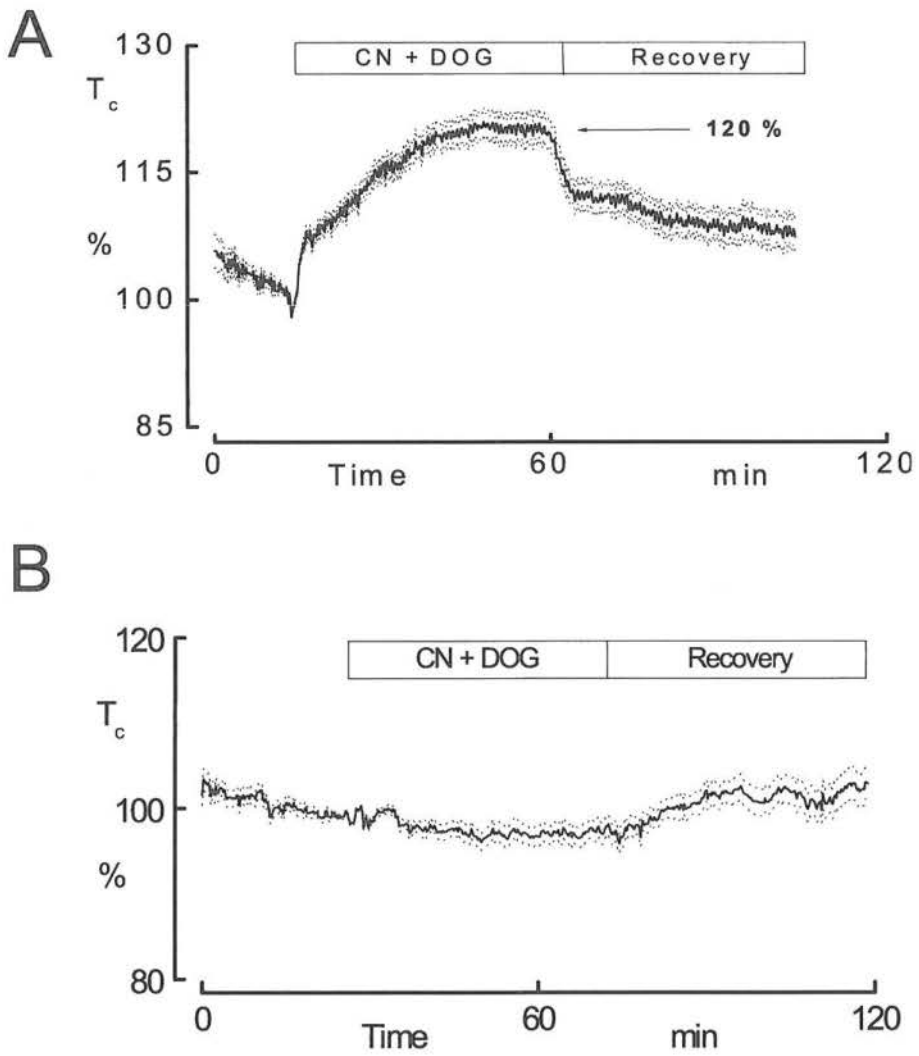

Figure 7.1 Effect of metabolic inhibition (MI) on cell thickness (T_c) of A6 epithelia. *MI was realised by superfusing the tissues at both sides during 45 min with 2.5 mM CN and 20 mM DOG. In the subsequent 45 min CN and DOG were removed from the Ringer solution and pyruvate was used as a substrate.* ***(A)*** *During MI T_c increases up to 120 % in tissues with high rates of Na^+ transport (22.3 ± 0.8 $\mu A/cm^2$) (solid line). Tonicity of the Ringer solution was 200 mOsm/kgH_2O at both sides. The initial absolute T_c value was 9.32 ± 0.33 μm (N=6, n_g=92). Dotted lines represent SEM.* ***(B)*** *T_c response to MI for low rate salt transporting (2.8 ± 0.3 $\mu A/cm^2$) epithelia. The initial absolute T_c values was 9.15 ± 0.27 μm (N=4, n_g=54). Tonicity of the Ringer solution was 260 mOsm/kgH_2O. Dotted lines represent SEM.*

Since no volume regulation was observed after the pronounced volume increase during MI in high salt transporting epithelia (200 mOsm/kgH_2O Ringer), we checked whether ischemia had an influence on cellular mechanisms of cell volume regulation. Therefore, metabolically inhibited epithelia in isotonic Ringer were exposed to a bl. hypotonic solution of 140 mOsm/kgH_2O, which is a severe volume-disturbing treatment.

7.3.2 T_c changes after a basolateral hypotonic shock in metabolically inhibited cells with low rate Na^+ transport

Fig. 7.2 (dotted line) illustrates the control behaviour of T_c during a bl. hyposmotic shock from 260 mOsm/kgH_2O to 140 mOsm/kgH_2O and subsequent perfusion with isotonic Ringer. When bl. osmolality is lowered, A6 cells swell fast due to bl. water influx. Subsequently, this volume increase is rapidly counteracted by a volume regulatory mechanism called the regulatory volume decrease, RVD. During this phase A6 cells lose solutes, predominantly K^+, Na^+ and Cl^- (De Smet et al., 1995b; Grosse et al., 2001) and to a lesser extent amino acids (De Smet et al., 1995a). The behaviour of metabolically inhibited cells with a low rate of Na^+ transport (2.7 ± 0.2 $\mu A/cm^2$, N=5) during a bl. hypotonic shock is indicated with a solid line. A 45 min pre-incubation period with CN and DOG did not alter the cell volume significantly (see also Fig. 7.1B), but a subsequent hyposmotic shock revealed the complete disappearance of RVD. So, ischemic cells completely lost their ability to regulate their volume during a bl. hypotonic shock.

7.3.3 Effect of metabolic inhibition with minimised Na^+ influx on RVD

One possible explanation for the absence of RVD seen in ischemic cells might be that the inhibition of active Na^+ extrusion from the cell leads to an accumulation of Na^+ in exchange for K^+. Since the swelling-activated cation channels in A6 cells are impermeable to Na^+ (Li et al., 1998), cellular K^+ depletion will impede cell volume regulation as observed after Na^+ pump inhibition with ouabain (De Smet et al., 1995c). To test the role of Na^+ accumulation in the inhibition of RVD after MI, we designed a protocol to minimise Na^+ influx into the cells. First, ap. Na^+ was replaced with $NMDG^+$. This ap. Na^+ uptake abolishing manipulation does not affect cell volume in isotonic conditions (De Smet et al., 1995c). Secondly, the bl. Na^+ concentration was lowered to 10 mmol/l to reduce the chemical driving force for Na^+ influx. In this protocol metabolic inhibition was realised with DOG (20 mmol/l) on both sides of the monolayer and NaCN (2.5 mmol/l) exclusively at the bl. side to maintain Na^+-free conditions at the ap. side.

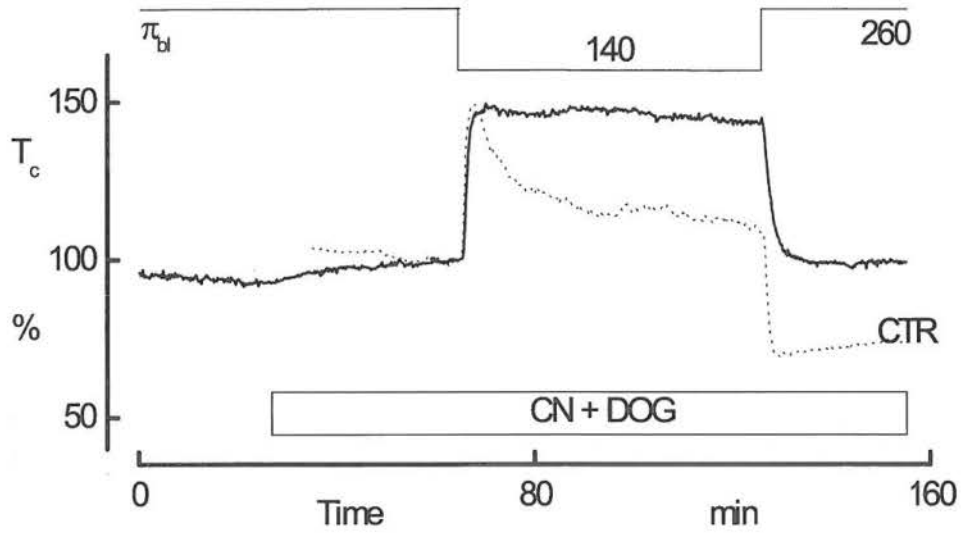

Figure 7.2 Effect of metabolic inhibition on the ability of A6 cells to regulate volume during a hypotonic shock. *All apical solutions were hyposmotic (140 mOsm/kgH_2O). The hyposmotic shock from 260 mOsm/kgH_2O to 140 mOsm/kgH_2O was applied during 60 min at the bl. side of the epithelium. In the subsequent 30 min cells were superfused again with isotonic Ringer solution of 260 mOsm/kgH_2O. The T_c response of control (CTR) tissues (dotted line) (N=6, n_B=59) to hypotonicity indicates a pronounced RVD. For metabolically inhibited tissues (solid line) (N=5, n_B=55), cells were bilaterally exposed to CN and DOG containing solutions 45 min before the hypotonic challenge and during subsequent changes in bl. osmolality. Absolute T_c values in isosmotic conditions were 10.34 ± 0.42 μm (N=6, n_B=59) and 10.08 ± 0.44 μm (N=5, n_B=55) for control and metabolically inhibited tissues respectively. Standard error bars were omitted for clarity.*

The solid line in Fig. 7.3 illustrates the behaviour of cells that were exposed to CN and DOG 45 min before and during the hyposmotic challenge. Although Na^+ accumulation and K^+ depletion were prevented, these ischemic cells still failed to downregulate their volume after a hypotonic shock. Since the reduction of the bl. Na^+ concentration had a pronounced volume decreasing effect in isotonic conditions (T_c dropped from 8.4 μm to 5.6 μm), we checked (dashed line) whether this manipulation as such had an influence on RVD evoked by a hypotonic shock. However, RVD was still present in cells that were superfused during 75 min with a bl. Ringer that contained only 10 mmol/l Na^+. These results suggest that RVD inhibition in metabolically inhibited cells is not caused by a depletion of cellular K^+, but rather by another MI-associated phenomenon.

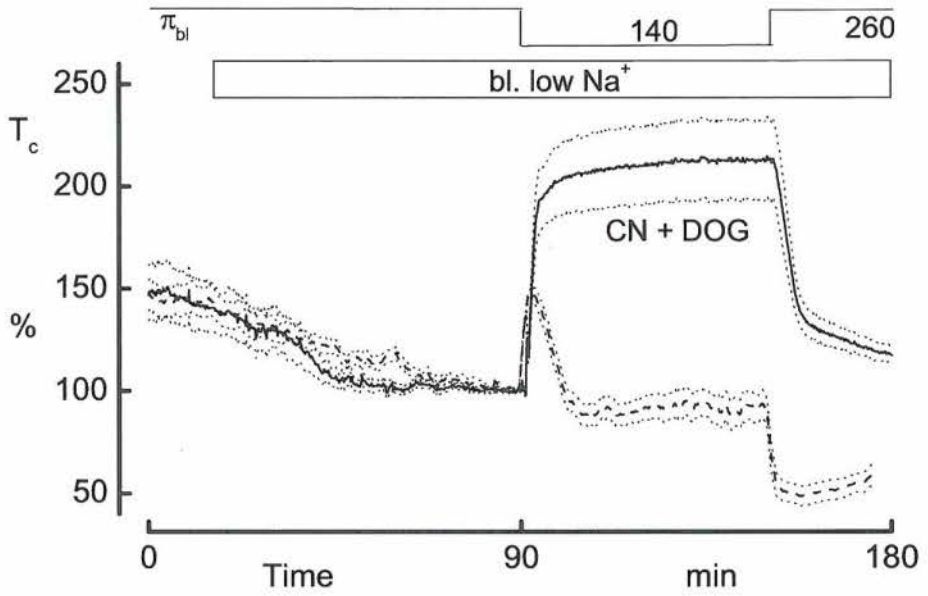

Figure 7.3 Effect of metabolic inhibition with minimised Na^+ influx on RVD. *Apical Na^+ influx was minimised by replacing ap. Na^+ with $NMDG^+$. The dashed line represents epithelia incubated in a bl. low Na^+ solution (10 mmol/l Na^+ and 45 mmol/l $NMDG^+$ instead of 55 mmol/l Na^+) for 75 min before and during the bl. hypotonic challenge from 260 mOsm/kgH_2O to 140 mOsm/kgH_2O. The solid line represents epithelia incubated in low Na^+ solutions that were treated with 20 mmol/l DOG (ap. + bl.) and 2.5 mmol/l CN (bl.) from 45 min before the hypotonic shock until the end of the experiment. Dotted lines represent SEM. The absolute T_c value in isosmotic conditions was 5.57 ± 0.45 µm (N=5, n_B=30) for tissues only incubated in a low Na^+ solution and 5.58 ± 0.40 µm (N=4, n_B=36) for metabolically inhibited cells.*

7.3.4 Intracellular acidification during metabolic inhibition in A6 cells

In Chapter 4 we showed that intracellular protons are able to close Na^+ channels in A6 cells. As a consequence, the hypothesis arose that intracellular protons might also inhibit volume-activated channels which are responsible for the RVD. To verify this hypothesis, intracellular pH (pH_c) was monitored during a 45 min period of MI. As shown in Fig. 7.4 the mean pH_c for 7 different monolayers displayed a pronounced acidification from pH_c 6.93 ± 0.04 to 6.54 ± 0.02 during MI. Since this acidification was maintained during the subsequent bl. hypotonic shock (N=4), intracellular protons are indeed candidates for interaction with volume-activated channels which are responsible for the RVD.

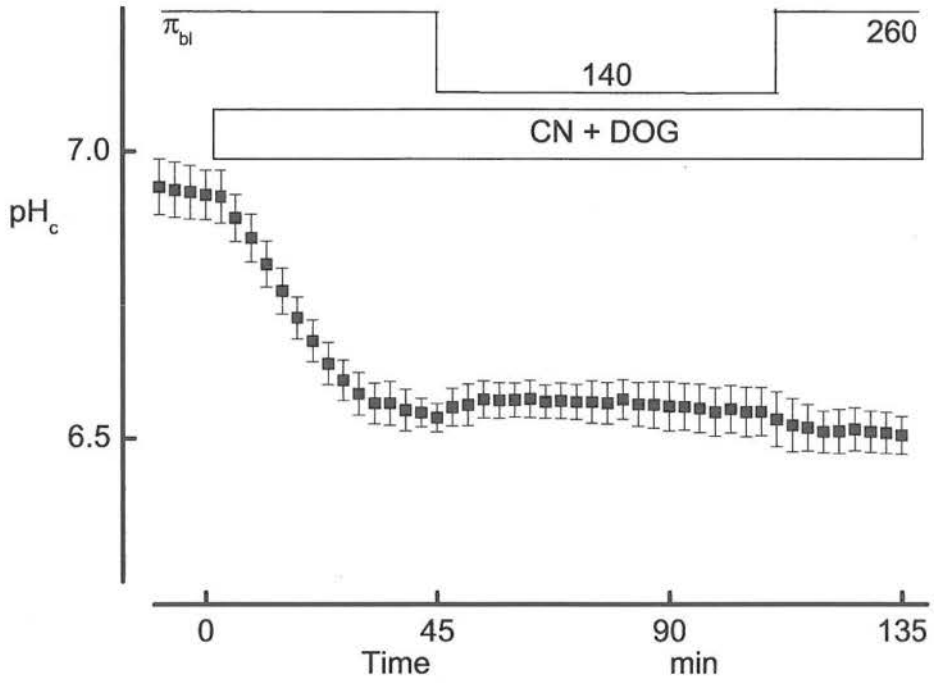

Figure 7.4 Intracellular acidification during MI in A6 cells. *Mean pH_c values during MI are shown for 7 monolayers ± SEM. The acidic pH_c was maintained during the hyposmotic challenge as shown for 4 monolayers.*

7.3.5 Influence of intracellular acidification on volume recovery after a hyposmotic challenge.

Since pH_c changes affect transepithelial Na^+ transport (I_{Na}) changes in A6 cells (Chapter 4) and even a small I_{Na} has an inhibiting effect on RVD (De Smet et al., 1995c), effects of pH_c on RVD were examined in non-transporting conditions where NaCl was replaced with NMDGCl in the ap. saline. As mentioned earlier, this ap. Na^+ uptake abolishing manipulation does not affect cell volume in isotonic conditions (De Smet et al., 1995c).

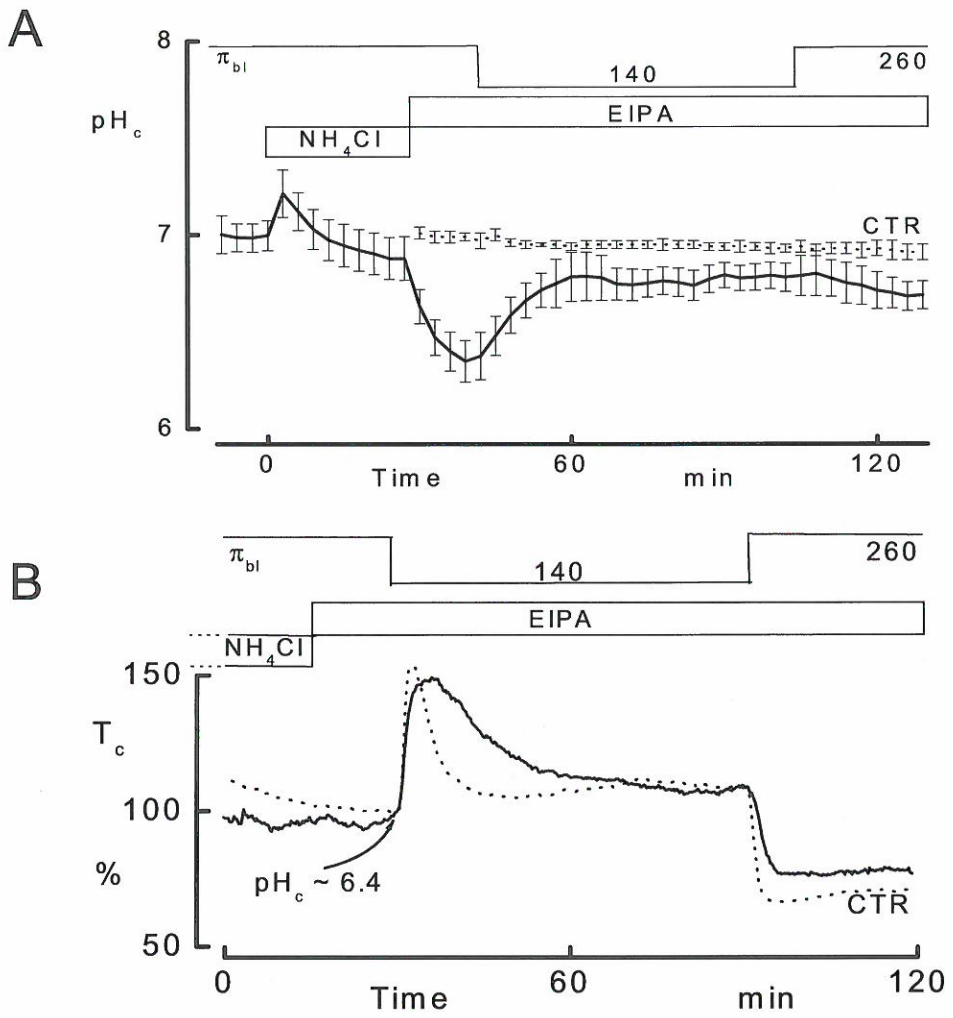

Figure 7.5 Influence of intracellular acidification on volume recovery after a hyposmotic challenge. ***(A)*** *A6 monolayers were exposed to a bl. solution containing 20 mM NH_4Cl during 25 min. Subsequently, NH_4Cl was isosmotically removed and 50 M EIPA was added to ap. and bl. solutions (N=4). Mean values (solid line) are given ± SEM. The dotted line represents mean values for 6 control (CTR) monolayers were the bl. isotonic Ringer was replaced with a hypotonic Ringer solution during 1 hour.* ***(B)*** *Comparison of the T_c response to a hypotonic shock in control (CTR) tissues (dotted line) and in tissues where the NH_4Cl prepulse method in combination with EIPA was applied before the hyposmotic challenge (solid line). The absolute T_c value in isosmotic conditions for these acidified cells was 10.05 ± 0.36 μm (N=6, n_B=83) and 8.22 ± 0.27 μm (N=8, n_B=85) for control tissues. For clarity, we omitted the SEM.*

7.3.5.1 Intracellular acidification via the NH_4Cl prepulse method in combination with EIPA.

First, the NH_4Cl pre-pulse technique (see Sections 4.1 and 4.4.5) was used to acidify the A6 cells without changing external pH. The bl. NH_4Cl pulse was performed under strict and volume-controlled experimental conditions (see Section 4.4.1): 40 mM sucrose in the bl. control saline was isotonically replaced with 20 mM NH_4Cl during 25 min. Subsequently, cells were bilaterally superfused during 15 min with control saline containing 50 μM of EIPA that arrests the bl. Na^+/H^+ exchanger (Casavola et al., 1992). As shown in Fig. 7.5A (solid line) this method evoked an intracellular acidification from pH_c 7.00 ± 0.08 to 6.4 ± 0.1 (N=4). Although EIPA was used, the cells gradually recovered from this pronounced acidification during the subsequent bl. hypotonic shock (pH_c = 6.8 ± 0.1 after 20 min). Further attempts (including the use of 30 mM sodium propionate, a continuous gazification with 5% CO_2 and the use of other Na^+/H^+ exchanger blockers: 10 μM HOE642 and 10 μM S3226) to keep the cells acidic for a longer period failed (results not shown). Possibly, gazification with only 5% CO_2 was insufficient, since in some cell types gazification with 15% CO_2 is applied to generate a substantial intracellular acidification (Sullivan et al., 1991). In general, cell swelling leads to cytosolic acidification (Lang et al., 1998). Nevertheless, we investigated in control experiments whether the bl. hyposmotic treatment -as such- was not a pH_c increasing manipulation in A6 cells. If this were the case, it would neutralise previous acid-inducing manipulations. Replacement of bl. isotonic Ringer with a hypotonic Ringer solution during 1 hour induced no significant pH_c change in 6 different monolayers (Fig. 7.5A, dotted line). T_c experiments (Fig. 7.5B) reveal that a hyposmotic challenge still elicits a complete RVD in cells that were previously acidified to pH_c 6.4 with the NH_4Cl pre-pulse technique (solid line). However, RVD was profoundly slowed down during the first 20 min compared to control experiments (dotted line). This delay in RVD might be attributed to the presence of intracellular protons that gradually leave the cells during the hypotonic shock.

7.3.5.2 Intracellular acidification via lowering of external Ringer pH (pH_{sol})

Secondly, pH_c was modified by lowering pH_{sol} at both sides of the epithelium. As indicated in Fig. 7.6A, a 30 min exposure period to pH_{sol} 6 reduced the intracellular pH from 7.06 ± 0.02 to 6.59 ± 0.03 (N=6). A subsequent bl. hypotonic shock of 60 min acidified the cells further to pH_c = 6.3 ± 0.2 (N=3). These acidified cells still elicited an RVD that was however partially inhibited as shown in the T_c measurements of Fig. 7.6B (solid line).

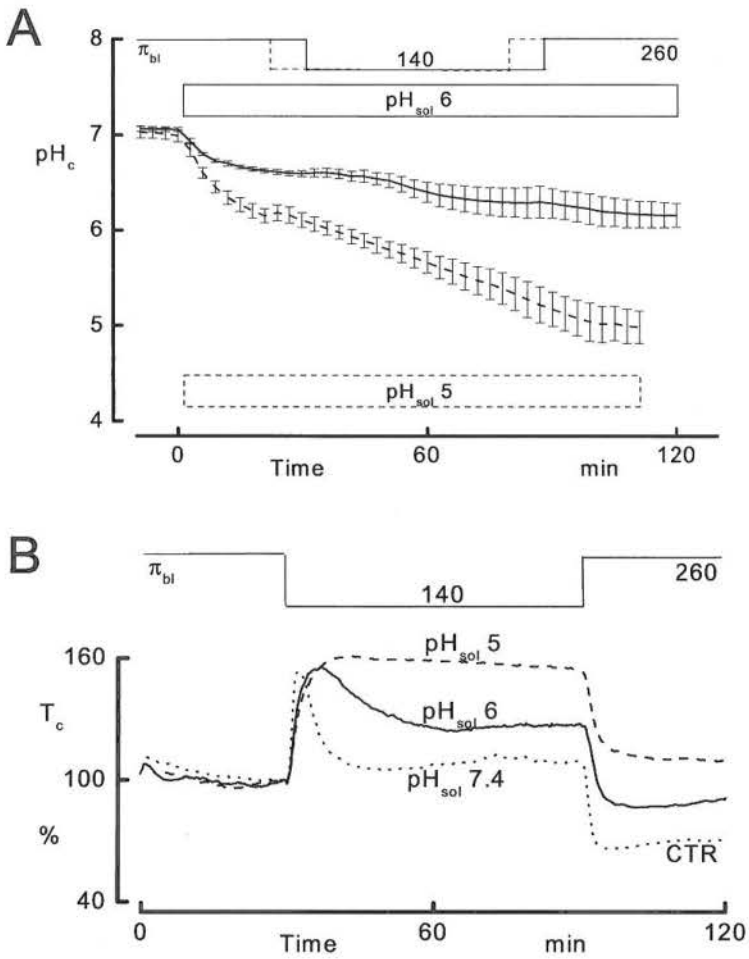

Figure 7.6 Influence of lowering external solution pH (pH_{sol}) on intracellular pH (pH_c) and regulatory volume decrease (RVD) during a hypotonic shock. *Non-transporting epithelia were incubated at both sides in a Ringer solution with pH_{sol} = 6 during 30 min before - and during - the hypotonic shock (solid line). Other monolayers were incubated in a Ringer solution with pH_{sol} = 5 during 20 min before and during a subsequent hypotonic challenge (dashed line).* ***(A)*** *Changes in pH_c are shown for the pre-incubation (before the hyposmotic shock) in Ringer with a pH_{sol} = 6 (N=6) or a pH_{sol} = 5 (N=6) and during the subsequent hyposmotic challenge (N=3). Mean pH_c values are indicated with SEM.* ***(B)*** *Comparison of the T_c response to a hypotonic shock in control tissues (CTR, dotted line) or in previous acidified tissues where external pH_{sol} was 6 (solid line) or 5 (dashed line). Initial absolute T_c values were 8.22 ± 0.27 μm (N=8, n_B=85), 8.61 ± 0.34 μm (N=6, n_B=72) and 7.13 ± 0.39 μm (N=6, n_B=45) respectively. The CTR curve was copied from Fig. 6B. For clarity, we omitted the SEM.*

In order to obtain a more pronounced pH_c drop (from 6.99 ± 0.06 to 6.15 ± 0.07, N=6), other monolayers were superfused during 20 min with a Ringer of pH_{sol} = 5 (Fig. 7.6A, dashed line). The acidifying process continued during the hypotonic shock. Fig. 7.6A shows that in these conditions (dashed line) RVD was completely inhibited. The fact that shrinking of the cells still occurred when isotonic Ringer was applied, demonstrated that this very low pH_{sol} did not damage cell membranes. Moreover, the mean transepithelial conductance for these acidic monolayers did not exceed a value of 0.85 mS/cm^2 during this experimental protocol.

To verify whether the RVD inhibition was due to the pronounced intracellular acidification or just caused by the action of external protons, it was necessary to distinguish between 'chronic' and 'acute' treatment with an external acidic solution (pH_{sol} 5). 'Chronic' treatment refers to the protocol described earlier in this section where external pH was lowered 20 min before and during the hypotonic challenge (Fig. 7.6, dashed line), whereas 'acute' treatment involves lowering of external pH_{sol} simultaneously with the hypotonic shock. If protons exerted their inhibitory action on RVD from the extracellular side, acute administration of protons would allow a rapid blockage of RVD. In contrary, it took at least 10 min to arrest the RVD as depicted in Fig 7.7A (solid line). The pH_c experiments in Fig 7.7B reveal that in the first 10 min of acute treatment with a pH_{sol} of 5, pH_c drops from 6.99 ± 0.05 to 6.39 ± 0.06 (N=5). The clear delay in RVD blockage in 'acutely' treated cells might indicate the necessity of a pronounced intracellular acidification for RVD inhibition. Therefore, this study suggests that the proton-sensitivity of RVD (Li et al., 1998) elicited by a bl. hypotonic shock in A6 cells, is caused by the inhibitory action of intracellular protons and probably not of extracellular protons. This inhibitory effect of internal protons might -at least partly- account for the absence of RVD seen in metabolically inhibited, and thus acidified, A6 cells.

7.4 DISCUSSION

One of the mechanisms that can reduce the GFR during renal ischemia is swelling of tubular epithelial cells in different nephron segments. In the present chapter, MI with CN and DOG was used as an experimental model to simulate ischemic cell injury. We investigated the effects of MI on cell volume and cell volume regulation of a tight epithelium, A6.

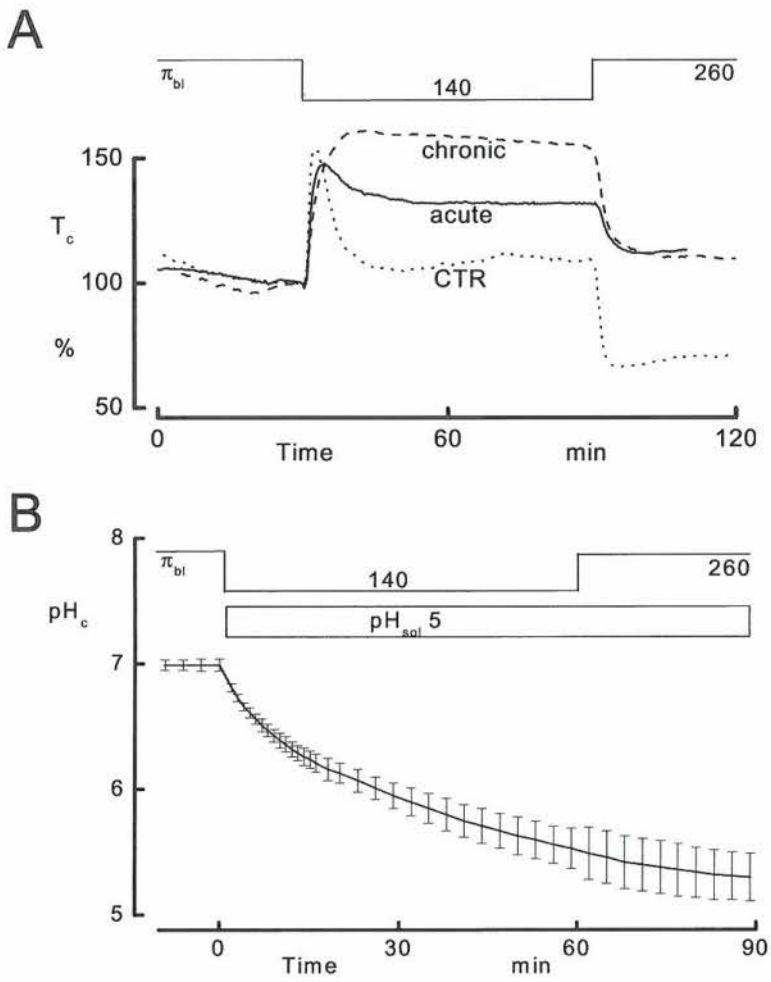

Figure 7.7 Comparison of chronic and acute effect of lowering pH_{sol} on RVD. (A) *To discriminate between the action of external and internal protons on RVD, external pH was bilaterally lowered to pH 5 'chronically' (20 min before and during the hypotonic shock) or 'acutely', i.e. simultaneously with the hyposmotic challenge. Acute treatment (solid line) resulted in a clear delay (~10 min) of RVD inhibition in contrast with the immediate RVD inhibition in chronically treated monolayers. The control CTR (dotted line) and 'chronic' curve (dashed line) were copied from Fig. 7B. The absolute T_c value in isosmotic conditions for acutely treated cells was 9.89 ± 0.30 μm (N=5, n_g=68). Standard error bars were omitted for clarity.* ***(B)*** *Changes in pH_c during 'acute' lowering of pH_{sol} are shown for 5 monolayers. The acidifying process continued during subsequent bl. superfusion with isotonic Ringer (N=4) after the hypotonic shock. Mean pH_c values are indicated with SEM.*

7.4.1 Metabolic inhibition induces cell swelling in high rate Na^+ transporting A6 epithelia

Under steady-state conditions, epithelial cell volume is maintained by balancing the rates of ap. and bl. ion transport in such a way that intracellular solute content remains constant. When MI is applied, cellular ATP depletion will inhibit the active bl. Na^+ extrusion from the cells. This can lead to an accumulation of Na^+ via ap. ENaCs in exchange for K^+ that leaves the cells via bl. K^+ channels. The resulting cellular depolarisation allows chloride to enter the cells and, when the net gain of Na^+ and Cl^- exceeds cellular K^+ loss, the increase in cellular solute content will draw in water and finally the cells will swell (Lang et al., 1998; Macknight and Leaf, 1977). As shown in Fig. 7.1A this sequence of events seems to occur in A6 epithelia with high rates of Na^+ transport where reduced pump rates during MI are insufficient to match massive ap. Na^+ influx. During the first 25 minutes of ischemia cell volume gradually increases up to a plateau-value of 120 %. A further rise of cell volume might be prevented via reduction of ap. Na^+ entry by the action of intracellular protons (Chapter 4) elicited during MI (Fig. 7.4). The constant T_c value in Fig. 7.1A probably indicates that, at the plateau-phase, the reduction of ap. Na^+ influx is sufficient to allow the hindered bl. Na^+ pump to preserve cellular volume. Hence, it seems that this plateau-phase is comparable with the situation in low salt transporting epithelia (Fig. 7.1B). There, the hindered Na^+ pump is still able to offset ap. Na^+ influx and therefore accumulation of intracellular osmolytes and cell swelling could be avoided during MI.

The cell swelling during MI in high salt transporting epithelia could also be a consequence of bl. Na^+ influx rather than ap. Na^+ influx as described above. A candidate for bl. Na^+ influx is the bl. Na^+/H^+ exchanger (Casavola et al., 1992) that probably is activated in these acidic (Fig. 6.7 of previous chapter) cells. However, this explanation is not plausible since low rate salt transporting epithelia (Fig. 7.1B) displayed no change in cell volume during MI, although these epithelia acidified to the same extent (Fig. 7.4) and therefore, at least a similar activation of the bl. Na^+/H^+ exchanger could be expected.

7.4.2 Absence of isosmotic volume regulation in metabolically inhibited A6 cells

High rate salt transporting A6 cells displayed no volume regulatory event after cell swelling due to MI. A similar behaviour was seen when Madin-Darby canine kidney (MDCK) cells, which are mammalian distal tubular cells, were exposed to MI (Fig. 7.8). Application of metabolic inhibitors resulted in a rapid increase in cell volume to 108 %. A plateau was reached in about 15-20 minutes. No volume regulatory response to this swelling was seen. However, it has been shown that, in control conditions, MDCK cells are able to respond with RVD to an acute increase in cell volume induced by a sudden hypotonic shock (Rothstein and Mack, 1990; Banderali and Roy, 1992; Lang and

Paulmichl, 1995). The similar behaviour of MDCK cells during MI, indicates that the absence of cell volume regulation in metabolically inhibited cells, as described in this chapter, is not limited to amphibian epithelial cells.

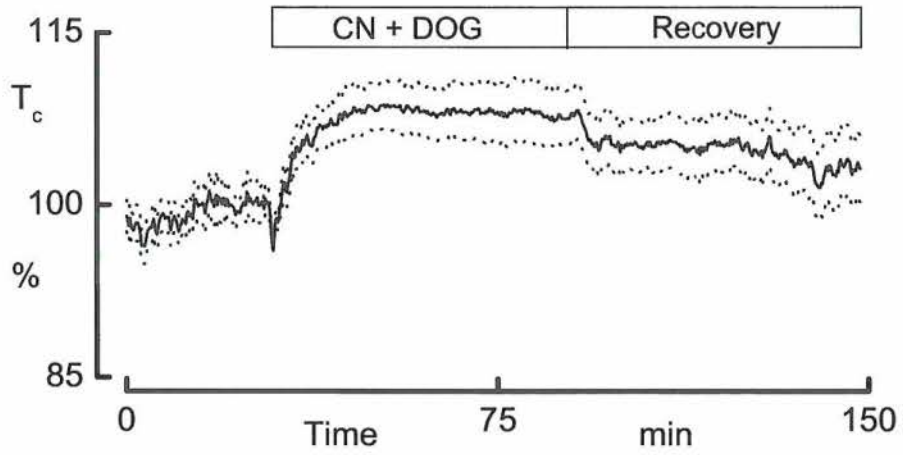

Figure 7.8 Effect of metabolic inhibition (MI) on cell thickness (T_c) in MDCK cells.
MDCK cells were cultured in a humidified 5% CO_2 atmosphere at 37 °C (De Strooper et al., 1995). Cells grown on permeable filter supports (Nunc Anopore, 10^5 cells/cm^2) were used for experiments after 7-10 days of growth. The normal Ringer solution contained (in mM): 140 NaCl, 5 KCl, 1.5 $CaCl_2$, 1 $MgSO_4$, 10 HEPES and 5.5 glucose (pH_{sol} = 7.4 with TRIS). MI was realised by superfusing the tissues basolaterally during 60 min with 'CN + DOG' Ringer (in mM): 135 NaCl, 5 KCl, 1.5 $CaCl_2$, 1 MgSO4, 10 HEPES, 10 DOG and 2.5 CN (pH_{sol} = 7.4). During 'recovery' CN and DOG were removed and 7.5 mM pyruvate substituted for glucose in the saline solution. All solutions had an osmolality of 300 mOsm/kgH_2O. Shown are the mean (solid line) and the SEM (dotted lines) from 4 different monolayers (n_s = 57). Experiments were performed at room temperature. The initial absolute T_c value was 10.97 ± 0.90 μm.

7.4.3 Absence of anisosmotic volume regulation in metabolically inhibited A6 cells

This study further explored the capacity of distal epithelial cells (A6) to regulate cellular volume during MI by challenging them with a bl. hyposmotic shock. After hyposmotic swelling, non-ischemic A6 cells exhibit a RVD by activating predominantly conductive pathways for K^+ and Cl^- efflux (De Smet et al., 1995b; Grosse et al., 2001), and, to a lesser extent, by extruding amino acids (De Smet et al., 1995a). Our results demonstrate that CN and DOG treated A6 cells completely lost the ability to regulate their volume after a bl. hyposmotic shock. This result is consistent with previous

reports were RVD was completely inhibited in hypotonically suspended glial cells in anoxic conditions in the presence of iodoacetate (Kempski et al., 1987) or partially inhibited by inhibitors of mitochondrial electron transport in cerebral astrocytes (Olson et al., 1986). Recently, the RVD inhibition seen during metabolic inhibition was linked to the impairment of the volume-regulated anion channels (VRAC) in ATP depleted cells. Some studies ascribe the dependence of VRAC activation on cytosolic ATP to a direct interaction of ATP with the channel, without the necessity of ATP hydrolysis. This was reported for different cell types including cerebellar granule neurons (Patel et al., 1998) and human intestinal epithelial cells (Okada, 1998). However, other reports state that ATP dependent phosphorylation steps may be involved in Cl^- channel activation for RVD (Chou et al., 1998; Light et al., 1998; Estevez et al., 1999; Idriss et al., 2000). The latter group includes studies on renal epithelia: cultured mouse cortical collecting duct cells (Meyer and Korbmacher, 1996) and isolated proximal tubule cells of Rana temporaria (Robson and Hunter, 1994).

In addition, cellular ATP depletion during MI leads to a reduced activity of the Na^+ pump. As shown for ouabain experiments in A6 cells (Borgmann et al., 1994) this results in an intracellular accumulation of Na^+ in exchange for K^+. A severe loss of cellular K^+ during a prolonged (60 min) ouabain treatment impedes RVD in A6 cells (De Smet et al., 1995c). In the present study, experiments that were designed to minimise Na^+ influx and thus to avoid K^+ depletion during MI, revealed that RVD was still impaired (Fig. 7.3). Hence, RVD inhibition in metabolically inhibited A6 cells cannot be ascribed to the indirect effect of ATP depletion on the intracellular K^+ concentration. However, it cannot be ruled out that the lack of ATP caused RVD inhibition in our cells. As described for other cell types above, internal ATP might regulate the activation of swelling-activated Cl^- channels in A6 cells. Furthermore, it was reported that ATP dependent tyrosine phosphorylations represent an essential step in the RVD response of a human intestine cell line (Tilly et al., 1993), Hence, impaired tyrosine kinases might also underlie RVD inhibition in ATP-depleted cells.

7.4.4 Role of intracellular pH on RVD inhibition in metabolically inhibited A6 cells

Other well-known regulators of ion channels in A6 cells are internal protons. Recently, the inactivation of ap. ENaCs (Harvey, 1995)(Chapter 4) and bl. K^+ channels (Harvey, 1995) by internal protons was reported. Therefore, we examined whether intracellular acidification can play a role in RVD inhibition maybe via inactivation of volume regulatory ion channels. A pronounced intracellular acidification develops in metabolically inhibited A6 cells perfused with iso- (Fig. 7.4) or hypotonic Ringer solutions (Fig. 6.7). Acidosis developed because the proton released during hydrolysis of ATP could not be converted to water by normal oxidative metabolism (Hochachka

and Mommsen, 1983), see also Chapter 6. Moreover, ATP depletion might impede the transport mechanisms that normally maintain intracellular acid-base balance and counteract the constant passive influx of protons (Hochachka and Mommsen, 1983; Demaurex and Grinstein, 1994). Probably, this explains why in metabolically inhibited A6 cells the intracellular acidification is conserved (Fig. 7.4), while in non-ATP-depleted cells with normal external pH_{sol} cellular acidity was not maintained (Fig. 7.5A) even in the presence of EIPA to block the bl. Na^+/H^+ antiporter (Casavola et al., 1992).

Li et al. (Li et al., 1998) have shown that lowering of the external pH_{sol} exhibits an RVD-inhibitory effect in A6 cells. Our data suggest that this inhibitory action is exerted by internal protons rather than by external protons. As shown in Fig 7.5B, RVD was clearly delayed in A6 cells, acidified by means of the NH_4Cl pre-pulse technique, with normal external pH_{sol}. This is consistent with findings of Sullivan et al. (Sullivan et al., 1990) who described that mild intracellular acidosis reduced the rate of volume regulation in response to hypotonic media in rabbit proximal tubules. The RVD in acidified A6 cells was only delayed rather than completely inhibited. This might be attributed to the fact that the extra internal protons were extruded out of the cells in the first 20 min of the hypotonic shock and hence, their inhibitory action was limited in time. This re-alkalinisation in Fig. 7.5A was not due to H^+ efflux via swelling-activated ion channels triggered by the bl. hypotonic shock, since this alkalinisation occurred with a similar time course in an identical experimental protocol but without lowering of the bl. osmolality (results not shown). Further experiments are needed to elucidate the identity of the H^+ extruding mechanism(s) as for instance the ubiquitous V-type ATPase which is present in frog skin (Harvey, 1992; Klein et al., 1997). However, the fact that hypotonic cell swelling was suggested to inactivate the H^+ ATPase in endocytotic vesicles of rat hepatocytes (Schreiber and Haussinger, 1995) argues against the involvement of a putative H^+ ATPase in the re-alkalinisation during the hypotonic shock.

Our results indicate that a complete and immediate inhibition of RVD after a hyposmotic challenge is only achieved when the following conditions are fulfilled. First, the extra amount of internal protons needs to be 'trapped' inside the cell. This was the case in ATP-depleted cells (Fig. 7.4) and, in non-ATP-depleted cells, we kept protons inside by lowering the external pH_{sol} and thus by reducing the chemical driving force for H^+ efflux. Secondly, a profound acidification is necessary. This was evidenced by the fact that RVD was only retarded (Fig. 7.6B) in cells that were acidified to some extent (pH_c 6.59) by incubation during 30 min in a pH_{sol} of 6. RVD was still arrested in these cells 30 min after the onset of the hyposmotic challenge, probably because of the further drop of pH_c during the hypotonic treatment (Fig. 7.6A). In contrast, an immediate and complete blockage of RVD was seen in cells that were profoundly acidified to pH_c values as low as 6.15 by incubation during 20 min before the hypotonic shock in a pH_{sol} of 5. 'Acute' addition of external protons (pH_{sol} 5), simultaneously with

the hypotonic shock, could not inhibit RVD immediately (Fig. 7.7A). The clear delay in RVD blockage seen in 'acutely' treated cells is accompanied with a rapid intracellular acidification (Fig. 7.7B). These results point to the necessity of a profound intracellular acidification for complete RVD inhibition in A6 cells. Although it is conceivable that external protons could also interact with the volume regulated ion channels either directly or indirectly at a site unrelated to the pore, the slow time course of the effect of lowering external pH_{sol} acutely on RVD argues against this explanation. Recently it has been shown that inactivation of cloned amphibian (derived from A6 cells) and mammalian (human) renal chloride channels (ClC-5) following exposure to external acidic solutions occurred very rapidly (within 1 min) (Mo et al., 1999). Therefore, the involvement of external protons in RVD inhibition is less likely.

The mechanism of RVD inhibition by internal protons in A6 cells was not identified in this chapter. Further experiments are needed to resolve this issue.
Previous studies mention effects of intracellular pH on VRAC channels as well as on volume activated K^+ channels. Recently, it was shown that VRAC channels of endothelial cells are markedly pH-sensitive (Sabirov et al., 2000). Sabirov described that VRACs are only active in a narrow pH range around physiological pH but are shut down whenever the cytoplasm becomes more acidic than approximately 6.5 (Sabirov et al., 2000). This is consistent with our findings in A6 cells that a pronounced acidification is necessary for complete RVD blockage. Internal protons seem to bind directly to group(s) on the ion channel with an apparent pK of ~ 6.5 which suggests protonation of His (Sabirov et al., 2000). Note however that no evidence for the presence of RVD was shown in the latter study. On the other hand, also the activation of volume-regulated K^+ channels might be impaired by intracellular acidification as described for jejunal villus epithelial cells (MacLeod and Hamilton, 1996; MacLeod and Hamilton, 1999a; MacLeod and Hamilton, 1999b) and for Ehrlich ascites tumor cells (Hoffmann, 2000). The underlying molecular mechanism of this inhibitory effect of protons on volume-regulated K^+ channels is still unknown.

7.4.5 Summary

With respect to our data, we arrive at the following conclusions. Cell swelling during metabolic inhibition in A6 cells is dependent on the rate of Na^+ reabsorption and the swelling is not followed by a volume regulatory response. Furthermore, A6 cells treated with CN and DOG lose completely their ability to regulate their volume when exposed to a bl. hypotonic shock. The intracellular acidification seen during MI in A6 cells might be one of the RVD inhibiting events. This is evidenced by the fact that NH_4Cl pre-pulse acidified cells, which gradually alkalinise during a hypotonic shock, show a marked delay in their RVD response to a hypotonic shock with normal external pH_{sol}. Moreover, a striking difference is seen in the RVD response when cells are treated

with external pH 5 depending on the mode of administration. When cells are *chronically* treated, RVD is absent since the cells are well acidified when the hypotonic shock is applied. Whereas a*cute* treatment allows RVD to start and the subsequent time course of RVD inhibition is rather slow. Complete RVD inhibition required at least 10 minutes, a time period in which a steady acidification of the cells occurred. Therefore, the intracellular acidification seen in metabolically inhibited A6 cells might, at least partly, account for the RVD inhibition seen during hypotonic treatment. It should be mentioned, however, that the mechanisms involved in 'anisosmotic volume regulation' may be different from the mechanisms seen after alterations of the intracellular solute content under isosmotic conditions. Nevertheless, a failure in cell volume regulation secondary to a severe disturbance of the cell metabolic processes and intracellular acidification, can be an instrumental factor for the drop of GFR and the impaired reflow observed after temporary interruption of the circulation in ischemic kidneys.

Summary and general discussion

The aim of this study was to investigate the cellular processes with respect to Na^+ handling, intracellular pH and volume regulation occurring in renal tubular cells facing ischemic conditions. Since the regeneration of the kidney after an ischemic insult is based on the capacity of surviving cells to recover and to proliferate, the present study was designed to unravel some putative cellular defence mechanisms of sub-lethally injured renal tubular cells. To mimic renal ischemia in distal tubular cells, metabolic inhibition (MI) of A6 cells was used as an *in vitro* experimental model.

In general, renal ischemia is associated with a dramatic drop of tubular reabsorption processes (Tanner et al., 1973; Brady et al., 2000; Hanley, 1980; Johnston P.A. et al., 1984; Brady et al., 2000). Since, in normal conditions, most salt is reabsorbed in the proximal nephron segments (proximal tubule and thick ascending limb), distal tubular epithelial cells usually don't face a high apical salt concentration. A normal sodium concentration in the lumen of distal tubules of the rat are ~ 45-65 mM (Schnermann et al., 1966; Seney et al., 1987). Schnermann and co-workers reported an increase of the distal tubular Na^+ concentration upto 98-143 mM after 30 to 60 min renal arterial clamping (Schnermann et al., 1966). Hence, the increase in luminal Na^+ content in the distal tubular lumen (Braam et al., 1993) might overload the tubular epithelial cells and have deleterious consequences. In Chapter 3 we evaluated how A6 cells handle an increasing apical Na^+ concentration in normal non-ischemic conditions. Our results are consistent with the literature in that the Na^+ uptake through the apical ENaCs saturates with increasing apical Na^+ concentrations. Current fluctuation analysis revealed that the saturating dependence of the transepithelial Na^+ current (I_{Na}) on the apical sodium concentration ($[Na^+]_{ap}$) was generated by both the Na^+-dependence of the open channel density, N_o, and the saturation of the single channel current, i. When increasing $[Na^+]_{ap}$ from 3 to ~ 20 mmol/l the density of conducting pores decreases sharply and behaves again as an almost $[Na^+]_{ap}$-independent parameter between 20 and 110 mmol/l. The single channel current clearly saturates with an apparent Michaelis-Menten constant (K_m) of ~ 17 mmol/l. A saturating single channel conductance may account for saturation of i as suggested from experiments with reconstituted A6 Na^+ channels in planar lipid bilayers (Olans et al., 1984), where the K_m was also ~ 17 mmol/l. Physiologically, the limited transport capacity of the amiloride-sensitive ENaC may be an important property to protect the cells from Na^+ overloading and subsequent changes in intracellular electrolyte composition in situations with increased outer Na^+ concentrations, such as those occurring during ischemia.

A fall in intracellular pH (pH_c) occurs in most cells exposed to ischemic conditions, for review see (Brady et al., 2000). As expected, metabolic inhibition also induced a pronounced intracellular acidification (from pH_c 7.02 to 6.46) in our experimental A6 model. Therefore, we examined in Chapter 4 whether a reduction of pH_c

in 'non-ischemic' A6 cells modulates the ap. Na^+ permeability (P_{Na}) and whether pH_c influences the I_{Na}-kinetics as described in Chapter 3. We could show that I_{Na} and G_T generally follow the time course of pH_c during different pH_c changing manipulations such as an ap. or bl. NH_4Cl pulse. Moreover, we established that the sole pH_c-sensitive parameter underlying I_{Na} was N_o. Furthermore, we showed that only the saturation value (I_{max}) of I_{Na} kinetics was subject to changes in pH_c. The pH_c-independency of K_m suggests that we deal with an allosteric site where the interaction of the internal protons with the ENaC should be non-competitive with external Na^+. This 'non-competitive' feature of ENaC modulation by external Na^+ ions and internal protons might explain the pH_c-independency of i, since this parameter is under dominant influence of external Na^+ as described in Chapter 3. pH_c-dependent changes in N_o may be caused by influencing P_o, the ENaC open probability, or/and the total channel density, N_T. Recently, the pH_c-dependency of P_o was demonstrated for the rat α-ENaC expressed in *Xenopus* oocytes or reconstituted in planar lipid bilayers (Chalfant et al., 1999). Cytosolic-side acidification reduced the mean open time and increased the mean closed time of the rat α-ENaC whereas single channel conductance remained unaffected. However, since several hormones are known to regulate P_{Na} via reversible insertion of channels residing in intracellular pools in several tight epithelia (Garty and Palmer, 1997) including A6 cells (Erlij et al., 1999), we are presently unable to conclude whether pH_c affects only P_o or also N_T of the ap. ENaCs.

To date a variety of messenger roles for intracellular protons have been proposed, including the concerted 'cross talk' modulation of ap. Na^+ and bl. K^+ permeabilities in tight, Na^+-transporting epithelia (Harvey, 1995). pH_c changes are known as a direct consequence of hormonal action (Lyall et al., 1995), e.g. stimulation of the Na^+/H^+ exchanger by steroid hormones (Urbach et al., 1996). A change in pH_c is not only induced by hormonal actions, but ion channels themselves have been shown to be a permanently threatening source of protons from the extracellular reservoir (Lyall et al., 1993; Lyall et al., 1995) as the net driving force for protons is almost always inward-directed. Therefore, protons will pile up in the cell when energy supply for H^+ extrusion is short as in the condition of ischemia. Moreover, glycolysis as well as ATP splitting without regeneration (Hochachka and Mommsen, 1983) will add even more to intracellular acidification which, in the end, would tend to deregulate cell life. This adverse, positive-feedback reaction chain may, however, be brought to a halt if the influx pathways for protons, the alkali ion channels, are closed down in a negative feedback loop by cytosolic protons. This might be a self-protection of the cells from lethal acidification.

To conclude, Chapters 3 and 4 provide us with valuable information on the ENaC characteristics in normal functioning epithelial cells. The amiloride-sensitive ENaC displays a limited transport capacity, which might protect the cells from Na^+

overloading (Chapter 3), and the open ENaC density is pH_c-sensitive in the sense that a pH_c drop downregulates N_o and a pH_c increase upregulates N_o (Chapter 4). The downregulation of N_o in acidic cells might serve as a cellular defence against extreme intracellular acidification. In addition, and perhaps even more important, a pH_c-induced closure of ENaCs contributes to the blockage of salt entry which may be crucial in cells with a hindered Na^+K^+-ATPase as discussed below. Hence, the ENaC features described above are important for the understanding of the different cellular processes occurring in metabolically inhibited cells and their correlations (Chapters 5, 6 and 7).

In this study (Chapters 5, 6 and 7) ATP depletion was introduced in A6 cells by incubation with the metabolic inhibitors cyanide (2.5 mM, CN) and 2-deoxyglucose (20 mM, DOG). Metabolic inhibition with CN and DOG is mostly used to simulate ischemia for *in vitro* models (Eisner et al., 1989; Esumi et al., 1991; Sheridan et al., 1993; Doctor et al., 1994; Leyssens et al., 1996; Karwatowska-Prokopczuk et al., 1998). CN has the advantage of being readily reversible on washout (as shown in Chapter 6 by the immediate decrease in the NAD(P)H/$NAD(P)^+$ ratio). However, a number of non-specific interactions of cyanide have been reported. At very low concentrations (10-100 μM), CN interferes with signal transduction pathways by interacting directly with some receptors (Yang et al., 1996; Sun et al., 1997). For example, CN interacts with the N-methyl-D-aspartate receptor channel complex in cerebellar granule cells to enhance receptor-mediated responses (Sun et al., 1997). CN was also found to reduce K^+ currents in the type I cells of the carotid body (Peers and O'Donnell, 1990) and this reduction occurred regardless of the presence of intracellular ATP. Direct effects of CN, unrelated to metabolic interference, have been reported also for K^+ channels in mouse motor nerve terminals (Chao et al., 1996). CN might also inhibit the Na^+-independent Ca^{2+} efflux from mitochondria (Gunter et al., 1994), which is the dominant mechanism of Ca^{2+} extrusion from the mitochondrial matrix in renal cells (Gunter et al., 1994). Despite these reports on the non-specific actions of cyanide in some cell types, the comparison of the action of 5 different chemical inhibitors of oxidative phosphorylation (antimycin A, rotenone, cyanide, oligomycin and carbonyl cyanide m-chlorophenyl hydrazone) revealed no significant differences in their effects on tubule cell integrity, intracellular ATP levels, cellular K^+ depletion and the decrease of intracellular glutathione levels in isolated rabbit proximal tubules (Weinberg et al., 1990). Similarly, the increase in NAD(P)H autofluorescence with CN incubation was indistinguishable from that with amytal (a site I blocker of the electron transport chain) incubation in rat myocytes (Esumi et al., 1991).

In Chapter 5, we evaluated the time course of cell viability during metabolic inhibition and examined whether it provokes apoptosis, necrosis or intermediate forms of cell death in A6 cells. Independent methods (light microscopy, fluorescence microscopy and transmission electron microscopy) showed that almost all A6 cells died

via the necrotic cell death pathway after prolonged (> ~ 8 hours) exposure to metabolic inhibitors. It has long been recognised that necrosis is a major form of cell death associated with ischemic acute renal failure (Ueda and Shah, 2000). However, there is accumulating evidence indicating a role of apoptotic pathways in *in vitro* and *in vivo* models of acute renal failure. The *in vivo* studies of ischemia/reperfusion so far demonstrate apoptosis only during the reperfusion period (Ueda et al., 2000). In general, the *in vitro* studies have shown apoptosis and DNA fragmentation in renal tubular cells during 'hypoxia' as well as 'reoxygenation' (Allen et al., 1992; Wiegele et al., 1998; Lieberthal et al., 1998; Saikumar et al., 1998). Since most *in vitro* models mimicked 'hypoxia' via metabolic inhibition in the presence of oxygen, this discrepancy between *in vivo* and *in vitro* studies might be ascribed to the presence of oxygen and the resulting reactive oxygen metabolites (ROM) (Ueda et al., 2000). ROM can induce apoptosis in a variety of cells, including renal tubular cells (Ueda et al., 2000). In our A6 model only some occasional apoptotic cells or apoptotic remnants in neighbouring epithelial cells were detected (via transmission electron microscopy) after 1 hour of MI. Although apoptosis usually is difficult to detect in tissue sections, even when responsible for extensive cell loss (Lieberthal, 1997), supposing substantial apoptotic cell death is unrealistic in our experimental model since A6 monolayers were able to restore their transepithelial transport function completely in 2 hours time from total loss of function after 45 min of MI (Chapter 6).

At present, it is generally accepted that it is the severity of the insult, rather than the type of the insult, that determines whether the cell will undergo apoptosis or necrosis (Bonfoco et al., 1995; Formigli et al., 2000). Actually, the intracellular ATP content is believed to be the downstream controller directing the cells either towards apoptosis, if intracellular ATP levels are sufficient to supply for this active cell death program, or either towards necrosis, in energy-deprived cells (Eguchi et al., 1997; Leist et al., 1997; Lieberthal et al., 1998; Formigli et al., 2000). The decrease of intracellular ATP content to ~ 20 % of the initial level in the early phase of the insult has been reported to represent a threshold that determines whether cells die by necrosis (< 20 %) or apoptosis (> 20 %) in the later phases of the insult (Lieberthal et al., 1998; Formigli et al., 2000). Since in A6 cells, intracellular ATP levels dropped to less than 20 % of the initial level during the first 45 min of MI (Chapter 6), a necrotic cell death could indeed be expected after prolonged MI.

The results in Chapter 5 illustrated that distal tubular A6 cells are very resistant to metabolic arrest. The higher resistance of distal tubular cells, in comparison with more proximal nephron segments, to a severe reduction in the cellular ATP content is well documented (Brady et al., 2000) but the mechanisms responsible for this effect are largely unknown. One can speculate that the profound intracellular acidification observed in this study (Chapters 6 and 7) protects the cells during ATP depletion. In

literature, the role of cytosolic acidification is ambivalent. Whereas massive cytosolic acidosis is harmful to the cell, mild acidosis has been shown to have a protective effect during ischemia in several organ systems, including the kidney (Weinberg, 1991; Weinberg et al., 1991; Edelstein et al., 1996). Cellular acidification was found to occur during anoxia in cultured, but not in freshly isolated rabbit proximal tubular cells (Rose et al., 1995). However, the differences in susceptibility to anoxic injury between cultured and freshly isolated proximal tubular cells could not be explained by cellular acidification in cultured cells because prevention of acidification in cultured proximal tubular cells did not lead to increased cell death (Rose et al., 1995). Nevertheless, it is most interesting that EIPA and similar drugs that stop the Na^+/H^+ exchanger –and thus lead to intracellular acidosis- have been shown to be protective in conditions of cardiac ischemia (Bugge and Ytrehus, 1995; Scholz et al., 1993). The presence of pH_c-dependent solute transport pathways in some cell types might allow cytoprotective pH_c-mediated modulation of transport activity.

Hochachka described that the most serious perturbations of hypoxia arise from an imbalance between (i) the extent of depression of ATP synthesis rates and (ii) the depression of processes requiring ATP (Hochachka, 1986). Careful analysis of hypoxia-tolerant animals (e.g. hibernators) revealed that the coupling of metabolic arrest to 'channel-arrest' could be an important defence strategy against hypoxia. Hypoxia tolerant tissues compensate for reduced ATP-dependent ion pumping capacities during O_2 lack by reducing the densities of functional ion channels in proportion to declining metabolic rate. The net effect of that mechanism is to maintain the ratio of ion influx rates to pumping rates at ~ unity, even during metabolic inhibition of varying degrees (Hochachka, 1986). A6 cells might defend themselves in a similar way against the harmful consequences of ATP depletion. The gradual pH_c drop from ~7 to ~6.6 in the first 25 min of MI (Chapter 6) is –according to Harvey's titration curve for ENaCs in A6 cells (Harvey, 1995)- sufficient to maximally reduce the open probability P_o and thus, to inactivate a major amount of ENaCs. The closure of ENaCs during MI was also confirmed by the drastic decrease in apical P_{Na} during 45 min of MI as shown in combined I_{sc} and G_T experiments (Chapter 6). The pronounced inhibition of ap. Na^+ entry after 25 min of MI is consistent with the cell swelling of metabolically inhibited A6 cells only in the first ~25 min of MI (Chapter 7). Afterwards, reduction of apical Na^+ influx is probably sufficient to allow the hindered bl. Na^+ pump to preserve cellular volume. Other A6 monolayers, which displayed low Na^+ transport rates in control conditions, were – just because of the low intrinsic Na^+ entry – less susceptible to metabolic arrest, since no cell swelling at all was detected in these epithelia (Chapter 7). The parallel course of both recovery of I_{sc} and re-alkalinisation of pH_c after MI in originally high rate Na^+ transporting epithelia (Chapter 6), further support the proposition of ENaC modulation by protons and consequently inhibition by intracellular acidification during MI.

Another defence strategy of metabolically challenged A6 cells might consist of the reversal action of the mitochondrial F_1F_0-ATPase during the first phase of MI in A6 cells: it might hydrolyse ATP to pump protons out of the mitochondrial matrix in an attempt to preserve the mitochondrial potential in the absence of electron transport (Chapter 6). This was suggested by measurements of the intracellular ATP content and the mitochondrial membrane potential ($\Delta\Psi_m$) during metabolic arrest in the absence and presence of oligomycin, a specific blocker of the mitochondrial ATP synthase. The reversal of the mitochondrial F_1F_0-ATPase in an attempt to preserve $\Delta\Psi_m$ was reported earlier for different cell types (Rouslin, 1991; Duchen and Biscoe, 1992; Di Lisa et al., 1995; Leyssens et al., 1996; Duchen, 1999). The conservation of $\Delta\Psi_m$ is important since it prevents mitochondrial swelling (Duchen, 1999) and allows mitochondria to accumulate Ca^{2+} via the Ca^{2+} uniporter, thus avoiding a Ca^{2+} overload of the cytoplasm (Gunter et al., 1994).

As discussed above, cell swelling during metabolic inhibition in A6 cells is dependent on the rate of Na^+ transport. In high rate Na^+ transporting cells, cell swelling occurs until massive salt influx is prevented by closure of the ap. Na^+ influx pathways. The arrest of tubular cell swelling is an important intervention to prevent extreme occlusion of the tubular lumen. The distal nephron segments, e.g. thick ascending limbs, are known to swell in the luminal direction –therefore contributing to tubular obstruction-, whereas cell swelling of the proximal tubule proceeds in the serosal direction at the expense of vascular space (Mason et al., 1989). Hence, epithelial cell swelling during metabolic arrest contributes to renal dysfunction via tubular obstruction, raised tubular pressure and decreased GFR on the one hand, and by compression of blood vessels and vascular congestion on the other hand. Therefore, it is not surprising that the experience of the last few decades in the improvement of *ex-vivo* kidney preservation solutions indicate that the addition of mannitol, or otherwise insuring hypertonicity of the perfusate, to prevent cell swelling, is critical to the efficacy of prevention of post-transplant acute renal failure (Better et al., 1997).

The results of Chapter 7 further indicate that MI inhibits the regulatory volume decrease (RVD) in response to isosmotic cell swelling (due to MI itself) as well as to anisosmotic swelling (elicited via a reduction of the basolateral tonicity). Our findings suggest that the intracellular acidification that accompanies MI might play a role in RVD inhibition. The RVD inhibiting effect of intracellular acidification was deduced from the marked delay of RVD in response to a hypotonic shock during a transient acidification induced by a NH_4Cl pre-pulse. Moreover, a striking difference was seen in RVD response when cells were chronically or acutely treated with external acidic solutions (pH 5). Chronic treatment of A6 monolayers resulted in the absence of RVD, since the cells were well acidified at the moment when the hypotonic shock was applied. In contrast, acute treatment with external pH 5 allowed the onset of RVD but

subsequently, RVD was completely inhibited after at least 10 minutes. The latter time period allowed a steady acidification of the cells. The mechanism of the suggested RVD inhibition by internal protons was not identified in this study. Whatever the exact mechanism may be, a failure in cell volume regulation secondary to a severe disturbance of the cell metabolic processes and intracellular acidification, can cause the drop of GFR and the impaired reflow observed after temporary interruption of the circulation in ischemic kidneys.

A last point that must be discussed here is the significance of the *in vitro* results for the *in vivo* situation. The experiments shown in Chapters 6 and 7 were designed to investigate the cellular effects of energy deprivation as they occur in the non-lethally injured renal cells exposed to hypoxia/ischemia. However, due to long-term cultivation, the cells underwent a process of dedifferentiation so that they do not maintain all the structural and functional properties of the nephron segment of origin. Certainly, cell culture models do not necessarily reflect the issues in human acute renal failure, and results obtained in cell cultures cannot be transferred directly onto the human situation. On the other hand, cultured cells offer the advantage of having a high resistance to ATP depletion. A6 cells, a well-characterised and established distal kidney cell culture model in epithelial research which is derived from amphibian origin, are even more resistant to metabolic inhibition as compared to other mammalian cell types in culture, presumably because of their lower metabolism. Their long term (> 6 hours) survival in face of metabolic inhibitors allows a detailed study of the cellular and the subcellular events that occur and enables to identify the relationships between them. These aspects are more difficult to investigate in primary cultures or freshly isolated cells, because the survival period is confined to a significantly shorter time interval (generally, tens of minutes). Consequently, although the results obtained in A6 cells have to be confirmed in conditions closer to the *in vivo* situation (in primary cultures and freshly isolated cells), they indicate the main mechanisms one should look for in other renal models. Further basic research is necessary to improve the understanding of the cellular events occurring in renal cells facing ischemic conditions and their implications for cell survival. Hopefully, insights derived from experimental models of renal ischemia finally will provide therapeutic tools to improve the bad prognosis of acute renal failure in the future.

Nederlandstalige samenvatting en algemene discussie

Het doel van deze studie was het onderzoeken van bepaalde aanpassingen van cellulaire processen met betrekking tot Na^+ reabsorptie, intracellulaire pH en volumeregeling in tubulaire niercellen tijdens ischemische omstandigheden. Aangezien de regeneratie van de nier na ischemie bepaald wordt door de capaciteit van de overlevende cellen om zich te herstellen en te vermenigvuldigen, was deze studie erop gericht mogelijke cellulaire beschermingsmechanismen te ontrafelen van niertubuluscellen die slechts sub-letaal beschadigd worden tijdens ischemische condities. Om nierischemie in distale tubuluscellen na te bootsen werd metabolische inhibitie (MI) van A6 cellen toegepast als een *in vitro* experimenteel model.

In het algemeen gaat nierischemie gepaard met een uitgesproken daling van de tubulaire reabsorptieprocessen mede bepaald door de verminderde filtratie (Tanner et al., 1973; Brady et al., 2000; Hanley, 1980; Johnston P.A. et al., 1984; Brady et al., 2000). Vermits in normale omstandigheden het grootste deel van de gefilterde zouten gereabsorbeerd wordt in de proximale tubulussegmenten en de dikke stijgende tak van de lis van Henle, worden distale tubulusepitheelcellen meestal niet geconfronteerd met hoge apicale zoutconcentraties. De normale Na^+ concentratie in de distale tubulus van de rat bedraagt ongeveer 45-65 mM (Schnermann et al., 1966; Seney et al., 1987). Schnermann en zijn medewerkers meldden een toename van de distale Na^+ concentratie tot 98-143 mM na 30 tot 60 minuten afklemming van de nierarterie (Schnermann et al., 1966). Het gestegen Na^+ gehalte in het lumen van de distale tubuli (Braam et al., 1993) zou bijgevolg de distale epitheelcellen kunnen bedreigen met een te hoge Na^+ influx en de hiermee gepaard gaande schadelijke gevolgen. In Hoofdstuk 3 werd onderzocht hoe A6 cellen reageren op een verhoogde apicale Na^+ concentratie in normale (niet-ischemische) omstandigheden. De resultaten gaven aan dat de apicale Na^+ opname doorheen ENaC's verzadigde met stijgende apicale Na^+ concentraties ($[Na^+]_{ap}$). Aan de hand van ruisexperimenten werd bovendien aangetoond dat deze verzadiging van de transepitheliale Na^+ stroom (I_{Na}) gegenereerd wordt door zowel de Na^+ afhankelijkheid van de densiteit van open kanalen, N_o, als door de verzadiging van de stroom doorheen één enkel kanaal, i. Bij een toename van $[Na^+]_{ap}$ van 3 tot 20 mmol/l daalt de densiteit N_o sterk en gedraagt zich verder als een $[Na^+]_{ap}$-onafhankelijke parameter tussen 20 en 110 mmol/l. De stroom doorheen één kanaal verzadigt met een schijnbare Michaelis-Menten konstante (K_m) van ~17 mmol/l. De verzadiging van de conductantie van het kanaal kan aan de basis liggen van de verzadiging van i zoals reeds werd gesuggereerd door experimenten met gereconstrueerde A6 ENaC kanalen in planaire lipide dubbellagen (Olans et al., 1984). In deze laatste studie werd eveneens een K_m van ongeveer 17 mmol/l vastgesteld. Vanuit fysiologisch standpunt bekeken, kan de beperkte transportcapaciteit van het amiloride-gevoelige Na^+ kanaal een belangrijke eigenschap zijn om het overspoelen van de cel met extracellulair Na^+, en de gevolgen

hiervan voor de intracellulaire ionen homeostasen, te voorkomen in situaties met een gestegen apicale Na^+ concentratie zoals o.a. tijdens ischemie.

Een daling van de intracellulaire pH (pH_c) tijdens ischemie treedt op in de meeste cellen (Brady et al., 2000). Zoals verwacht induceerde metabolische inhibitie ook een uitgesproken intracellulaire verzuring (van pH_c 7.02 tot 6.46) in het gebruikte experimenteel A6 model. Daarom onderzochten we in Hoofdstuk 4 of een daling van pH_c in niet-ischemische omstandigheden de apicale Na^+ permeabiliteit (P_{Na}) moduleert en of pH_c een effect heeft op de I_{Na}-kinetiek zoals beschreven werd in Hoofdstuk 3. We konden aantonen dat wijzigingen in pH_c tijdens verscheidene manipulaties, zoals bijvoorbeeld tijdens een apikale of basolaterale NH_4Cl-puls, weerspiegeld worden in I_{Na} en G_T veranderingen. Verder constateerden we dat N_o de enige parameter is die door pH_c wordt bepaald en zo de I_{Na} beïnvloedt. Bovendien bleek dat de maximale stroomwaarde (I_{max}), als enige kinetische parameter van de I_{Na} verzadiging, pH_c afhankelijk is. De pH_c-onafhankelijkheid van K_m suggereert een interactieplaats op het ENaC waar interne protonen en extracellulaire Na^+ ionen niet competitief zijn. Dit niet-competitieve aspect van de ENaC modulatie door externe Na^+ ionen en interne protonen kan de pH_c-onafhankelijkheid van i verklaren, vermits i vooral bepaald wordt door externe Na^+ ionen zoals beschreven in Hoofdstuk 3. pH_c-afhankelijke veranderingen in N_o kunnen veroorzaakt worden door veranderingen in de open probabiliteit van het ENaC, P_o, en/of door wijzigingen in de totale densiteit van kanalen, N_T. De pH_c-afhankelijkheid van P_o werd recent aangetoond voor de α-ENaC subeenheid van rattennieren die tot expressie gebracht was in *Xenopus* oöcyten of ingebouwd werd in planaire lipiden dubbellagen (Chalfant et al., 1999). Intracellulaire verzuring reduceerde de gemiddelde tijd dat het kanaal open was en veroorzaakte een verlenging van de gemiddelde tijd dat het kanaal dicht was. De conductantie van het kanaal bleef echter konstant. Er zijn verscheidene hormonen bekend die P_{Na} kunnen regelen in dichte epithelen (Garty and Palmer, 1997), met inbegrip van A6 cellen (Erlij et al., 1999). Dit gebeurt door het reversiebel inbouwen van kanalen in het plasmamembraan vanuit intracellulaire vesikels. Het is momenteel onmogelijk om te besluiten of pH_c enkel P_o moduleert of ook N_T van de apikale ENaC's.

Een grote verscheidenheid aan boodschapperfuncties wordt toegeschreven aan intracellulaire protonen, zoals ook de simultane 'cross talk' modulatie van apikale Na^+ en basolaterale K^+ permeabiliteiten in dichte, Na^+-transporterende epithelen (Harvey, 1995). Het is bekend dat veranderingen in pH_c kunnen optreden als onmiddellijk gevolg van hormonale acties (Lyall et al., 1995), zoals bijvoorbeeld de stimulatie van de Na^+/H^+ uitwisselaar door steroid hormonen (Urbach et al., 1996). Een verandering in pH_c wordt echter niet enkel veroorzaakt door hormonen. Ook ionenkanalen kunnen een permanente bedreiging vormen voor de cel als bron van extracellulaire protonen (Lyall et al., 1993; Lyall et al., 1995), aangezien de netto drijvende kracht voor protonen

bijna altijd inwaarts gericht is. Zo kunnen protonen zich opstapelen in het cytosol in omstandigheden waarbij de energievoorziening voor de extrusiemechanismen van protonen onvoldoende is, zoals tijdens ischemie. Bovendien zullen de glycolyse en ook de hydrolyse van ATP zonder regeneratie (Hochachka and Mommsen, 1983) bijdragen tot de intracellulaire verzuring, die uiteindelijk de homeostase van de cel totaal zal ontregelen. Deze reactieketen kan echter eindigen indien het binnenstromen van extracellulaire protonen doorheen de alkali-ionenkanalen kan verhinderd worden door het sluiten van deze laatste onder invloed van een negatieve terugkoppeling van intracellulaire protonen. Hierdoor kunnen de cellen zich beschermen tegen een dodelijke intracellulaire verzuring.

Hoofdstukken 3 en 4 verschaffen waardevolle informatie over de ENaC karacteristieken in normaal functionerende cellen. Het amiloride-gevoelige ENaC vertoont een beperkte transportcapaciteit, die de cellen kunnen behoeden tegen een overdreven Na^+ influx in omstandigheden met een gestegen $[Na^+]_{ap}$ (Hoofdstuk 3). N_o is pH_c-gevoelig in die zin dat een pH_c daling N_o doet dalen en een pH_c toename N_o doet stijgen (Hoofdstuk 4). De afname van N_o in zure cellen kan de cellen beschermen tegen extreme intracellulaire verzuring. Daarenboven draagt het sluiten van ENaC's bij tot het verminderen van zoutinflux. Dit is uiteraard van cruciaal belang in cellen met een gehinderde basolaterale Na^+/K^+-ATPase activiteit, zoals hieronder aangegeven. De ENaC aspecten zoals hierboven beschreven, zijn belangrijk voor het situeren van de verschillende cellulaire processen die optreden in metabolisch geïnhibeerde cellen (Hoofdstukken 5, 6 en 7).

In deze studie (Hoofdstukken, 5, 6 en 7) werd een ATP-depletie gerealiseerd in A6 cellen met behulp van de metabolische inhibitoren cyanide (2.5 mM, CN) en 2-deoxyglucose (20 mM, DOG). MI met CN en DOG wordt meestal gebruikt om ischemie te simuleren in *in vitro* modellen (Eisner et al., 1989; Esumi et al., 1991; Sheridan et al., 1993; Doctor et al., 1994; Leyssens et al., 1996; Karwatowska-Prokopczuk et al., 1998). CN heeft het voordeel van goed uitwasbaar te zijn (zoals aangetoond in Hoofdstuk 6 door de onmiddellijke daling van de $NAD(P)H/NAD(P)^+$ ratio). Er werden echter een aantal niet-specifieke effecten van cyanide beschreven. Bij zeer lage concentraties (10-100 μM), kan CN interfereren met signaaltransductiewegen door een directe interactie met bepaalde receptoren (Yang et al., 1996; Sun et al., 1997). CN kan bijvoorbeeld interageren met het N-methyl-D-aspartaat receptorkanaalcomplex in cerebellaire granulaire cellen en daar de receptor gemedieerde respons versterken (Sun et al., 1997). Er werd bovendien beschreven dat CN K^+ stromen kan reduceren in type I cellen van het carotisch lichaam (Peers and O'Donnell, 1990). Deze reductie gebeurde onafhankelijk van de aanwezigheid van ATP. Directe effecten van CN, ongerelateerd aan metabolische

effecten, werden ook beschreven op K^+ kanalen in de uiteinden van motorneuronen van muizen (Chao et al., 1996). CN kan ook de Na^+-onafhankelijke Ca^{2+} efflux uit mitochondriën inhiberen (Gunter et al., 1994), hetgeen het belangrijkste Ca^{2+} extrusiemechanisme is in niercellen (Gunter et al., 1994). Ondanks deze niet-specifieke effecten van CN in bepaalde celtypes, leverde de vergelijking van 5 verschillende chemische inhibitoren van de oxidatieve fosforylatie (antimycine A, rotenone, cyanide, oligomycine en carbonyl cyanide m-chlorophenyl hydrazone) geen significante verschillen op in hun effecten op de celintegriteit, intracellulaire ATP gehaltes, cellulaire K^+ depletie en de afname van het intracellulaire glutathiongehalte in geïsoleerde proximale tubuli van het konijn (Weinberg et al., 1990). Analoog hiermee is de vaststelling dat de stijging in NAD(P)H autofluorescentie geïnduceerd door incubatie met CN niet te onderscheiden is van deze geïnduceerd met amytal (een inhibitor van het complex I in de elektronentransportketen) in myocyten van de rat (Esumi et al., 1991).

In Hoofdstuk 5 werd het tijdsverloop van de celleefbaarheid tijdens metabolische inhibitie onderzocht en werd nagegaan of apoptose, necrose of intermediaire vormen van celdood optreden in A6 cellen. Verscheidene onafhankelijke methoden (lichtmikroscopie, fluorescentiemikroscopie en transmissie-elektronenmikroscopie) toonden aan dat bijna alle A6 cellen stierven aan necrotische dood na een blootstelling van meer dan 8 uur aan metabolische inhibitoren. Het is reeds lang bekend dat necrose de belangrijkste vorm van celdood uitmaakt bij ischemisch nierfalen (Ueda and Shah, 2000). Er zijn echter meer en meer evidenties voor een rol van apoptose in *in vitro* en *in vivo* modellen van acuut nierfalen. De *in vivo* studies van ischemie en reperfusie geven tot nu toe enkel apoptose aan tijdens de reperfusieperiode (Ueda et al., 2000). In het algemeen tonen *in vitro* studies apoptose en DNA fragmentatie aan zowel tijdens de hypoxische periode als tijdens de reoxygenatie (Allen et al., 1992; Wiegele et al., 1998; Lieberthal et al., 1998; Saikumar et al., 1998). Aangezien de meeste *in vitro* modellen hypoxie nabootsen via MI in de aanwezigheid van zuurstof, kan deze discrepantie mogelijkerwijze toegeschreven worden aan de aanwezigheid van zuurstof en de resulterende reactieve zuurstofmetabolieten (ROM) (Ueda et al., 2000). ROM kunnen apoptose induceren in verscheidene celtypen, met inbegrip van niertubuluscellen (Ueda et al., 2000). In het A6 model van deze studie werden slechts occasioneel apoptotische cellen of apoptotische celresten gedetecteerd (via transmissie-elektronenmikroscopie) na 1 uur van MI. Het is moeilijk apoptose te detecteren in weefselcoupes, zelfs wanneer dit proces verantwoordelijk is voor een aanzienlijk verlies aan cellen (Lieberthal, 1997). Desondanks is het onrealistisch om een substantiële apoptotische celdood te veronderstellen in het bestudeerde modelpreparaat, vermits A6 cellen in staat waren

hun transepitheliale transport functie volledig te herstellen in twee uur tijd na volledig functieverlies ten gevolge van een MI gedurende 45 minuten (Hoofdstuk 6).

Tegenwoordig wordt algemeen aanvaard dat het eerder de sterkte van de bedreiging is die bepaalt of een cel apoptose of necrose zal ondergaan in plaats van het type van de bedreiging (Bonfoco et al., 1995; Formigli et al., 2000). Vermoedelijk is het niveau van intracellulaire ATP bepalend. Indien de intracellulaire ATP concentraties voldoende hoog zijn kan het actieve celdoodprogramma (apoptose) voorzien worden van energie, in het andere geval volgt necrose (Eguchi et al., 1997; Leist et al., 1997; Lieberthal et al., 1998; Formigli et al., 2000). De daling van het intracellulaire ATP gehalte tot ~ 20% van de initiële hoeveelheid in de eerste fase van de bedreigende situatie werd beschreven als een drempelwaarde, die zou bepalen of een cel gaat afsterven via necrose (< 20 %) of apoptose (> 20 %) (Lieberthal et al., 1998; Formigli et al., 2000). Vermits de intracellulaire ATP concentratie in A6 cellen afnam tot minder dan 20% van het initiële niveau tijdens de eerste 45 minuten van MI (Hoofdstuk 6), kon een necrotische celdood verwacht worden bij langere incubaties met metabolische inhibitoren.

De resultaten van Hoofdstuk 5 illustreren dat de distale A6 cellen zeer resistent zijn tegen MI. De hogere resistentie van distale cellen in vergelijking met meer proximale tubuluscellen is alom bekend (Brady et al., 2000), maar de mechanismen die verantwoordelijk zijn voor deze resistentie zijn grotendeels onbekend. Men kan speculeren dat de uitgesproken intracellulaire verzuring die geobserveerd werd in deze studie (Hoofdstukken 6 en 7) de cel beschermt tijdens de ATP-depletie. Volgens de literatuur is de rol van een intracellulaire verzuring echter ambivalent. Terwijl een extreme verzuring schadelijk is voor de cel, werd aangetoond dat een milde verzuring een beschermende invloed kan hebben in verschillende organen zoals ook in de nieren (Weinberg, 1991; Weinberg et al., 1991; Edelstein et al., 1996). Er werd vastgesteld dat een anoxie-geïnduceerde intracellulaire verzuring optrad in proximale tubuluscellen van het konijn in cultuur, maar niet in vers geïsoleerde tubuluscellen (Rose et al., 1995). Desalniettemin is het een interessante waarneming dat EIPA en gelijkaardige substanties die de Na^+/H^+ uitwisselaar blokkeren -en bijgevolg leiden tot acidose- protectief werken in hartcellen tijdens ischemische condities (Bugge and Ytrehus, 1995; Scholz et al., 1993). De aanwezigheid van pH_c-gevoelige transportsystemen in bepaalde celtypen kan een beschermende pH_c-gemedieerde modulatie van de transportactiviteit toelaten, wat energie-besparend zou kunnen werken.

Hochachka beschreef dat de meest ernstige storingen door hypoxie te wijten zijn aan een onevenwicht tussen (i) de graad van onderdrukking van ATP-synthese processen in de cellen en (ii) de onderdrukking van de ATP-verbruikende processen

(Hochachka, 1986). Zorgvuldige analyse van hypoxie-tolerante dieren (bijvoorbeeld van dieren die een winterslaap houden) toonde aan dat de koppeling tussen metabolische inhibitie en het sluiten van kanalen een belangrijke verdedigingsstrategie kan zijn tegen hypoxie. Dieren, die tolerant zijn voor hypoxische condities, compenseren voor de vermindering van het ATP-afhankelijke pompen van ionen tijdens een periode van zuurstoftekort door de densiteit van functionele ionenkanalen proportioneel aan te passen aan het gereduceerd metabolisme. Het netto-effect van dit mechanisme is het behoud van de verhouding van ionenfluxen tot pompsnelheden rond 1, zelfs tijdens variërende graden van MI (Hochachka, 1986). Mogelijkerwijze kunnen A6 cellen zich verdedigen op een gelijkaardige manier tegen de schadelijke gevolgen van ATP-depletie. De geleidelijke daling van pH_c van ~7 tot ~6.6 tijdens de eerste 25 minuten van MI (Hoofdstuk 6) is -volgens de titratiecurve in A6 cellen (Harvey, 1995)- voldoende om P_o maximaal te reduceren en dus om het grootste deel van de ENaC's te sluiten. Het sluiten van de ENaC kanalen tijdens MI werd bevestigd door de drastische afname van P_{Na} zoals te zien in de gecombineerde metingen van I_{sc} en G_T (Hoofdstuk 6). De uitgesproken inhibitie van de Na^+ influx na 25 minuten van MI is in overeenstemming met het feit dat de cel zwelling tijdens MI beperkt blijft tot de eerste 25 minuten van MI (Hoofdstuk 7). Nadien is de reductie van de apicale Na^+ influx waarschijnlijk voldoende om de gehinderde basolaterale Na^+ pomp toe te laten het celvolume te behouden. A6 monolagen, die lage Na^+ transportsnelheden vertoonden, waren -juist omwille van hun lage intrinsieke Na^+ influx- minder vatbaar voor MI, aangezien geen celzwelling gedetecteerd werd in deze epithelen (Hoofdstuk 7). Het parallelle verloop van, enerzijds het herstel van I_{sc} en, anderzijds de re-alkalinisatie na MI in epithelen met een hoge initiële Na^+ transportsnelheid (Hoofdstuk 6), vormt een bijkomend argument voor de suggestie van ENaC modulatie door interne protonen.

Een andere mogelijke verdedigingsstrategie van A6 cellen, blootgesteld aan metabolische inhibitoren, kan eruit bestaan de mitochondriale F_1F_0-ATPase om te keren tijdens de eerste fase van MI: de pomp zou dan ATP kunnen hydrolyseren om protonen uit de mitochondriale matrix te pompen in een poging om zo de mitochondriale potentiaal te behouden in afwezigheid van de elektronentransportketen (Hoofdstuk 6). Dit werd gesuggereerd door metingen van het intracellulaire ATP-gehalte en de mitochondriale potentiaal ($\Delta\Psi_m$) tijdens MI in afwezigheid en aanwezigheid van oligomycine, een specifieke blokker van de mitochondriale ATP-synthase. Het omkeren van de mitochondriale F_1F_0-ATPase in een poging om $\Delta\Psi_m$ te bewaren werd reeds beschreven voor verschillende celtypen (Rouslin, 1991; Duchen and Biscoe, 1992; Di Lisa et al., 1995; Leyssens et al., 1996; Duchen, 1999). Het behoud van $\Delta\Psi_m$ is belangrijk vermits het de mitochondriale zwelling kan voorkomen (Duchen, 1999) en de mitochondriën toelaat Ca^{2+} te accumuleren via de Ca^{2+} uniporter waardoor een te hoge Ca^{2+} concentratie in het cytosol vermeden wordt (Gunter et al., 1994).

Zoals reeds eerder vermeld is de cel zwelling van A6 cellen tijdens MI afhankelijk van de Na^+ transportsnelheid. In cellen met een hoog Na^+ transport treedt celzwelling op totdat de extreme Na^+ influx drastisch verminderd is door het sluiten van de apikale Na^+ influxwegen. Het verhinderen van een verdere celzwelling is belangrijk om extreme vernauwing van het tubulaire lumen te voorkomen. De distale nefronsegmenten, bijvoorbeeld de dikke stijgende tak van de lis van Henle, zwellen in de luminale richting en dragen daarom bij tot luminale obstructie. Celzwelling van de proximale tubulus daarentegen gebeurt in de serosale richting ten koste van ruimte voor de bloedvaten (Mason et al., 1989). Celzwelling tijdens MI draagt daardoor bij tot een verstoring van de nierfunctie door tubulaire obstructie, een gestegen tubulaire druk en een hierdoor gedaalde GFR enerzijds, en door compressie van de bloedvaten en bijgevolg vasculaire obstructie anderzijds. Daarom is het niet verrassend dat de ervaring van de laatste decaden m.b.v. de verbetering van het behoud van een goede nierfunctie *ex vivo* leert dat de toevoeging van mannitol, of ook de hypertoniciteit van het perfusaat, kritisch is voor een doelmatige preventie van acuut nierfalen na de transplantatie (Better et al., 1997).

De resultaten van Hoofdstuk 7 geven verder aan dat MI de RVD (regulatory volume decrease) inhibeert die normaal optreedt na zowel isosmotisch celzwellen (geïnduceerd door MI zelf) als na anisosmotisch celzwellen (uitgelokt door een reductie van de basolaterale toniciteit). Onze bevindingen suggereren dat de intracellulaire acidificatie die gepaard gaat met MI een rol zou kunnen spelen in deze RVD inhibitie. Het RVD inhiberende effect van een intracellulaire verzuring werd afgeleid uit de duidelijke vertraging van de RVD na een hypotone shock tijdens een transiënte verzuring geïnduceerd door een NH_4Cl-puls. Bovendien stelden we een uitgesproken verschil vast in de RVD respons wanneer cellen chronisch of acuut behandeld werden met externe zure oplossingen (pH=5). Een chronische behandeling van A6 monolagen resulteerde in de afwezigheid van RVD, aangezien de cellen reeds voldoende verzuurd waren op het moment dat de basolaterale toniciteit werd verlaagd. Daartegenover staat de acute behandeling met een externe zure pH (pH=5) die het begin van een RVD respons toeliet, maar waarbij de RVD vervolgens volledig geïnhibeerd werd na tenminste 10 minuten. Tijdens deze 10 minuten trad er een duidelijke intracellulaire verzuring op. Het mechanisme van een mogelijke RVD inhibitie door interne protonen werd niet bepaald in deze studie. Wat ook het exacte mechanisme is, het ontbreken van een celvolumeregeling ten gevolge van een verstoring in het celmetabolisme en een intracellulaire verzuring, kunnen mede aan de basis liggen van de daling in GFR en de verhinderde doorbloeding die men vaststelt na een tijdelijke verbreking van de circulatie in ischemische nieren.

Tenslotte bespreken we het belang van deze *in vitro* resultaten voor de *in vivo* situatie. De experimenten die getoond werden in Hoofdstukken 6 en 7 waren ontworpen om bepaalde cellulaire gevolgen van energie-depletie te onderzoeken zoals deze voorkomen in niet-dodelijk beschadigde niercellen die bloot gesteld werden aan hypoxie/ischemie. Omwille van het kweken van de niercellen gedurende lange termijn ondergingen deze een proces van dedifferentiatie zodat ze niet meer alle structurele en functionele eigenschappen vertonen van het oorspronkelijke nefronsegment. Uiteraard weerspiegelen deze celcultuurmodellen niet noodzakelijk hetgeen er gebeurt tijdens acuut nierfalen bij de mens. De resultaten die verkregen worden op celculturen kunnen dan ook niet onmiddellijk geextrapoleerd worden naar de menselijke situatie. Anderzijds bieden cellen in cultuur het voordeel dat ze een hogere weerstand bezitten tegen ATP depletie. De A6 cellijn, die afkomstig is van een amfibie, is een alom gekend model voor de distale tubuluscellen in het domein van epitheelonderzoek. Deze cellijn heeft meer weerstand tegen metabolische inhibitie dan andere cellijnen afkomstig van zoogdieren, vermoedelijk omwille van hun lager metabolisme. De lange overlevingstermijn (> 6 uren) tijdens blootstelling aan metabolische inhibitoren laat een gedetailleerde studie toe van de cellulaire en subcellulaire gebeurtenissen tijdens MI en hun onderlinge verbanden. Deze aspecten zijn veel moeilijker te onderzoeken in primaire culturen of vers geïsoleerde cellen omdat de overlevingsperiode daar beperkt blijft tot een duidelijk korter tijdsinterval (in het algemeen slechts minuten). Ondanks het feit dat de resultaten van deze studie op A6 cellen dienen bevestigd te worden in omstandigheden die de *in vivo* situatie beter benaderen (in primaire culturen en vers geïsoleerde niercellen bijvoorbeeld), kan deze studie toch de belangrijke mechanismen aangeven waarnaar men moet zoeken in andere modellen. Meer onderzoek is nodig om de cellulaire gebeurtenissen in niercellen tijdens ischemie beter te verstaan. Hopelijk kunnen de inzichten verworven uit relevante experimentele modellen van nierischemie uiteindelijk therapeutische middelen aanreiken om de slechte prognose van acuut nierfalen te verbeteren.

References

Abramcheck FJ, Van Driessche W, and Helman SI. (1985). Autoregulation of apical membrane Na^+ permeability of tight epithelia. Noise analysis with amiloride and CGS 4270. *J Gen Physiol* 85: 555-582

Abriel H and Horisberger J-D. (1999). Feedback inhibition of rat amiloride-sensitive epithelial sodium channels expressed in Xenopus laevis oocytes. *J Physiol* 516: 31-43

Al-Awqati Q, Gluck S, Reeves W, and Cannon C. (1983). Regulation of proton transport in urinary epithelia. *J Exp Biol* 106: 135-141

Allen J, Winterford C, Axelsen RA, and Gobe GC. (1992). Effects of hypoxia on morphological and biochemical characteristics of renal epithelial cell and tubule cultures. *Renal Fail* 14: 453-460

Alvarez de la Rosa D, Canessa CM, Fyfe GK, and Zhang P. (2000). Structure and regulation of amiloride-sensitive sodium channels. *Annu Rev Physiol* 62: 573-594

Atia F, Zeiske W, and van Driessche W. (1999). Secretory apical Cl- channels in A6 cells: possible control by cell Ca2+ and cAMP. *Pflugers Arch* 438: 344-53

Banderali U and Roy G. (1992). Activation of K^+ and Cl^- channels in MDCK cells during volume regulation in hypotonic media. *J Membrane Biol* 126: 219-234

Bastin J, Cambon N, Thompson M, Lowry OH, and Burch HB. (1987). Change in energy reserves in different segments of the nephron during brief ischemia. *Kidney Int* 31: 1239-1247

Beeri R, Symon Z, Brezis M, Ben-Sasson SA, Baehr PH, and Zager RA. (1995). Rapid DNA fragmentation from hypoxia along the thick ascending limb of rat kidneys. *Kidney Int* 47: 1806-1810

Better OS, Rubinstein I, Winaver JM, and Knochel JP. (1997). Mannitol therapy revisited (1940-1997). *Kidney Int* 51: 886-894

Biber TU and Curran PF. (1970). Direct measurement of uptake of sodium at the outer surface of the frog skin. *J Gen Physiol* 56: 83-99

Bing OH, Brooks WW, and Messer JV. (1973). Heart muscle viability following hypoxia: protective effect of acidosis. *Science* 180: 1297-1298

Blokkebak-Poulsen J, Sheikh MI, and Jacobsen C. (1991). Effects of divalent cations and pH on amiloride-sensitive Na^+ fluxes into luminal membrane vesicles from pars recta of rabbit proximal tubule. *Biochim Biophys Acta* 1068: 125-132

Boleti H, Ojcius DM, and Dautry-Varsat A. (2000). Fluorescent labeling of intracellular bacteria in living host cells. *J Microbiol Methods* 40: 265-274

Bonfoco E, Krainc D, Ankarcrona M, Nicotera P, and Lipton S. (1995). Apoptosis and necrosis: two distinct events induced, respectively, by mild and intense insults with N-Methyl-D-Aspartate or nitric oxide/superoxide in cortical cell cultures. *PNAS* 92: 7162-7166

Bonventre JV. (1998). Pathogenetic and regenerative mechanisms in acute tubular necrosis. *Kidney Blood Press Res* 21: 226-229

Bonventre JV, Brezis M, Siegel N, Rosen S, Portilla D, and Venkatachalam M. (1998). Acute renal failure. I. Relative importance of proximal vs. distal tubular injury. *Am J Physiol Renal Physiol* 275: F623-632

Bonventre JV and Cheung JY. (1985). Effects of metabolic acidosis on viability of cells exposed to anoxia. *Am J Physiol Cell Physiol* 249: C149-159

Bonventre JV, Leaf A, and Malis CD. (1988). Nature of the cellular insult in ischemic acute renal failure. In *Acute Renal Failure.*, 2nd . New York: Churchill Livingstone., ed. Brenner, BM and Lazarus, JM

Borgmann S, Granitzer M, Crabbe J, Beck FX, Nagel W, and Dorge A. (1994). Electron microprobe analysis of electrolytes in whole cultured epithelial cells. *Scanning Microsc* 8: 139-147

Boron WF. (1992). Control of intracellular pH. In *The Kidney: Physiology and pathophysiology* 2nd Edition: p 219-263. New York: Raven Press, Ltd., ed. Seldin DW and Giebisch G

Boron WF and Boulpaep EL. (1983). Intracellular pH regulation in the renal proximal tubule of the salamander. Basolateral HCO_3^- transport. *J Gen Physiol* 81: 53-94

Boyarsky G, Ganz MB, Sterzel RB, and Boron WF. (1988). pH regulation in single glomerular mesangial cells. II. Na^+-dependent and -independent Cl^--HCO_3^-- exchangers. *Am J Physiol Cell Physiol* 255: C857-869

Braam B, Mitchell KD, Koomans HA, and Navar LG. (1993). Relevance of the

tubuloglomerular feedback mechanism in pathophysiology. *J Am Soc Nephrol* 4: 1257-1274

Brady HR, Brenner BM, Clarkson MR, and Lieberthal W. (2000). Acute Renal Failure. In *Brenner & Rector's The kidney*, 6th edition: 1201-1262. Philadelphia: W.B. Saunders Company., ed. Brenner, B. M.

Brezis M and Rosen S. (1995). Hypoxia of the renal medulla -its implications for disease. *N Engl J Med* 332: 647-655

Brezis M, Rosen S, Silva P, and Epstein FH. (1984). Selective vulnerability of the thick ascending limb to anoxia in the isolated perfused kidney. *J Clin Invest* 73: 182-189

Brochiero E, Banderali U, Lindenthal S, Raschi C, and Ehrenfeld J. (1995). Basolateral membrane chloride permeability of A6 cells: implication in cell volume regulation. *Pflugers Arch* 431: 32-45

Brochiero E and Ehrenfeld J. (1997). Characterisation of Ca^{2+} membrane permeability of renal A6 cells upon different osmotic conditions. *Kidney blood Press Res* 20: 381-390

Brochiero E, Raschi C, and Ehrenfeld J. (1995). Na/Ca exchange in the basolateral membrane of the A6 cell monolayer: role in Ca_i homeostasis. *Pflügers Arch* 430: 105-114

Bugge E and Ytrehus K. (1995). Inhibition of sodium-hydrogen exchange reduces infarct size in the isolated rat heart-a protective additive to ischemic preconditioning. *Cardiovasc Res* 269: 269-274

Cala PM. (1985). Volume regulation by Amphiuma red blood cells: strategies for identifying alkali metal/H^+ transport. *Fed Proc* 44: 2500-2507

Canessa CM, Schild L, Buell G, Thorens B, Gautschi I, Horisberger JD, and Rossier BC. (1994). Amiloride-sensitive epithelial Na^+ channel is made of three homologous subunits. *Nature* 367: 463-467

Canfield PE, Geerdes AM, and Molitoris BA. (1991). Effect of reversible ATP depletion on tight-junction integrity in LLC- PK1 cells. *Am J Physiol* 261: F1038-F1045

Cannon C, van Adelsberg J, Kelly S, and Al-Awqati Q. (1985). Carbon-dioxide induced exocytotic insertion of H^+ pumps in turtle bladder luminal membrane: role of cell pH and calcium. *Nature* 314: 443-446

Cantiello HF, Stow JL, Prat AG, and Ausiello DA. (1991). Actin filaments regulate epithelial Na^+ channel activity. *Am J Physiol Cell Physiol* 261: C882-888

Casavola V, Guerra L, Helmle-Kolb C, Reshkin SJ, and Murer H. (1992). Na^+/H^+ exchange in A6 cells: polarity and vasopressin regulation. *J Membrane Biol* 130: 105-114

Casavola V, Guerra L, Reshkin SJ, Jacobson KA, and Murer H. (1997). Polarization of adenosine effects on intracellular pH in A6 renal epithelial cells. *Molecular Pharmacology* 51: 516-523

Chalfant ML, Coupaye-Gerard B, and Kleyman TR. (1993). Distinct regulation of Na^+ reabsorption and Cl^- secretion by arginine vasopressin in the amphibian cell line A6. *Am J physiol Cell Physiol* 264: C1480-1488

Chalfant ML, Denton JS, Berdiev BK, Ismailov II, Benos DJ, and Stanton BA. (1999). Intracellular H^+ regulates the ?-subunit of ENaC, the epithelial Na^+ channel. *Am J Physiol Cell Physiol* 276: C477-486

Chao KF, Liu SH, and Lin-Shiau SY. (1996). Suppression of potassium currents by cyanide on the mouse motor nerve terminal. *Neuroscience Letters* 203: 105-108

Chen LK and Boron WF. (1991). Intracellular pH regulation in epithelial cells. *Kidney Int Suppl* 33: S11-S17

Chen W and Gueron M. (1992). The inhibition of bovine heart hexokinase by 2-deoxy-D-glucose-6-phosphate: characterization by ^{31}P NMR and metabolic implications. *Biochimie* 74: 867-873

Choe H, Zhou H, Palmer LG, and Sackin H. (1997). A conserved cytoplasmic region of ROMK modulates pH sensitivity, conductance and gating. *Am J Physiol Renal Physiol* 273: F516-529

Chou CY, Shen MR, Hsu KS, Huang HY, and Lin H.C. (1998). Involvement of PKC-alpha in regulatory volume decrease responses and activation of volume-sensitive chloride channels in human cervical cancer HT-3 cells. *J Physiol* 512: 435-448

Christensen O and Bindslev N. (1982). Fluctuation analysis of short-circuit current in a warm blooded sodium retaining epithelium: site current, density and interaction with triamterene. *J Membrane Biol* 65: 19-30

Chuard F and Durand J. (1992). Coupling between the intracellular pH and the active transport of sodium in an epithelial cell line from *Xenopus laevis*. *Comp Biochem Physiol A Physiol* 102: 7-14

Collins RJ, Harmon BV, Gobe GC, and Kerr JFR. (1992). Internucleosomal DNA cleavage

should not be the sole criterion for identifying apoptosis. *Int J Radiat Biol* 61: 451-453

Cossarizza A, Baccarani-Contri M, Kalashnikova G, and Franceschi C. (1993). A new method for cytofluorimetric analysis of mitochondrial membrane potential using the J-aggregate forming lipophilic cation 5,5',6,6'-tetrachloro-1,1',3,3'-tetraethylbenzimidazolcarbocyanine iodide (JC-1). *Biochem Biophys Res Comm* 197: 40-45

Cougnon M, Bouyer P, Hulin P, Anagnostopoulos T, and Planelles G. (1996). Further investigation of ionic diffusion properties and of NH_4^+ pathways in *Xenopus laevis* oocyte cell membrane. *Pflügers Arch* 431: 658-667

Cuthbert A and Wilson SA. (1981). Mechanisms for the effect of acetylcholine on sodium transport in frog skin. *J Membrane Biol* 59: 65-75

De Greef K, Ysebaert D, Vercauteren S, Persy V, Mey D, Dauwe S, and De Broe M. (2001). Anti-B7-1 improves kidney function and blocks mononuclear cell adherence in vasa recta after acute renal ischemic injury. *Kidney Int (In Press)*

De Smet P, Simaels J, Declercq PE, and Van Driessche W. (1995a). Regulatory volume decrease in cultured kidney cells (A6): role of amino acids. *J Gen Physiol* 106: 525-542

De Smet P, Simaels J, and Van Driessche W. (1995b). Regulatory volume decrease in a renal distal tubular cell line (A6). I. Role of K^+ and Cl^-. *Pflügers Arch* 430: 936-944

De Smet P, Simaels J, and Van Driessche W. (1995c). Regulatory volume decrease in a renal distal tubular cell line (A6). II. Effect of Na^+ transport rate. *Pflügers Arch* 430: 945-953

De Smet P and Van Driessche W. (1992). Inhibition of Cl^- currents in A6 epithelia by mefenamic acid. *Arch Int Pharmacodyn Ther* 315: 123-124 (Abstr.)

De Strooper B, Craessaerts K, Dewachter I, Moechars D, Greenberg B, Van Leuven F, and Van Den Berghe H. (1995). Basolateral secretion of amyloid precursor protein in Madin-Darby Canine Kidney cells is disturbed by alterations of intracellular pH and by introducing a mutation associated with familial alzheimer's disease. *J Biol Chem* 270: 4058-4065

De Weer P. (1978). Intracellular pH transients induced by CO_2 or NH_3. *Respiration Physiology* 33: 41-50

De Wolf I and Van Driessche W. (1986). Voltage-dependent Ba^{2+} block of K^+ channels in apical membrane of frog skin. *Am J Physiol Cell Physiol* 251: C696-706

Delhumeau G, Cruz-Mendoza AM, and Gomez Lojero C. (1994). Protection of cytochrome c oxidase against cyanide inhibition by pyruvate and ?-ketoglutarate: Effect of aeration *in Vitro*. *Tox Appl Pharm* 126: 345-351

Demaurex N and Grinstein S. (1994). Na^+/H^+ antiport: modulation by ATP and role in cell volume regulation. *J Exp Biol* 196: 389-404

Dezaki K, Tsumura T, Maeno E, and Okada Y. (2000). Receptor-mediated facilitation of cell volume regulation by swelling-induced ATP release in human epithelial cells. *Jpn J Physiol* 50: 235-241

Di Lisa F, Blank PS, Colonna R, Gambassi G, Silverman HS, Stern MD, and Hansford RG. (1995). Mitochondrial membrane potential in single living adult rat cardiac myocytes exposed to anoxia or metabolic inhibition. *J Physiol* 486: 1-13

Di Mari JF, Davis R, and Safirstein RL. (1999). MAPK activation determines renal epithelial cell survival during oxidative injury. *Am J Physiol Renal Physiol* 277: F195-203

Diaz G, Setzu MD, Zucca A, Isola R, Diana A, Murru R, Sogos V, and Gremo F. (1999). Subcellular heterogeneity of mitochondrial membrane potential: relationship with organelle distribution and intercellular contacts in normal, hypoxic and apoptotic cells. *J Cell Sci* 112: 1077-1084

Dinudom A, Harvey KF, Komwatana P, Young JA, Kumar S, and Cook DI. (1998). Nedd4 mediates control of an epithelial Na^+ channel in salivary duct cells by cytosolic Na^+. *Proc Natl Acad Sci U S A* 95: 7169-7173

Doctor RB, Bacallao R, and Mandel LJ. (1994). Method for recovering ATP content and mitochondrial function after chemical anoxia in renal cell cultures. *Am J Physiol Cell Physiol* 266: C1803-1811

Dong Z, Saikumar P, Weinberg JM, and Venkatachalam MA. (1997). Internucleosomal DNA cleavage triggered by plasma membrane damage during necrotic cell death. *Am J Pathol* 151: 1205-1213

Donoso P, Mill JG, O'Neill SC, and Eisner DA. (1992). Fluorescence measurements of cytoplasmic and mitochondrial sodium concentrations in rat ventricular myocytes. *J Physiol* 448: 493-509

Dube L, Parent L, and Sauve R. (1990). Hypotonic shock activates a maxi K^+ channel in primary cultured proximal tubule cells. *Am J Physiol Renal Physiol* 259: F348-356

Duchatelle P, Ohara A, Ling BN, Kemendy AE, Kokko KE, Matsumoto PS, and Eaton DC. (1992). Regulation of renal epithelial sodium channels. *Mol Cell Biochem*: 27-34

Duchen MR. (1999). Contributions of mitochondria to animal physiology: from homeostatic sensor to calcium signalling and cell death. *J Physiol* 516: 1-17

Duchen MR and Biscoe TJ. (1992). Relative mitochondrial membrane potential and $[Ca^{2+}]_i$ in type I cells isolated from the rabbit carotic body. *J Physiol* 450: 33-61

Duranton C, Mikulovic E, Tauc M, Avella M, and Poujeol P. (2000). Potassium channels in primary cultures of seawater fish gill cells. I. Stretch-activated K^+ channels. *Am J Physiol Regulatory Integrative Comp Physiol* 279: R1647-1658

Eaton DC. (1981). Intracellular sodium ion activity and sodium transport in rabbit urinary bladder. *J Physiol* 316: 527-544

Eaton DC, Becchetti A, Heping M, and Ling BN. (1995). Renal sodium channels: regulation and single channel properties. *Kidney Int* 48: 941-945

Eaton DC, Hamilton KL, and Johnson KE. (1984). Intracellular acidosis blocks the basolateral Na/K-pump in rabbit urinary bladder. *Am J Physiol Renal Physiol* 247: F946-954

Eaton DC and Marunaka Y. (1990). Ion channel fluctuations; "noise" and single-channel measurements. *Curr Top Membr Transp* 37: 61-114

Edelstein CL and Schrier RW. (1995). The role of calcium in cell injury. In *Acute renal failure. New concepts and therapeutic strategies.*: 3-21. New York: Curchill Livingstone., ed. Stein, J.

Edelstein CL, Yaqoob MM, Alkunaizi AM, Gengaro AM, Nemenoff PE, Wanh KK, and Schrier RW. (1996). Modulation of hypoxia-induced calpain activity in rat renal proximal tubules. *Kidney Int* 50: 1150-1157

Eguchi Y, Shimizu S, and Tsujimoto Y. (1997). Intracellular ATP levels determine cell death fate by apoptosis or necrosis. *Cancer Res* 57: 1835-1840

Ehrenfeld J, Lacoste I, and Harvey BJ. (1992). Effects of intracellular signals on Na^+/K^+-ATPase activity in the frog skin epithelium. *Biochim Biophys Acta* 1106: 197-208

Eisner DA, Nichols CG, O'Neill SC, Smith GL, and Valdeolmillos M. (1989). The effects of metabolic inhibition on intracellular calcium and pH in isolated rat ventricular cells. *J Physiol* 411: 393-418

Els WJ and Helman SI. (1991). Activation of epithelial sodium channels by hormonal and autoregulatory mechanisms of action. *J Gen Physiol* 98: 1197-1220

Epel D. (1990). The initiation of development at fertilization. *Cell Differ Dev* 29: 1-12

Erlij D, De Smet P, Mesotten D, and Van Driessche W. (1999). Forskolin increases apical sodium conductance in cultured toad kidney cells (A6) by stimulating membrane insertion. *Pflügers Arch* 438: 195-204

Erlij D, De Smet P, and Van Driessche W. (1994). Effect of insulin on area and Na+ channel density of apical membrane of cultured toad kidney cells. *J Physiol* 481 : 533-542

Erlij D and Van Driessche W. (1983). Noise analysis of inward and outward Na^+ currents across the apical border of ouabain-treated frog skin. *Pflügers Arch* 398: 179-188

Eskelinen S, Huotari V, Sormunen R, Palovuori R, Kok JW, and Lehto VP. (1992). Low intracellular pH induces redistribution of fodrin and instabilisation of lateral walls in MDCK cells. *J Cell Physiol* 150: 122-133

Estevez AY, O'Regan MH, Song D, and Phillis JW. (1999). Hyposmotically induced amino acid release from the rat cerebral cortex: role of phospholipases and protein kinases. *Brain Res* 844: 1-9

Esumi K, Nishida M, Shaw D, Smith TW, and Marsh J.D. (1991). NADH measurements in adult rat myocytes during simulated ischemia. *Am J Physiol Heart Circ Physiol* 260: H1743-1752

Fakler B, Schultz JH, and Yang J. (1996). Identification of a titratable lysine residue that determines sensitivity of kidney potassium channels (ROMK) to intracellular pH. *EMBO J* 15: 4093-4099

Fidelman ML, May JM, Biber TU, and Watlington CO. (1982). Insulin stimulation of Na^+ transport and glucose metabolism in cultured kidney cells. *Am J Physiol Cell Physiol* 242: C121-123

Formigli L, Papucci L, Tani A, Schiavone N, Tempestini A, Orlandini GE, Capaccioli S, and Orlandini SZ. (2000). Aponecrosis: morphological and biochemical exploration of a syncretic process of cell death sharing apoptosis and necrosis. *J Cell Physiol* 182: 41-49

Fuchs W, Hviid -Larsen E, and Lindemann B. (1977). Current-voltage curve of sodium channels and concentration dependence of sodium permeability in frog skin. *J Physiol*

267: 137-166

Gabellini N, Zatti A, and Carafoli E. (2000). The Na^{+}/Ca^{2+} exchanger: structural aspects, function and regulation. In *Topics in biological inorganic chemistry: Calcium homeostasis*: 173-188. Berlin: Springer Verlag., ed. Carafoli, E. and Krebs, J.

Ganapathy V and Leibach FH. (1991). Protons and regulation of biological functions. *Kidney Int Suppl* 33: S4-S10

Garty H and Benos DJ. (1988). Characteristics and regulatory mechanisms of the amiloride-blockable channel. *Physiol Rev* 68: 309-373

Garty H and Palmer LG. (1997). Epithelial sodium channels: function, structure and regulation. *Physiol Rev* 77: 359-396

Giebisch G and Wang W. (2000). Renal tubule potassium channels: function, regulation and structure. *Acta Physiol Scand* 170: 153-173

Glaumann B, Glaumann H, Berezesky IK, and Trump BF. (1975). Studies on the pathogenesis of ischemic cell injury. II. Morphological changes of the pars convoluta (P1 and P2) of the proximal tubule of the rat kidney made ischemic in vivo. *Virchows Arch B Cell Pathol* 19: 281-302

Gores GJ, Nieminen AL, Wray BE, Herman B, and Lemasters JJ. (1989). Intracellular pH during chemical hypoxia in cultured rat hepatocytes. Protection by intracellular acidosis against the onset of cell death. *J Clin Invest* 83: 386-396

Granitzer M, Leal T, Nagel W, and Crabbé J. (1991). Apical and basolateral conductance in cultured A6 cells. *Pflügers Arch* 417: 463-468

Greene EL and Paller MS. (1991). Oxygen free radicals in acute renal failure. *Miner Electrolyte Metab* 17: 124-132

Grinstein S and Foskett JK. (1990). Ionic mechanisms of cell volume regulation in leukocytes. *Annu Rev Physiol* 52: 399-414

Grosse T, Heid I, Simaels J, Beck F, Nagel W, Van Driessche W, and Dorge A. (2001). Changes in element composition of A6 cells following hypotonic stress. *Pflügers Arch* 442: 297-303

Guerrero ML, Beron J, Spindler B, Groscurth P, Wallimann T, and Verrey F. (1997). Metabolic support of Na+ pump in apically permeabilized A6 kidney cell epithelia: role of creatine kinase. *Am J Physiol Cell Physiol* 272: C697-706

Gunter TE, Gunter KK, Sheu SS, and Gavin CE. (1994). Mitochondrial calcium transport: physiological and pathophysiological relevance. *Am J Physiol Cell Physiol* 267: C313-339

Hall AC, Bianchini L, and Ellory JC. (1989). Pathways for cell volume regulation via potassium and chloride loss. In *Ion Transport.*: 217-235. London: Academic Press Limited., ed. Keeling, D. and Benham, C.

Hamilton KL and Eaton DC. (1985). Single channel recordings from amiloride-sensitive epithelial sodium channel. *Am J Physiol Cell Physiol* 249: C200-207

Handler JS, Perkins FM, and Johnson JP. (1980). Studies of renal cell function using cell culture techniques. *Am J Physiol Renal Physiol* 238: F1-9

Handler JS, Perkins FM, and Johnson JP. (1981). Hormone effects on transport in cultured epithelia with high electrical resistance. *Am J Physiol Cell Physiol* 240: C103-105

Hanley MJ. (1980). Isolated nephron segments in a rabbit model of ischemic acute renal failure. *Am J Physiol Renal Physiol* 239: F17-23

Harvey BJ. (1992). Energization of sodium absorption by the H^+-ATPase pump in mitochondria-rich cells of frog skin. *J Exp Biol* 172: 289-309

Harvey BJ. (1994). Cross-talk and epithelial ion transport. *Curr Opin Nephrol Hypertens* 3: 523-528

Harvey BJ. (1995). Cross-talk between sodium and potassium channels in tight epithelia. *Kidney Int* 48: 1191-1199

Harvey BJ and Ehrenfeld J. (1988). Role of Na^+/H^+ exchange in the control of intracellular pH and cell membrane conductances in frog skin epithelium. *J Gen Physiol* 92: 793-810

Harvey BJ, Thomas SR, and Ehrenfeld J. (1988). Intracellular pH controls cell membrane Na^+ and K^+ conductances and transport in frog skin epithelium. *J Gen Physiol* 92: 767-791

Haussinger D and Lang F. (1991). Cell volume in the regulation of hepatic function: a mechanism for metabolic control. *Biochim Biophys Acta* 1071: 331-350

Hayslett JP, Macala. L.J., Smallwood JI, Kalghatgi L, Gassala-Herraiz J, and Isales C. (1995). Vasopressin-stimulated electrogenic sodium transport in A6 cells is linked to a Ca^{2+}-mobilizing signal mechanism. *J Biol Chem* 270: 16082-16088

Hayworth RA, Hunter DR, and Berkoff HA. (1980). Na^+ releases Ca^{2+} from liver, kidney and lung mitochondria. *FEBS Lett* 110: 216-218

Helman SI and Baxendale LM. (1990). Blocker related changes of channel density: analysis of a three state model for apical sodium channels of frog skin. *J Gen Physiol* 95: 647-678

Helman SI, Baxendale LM, Sariban Sohrabi S, and Benos DJ. (1986). Blocker-induced noise of Na^+ channels in cultured A6 epithelia. *Fed Proc* 45:516 (Abstr.)

Helman SI, Liu X, Baldwin K, Blazer-Yost BL, and Els WJ. (1998). Time-dependent stimulation by aldosterone of blocker-sensitive ENaCs in A6 epithelia. *Am J Physiol Cell Physiol* 274: C947-957

Hillered L, Siesjo BK, and Arfors KE. (1984). Mitochondrial response to transient forebrain ischemia and recirculation in the rat. *J Cereb Blood Flow Metab* 4: 438-446

Hochachka PW. (1986). Defense strategies against hypoxia and hypothermia. *Science* 231: 234-241

Hochachka PW and Mommsen TP. (1983). Protons and anaerobiosis. *Science* 219: 1391

Hoffmann EK. (1987). Volume regulation in cultured cells. *Curr Top Membr Tr* 30: 125-180

Hoffmann EK. (1992). Cell swelling and volume regulation. *Can J Physiol Pharmacol* 70 Suppl:S310-313

Hoffmann EK. (2000). Intracellular Signalling Involved in Volume Regulatory Decrease. *Cell Physiol Biochem* 10: 273-288

Homareda H and Matsui H. (1985a). Effect of pH on Na^+ and K^+ binding to Na,K ATPase. In *The sodium pump, 4th Annual Intnl Conf on Na,K ATPase*: 251-254. Huddersfield, UK: The Company of Biologists-Charlesworth & Co., ed. Glynn, I. and Ellory, C.

Homareda H and Matsui H. (1985b). Effect of pH on Na^+ and K^+ binding to Na,K ATPase. In *The sodium pump, 4th Annual Intnl Conf on Na,K ATPase*: 251-254. Huddersfield, UK: The Company of Biologists-Charlesworth & Co., ed. Glynn, I. and Ellory, C.

Idriss HT, Hannun YA, Boulpaep E, and Basavappa S. (2000). Regulation of volume-activated chloride channels by P-glycoprotein: phosphorylation has the final say! *J Physiol* 524: 629-636

Ismailov II, Shlyonsky VG, Alvarez O, and Benos DJ. (1997). Cation permeability of a cloned rat epithelial amiloride-sensitive Na^+ channel. *J Physiol* 504: 287-300

Ives HE and Rector FC. (1984). Proton transport and cell function. *J Clin Invest* 73: 285-290

Johnson I. (1998). Fluorescent probes for living cells. *Histochem J* 30: 123-140

Johnston P.A., Rennke H, and Levinsky NG. (1984). Recovery of proximal tubular function from ischemic injury. *Am J Physiol Renal Physiol* 246: F159-166

Karwatowska-Prokopczuk E, Nordberg JA, Li HL, Engler RL, and Gottlieb RA. (1998). Effect of vacuolar proton ATPase on pH_i, Ca^{2+}, and apoptosis in neonatal cardiomyocytes during metabolic inhibition/recovery. *Circ Res* 82: 1139-1144

Kempski O, Zimmer M, Neu A, von Rosen F, Jansen M, and Baethmann A. (1987). Control of glial cell volume in anoxia. In vitro studies on ischemic cell swelling. *Stroke* 18: 623-628

Kerr JFR, Gobe GC, Winterford CM, and Harmon BV. (1995). Anatomical methods in cell death. In *Methods in cell biology. Cell death.* 1-27. San Diego: Academic Press, Inc., ed. Schwartz, L. M. and Osborne, B. A.

Klein U, Timme M, Zeiske W, and Ehrenfeld J. (1997). The H^+ pump in frog skin (*Rana esculenta*): identification and localisation of V-ATPase. *J Membrane Biol* 157: 117-126

Knepper MA. (1991). NH_4^+ transport in the kidney. *Kidney Int Suppl* 33: S95-S102

Kobryn CE and Mandel LJ. (1994). Decreased protein phosphorylation induced by anoxia in proximal renal tubules. *Am J Physiol* 267: C1073-C1079

Konstas AA, Mavrelos D, and Korbmacher C. (2000). Conservation of pH sensitivity in the epithelial sodium channel (ENaC) with Liddle's syndrome mutation. *Pflügers Arch* 441: 341-350

Kriz W and Bankir L. (1988). A Standard nomenclature for structure of the kidney. The renal commission of the international union of physiological sciences (IUPS). *Anat Embryol (Berl)* 178: N1-8

Kroemer G, Dallaporta B, and Resche-Rigon M. (1998). The mitochondrial death/life regulator in apoptosis and necrosis. *Annu Rev Physiol* 60: 619-642

Lameire N and Vanholder R. (2001). Pathophysiologic features and prevention of human

and experimental acute tubular necrosis. *J Am Soc Nephrol* 12: S20-S32

Lang F, Busch GL, and Gulbins E. (1995). Physiology of cell survival and cell death: implications for organ conservation. *Nephrol Dial Transplant* 10: 1551-1555

Lang F, Busch GL, Ritter M, Volkl H, Waldegger S, Gulbins E, and Haussinger D. (1998). Functional significance of cell volume regulatory mechanisms. *Physiol Rev* 78: 247-306

Lang F, Friedrich F, Paulmichl M, Schobersberger W, Jungwirth A, Ritter M, Steidl M, Weiss H, Woll E, Tschernko E, and et al. (1990). Ion channels in Madin-Darby canine kidney cells. *Ren Physiol Biochem* 13: 82-93

Lang F and Paulmichl M. (1995). Properties and regulation of ion channels in MDCK cells. *Kidney Int* 48: 1200-1205

LaPointe MS and Battle DC. (1994). Na^+/H^+ exchange and vascular smooth muscle proliferation. *Am J Med Sci* 307: S9-16

Leist M, Single B, Castoldi AF, Kuhnle S, and Nicotera P. (1997). Intracellular adenosine triphosphate (ATP) concentration: a switch in the decision between apoptosis and necrosis. *J Exp Med* 185: 1481-1486

Lemasters JJ. (1999). Necrapoptosis and the mitochondrial permeability transition: shared pathways to necrosis and apoptosis. *Am J Physiol* 276: G1-G6

Lewis FA, Ifshin MS, Loo DDF, and Diamond JM. (1984). Studies of sodium channels in rabbit urinary bladder by noise analysis. *J Membrane Biol* 80: 135-151

Leyssens A, Nowicky AV, Patterson L, Crompton M, and Duchen MR. (1996). The relationship between mitochondrial state, ATP hydrolysis, $[Mg^{2+}]_i$ and $[Ca^{2+}]_i$ studied in isolated rat cardiomyocytes. *J Physiol* 496: 111-128

Li HY, Dai LJ, Krieger C, and Quamme GA. (1993). Intracellular Mg^{2+} concentrations following metabolic inhibition in opposum kidney cells. *Biochim Biophys Acta* 1181: 307-315

Li J, De Smet P, Jans D, Simaels J, and Van Driessche W. (1998). Swelling-activated cation-selective channels in A6 epithelia are permeable to large cations. *Am J Physiol Cell Physiol* 275: C358-366

Lieberthal W. (1997). Biology of acute renal failure: therapeutic implications. *Kidney Int* 52: 1102-1115

Lieberthal W, Menza SA, and Levine JS. (1998). Graded ATP depletion can cause necrosis or apoptosis of cultured mouse proximal tubular cells. *Am J Physiol* 274: F315-F327

Light DB, Adler MR, Ter Beest JK, Botsford SA, and Gronau RT. (1998). Protein kinase C and regulatory volume decrease in mudpuppy red blood cells. *J Membrane Biol* 166: 119-132

Lindemann B. (1984). Fluctuation analysis of sodium channels in epithelia. *Annu Rev Physiol* 46: 497-515

Lindemann B and Van Driessche W. (1977). Sodium-specific membrane channels of frog skin are pores: current fluctuations reveal high turnover. *Science* 195: 292-294

Ling BN and Eaton DC. (1989). Effects of luminal Na^+ on single Na^+ channels in A6 cells, a regulatory role for protein kinase C. *Am J Physiol Renal Physiol* 256: F1094-1103

Ling BN, Webster CL, and Eaton DC. (1992). Eicosanoids modulate apical Ca^{2+}-dependent K^+ channels in cultured rabbit principal cells. *Am J Physiol Renal Physiol* 263: F116-126

Lyall V, Belcher TS, and Biber TU. (1993). Na^+ channel blockers inhibit voltage-dependent intracellular pH changes in principal cells of frog (*Rana pipiens*) skin. *Comp Biochim Physiol A Physiol* 105: 503-511

Lyall V, Feldman GM, and Biber TU. (1995). Regulation of apical Na^+ conductive transport in epithelia by pH. *Biochim Biophys Acta* 1241: 31-44

Lynch RM and Balaban RS. (1987). Energy metabolism of renal cell lines, A6 and MDCK: regulation by Na-K-ATPase. *Am J Physiol Cell Physiol* 252: C225-231

Macknight AD and Leaf A. (1977). Regulation of cellular volume. *Physiol Rev* 57: 510-573

MacLeod RJ and Hamilton JR. (1999a). Ca^{2+}/calmodulin kinase II and decreases in intracellular pH are required to activate K^+ channels after substantial swelling in villus epithelial cells. *J Membrane Biol* 172: 59-66

MacLeod RJ and Hamilton JR. (1999b). Increases in intracellular pH and Ca^{2+} are essential for K^+ channel activation after modest 'physiological' cell swelling in villus epithelial cells. *J Membrane Biol* 172: 47-58

MacLeod RJ and Hamilton JR. (1996). Activation of Na^+/H^+ exchange is required for regulatory volume decrease after modest "physiological" volume increases in jejunal

villus epithelial cells. *J Biol Chem* 271: 23138-23145

Majno G and Joris I. (1995). Apoptosis, oncosis, and necrosis. An overview of cell death. *Am J Pathol* 146: 3-15

Malik B, Schlanger L, Al-Khalili O, Bao HF, Yue G, Price SR, Mitch WE, and Eaton DC. (2001). Enac degradation in A6 cells by the ubiquitin-proteosome proteolytic pathway. *J Biol Chem* 276: 12903-12910

Marunaka Y and Eaton DC. (1990). Chloride channels in the apical membrane of a distal nephron A6 cell line. *Am J Physiol Cell Physiol* 258: C352-368

Mason J, Joeris B, Welsch J, and Kriz W. (1989). Vascular congestion in ischemic renal failure: the role of cell swelling. *Miner Electrolyte Metab* 15: 114-124

McCoy CE, Selvaggio AM, Alexander EA, and Schwartz JH. (1988). Adenosine triphosphate depletion induces a rise in cytosolic free calcium in canine renal epithelial cells. *J Clin Invest* 82: 1326-1332

McNicholas CM and Canessa CM. (1997). Diversity of channels generated by different combinations of epithelial sodium channel subunits. *J Gen Physiol* 109: 681-692

Meister A and Anderson ME. (1983). Glutathione. *Annu Rev Biochem* 52: 711-760

Meyer K and Korbmacher C. (1996). Cell swelling activates ATP-dependent voltage-gated chloride channels in M-1 mouse cortical collecting duct cells. *J Gen Physiol* 108: 177-193

Mo L, Hellmich HL, Fong P, Wood T, Embesi J, and Wills NK. (1999). Comparison of amphibian and human ClC-5: Similarity of functional properties and inhibition by external pH. *J Membrane Biol* 168: 253-264

Moolenaar WH. (1986). Regulation of cytoplasmic pH by Na^+/H^+ exchange. *TIBS* 11: 141-143

Nakanishi T, Balaban RS, and Burg MB. (1988). Survey of osmolytes in renal cell lines. *Am J Physiol Cell Physiol* 255: C181-191

Nath KA and Norby SM. (2000). Reactive oxygen species and acute renal failure. *Am J Med* 109: 665-678

Nett W and Deitmer JW. (1996). Simultaneous measurements of intracellular pH in the leech giant glial cell using 2',7'-bis-(2-carboxyethyl)-5-,6-carboxyfluorescein and ion-

sensitive microelectrodes. *Biophys J* 71: 394-402

Newsholme EA and Leech AR. (1983). Integration of anabolic processes. In *Biochemistry for the medical sciences.* Chichester: John Wiley & Sons Ltd., ed.

Niisato N and Marunaka Y. (1997a). Hyposmolality-induced enhancement of ADH action on amiloride-sensitive I_{sc} in renal epithelial A6 cells. *Jpn J Physiol* 47: 131-137

Niisato N and Marunaka Y. (1997b). Regulation of Cl^- transport by IBMX in renal A6 epithelium. *Pflügers Arch* 434: 227-233

Niisato N, Van Driessche W, Liu M, and Marunaka Y. (2000). Involvement of protein tyrosine kinase in osmoregulation of Na^+ transport and membrane capacitance in renal A6 cells. *J Membrane Biol* 175: 63-77

Oberbauer R, Rohrmoser M, Regele H, Muhlbacher F, and Mayer G. (1999). Apoptosis of tubular epithelial cells in donor kidney biopsies predicts early renal allograft function. *J Am Soc Nephrol* 10: 2006-2013

Ojcius DM, Zychlinsky A, Zheng LM, and Young JDE. (1991). Ionophore-induced apoptosis: role of DNA fragmentation and calcium fluxes. *Exp Cell Res* 197: 43-49

Okada Y. (1998). Cell volume-sensitive chloride channels. In *Cell Volume Regulation*: 21-33. Basel: Karger., ed. Lang, F.

Olans L, Sariban-Sohrabi S, and Benos DJ. (1984). Saturation behaviour of single, amiloride-sensitive Na^+ channels in planar lipid bilayers. *Biophys J* 46: 831-835

Olson JE, Sankar R, Holtzman D, James A, and Fleischhacker D. (1986). Energy-dependent volume regulation in primary cultured cerebral astrocytes. *J Cell Physiol* 128: 209-215

Palmer LG. (1985). Modulation of apical Na permeability of the toad urinary bladder by intracellular Na, Ca, and H. *J Membrane Biol* 83: 57-69

Palmer LG, Corthesy-Theulaz I, Gaeggeler HP, Kraehenbuhl JP, and Rossier BC. (1990). Expression of epithelial Na^+ channels in *Xenopus* oocytes. *J Gen Physiol* 96: 23-46

Palmer LG and Frindt G. (1987). Effects of cell calcium and pH on Na channels from rat cortical collecting tubule. *Am J Physiol Renal Physiol* 253: F333-339

Palmer LG, Frindt G., Silver RB, and Strieter J. (1989). Feedback regulation of epithelial sodium channels. *Curr. Top Membr Transp* 34: 45-60

Panda M and Robinson NC. (1995). Kinetics and mechanism for the binding of HCN to cytochrome c oxidase. *Biochem* 34: 10009-10018

Parkinson NA and Hendry BM. (1995). Thapsigargin-induced changes in intracellular pH in Madin-Darby canine kidney (MDCK) cells. *J Physiol* 489:88 (Abstr.)

Patel AJ, Lauritzen I, Lazdunski M, and Honore E. (1998). Disruption of mitochondrial respiration inhibits volume-regulated anion channels and provokes neuronal cell swelling. *J Neurosci* 18: 3117-3123

Peers C and O'Donnell J. (1990). Potassium currents recorded in type I carotic body cells from the neonatal rat and their modulation by chemoexcitatory agents. *Brain Res* 522: 259-266

Penttila A and Trump BF. (1974). Extracellular acidosis protects Ehrlich ascites tumor cells and rat renal cortex against anoxic injury. *Science* 185: 277-278

Perkins FM and Handler JS. (1981). Transport properties of toad kidney epithelia in culture. *Am J Physiol Cell Physiol* 241: C154-C159

Peters SMA, tijsen MJH, bindels RJM, Van Os CH, and Wetzels JFM. (1995). Protection against hypoxic injury of rat proximal tubules by felodipine via a calcium-independent mechanism. *Pflügers Arch* 431: 20-27

Price PM, Megyesi J, Saggi S, and Safirstein RL. (1995). Regulation of transcription by the rat EGF gene promoter in normal and ischemic murine kidney cells. *Am J Physiol* 268: F664-670

Puoti A, May A, Canessa CM, Horisberger JD, Schild L, and Rossier BC. (1995). The highly selective low conductance epithelial channel of *Xenopus* laevis A6 kidney cells. *Am J Physiol Cell Physiol* 269: C188-197

Raffray M and Cohen GM. (1997). Apoptosis and necrosis in toxicology: a continuum or distinct modes of cell death? *Pharmacol Ther* 75: 153-77

Ramachandra S and Studzinski GP. (1995). Morphological and biochemical criteria of apoptosis. In *Cell growth and apoptosis. A practical approach.*: 119-142. Oxford: IRL Press at Oxford University Press., ed. Studzinski, G. P.

Reers M, Smiley ST, Mottola-Hartshorn C, Chen A, Lin M, and Chen MB. (1995). Mitochondrial membrane potential monitored by the JC-1 dye. *Methods in Enzymology* 260: 406-417

Reers M, Smith TW, and Chen LB. (1991). J-aggregate formation of a carbocyanine as a quantitative fluorescent indicator of membrane potential. *Biochem* 30: 4480-4486

Rehn M, Weber WM, and Clauss W. (1995). The use of kidney epithelial cell cultures (A6) in the study of Na^+ transport regulation. *Zoology* 99: 221-226

Reuss L. (1998). Focus on 'Effect of expressing the water channel aquaporin-1 on the CO_2 permeability of *Xenopus* oocytes'. *Am J Physiol Cell Physiol* 274: C297-298

Robson L and Hunter M. (1994). Role of cell volume and protein kinase C in regulation of a Cl^- conductance in single proximal tubule cells of Rana temporaria. *J Physiol* 480: 1-7

Rose UM, Abrahamse SL, Jansen JW, Bindels RJ, and van Os CH. (1995). Cellular acidification occurs during anoxia in cultured, but not in freshly isolated, rabbit proximal tubular cells. *Pflügers Arch* 429: 722-728

Rossier BC. (1997). 1996 Homer Smith Award Lecture. Cum grano salis: the epithelial sodium channel and the control of blood pressure. *J Am Soc Nephrol* 8: 980-992

Rothstein A and Mack E. (1990). Volume-activated K^+ and Cl^- pathways of dissociated epithelial cells (MDCK): role of Ca^{2+}. *Am J Physiol Cell Physiol* 258: C827-834

Rouslin W. (1991). Regulation of the mitochondrial ATPase in situ in cardiac muscle: role of the inhibitor subunit. *J Bioenerg Biomembr* 23: 873-888

Ruppersberg JP. (2000). Intracellular regulation of inward rectifier K^+ channels. *Pflügers Arch* 441: 1-11

Sabirov RZ, Prenen J, Droogmans G, and Nilius B. (2000). Extra- and intracellular proton-binding sites of volume-regulated anion channels. *J Membrane Biol* 177: 13-22

Sachs G, Munson K, Balaji VN, Aures-Fischer D, Hersey SJ, and Hall K. (1989). Functional domains of the gastric HK ATPase. *J Bioenerg Biomembr* 21: 573-588

Saikumar P, Dong Z, Patel Y, Hall K, Hopfer U, Weinberg JM, and Venkatachalam MA. (1998). Role of hypoxia-induced Bax translocation and cytochrome C release in reoxygenation injury. *Oncogene* 17: 3401-3415

Sariban-Sohrabi S, Burg MB, and Turner RJ. (1983). Apical sodium uptake in toad kidney epithelial cell line A6. *Am J Physiol Cell Physiol* 245: C167-171

Savill J. (1994). Apoptosis and the kidney. *J Am Soc Nephrol* 5: 12-21

Schild L, Schneeberger E, Gautschi I, and Firsov D. (1997). Identification of amino acid residues in the alpha, beta, and gamma subunits of the epithelial sodium channel (EnaC) involved in amiloride block and ion permeation. *J Gen Physiol* 109: 15-26

Schnermann J, Nagel W, and Thurau K. (1966). Die frühdistale natriumkonzentration in rattennieren nach renaler ischämie und hämorrhagischer hypotension. *Pflügers Arch* 287: 296-310

Scholz W, Albus U, Lang J, Linz W, Martorana PA, Englert HC, and Scholkens BA. (1993). Hoe 694, a new Na^+/H^+ exchange inhibitor and its effects in cardiac ischemia. *Br J Pharmacol* 109: 562-568

Schreiber R and Haussinger D. (1995). Characterization of the swelling-induced alkalinization of endocytotic vesicles in fluorescein isothiocyanate-dextran-loaded rat hepatocytes. *Biochem J* 309: 19-24

Selvaggio AM, Schwartz JH, Bengele HH, Gordon FD, and Alexander EA. (1988). Mechanisms of H^+ secretion by inner medullary collecting duct cells. *Am J Physiol Renal Physiol* 254: F391-400

Seney FDJR, Persson EG, and Wright FS. (1987). Modification of tubuloglomerular feedback signal by dietary protein. *Am J Physiol Renal Physiol* 252: F83-90

Shanley PF, Shapiro JI, Chan L, Burke TJ, and Johnson GC. (1988). Acidosis and hypoxic medullary injury in the isolated perfused kidney. *Kidney Int* 34: 791-796

Shapiro J.I., Cheung C, Itabashi A, Chan L, and Schrier RW. (1985). The effect of verapamil on renal function after warm and cold ischemia in the isolated perfused rat kidney. *Transplantation* 40: 596-600

Sheridan AM and Bonventre JV. (2001). Epidemiology and pathogenesis of ARF in ICU: Pathophysiology of ischemic acute renal failure. *Contrib Nephrol* 132: 7-21

Sheridan AM, Schwartz JH, Kroshian VM, Tercyak AM, Laraia J, Masino S, and Lieberthal W. (1993). Renal mouse proximal tubular cells are more susceptible than MDCK cells to chemical anoxia. *Am J Physiol Renal Physiol* 265: F342-350

Shimizu S, Eguchi Y, Kamiike W, Waguri S, Uchiyama Y, Matsuda H, and Tsujimoto Y. (1996). Retardation of chemical hypoxia-induced necrotic cell death by Bcl-2 and ICE inhibitors: possible involvement of common mediators in apoptotic and necrotic signal transductions. *Oncogene* 12: 2045-2050

Shimkets RA, Lifton RP, and Canessa CM. (1997). The activity of the epithelial sodium

channel is regulated by clathrin- mediated endocytosis. *J Biol Chem* 272: 25537-25541

Silverman HS. (1993). Mitochondrial free calcium regulation in hypoxia and reoxygenation: relation to cellular injury. *Basic Res Cardiol* 88: 483-494

Slavik J. (1992). Optical detection of intracellular ion concentrations. In *Fluorescence Spectroscopy. New methods and Applications*: 173-185. Berlin: Springer-Verlag., ed. Wolfbeis O.S.

Smets I, Zeiske W, Steels P, and Van Driessche W. (1998). Na^+ dependence of single channel current and channel density generate saturation of Na^+ uptake in A6 cells. *Pflügers Arch* 435: 604-609

Smiley ST, Reers M, Mottola-Hartshorn C, Lin M, Chen A, Smith TW, Steele GD Jr, and Chen LB. (1991). Intracellular heterogeneity in mitochondrial membrane potentials revealed by a J-aggregate-forming lipophilic cation JC-1. *Proc Natl Acad Sci U S A* 88: 3671-3675

Snyder PM, Price MP, McDonald FJ, Adams CM, Volk KA, Zeiher BG, Stokes JB, and Welsh MJ. (1995). Mechanism by which Liddle's syndrome mutations increase activity of a human epithelial Na^+ channel. *Cell* 83: 969-978

St-Pierre J, Brand MD, and Boutilier RG. (2000). Mitochondria as ATP consumers: cellular treason in anoxia. *Proc Natl Acad Sci U S A* 97: 8670-8674

Staub O, Dho S, Henry P, Correa J, Ishikawa T, McGlade J, and Rotin D. (1996). WW domains of Nedd4 bind to the proline-rich PY motifs in the epithelial Na^+ channel deleted in Liddle's syndrome. *EMBO J* 15: 2371-2380

Stobiecka A, Steels P, and Ameloot M. (2001). The effects of chemical ischemia on intracellular calcium in A6 cells. *Biophys J* 80:473 (Abstr.)

Stockand JD, Bao HF, Schenck J, Malik B, Middleton P, Schlanger LE, and Eaton DC. (2000). Differential effects of protein kinase C on the levels of epithelial Na^+ channel subunit proteins. *J Biol Chem* 275: 25760-25765

Stoner LC and Morley GE. (1995). Effect of basolateral or apical hyposmolarity on apical maxi K channels of everted rat collecting tubule. *Am J Physiol Renal Physiol* 268: F569-580

Sullivan LP, Wallace DP, Clancy RL, and Grantham JJ. (1990). Effect of cellular acidosis on cell volume in S2 segments of renal proximal tubules. *Am J Physiol Renal Physiol*

258: F831-839

Sullivan LP, Wallace DP, Clancy RL, Lechene C, and Grantham JJ. (1991). Cellular electrolyte and volume changes induced by acidosis in the rabbit proximal straight tubule. *J Am Soc Nephrol* 2: 1030-1040

Sun D and Gilboe DD. (1994). Effect of the platelet-activating factor antagonist BN 50739 and its diluents on mitochondrial respiration and membrane lipids during and following cerebral ischemia. *J Neurochem* 62: 1929-1938

Sun P, Rane SG, Gunasekar PG, Borowitz JL, and Isom GE. (1997). Modulation of the NMDA receptor by cyanide: enhancement of receptor-mediated responses. *J Pharmacol Exp Ther* 280: 1341-1348

Sutton TA and Molitoris BA. (1998). Mechanisms of cellular injury in ischemic acute renal failure. *Semin Nephrol* 18: 490-497

Tanner GA, Sloan KL, and Sophasan S. (1973). Effects of renal artery occlusion on kidney function in the rat. *Kidney Int* 4: 377-389

Taylor A and Windhager EE. (1979). Possible role of cytosolic calcium and Na-Ca exchange in regulation of transepithelial sodium transport. *Am J Physiol Renal Physiol* 236: F505-512

Thomas JA, Buchsbaum RN, Zimniak A, and Racker E. (1979). Intracellular pH measurements in Ehrlich ascites tumor cells utilizing spectroscopic probes generated in situ. *Biochem* 18: 2210-2218

Thompson CB. (1995). Apoptosis in the pathogenesis and treatment of disease. *Science* 267: 1456-1462

Tilly DC, van den Berghe N, Tertoolen LGJ, Edixhoven MJ, and de Jonge HR. (1993). Protein tyrosine phosphorylation is involved in osmoregulation of ionic conductances. *J Biol Chem* 268: 19919-19922

Trump BF and Berezesky IK. (1998). The reactions of cells to lethal injury: oncosis and necrosis - the role of calcium., ed. When cells die. A comprehensive evaluation of apoptosis and programmed cell death.: 57-96. New York: Wiley-Liss, Inc., ed. Lockshin, R., Zakeri, Z., and Tilly, J. L.

Turnheim K. (1991). Intrinsic regulation of apical sodium entry in epithelia. *Physiol Rev* 71: 429-445

Zeiske W, Atia F, and Van Driessche W. (1998). Apical Cl- channels in A6 cells. *J Membr Biol* 166: 169-178

Zeiske W, Smets I, Ameloot M, Steels P, and Van Driessche W. (1999). Intracellular pH shifts in cultured kidney (A6) cells: effects on apical Na^+ transport. *Am J Physiol Cell Physiol* 277: C469-479

Zeiske W and Van Driessche W. (1983). The interaction of 'K^+-like' cations with the apical K^+ channel in frog skin. *J Membrane Biol* 76: 57-72

Dankwoord

Het werk is geleverd, het boekje mag naar de drukker. Er valt wat van me af...wat een goed gevoel. Het is echt wel mooi geweest. De voorbije 7 jaren waren erg leerrijk op vele gebieden: ik heb mogen functioneren in een groep van toffe collega's waarmee ik in de loop van de jaren echt een fijne band heb opgebouwd , ik heb mogen lesgeven aan gemotiveerde en geïnteresseerde studenten, ik heb veel onderzoekservaring mogen opdoen en allerlei technieken geleerd, ik heb mogen ondervinden hoe fascinerend fysiologie kan zijn. En nu ligt het resultaat van de voorbije jaren onderzoek hier voor mij op tafel. Vooraan op het boekje zal mijn naam prijken... Nochtans is 'mijn pronkstuk' echt wel het resultaat van de inzet van velen, naar wie ik nu graag een welgemeend dankwoord richt.

Zeven jaar geleden ben ik mogen van start gaan voor een tocht van 6 jaar met als eindbestemming 'de doctoraatsthesis'. Om mij te behoeden voor al te veel moeilijkheden onderweg en om doodlopende straatjes te vermijden, werden mij toen 2 promotoren toegewezen: Prof. P. Steels en Prof. M. Ameloot. En ik ben er geraakt (wel één jaar later dan voorzien, maar daar zaten zij voor niets tussen)! Prof. Steels en Marcel, bedankt! Jullie hebben me elk op jullie eigen manier gesteund en begeleid op mijn tocht. Ik ben jullie in het bijzonder dankbaar voor jullie vertrouwen in mij. Ik heb het enorm geapprecieerd dat jullie me mijn eigen weg lieten gaan, maar toch steeds bereid waren om me -bij twijfel- de juiste weg te wijzen. Prof. Steels, van in mijn prille begin hier aan het LUC heb je me ingewijd in de wondere wereld van de fysiologie. Ik denk bijvoorbeeld aan de manier waarop je me in enkele weken tijd met veel enthousiasme nierfysiologie hebt bijgebracht door elke avond gedurende enkele uren privé-les te geven. Ook nadien hebben we vaak uren samen gezeten om bepaalde thema's van de fysiologie te behandelen, om practica's voor de studenten te bespreken, om onderzoeksresultaten te bediscussiëren. Het was voor mij enorm belangrijk te weten dat je deur steeds open stond en dat je steeds bereid was om tijd vrij te maken als ik dacht dat het nodig was. Ik heb enorm veel mogen leren van onze discussies en van de manier waarop je wetenschappelijke literatuur en wetenschappelijk onderzoek benadert. Bedankt daarvoor! Marcel, u moet ik het niet meer vertellen dat de fluorescentiemetingen in A6 cellen niet altijd van een leien dakje liepen...Ik herinner me maar al te goed die keren dat ik ten einde raad naar uw bureel kwam omdat ik weer maar eens geen fluorescentiesignaal had...Je bleef erin geloven en inderdaad, het is gelukt. Ik ben je dankbaar voor het doorgeven van je 'fluorescentie-microbe'. Ik ben erdoor gebeten en ik hoop dat ik -op mijn beurt- mijn enthousiasme kan doorgeven aan anderen. Bovendien was het vaak erg leerrijk te ondervinden hoe anders dat jij –als biofysicus- de zaken benadert. Onze discussies hebben me vaak dieper doen nadenken en tot nieuwe inzichten gebracht. Bedankt !

Uiteraard hebben niet alleen de promotoren maar ook de andere leden van de ondezoeksgroep fysiologie bijgedragen tot deze thesis. Bij het bespreken van artikels en bij het voorstellen van onderzoeksresultaten werden vaak zeer goede suggesties gegeven. Voor de vele interessante discussies over ischemie en metabolische inhibitie wil ik Frank, Robbert, Jerry, Yves en Sanda danken. Voor 'fluorescentie-problemen' kon ik steeds terecht bij Sanda, Mieke en Frank. Uiteraard wil ik hier ook graag de belangrijke bijdrage van het technisch personeel benadrukken. Bedankt Joke, Agnes, Wilfried en Jo omdat jullie ervoor zorgden dat mijn cellen zich steeds in optimale conditie bevonden om zich aan mijn grillen te onderwerpen. Bedankt Roland voor je hulp met de elektronische aspecten van mijn experimenten. Patrick, je hebt me vaak versteld doen staan van je vakkundig ontwerpen én realiseren van speciale meetkamertjes. Bedankt ook voor je snelle hulp als er weer juist op het 'moment suprême' van mijn experiment iets dreigde mis te lopen en ik niet direct een oplossing zag. Liters oplossingen met telkens weer andere samenstellingen en hoeveelheden werden bereid door Joke, Wilfried, Agnes en Jo. Roland, Jo en Wilfried wil ik hier ook graag speciaal bedanken voor hun hulp bij mijn onderwijstaken. Ik kon er echt op vertrouwen dat de practica zorgvuldig voorbereid werden. Ook jullie assistentie tijdens de practica werd geapprecieerd. Niet minder belangrijk waren de fijne babbels met de collega's aan de koffietafel! Bedankt voor jullie vriendschap en de aangename sfeer waarin zowel 'grappige zever' als serieuze gesprekken mogelijk waren! Tevens wil ik Isabelle, Ingrid, Nadine en Emmy speciaal danken voor onze plezierige uitwisselingen over zwangerschappen, bevallingen, kinder-kuren, opvoedingsaspecten, ... Josette, Paula en Kathleen ben ik dankbaar voor hun hulp bij administratieve aangelegenheden en Magda, Marc en Kathleen voor hun inzet om mijn posters en figuren er mooi te laten uitzien.

Naast de leden van 'de fysiologie' ben ik ook andere mensen op het LUC erg dankbaar voor het ter beschikking stellen van apparatuur en hulp bij bepaalde technieken: Prof. P. Stinissen en Annegret VanderAa voor hulp bij de ^{3}H-thymidine metingen, Prof. R. Valcke voor het gebruik van de luminometer, Prof. J. Creemers, Prof. I. Lambrichts en Frank Vandenabeele voor hulp bij de elektronenmikroscopie. Verder wil ik ook Mark Jans danken voor het maken van de coupes voor electronenmikroscopie.

Gedurende mijn tocht kon ik bovendien rekenen op de steun van mensen buiten het LUC. Hierbij wil ik Prof. W. Van Driessche (KULeuven, Fysiologie) speciaal danken voor de mogelijkheid die ik kreeg om verscheidene malen experimenten te doen in zijn labo en kennis te maken met enkele ingenieuze technieken zoals de ruisanalyse techniek en de celvolumemeting. De ruisexperimenten en volumemetingen leveren een belangrijke bijdrage tot mijn thesis. Bedankt ook, Prof. Van Driessche, voor de tijd die u telkens weer vrij maakte voor wetenschappelijke discussies over de resultaten. Het waren telkens aangename en zeer leerrijke periodes in uw labo. Hierbij wil ik zeker ook Jeannine danken voor haar hulp bij de ruisexperimenten en Els voor de volumemetingen. Ik heb bovendien herhaaldelijk mogen ervaren dat ik ook op jullie kon rekenen als er plots een probleem opdook in Diepenbeek. Bedankt daarvoor! Ook Dr. Wolfgang Zeiske (Universität Osnabrück)

ben ik erg dankbaar voor zijn belangrijke bijdrage tijdens de eerste fase van deze tocht. Wolfgang, jij hebt me de juiste weg gewezen en bent bovendien steeds blijven supporteren onderweg! Hartelijk bedankt!

Furthermore, I would like to express my gratitude to the members of the jury for their willingness to critically evaluate this thesis and for giving constructive suggestions that certainly have improved the quality of this work.

En dan kom ik nu tot de personen die eigenlijk de grootste bijdrage geleverd hebben om het eindpunt van deze tocht te bereiken. Niet alleen gedurende de voorbije zeven jaren, maar vooral gedurende de jaren die hieraan vooraf gingen. Moeke en papa, ik kan mijn dankbaarheid ten opzichte van jullie niet met woorden omschrijven. Jullie hebben me het mooiste geschenk gegeven wat een kind krijgen kan: een warme liefdevolle thuis. Jullie hebben steeds trots voor mij gesupporterd en hebben ervoor gezorgd dat ik telkens vol vertrouwen de juiste weg heb kunnen kiezen. Ik vond het lang de gewoonste zaak van de wereld dat ouders wel achter hun kinderen staan en hen alle kansen bieden, maar meer en meer besef ik dat ik toch wel héél veel geluk heb gehad. Bedankt voor me op zo'n fantastische manier te tonen hoe mooi het leven is en voor het aanreiken van zoveel kansen. Het boekje dat hier nu voor jullie ligt is voor een heel groot deel aan jullie te danken! Het is mijn grootste wens er samen met Danny in te slagen ook onze kindjes dat vertrouwen, die warmte en levenskunst mee te geven! Bedankt lieve ouders!

Danny, dit stukje laat ik je niet op voorhand lezen want dan zou je waarschijnlijk toch vinden dat ik een beetje overdrijf, want je hebt me toch maar 'gewoon' gesteund... Integendeel, het besef dat je steeds achter me stond en het enorme vertrouwen in mij heeft me vaak de kracht gegeven om even door te bijten als de weg wat te steil werd. Lieve schat, bedankt ook voor je geduld en voor je begrip in periodes waarin de gedachten aan onopgeloste vragen en mysteries mij bleven achtervolgen. Met de keuze voor onze kindjes, Lien en Joren, werd ons leven enorm verrijkt, maar tegelijkertijd werd het niet eenvoudiger en alles vroeg meer organisatie. Maar we hebben het toch maar mooi voor elkaar gekregen! Hieraan heb jij trouwens nooit getwijfeld! Ik kon die onderzoeks-mysteries soms net wat beter relativeren als ik je zo zag stoeien met de kinderen of als we ons (allevier!) eens lekker konden gaan uitleven op de speeltuin... Bedankt voor die zalige jaren samen, voor die vele intense momenten van echt geluk. We hebben al zoveel moois mogen meemaken. Laat ons samen aan onze volgende tocht beginnen, kom!

Ilse, november 2001

Curriculum Vitae

Ilse Smets was born on the 6th of November, 1971 in Hasselt (Belgium). From 1983 to 1989 she attended the Humaniora Virga Jesse in Hasselt (mathematics - sciences). Between 1989 and 1994, she studied at the Faculty of Applied Biological Sciences at the Katholieke Universiteit Leuven (Belgium). In June 1994, she graduated as Bio-engineer in Chemistry. In December 1994, she joined the group of Physiology at the Limburgs Universitair Centrum (LUC) in Diepenbeek where she taught physiology at the Faculty of Medicine and performed the research that is described in this thesis.

Publications in International Journals

Smets I., Zeiske W.*, Steels P., Van Driessche W. (**1998**)*
Na^+ dependence of single-channel current and channel density generate saturation of Na^+ uptake in A6 cells.
Pflügers Arch - Eur J Physiol, 435, 604-609
*authors equally contributed to the report

Zeiske W., **Smets I.***, Ameloot M., Steels P., Van Driessche W. (**1999**)*
Intracellular pH shifts in cultured kidney (A6) cells: effects on apical Na^+ transport.
Am J Physiol Cell Physiol, 277, C469-C479
*authors equally contributed to the report

***Smets I.**, Ameloot M., Steels P., Van Driessche W. (**2001**)*
Loss of cell volume regulation during metabolic inhibition in A6 cells: role of intracellular pH.
Am J Physiol Cell Physiol, in revision

Presentations of posters on regional, national or international symposia

***Smets I.**, Zeiske W., Ameloot M., Steels P. (**1995**)*
Alterations of intracellular pH in renal A6 cells during chemical anoxia and during the putative cytoprotective action of glycine.
Autumn meeting of the Belgian Society for Fundamental and Clinical Physiology and Pharmacology: 18 November 1995, Mons, Belgium
Pflügers Archiv - Eur J Physiol, 431, R6

Zeiske W., ***Smets I.***, *Ameloot M., Steels P., Kramp R.* ***(1996)***
How does intracellular acidosis inhibit sodium transport in A6 cells?
Annual Meeting of the American Society of Nephrology: 3-6 November 1996, New Orleans.
J Am Soc Nephrol, 7, 1295

Vecer J., Ameloot M., ***Smets I.***, *Steels P.* ***(1997)***
Steady-state and time-resolved microfluorimetry: determination of intracellular ion concentrations, membrane potential, cytoplasmic viscosity and order of lipids in membranes.
Spring meeting of the Belgian Society for Fundamental and Clinical Physiology and Pharmacology: 15 February 1997, Brussels, Belgium

Smets I., *Zeiske W., Steels P., Van Driessche W.* ***(1997)***
Saturating single channel currents generate saturation of transepithelial Na^+ transport in A6 cells.
American Physiological Society Conference: 29 October - 1 November 1997, Park City, Utah
The Physiologist, 40, A-6, 6.11

Smets I., *Vecer J., Steels P., Ameloot M.* ***(1998)***
Monitoring NAD(P)H levels in renal epithelial cells (A6) by microfluorometry.
Belgian Society of Cell Biology: 25 October 1997, Diepenbeek, Belgium
Cell Biology International, 22, 73

Vecer J., Ameloot M., ***Smets I.***, *Steels P.* ***(1998)***
Which intracellular characteristics are monitored by the pH indicators C. SNARF-1 and C. SNAFL-1? A time-resolved microfluorimetric study.
Meeting of the Belgian Society of Fundamental and Clinical Physiology and Pharmacology, 14 February 1998, Louvain-en-Woluwé, Belgium
Pflügers Archiv - Eur J Physiol, 435, R245

Smets I., *Zeiske W., Ameloot M., Steels P., Van Driessche W.* ***(1998)***
Intracellular protons reduce the apical open channel density without altering single channel currents in renal epithelial cells (A6).
European Kidney Research Forum, 3-6 July 1998, Manchester, England

Jans F., ***Smets I.***, *Ameloot M., Steels P.* ***(1998)***
Primary cultures of rabbit medullary thick ascending limb of Henle's loop
International Symposium: Renal tubular cells in culture. Tools for the study of tubulo-interstitial function in health and disease, 4-5 December 1998, Antwerpen, Belgium

Smets I., *Ameloot M., Steels P.* ***(1999)***
Chemical ischemia induces apoptosis and necrosis in renal epithelial cells (A6).
Belgian Society of Cell Biology: 6 March 1999, Gent, Belgium
Cell biology International, 23, 782

Smets I.**, Zeiske W., Ameloot M., Van Driessche W., Steels P. **(1999)
Effects of intracellular pH shifts on apical Na^+ transport in cultured kidney (A6) cells.
International Congress of Nephrology, Satellite symposium "Cell homeostasis: channels and transporters": 8-10 May 1999, Guaruja, Brazil

*Vandenabeele F., **Smets I.**, Creemers J., Steels P., Lambrichts I. **(1999)***
Early apoptosis in toad kidney epithelial cell cultures (A6): ultrastructural observations correlated with sodium transport and energy content.
Autumn meeting of the Dutch Society of Microscopy: 16-17 December 1999, Arnhem, The Netherlands

Smets I.**, Ameloot M., Steels P., Van Driessche W. **(2001)
The effects of external and internal protons on RVD in A6 cells.
Spring meeting of the Belgian Society for Fundamental and Clinical Physiology and Pharmacology: 3 March 2001, Leuven, Belgium
Pflügers Arch - Eur J Physiol, 442, R42

Smets I.**, Van Driessche W., Ameloot M., Steels P., **(2001)
Metabolic inhibition of transepithelial sodium transport in A6 epithelia is fully reversible: time course of intracellular ATP levels and modulation of apical sodium influx.
Meeting of the Belgian Society for Fundamental and Clinical Physiology and Pharmacology: 9 June 2001, Namur, Belgium
Pflügers Arch - Eur J Physiol

Smets I.**, Ameloot M., Van Driessche W., Steels P. **(2001)
Role of intracellular pH in cell volume regulation of metabolic inhibited A6 cells.
The 2001 ASN/ISN World Congress of Nephrology: 14-17 October 2001, San Francisco, California, USA
J Am Soc Nephrol, 12, 792A

Oral Communications

Smets I.**, Ameloot M., Steels P., Van Driessche W. **(2000)
Effects of chemical ischemia on cell volume and on cell volume regulation in a renal distal tubular cell line (A6).
Annual meeting of The Belgian Society of Nephrology: 8 April 2000, Aalst, Belgium

Smets I.**, Ameloot M., Steels P., Van Driessche W. **(2000)
Intracellular acidification is not the regulatory volume decrease inhibiting event during chemical ischemia in A6 cells.
Symposium sponsored by the bilateral agreement BIL96/23 (Belgium/Romenia): Cell behavior in stress situations: 26 May 2000, Leuven, Belgium

Award

***Smets I.**, Ameloot M., Steels P., Van Driessche W. (**2000**)*
Effects of chemical ischemia on cell volume and on cell volume regulation in a renal distal tubular cell line (A6).
Annual meeting of The Belgian Society of Nephrology: 8 April 2000, Aalst, Belgium

Award for the best oral communication